

Scoping MEMS Seismometers for Deployment on the Moon

Ceri Nunn (3226), William T. Pike (Imperial College, London),
Mark P. Panning (3226), Sharon Kedar (335N)



Fig. 1: Artist's Impression, MX-1E Lander
[MoonExpress]

1) INTRODUCTION

Commercial Lunar Payload Services (CLPS) is a NASA program to acquire end-to-end commercial payload services between the Earth and lunar surface.

Micro-Electro-Mechanical Systems (MEMS) sensors are small, lightweight sensors etched on a silicon wafer.

Here we aim to answer two important questions:

- 1) Are MEMS sensors suitable for deployment on the Moon?
- 2) Will the sensor detect sufficient moonquakes if the mission extends for a single lunar day (approximately two weeks in Earth-time)?

2) METHODOLOGY

To answer question 1), we estimated the impact of each required change for the seismometer on each of the components. We then compared the noise floor with a variety of events from the Apollo missions.

For each Apollo event, we removed the instrument response, and output the seismogram in acceleration. We estimated the maximum acceleration for many events, and compared to the estimated noise floor for the MEMS seismometer.

For question 2), we counted the number of events above the noise floor.

3) MEMS SEISMOMETERS

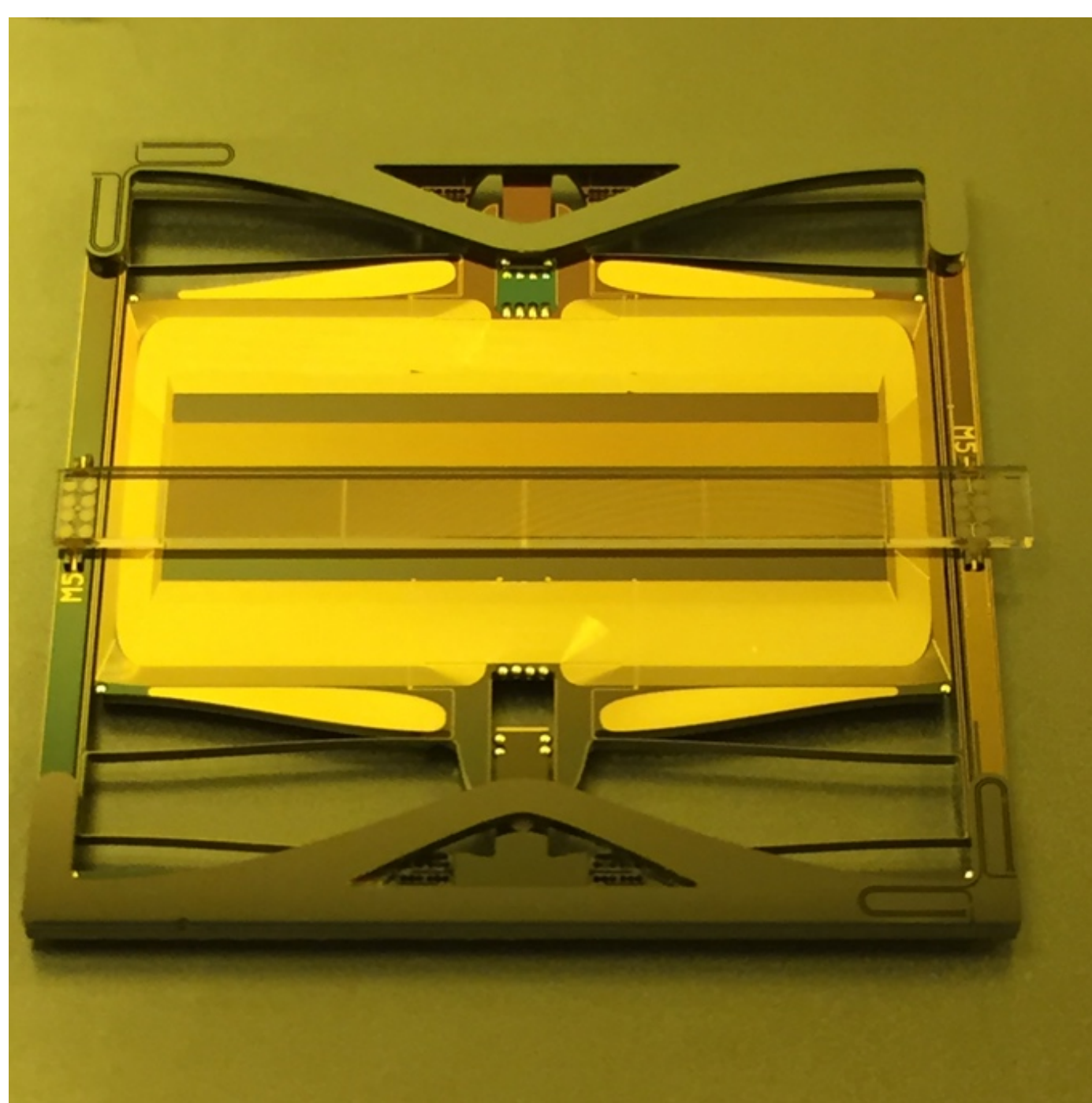


Fig 2: The sensor is a small and robust instrument. It is through-wafer etched and patterned in single-crystal silicon, with a 25 mm die size. Three sensors measure all three components of translational motion. The combined package for InSight had a total mass of 635 g for the three-axis SP delivery of packaged sensor heads, electronics board and associated connectors and cabling [1]. (© Imperial College London).

The performance of the current generation of SEIS-SP sensor is limited by the thermal noise floor from gas damping within the package [2]. The near-vacuum of the lunar surface will reduce the thermal noise floor.

6) CONCLUSIONS AND IMPACT ON THE FIELD

We conclude that:

- 1) MEMS seismometers are suitable for deployment on the Moon.
- 2) Although surviving the lunar night would increase the number of detectable events, just one lunar day would provide many high-quality observations.

We will use these results to propose a MEMS seismometer on a Commercial Lander.

A mission lasting a just one lunar day could test the technology for a future Lunar Geophysical Network (LGN). The LGN would have several seismometers deployed in different locations on the Moon. We are building on the expertise from Apollo, to make the LGN a reality. Forward to the Moon!

[1] Pike, W. T. et al. in Proc. 47th Lunar Planet. Sci. Conf. (2016).

[2] Pike, W. et al., 25 - European Lunar Symposium 2016 - NASA (2016).

4) RESULTS I - SENSOR IMPROVEMENTS

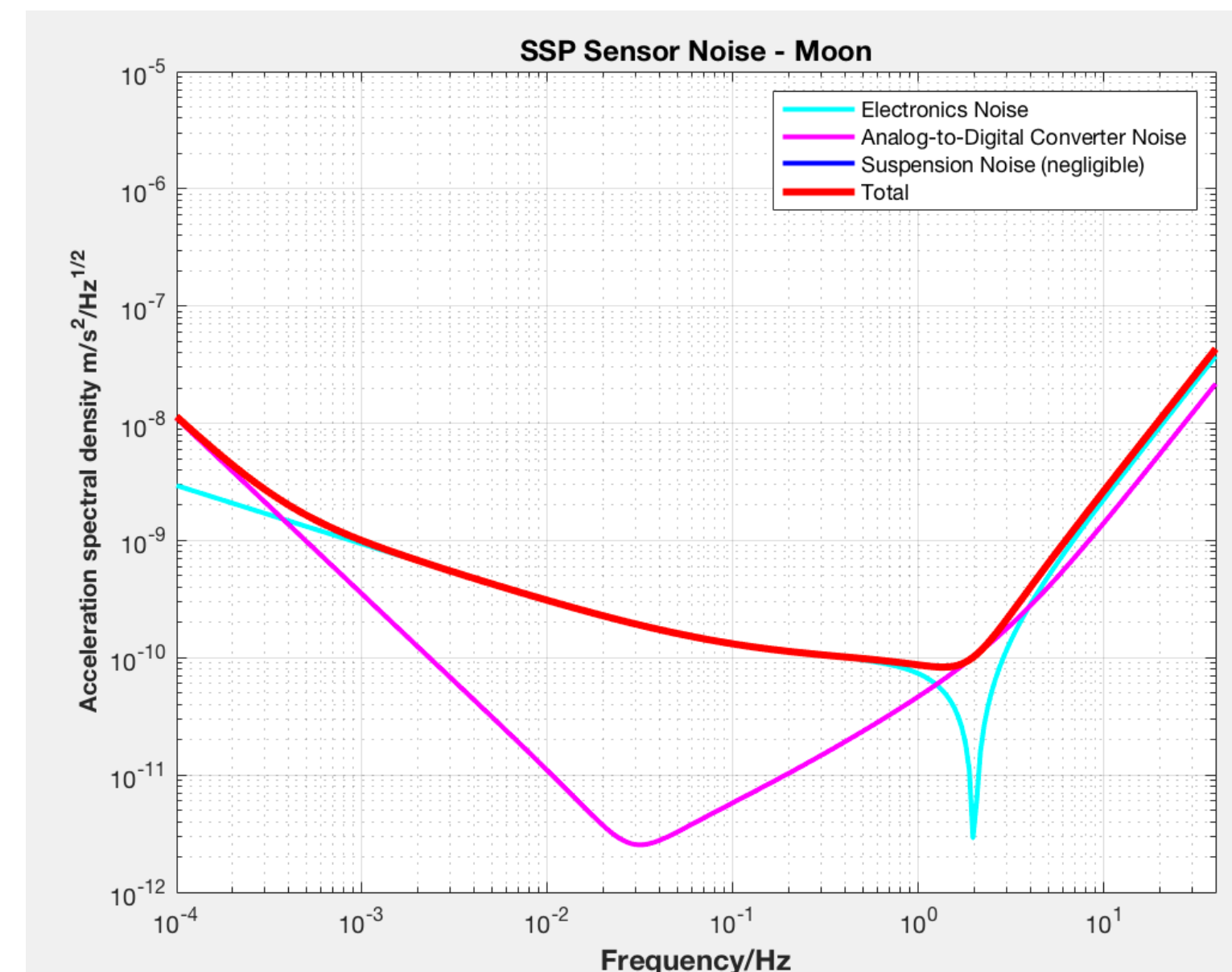


Fig 3: Noise floor of the SSP seismometer (estimated) after changes required for lunar operation. Several changes are required to make the seismometer work in lunar gravity. The noise floor is lowered relative to the operation on Mars or cruise to Mars.

Impact on the Noise Floor

- ↓ Lower Gravity (reduce resonant frequency)
- ↓ Airless Body (thermal noise on spring)
- ↓ Airless Body (Displacement transducer gain)
- ↓ Lower Radiation (lower noise pre-amp)
- ↑ Deck Deployment
- ↓ Digitisation (finer than Apollo)

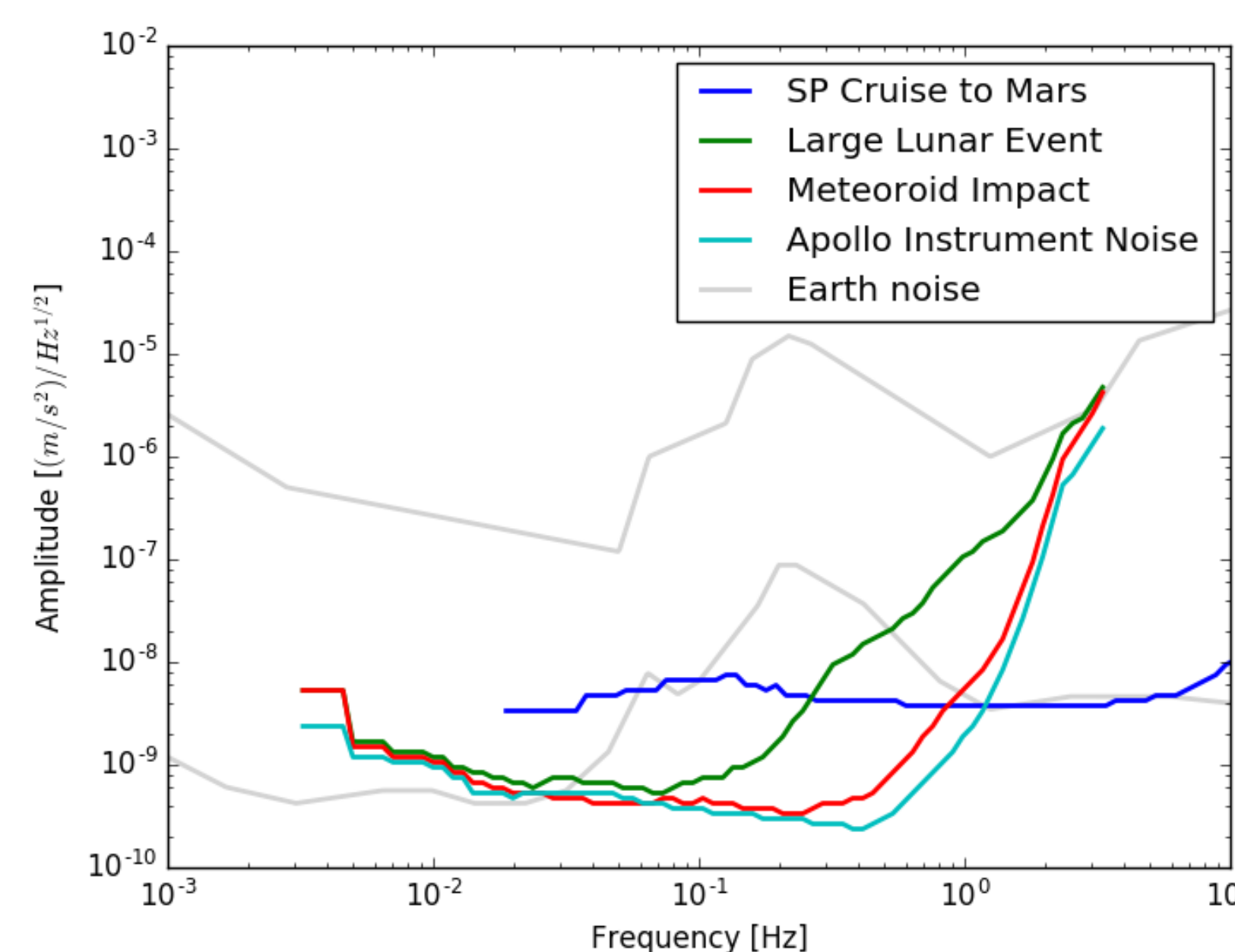


Fig 4: A selection of Apollo seismic events. These events would be detected by the SSP seismometer.

5) RESULTS II - EVENT DETECTION

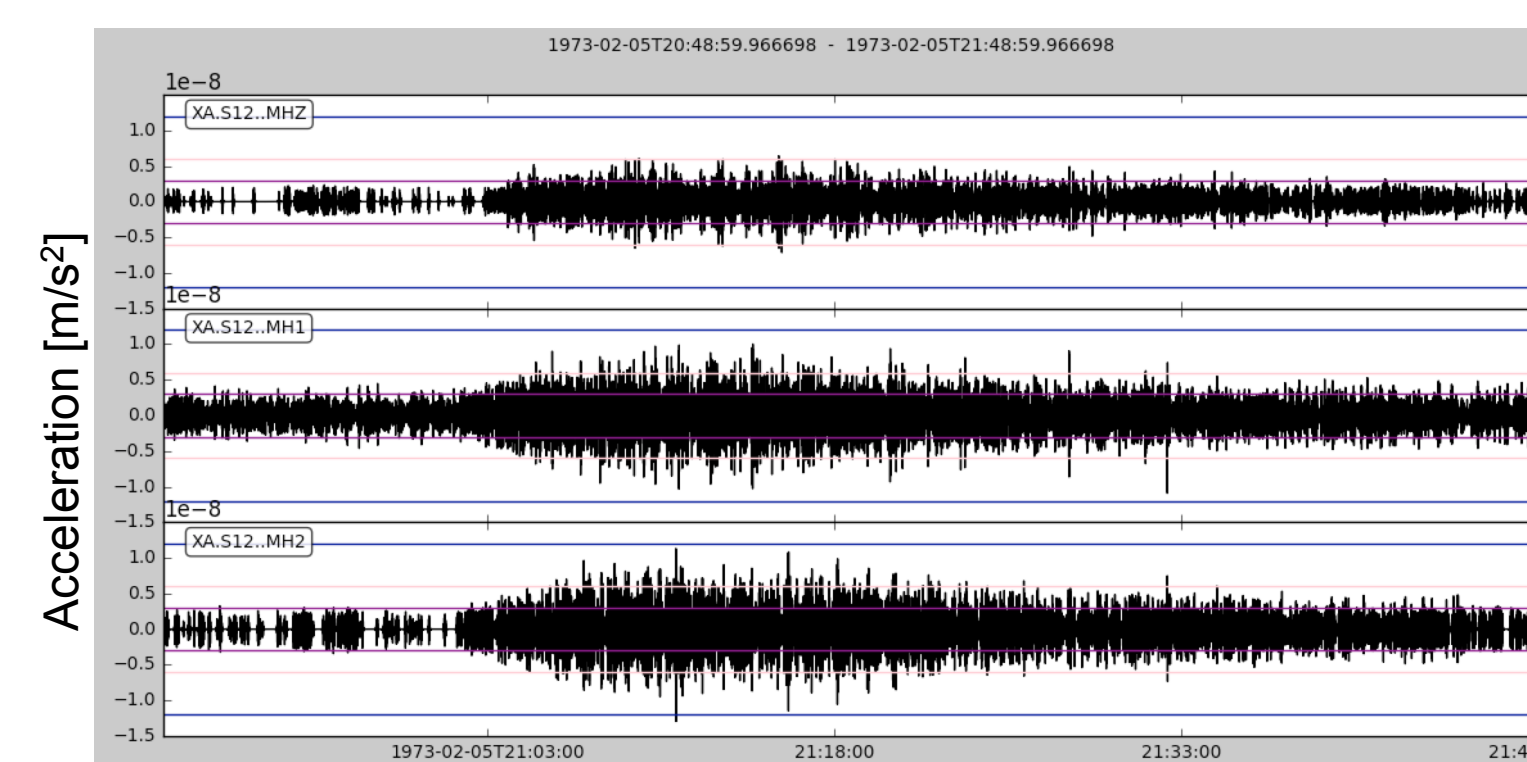


Fig 5: Meteoroid impact detected by Apollo 12's seismometer. The MEMS seismometer could detect a similarly small event.

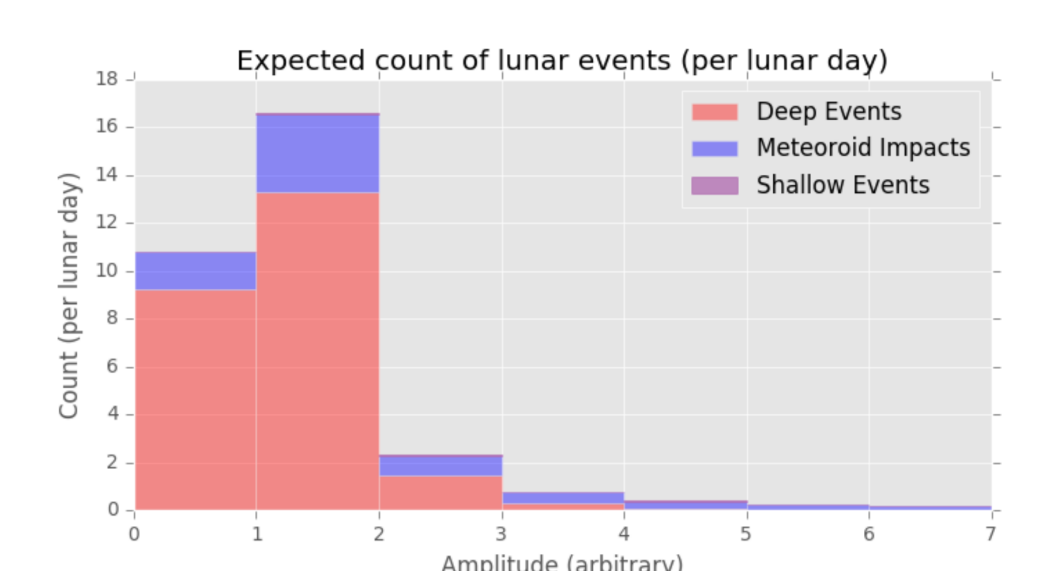


Fig 6: Estimated seismic event count for one lunar day.



Increased thermoelectric figure of merit through cobalt compositing in the Zintl phase $\text{Yb}_{14}\text{MnSb}_{11}$

Author: Giacomo Cerretti (3464)
Sabah K. Bux (3464), Jean-Pierre Fleurial (3462)

Objective and strategy

Increase the thermoelectric figure of merit (zT) to improve the efficiency of Radioisotope Thermoelectric Generators (RTGs), and provide higher power output during missions. The increase of zT can be achieved by compositing to decouple the optimization of thermoelectric properties. Cobalt (Co) has been chosen because it is a metal with a relatively high Seebeck coefficient ($|S| \approx 25 \mu\text{V/K}$ at 1100K), therefore the composite material should have a lower electrical resistivity while retaining high values of S .

Background



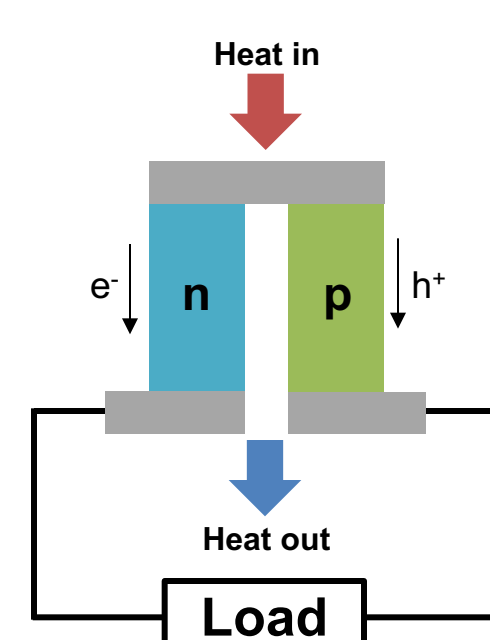
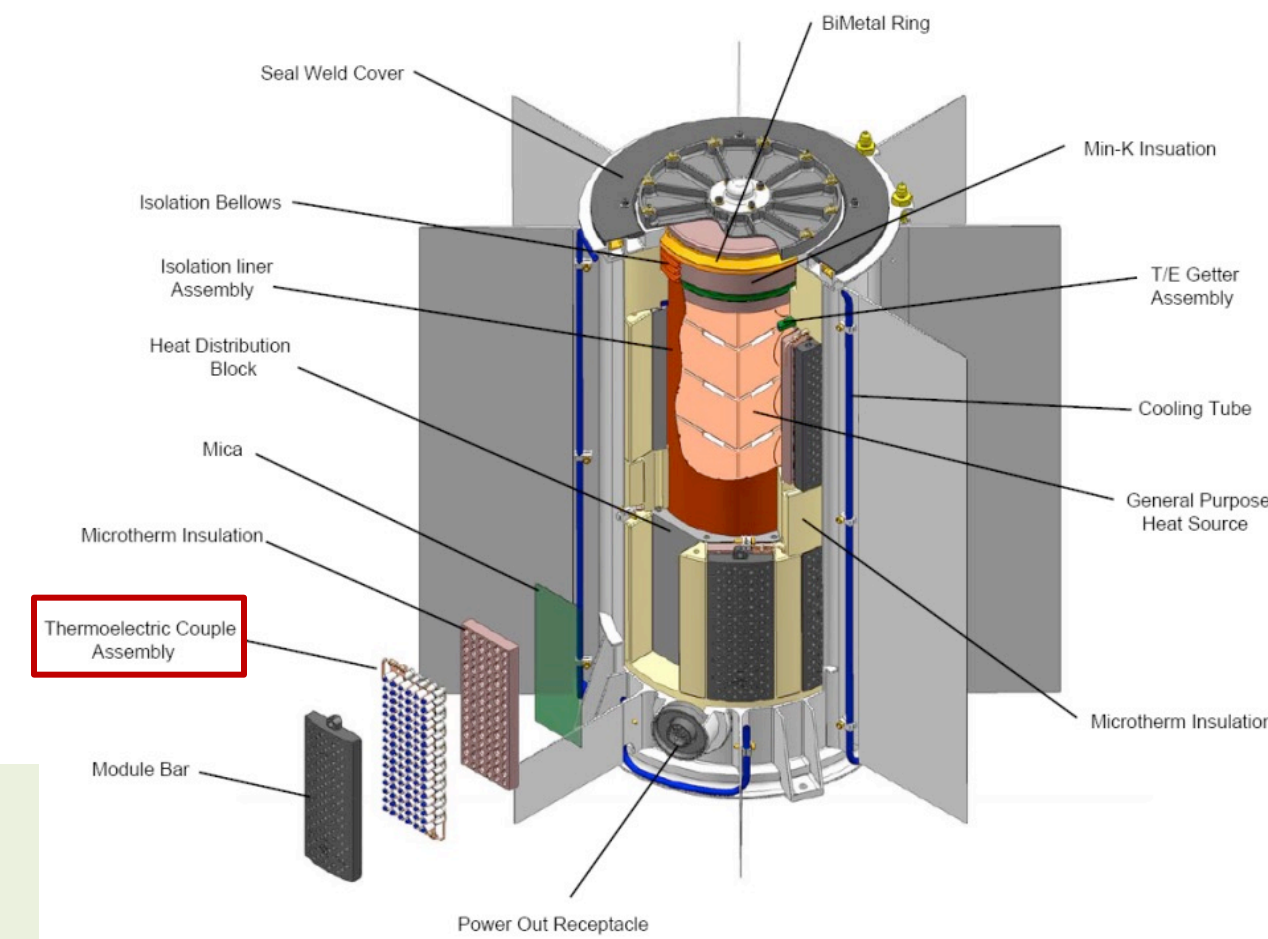
41 RTGs used successfully on 23 NASA missions since 1961.

Why RTGs:

- ✓ No moving parts.
- ✓ Very reliable technology (40+ years of proved operation).
- ✓ Independent from solar irradiance and environmental conditions.

Thermoelectric generation:

Temperature gradient applied to p - n junction induce migration of charge carriers (e^- ; h^+) from the hot to the cold side generating an electric potential.



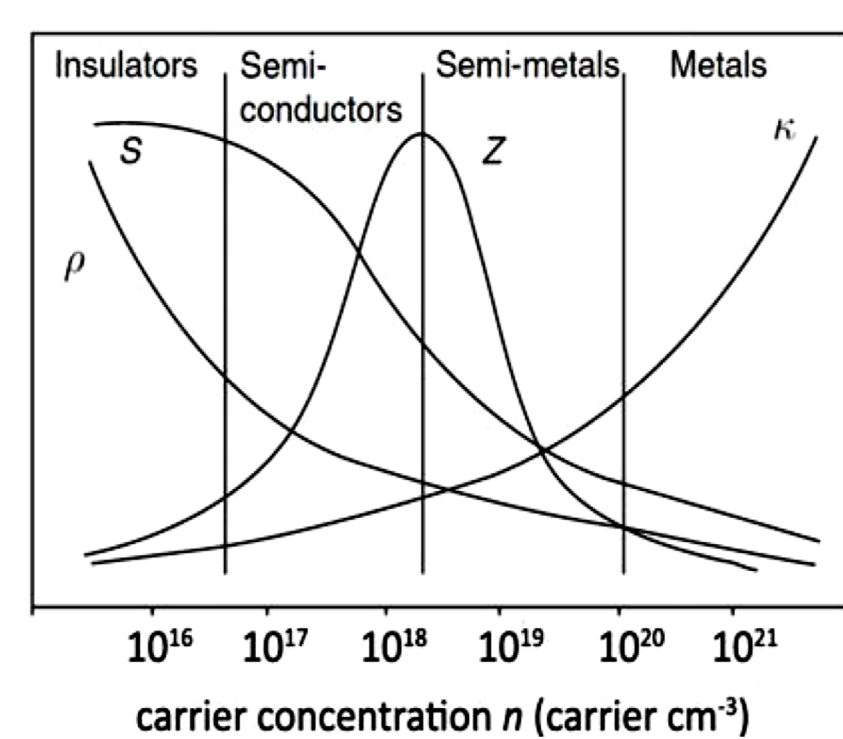
Efficiency

$$\eta_{\max} = \frac{T_{\text{hot}} - T_{\text{cold}}}{T_{\text{hot}}} \frac{\sqrt{1 + ZT} - 1}{\sqrt{1 + ZT} + \frac{T_{\text{cold}}}{T_{\text{hot}}}}$$

Thermoelectric Figure of Merit

$$zT = \frac{S^2 T}{\rho \kappa}$$

S = Seebeck coefficient
 ρ = Electrical resistivity
 κ = Thermal conductivity
 T = Absolute temperature

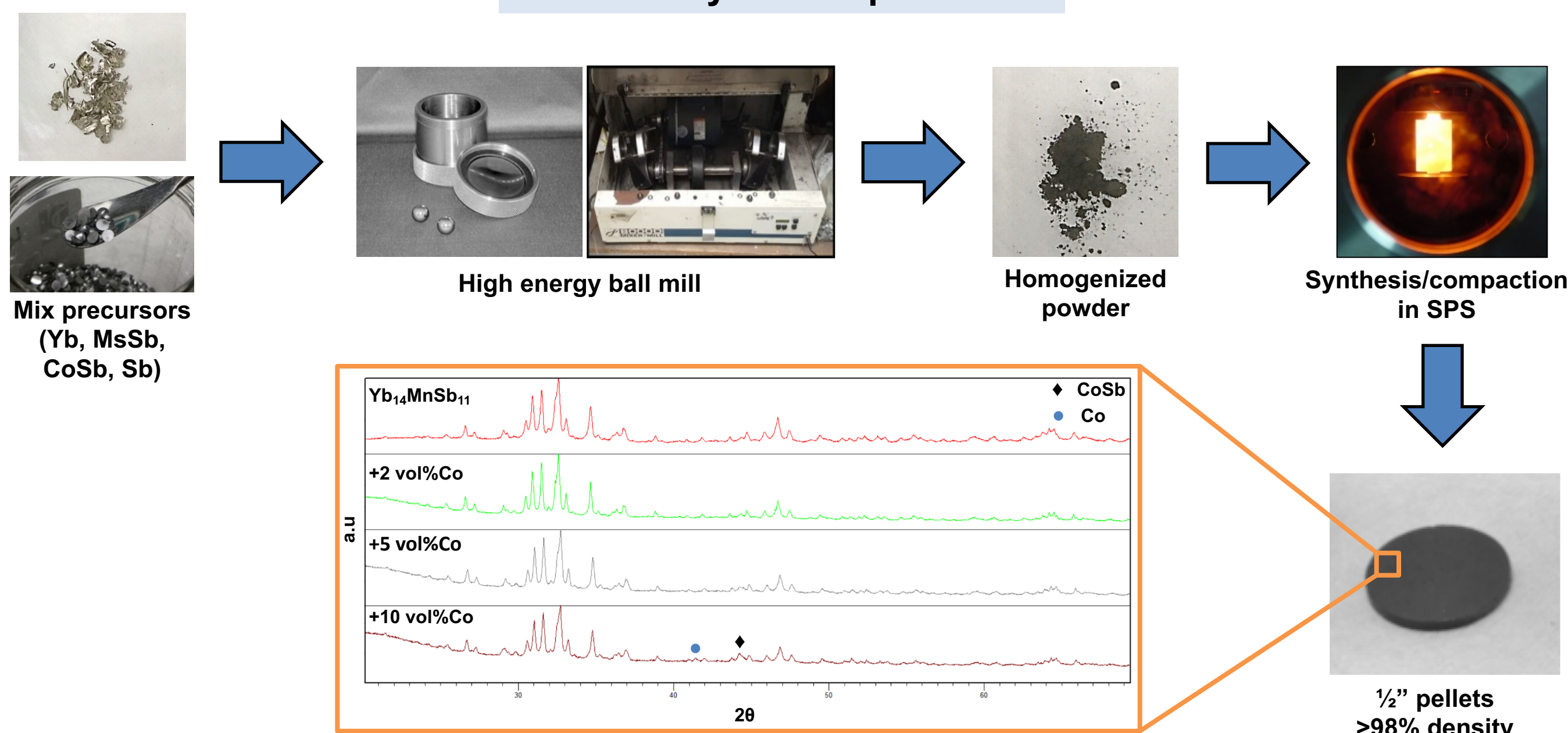


Challenges:

- SoA RTGs have low efficiencies (GPHS-RTG $\eta \approx 5\%$, MMRTG $\eta \approx 6.5\%$).
- Strategies for the independent optimization of material parameters need to be found in order to increase zT and η .

Methods

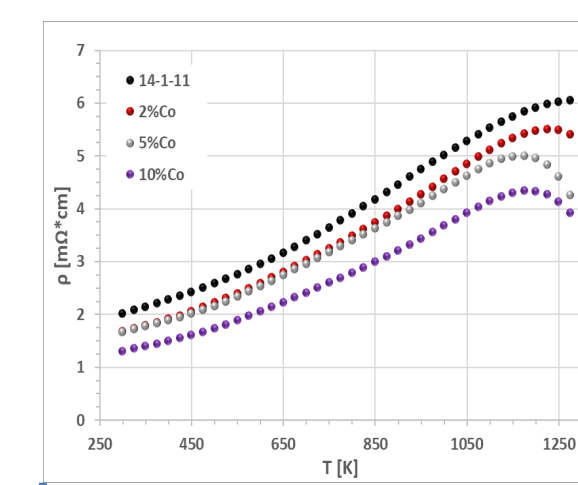
Materials synthesis procedure



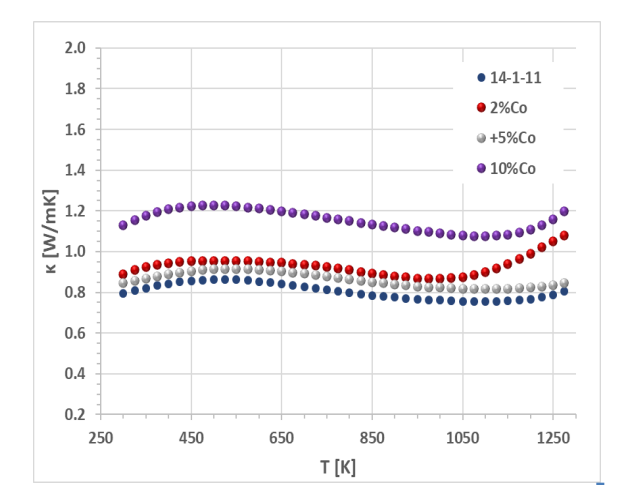
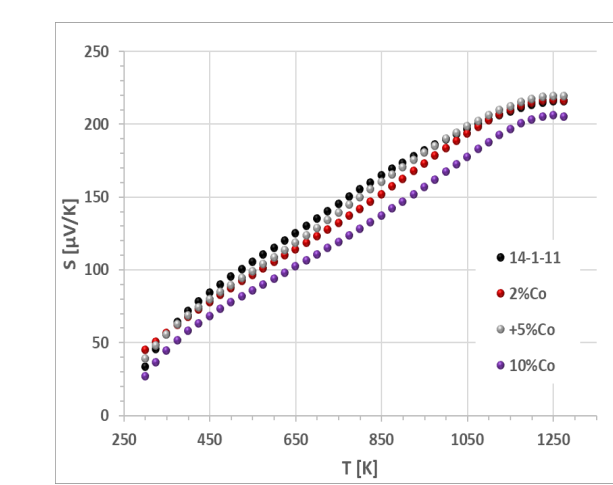
Results

Increasing Co content:

- Decreases ρ .
- Comparable S .
- Increases κ .



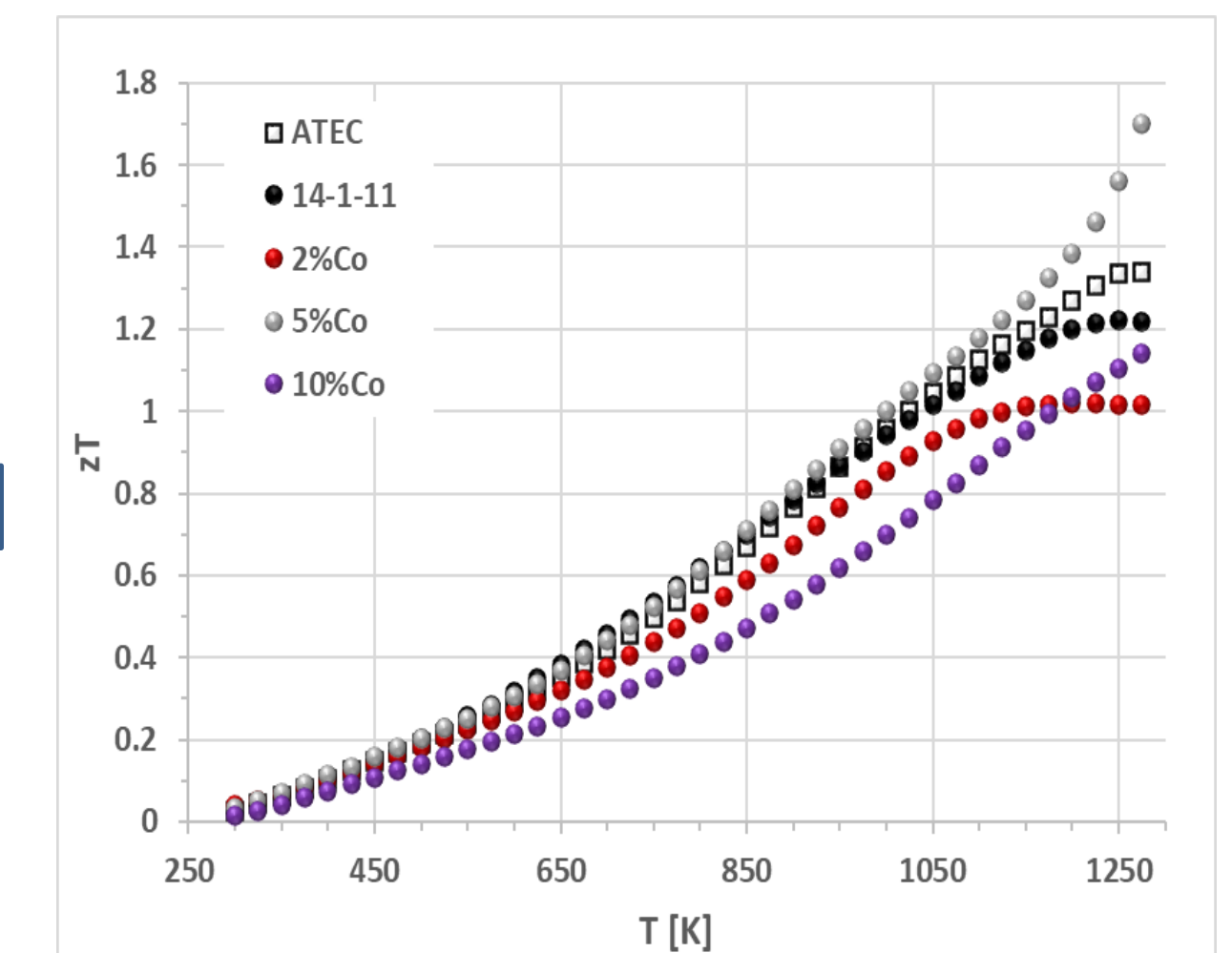
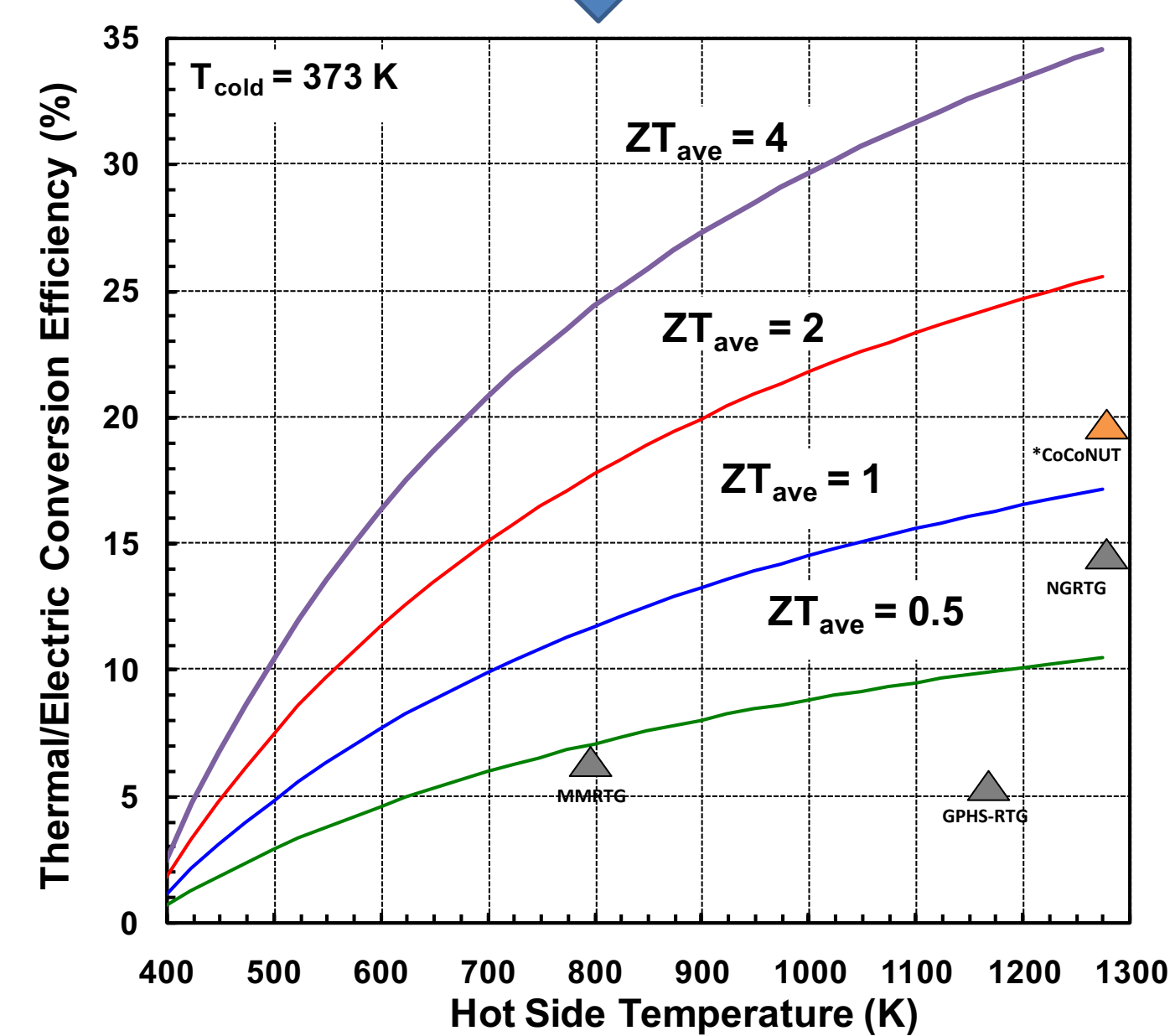
Transport properties



zT Improvement:

Adding 5vol% Co improved the thermoelectric performance of $\text{Yb}_{14}\text{MnSb}_{11}$ (14-1-11) reaching a peak zT of 1.7 @1273K.

Increased $zT \rightarrow$ Higher η



ATEC (Advanced ThermoElectric Converter) = JPL baseline for $\text{Yb}_{14}\text{MnSb}_{11}$.

Higher conversion efficiency:

Using segmented couple design having composite $\text{Yb}_{14}\text{MnSb}_{11}$ on the p -leg (p -1), and by impedance matching (electrical and thermal) and temperatures for each segment, a total efficiency of 18.7% can be achieved (CoCoNUT - Cobalt Composite Network Using Thermoelectric).

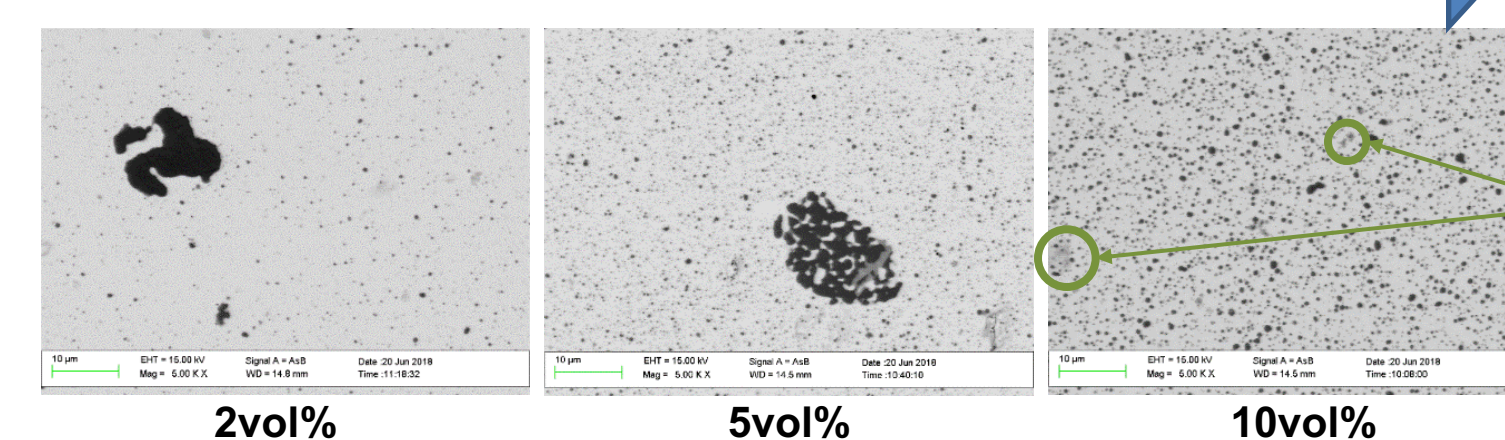
Materials efficiencies and leg segmentation

RTG	n-type		p-type		T_H [K]		T_C [K]		Couple η [%]
	1	2	1	2	1	2	1	2	
GPHS-RTG	PbTe	-	TAGS	-	775	-	566	-	5.1
MMRTG	SiGe	-	SiGe	-	1273	-	500	-	6.5
NGRTG	$\text{La}_{3-x}\text{Te}_4$	n-SKD	$\text{Yb}_{14}\text{MnSb}_{11}$	p-SKD	1273	875	875	475	13.5
*CoCoNUT	$\text{La}_{3-x}\text{Te}_4 + \text{Ni}$	n-SKD	$\text{Yb}_{14}\text{MnSb}_{11} + \text{Co}$	YbZn_2Sb_2	1273	850-775	850-775	325	18.7

* = Preliminary best configuration.

Microstructure

Better inclusions dispersion with higher Co content



At high cobalt concentration start appearing secondary phase regions, possible unreacted precursor (CoSb).

Conclusions

- Optimizing materials, design and temperatures of TE junction a conversion efficiency of 18.7% is achieved. This is a 3-fold improvement compared to heritage SiGe couples.
- $\text{Yb}_{14}\text{MnSb}_{11}$ +5vol% Co shows the highest zT , marking a +40% improvement compared to reference sample ($\text{Yb}_{14}\text{MnSb}_{11}$).
- Through compositing it was possible to decouple the optimization of the electronic properties and finally improve zT .

Acknowledgements

This work was performed at the California Institute of Technology/Jet Propulsion Laboratory under contract with the National Aeronautics and Space Administration, and it was supported by the NASA Science Missions Directorate's Radioisotope Power Systems Thermoelectric Technology Development Project.

G. Cerretti's research at Jet Propulsion Laboratory was supported by an appointment to the NASA Postdoctoral Program, administered by Universities Space Research Association under contract with NASA.

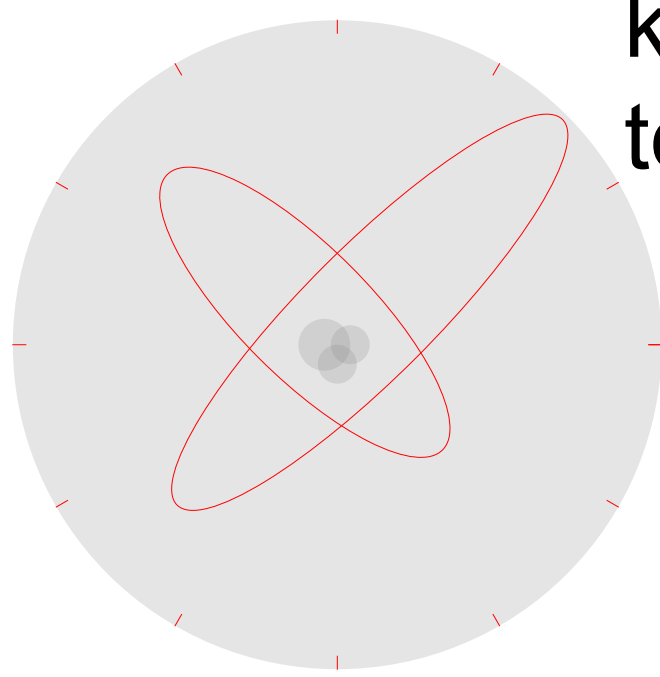
Micro Mercury Trapped Ion Clock (MMTIC)

Author: Thai M. Hoang (332J)

Sang K. Chung (332J), Thanh Le (332J), John D. Prestage (332J), Lin Yi (335E), Robert L. Tjoelker (335E), and Nan Yu (332J)
Sehyun Park (UIUC), Sung-Jin Park (UIUC), Gary Eden (UIUC), Chris Holland (SRI), Hao Wang (UC Davis), and Omeed Momeni (UC Davis)

1. Introduction: Atomic clock

- An atomic clock uses an atomic transition as a frequency standard for time keeping.
- A high accuracy and stability atomic clock will be key to many navigation applications and allow testing fundamental science. Examples include
 - The global positioning system, deep-space navigation
 - Theory of relativity, dark matter, and time variation of fundamental constants.



2. Objective: Develop a portable, low power, high stability clock



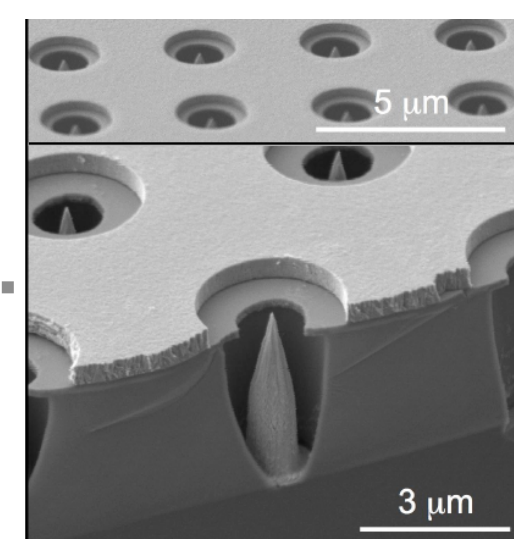
	CSAC Chip Scale Atomic Clock	DSAC Deep Space Atomic Clock	MMTIC (this work) Micro Mercury Trapped Ion Clock
Size	17 cc	17,000 cc	50 cc
Power	120 mW	50 W	250 mW
Stability $\sigma_y(\tau)$	$3 \times 10^{-10} / \sqrt{\tau}$	$2 \times 10^{-13} / \sqrt{\tau}$	$1 \times 10^{-11} / \sqrt{\tau}$
Stability σ_y	$1 \times 10^{-11} @ 10^3 s$	$1 \times 10^{-15} @ 10^4 s$	$1 \times 10^{-13} @ 10^4 s$

4. Results

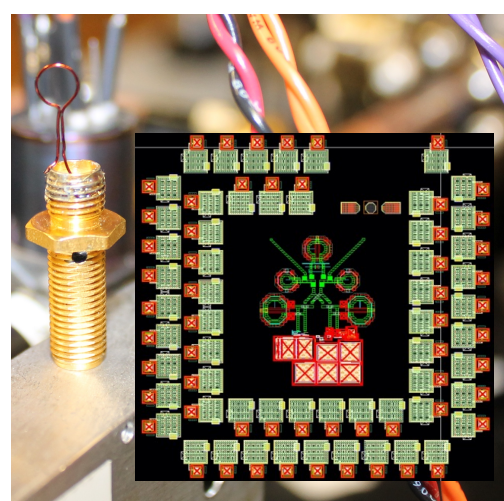
A linear ion trap



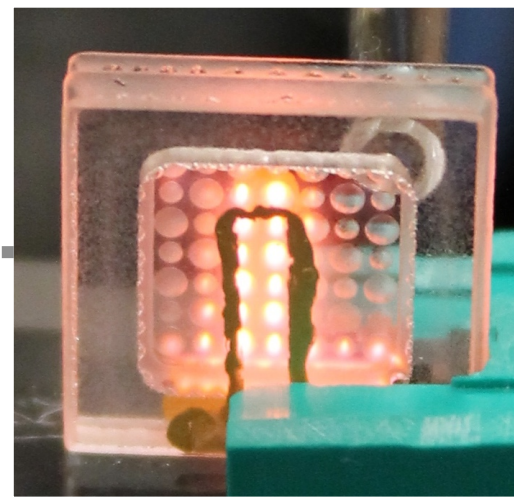
A field emitter array



Microwave synthesizer



Micro-cavity lamp



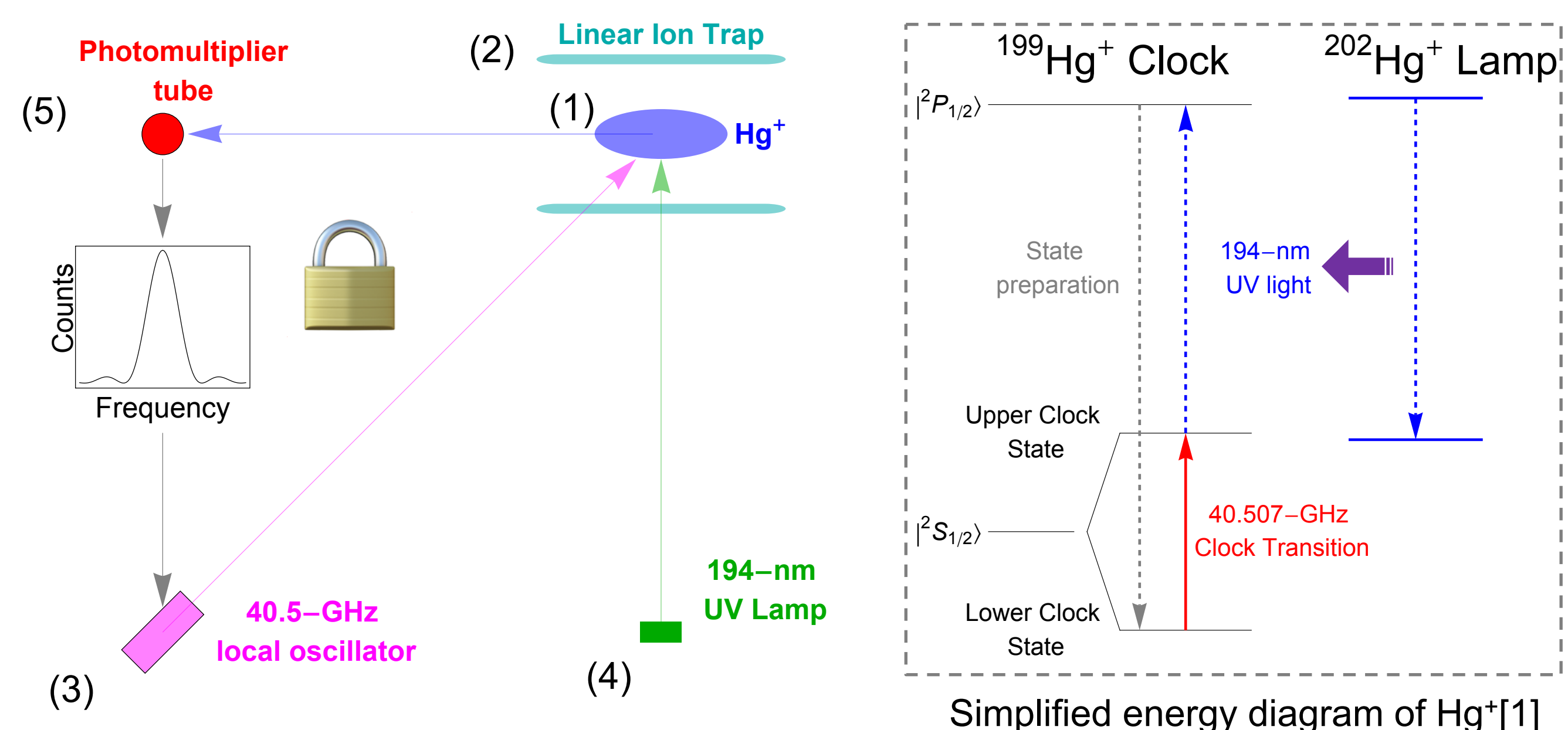
- Successfully integrating most clock components into the 130-cc Hg⁺ clock package (e.g., optics, FEA, linear ion trap, microwave antenna, micro-cavity lamp).

5. Conclusions

- The 130-cc Hg⁺ clock is assembled with most components and meets the stability requirement. We are working toward a completed clock package.
- A portable, miniaturized, low power-consumption, and high stability atomic clock can further advance navigation applications and allows testing fundamental science at different locations.
- The MMTIC technologies may be implemented into the future DSAC because of the power consumption and small size advantages.

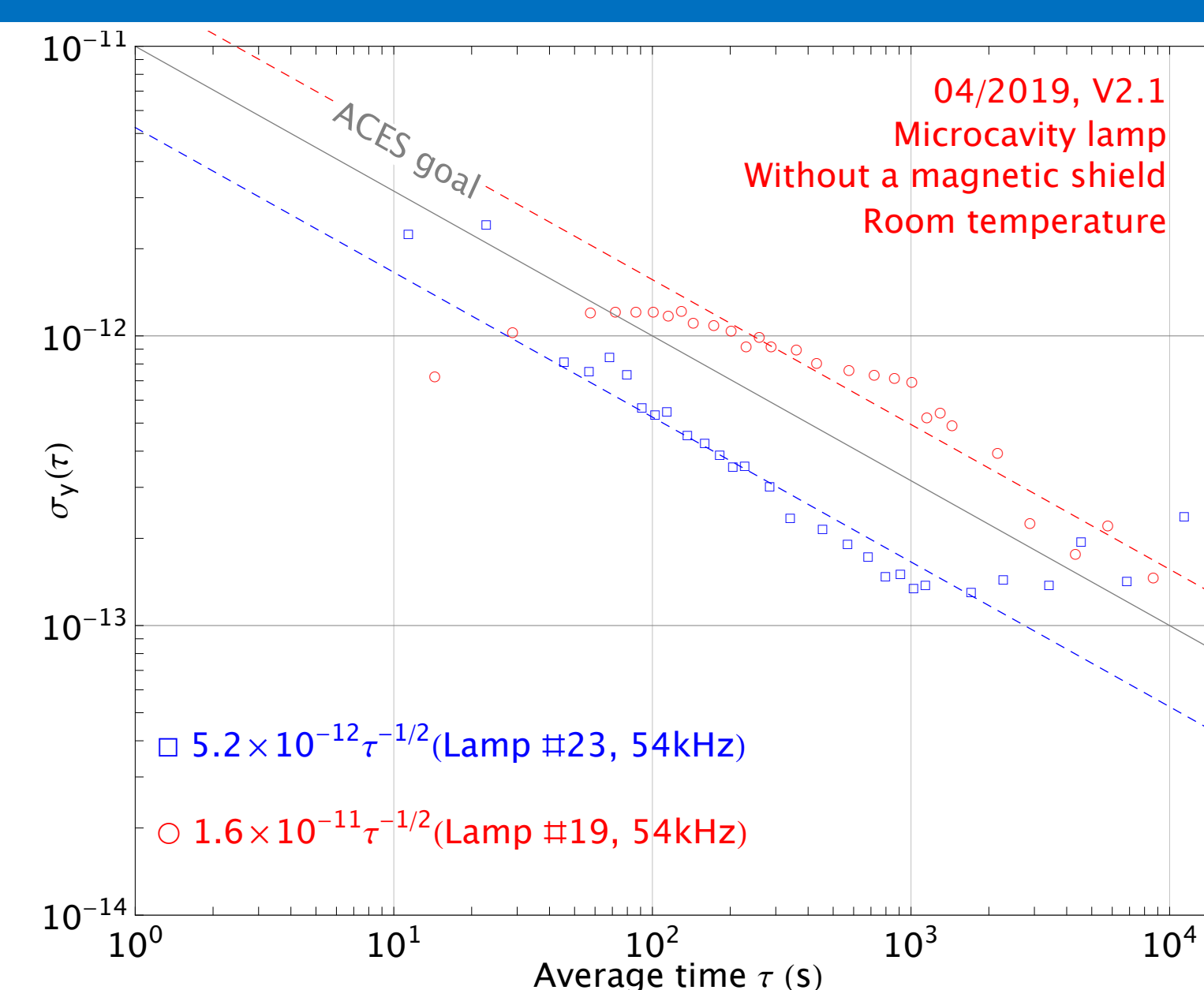
3. Method: Micro mercury trapped ion clock

Component	Hg ⁺ trapped ion clock	Advantage
Cooling	Helium buffer gas	No laser cooling/cryogenics
Vacuum	UHV, getter pumps	Zero power/maintenance-free
Atom	10 ⁶ - 10 ⁷ trapped Hg ⁺ ions	Small volume/long ion lifetime
Ion loading	Electron beam + Hg vapor	Negligible power consumption
Clock	40,507,347,996.8 Hz	Low magnetic sensitivity
Detection	A 194-nm lamp	No laser



¹⁹⁹Hg⁺ clock diagram:

- Loading ions using a low power field emitter array
- Trapping the ions using a linear ion trap.
- Interrogating the ions using a low power microwave synthesizer.
- Optically exciting the ions using a low power micro-lamp.
- Detecting the ion signal using a PMT and feedback to the synthesizer.



- The 130-cc Hg⁺ atomic clock meets the stability requirements: $\sigma_y(\tau) < 1 \times 10^{-11} / \sqrt{\tau}$ and $\sigma_y \sim 1 \times 10^{-13}$ at 10⁴ s

Acknowledgements

The research was carried out at the Jet Propulsion Laboratory, California Institute of Technology, under a contract with the National Aeronautics and Space Administration. Support from the Defense Advanced Research Projects Agency is acknowledged. The views, opinions and/or findings expressed are those of the author and should not be interpreted as representing the official views or policies of the Department of Defense or the U.S. Government. © 2019, California Institute of Technology.

References

- Prestage, John D., and Gregory L. Weaver. "Atomic clocks and oscillators for deep-space navigation and radio science." *Proceedings of the IEEE* 95.11 (2007)

Demonstration of optical frequency combs to cancel both clock noise and laser phase noise in time-delay interferometry

Quentin Vinckier (332J), Daniel Rieländer (University of Freiburg), Ivan Grudinin (Cruise Automation), Massimo Tinto (University of California, San Diego), Nan Yu (332J)

Laser Interferometry Space Antenna

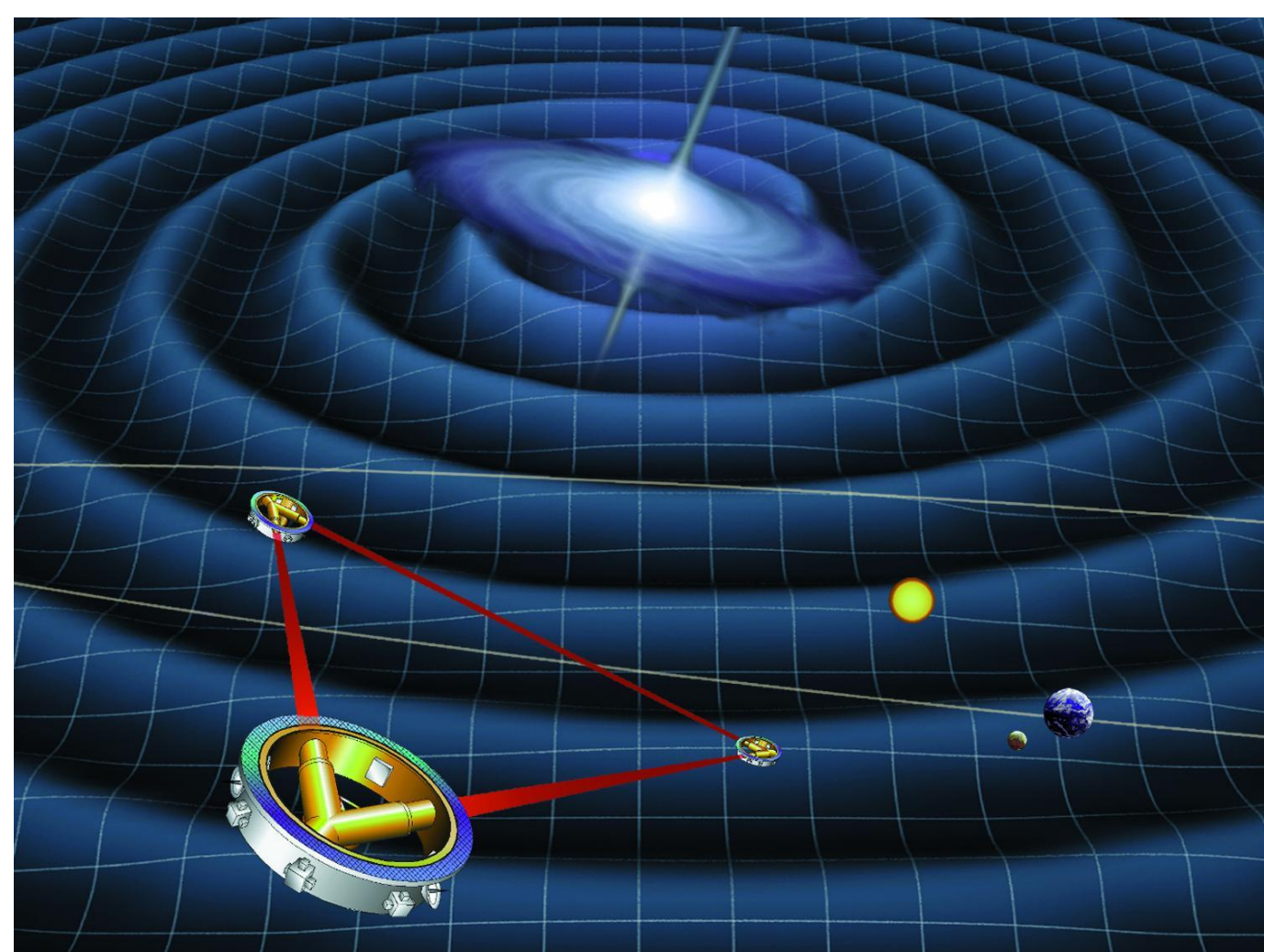


Image credit: NASA/ESA

Light Interferometer Space Antenna (LISA) mission goal is to detect gravitational waves (GW) in the frequency range from 0.1 mHz to 0.1 Hz with a strength sensitivity down to $\sim 10^{-20} 1/\sqrt{Hz}$ at 10^{-2} Hz. It consists of three spacecraft's exchanging laser signals, hence forming a triangular interferometer with arm length of 2.5 million km. LISA will orbit around the Sun following the Earth.

Time-delay interferometry

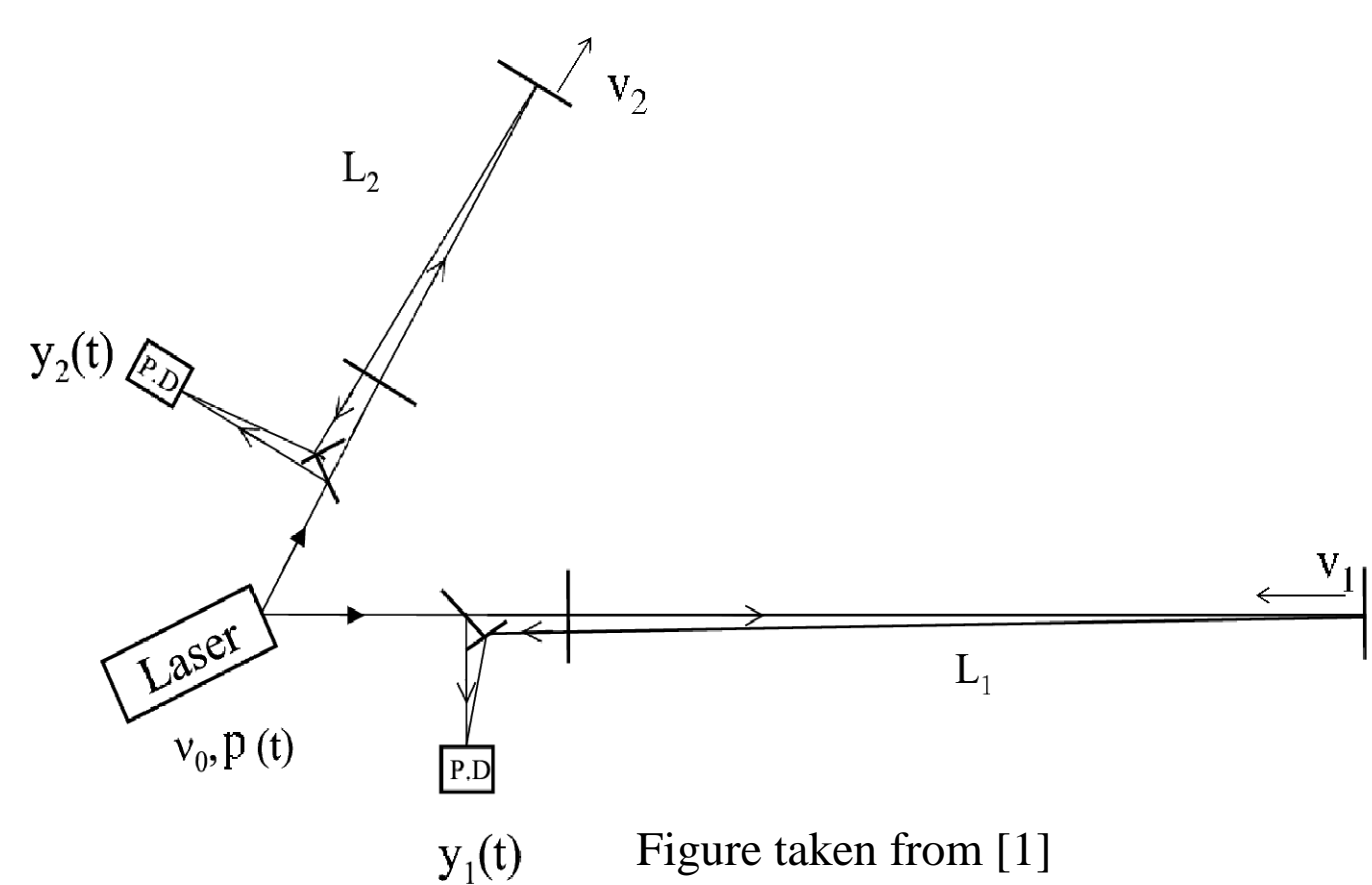


Figure taken from [1]

In order to recover gravitational-wave signals, time-delay interferometry (TDI) compensates variations in distance (L) and velocity (V : velocity normalized by the speed of light in vacuum) between the spacecraft's in post-processing by capturing digitalized laser phase measurements ($y_i(t)$) of each interferometer arm [1,2]. So far clocks are calibrated by additional inter spacecraft phase measurements to cancel laser phase noise and clock noise in post-processing [3].

Optical frequency comb

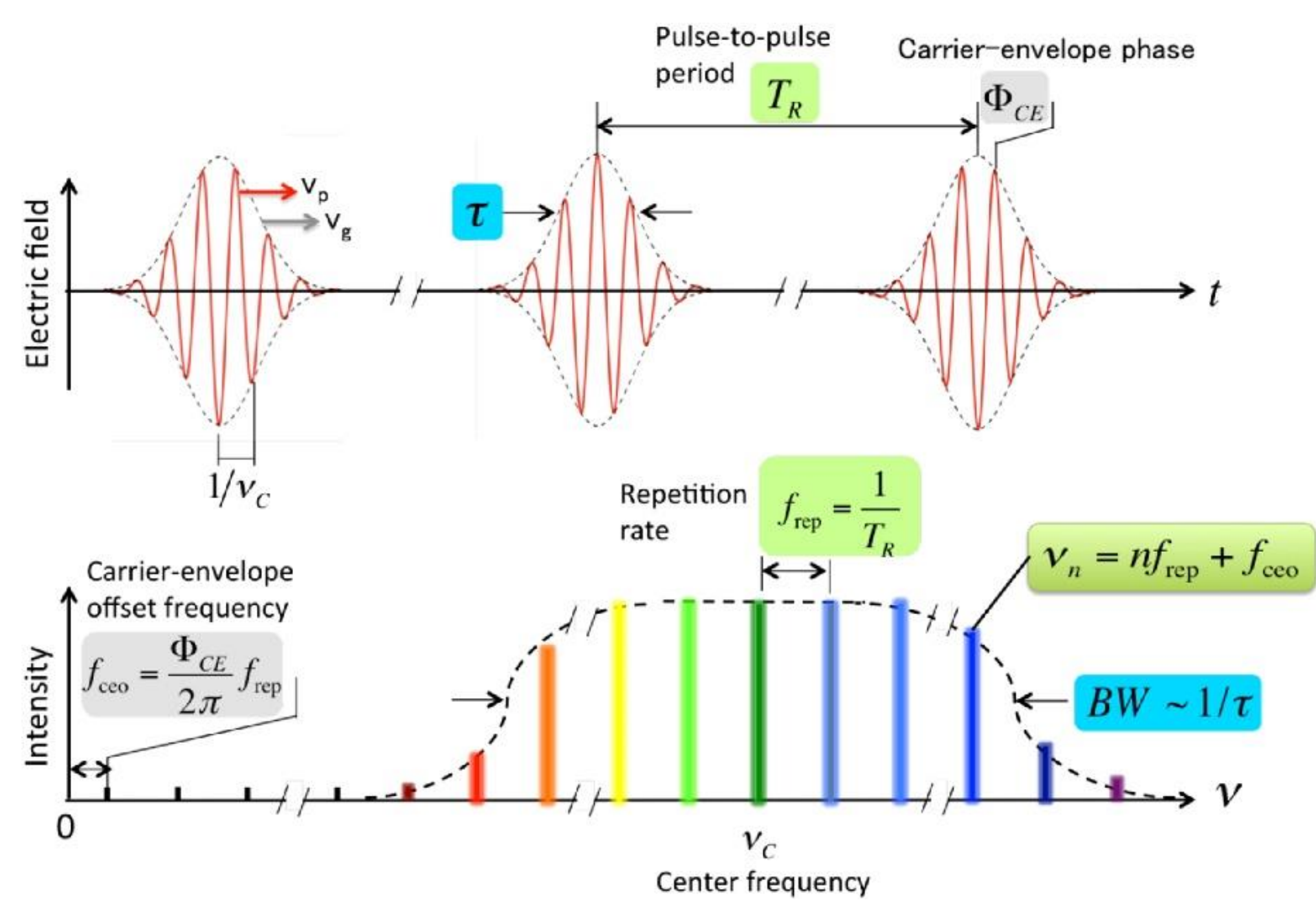
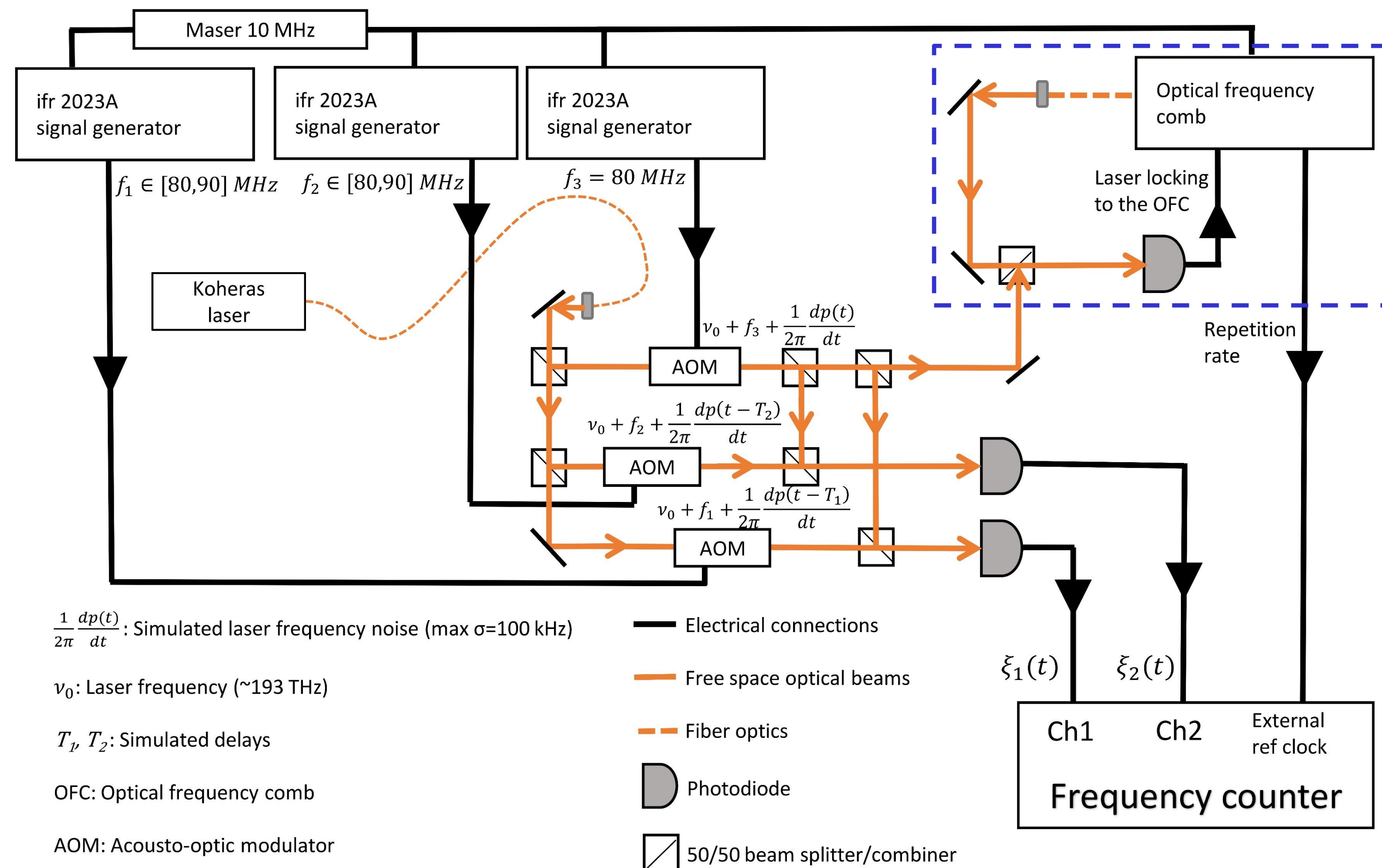


Figure taken from [4]

An optical frequency comb (OFC) is a device capable of generating equally spaced spectral lines in the Fourier domain, which corresponds to a pulse train with a stable repetition rate in the time domain. By beating an external laser to one of the comb lines, it is possible to lock the OFC to the external laser, enabling a coherent coupling between the external laser frequency and the microwave signal corresponding to the OFC repetition rate. Using a new generation of TDI combination (see Eq. (1) below: $X^{OFC}(t)$ is the post-processed GW signal; ξ_i are phase or frequency measurements) and an updated LISA design (see our experimental setup, a simulated 2-arm "LISA" interferometer), locking the LISA lasers to OFCs would enable to cancel out both the laser frequency noise and clock noise from the GW signal down to the LISA frequency noise requirement.

$$X^{OFC}(t) \equiv [\xi_1(t - 2L_2) - (1 - 2V_2)\xi_1(t)] - [\xi_2(t - 2L_1) - (1 - 2V_1)\xi_2(t)] \quad (1)$$

Experimental setup



$\frac{1}{2\pi} \frac{dp(t)}{dt}$: Simulated laser frequency noise (max $\sigma=100$ kHz)

ν_0 : Laser frequency (~ 193 THz)

T_1, T_2 : Simulated delays

OFC: Optical frequency comb

AOM: Acousto-optic modulator

— Electrical connections

— Free space optical beams

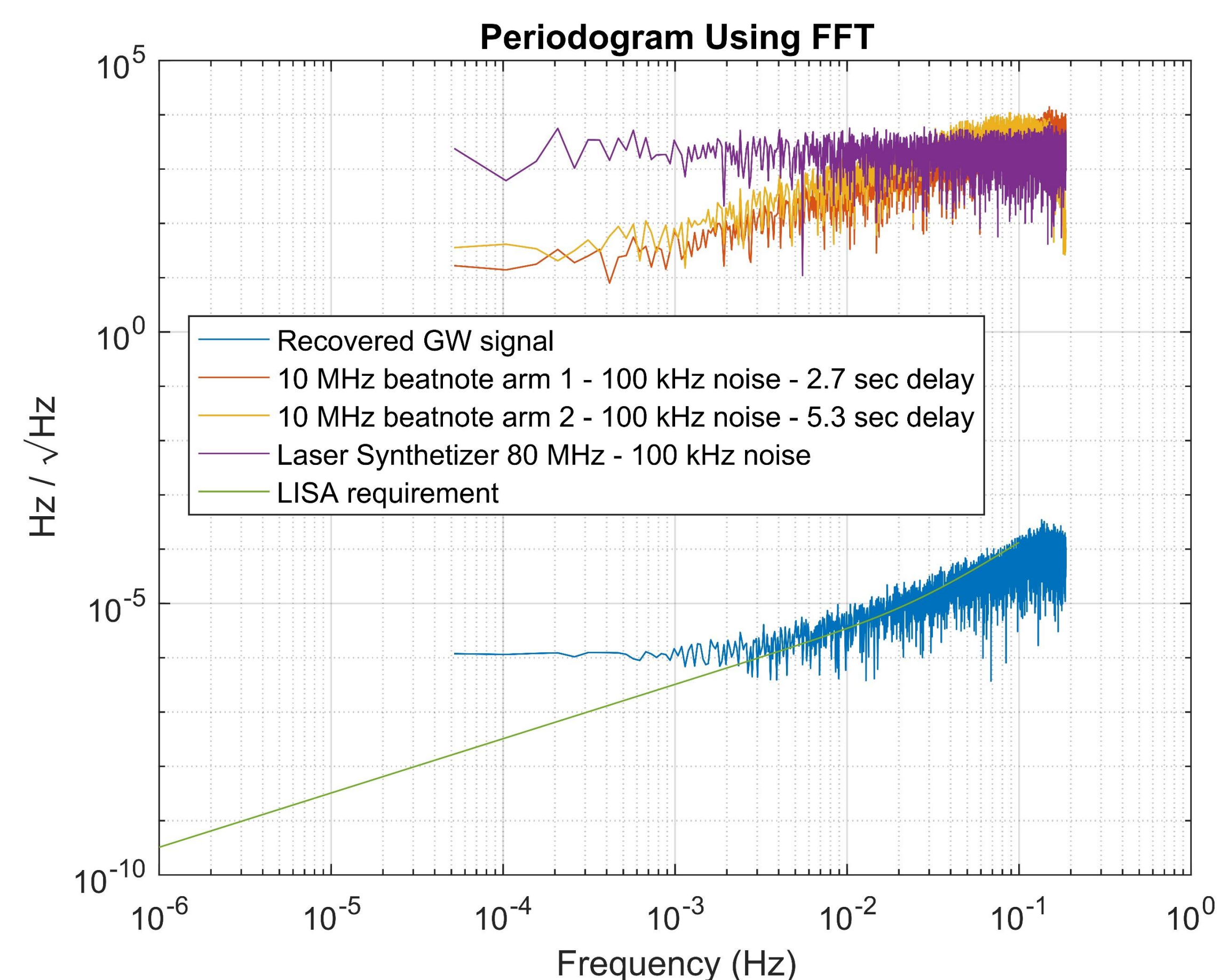
— Fiber optics

— Photodiode

— 50/50 beam splitter/combiner

In order to experimentally demonstrate the noise suppression with a compact setup, we use signal generators and acousto-optic modulators (AOM) to simulate Doppler frequency shifts ($f_1 - f_3$ and $f_2 - f_3$), laser frequency noise ($\frac{1}{2\pi} \frac{dp(t)}{dt}$), and arm length difference (T_1, T_2). The experimental bench (signal generators and frequency counter) is controlled by a computer using Python.

Preliminary results



So far we have experimentally demonstrated the cancellation of simulated laser frequency noise using the setup above, excluding the OFC (see blue curve "Recovered GW signal"). The frequency counter reference signal was directly provided by the maser. The noise floor shown by the blue curve is driven by the noise performance of the frequency counter.

Further measurements involving the optical frequency comb will show the suppression of both the simulated laser frequency noise and frequency counter clock noise.

References

- [1] Massimo Tinto and Nan Yu, *Time-delay interferometry with optical frequency comb*, Phys. Rev. D 92, 042002 (2015)
- [2] Massimo Tinto and Sanjeev V. Dhurandhar, *Time-delay Interferometry*, Livin Rev. Relativity, 17, 6 (2014)
- [3] Glenn de Vine et al., *Experimental Demonstration of Time-Delay Interferometry for the Laser Interferometer Space Antenna*, Phys. Rev. Lett. 104, 211103 (2010)
- [4] Jungwon Kim and Youjian Song, *Ultralow-noise mode-locked fiber lasers and frequency combs: principles, status, and applications*, Adv. Opt. Photon. 8, 465-540 (2016)

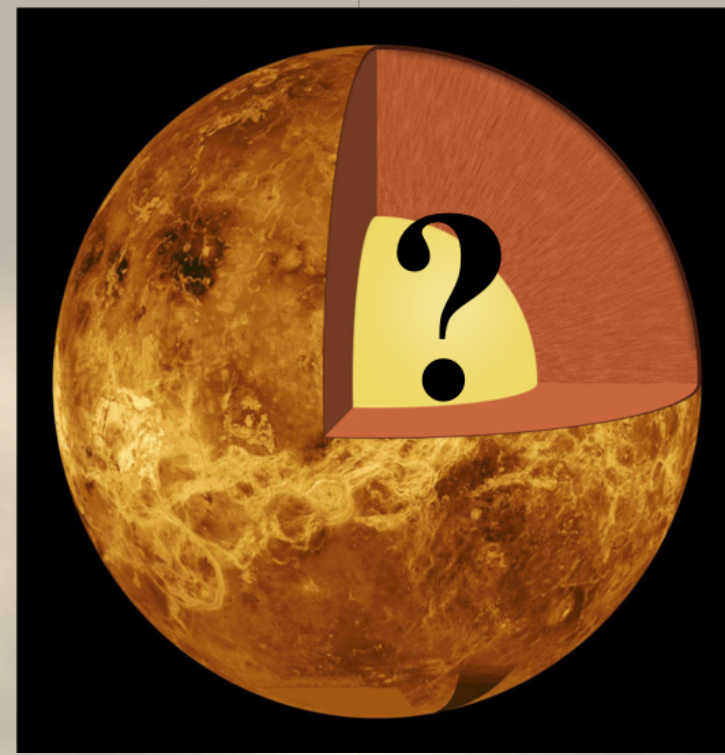
Balloon-Based Seismology for Venus Exploration

Author: Siddharth Krishnamoorthy (335)

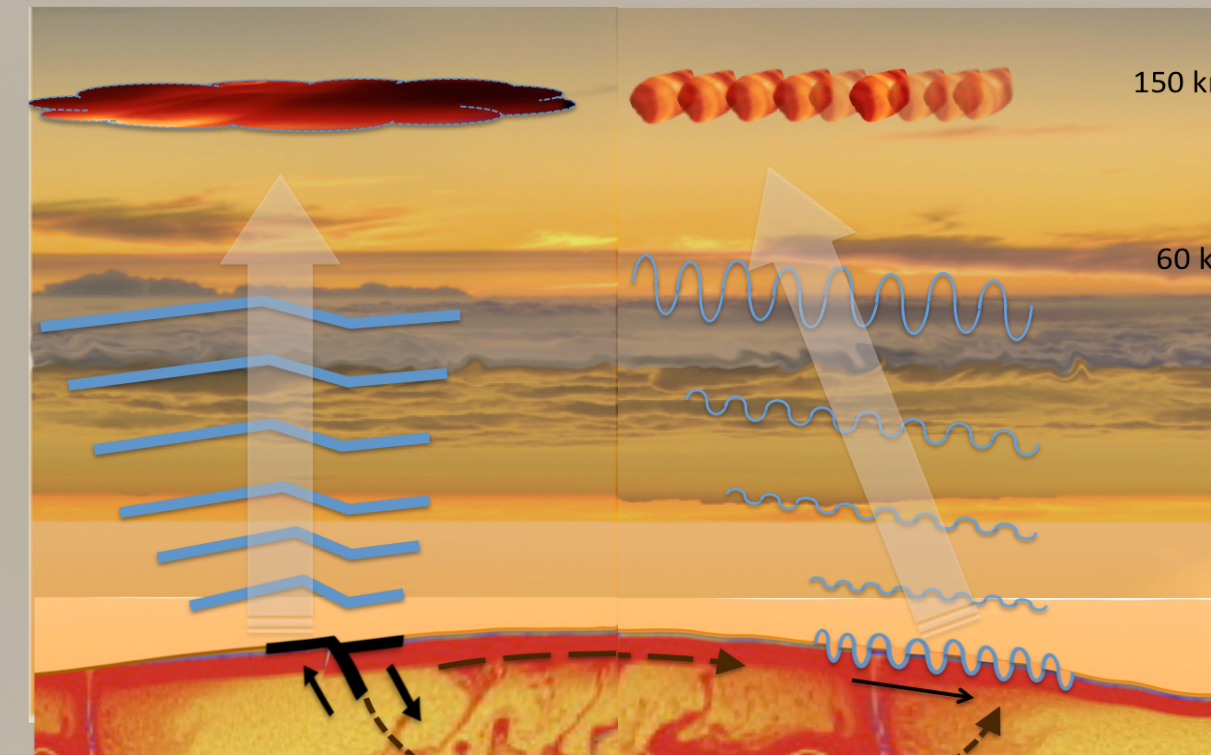
Attila Komjathy (335), Michael T. Pauken (353), and James A. Cutts (4300)

Introduction

The evolution and interior structure of Venus remain uncertain despite half a century of exploration. This is in large part due to the absence of seismological investigations, which have yielded much of the information about Earth's interior. **Extreme surface temperature (>460 C) and pressure (>90 atmospheres) result in extremely limited lifetimes for Venus surface missions, which prohibits traditional seismology.**



Venus' thick atmosphere allows for the efficient coupling of seismic waves between the solid planet and its atmosphere resulting in **low-frequency pressure waves, also known as infrasound**. Infrasound travels relatively unattenuated for large distances and may be used to study seismic activity on Venus without needing to land on it. Infrasound barometers may be deployed on balloons floating at 55-60 km altitude on Venus, where the temperature and pressure are much more benign and longer mission lifetimes can be guaranteed.



Cutts et al., 2015

Challenges with Performing Balloon-Based Seismology

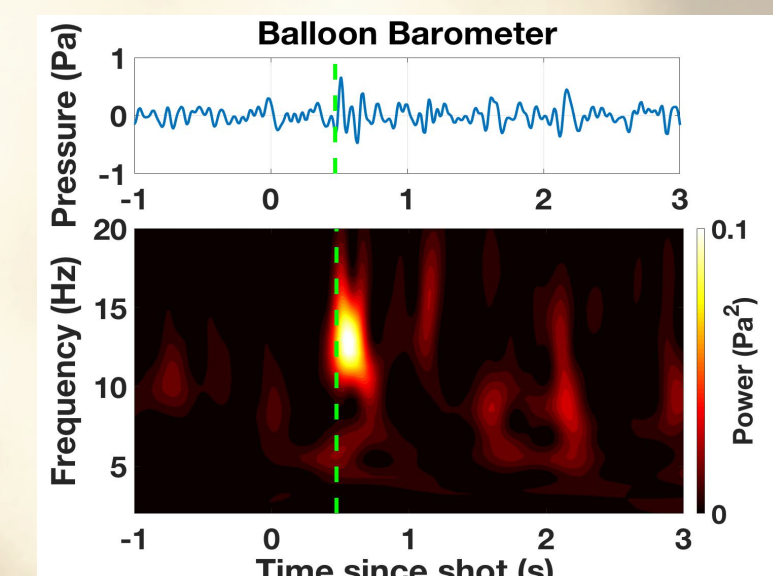
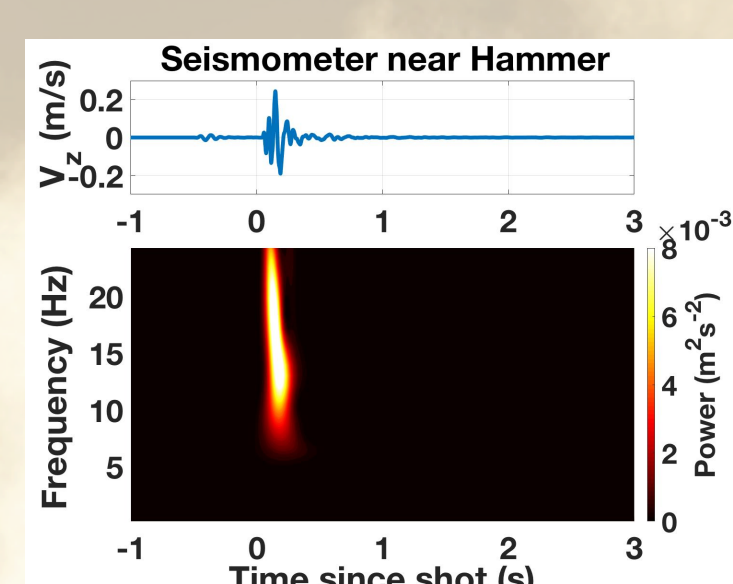
While mission lifetimes are long in Venus' upper atmosphere, there are major challenges associated with balloon-based seismology:

- Detection and geolocation of low-amplitude seismic infrasound signal for generating maps of seismic activity
- Determination of the infrasound noise background and classification of infrasound from different geophysical sources (such as quakes, volcanoes, lightning etc.)
- Sensor miniaturization and reduction of data volume so that the sensor can be accommodated on a balloon and deployed easily

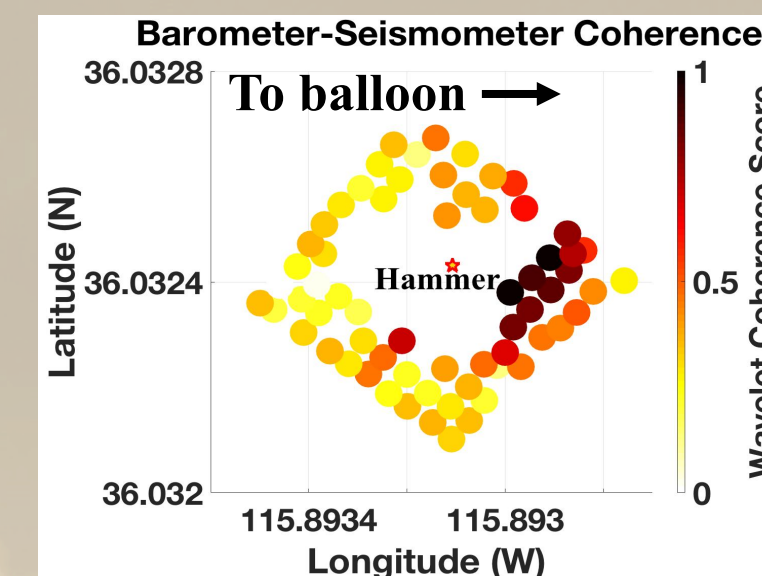
Since 2014, we have been conducting an Earth-based campaign to address these challenges and infuse infrasonic remote sensing technology into a balloon-based Venus exploration mission. Our team at JPL has led experimental campaigns to develop infrasound technology, while our international partners are focusing on Venus atmosphere and signal propagation modeling.

Mapping of Seismic Activity

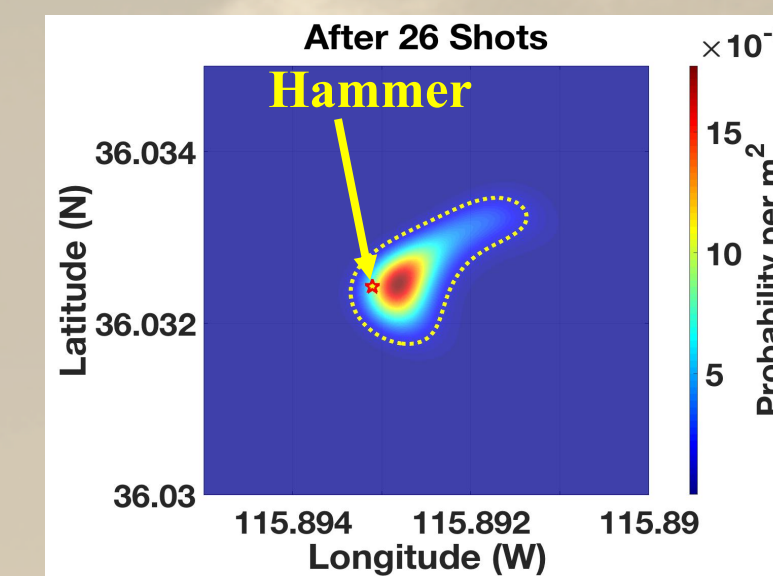
In June 2017, we generated artificial seismic signals by **striking the ground highly repeatedly with a seismic hammer** in Pahrump, NV and recorded the resulting signature using **an array of seismometers on the ground and two barometers on a tethered balloon** 300m above.



Infrasound from ground motion was detected by the balloon-borne barometers. The spectral signature of the acoustic signal seen by the barometer is similar to the ground motion signal seen by the seismometer near the hammer



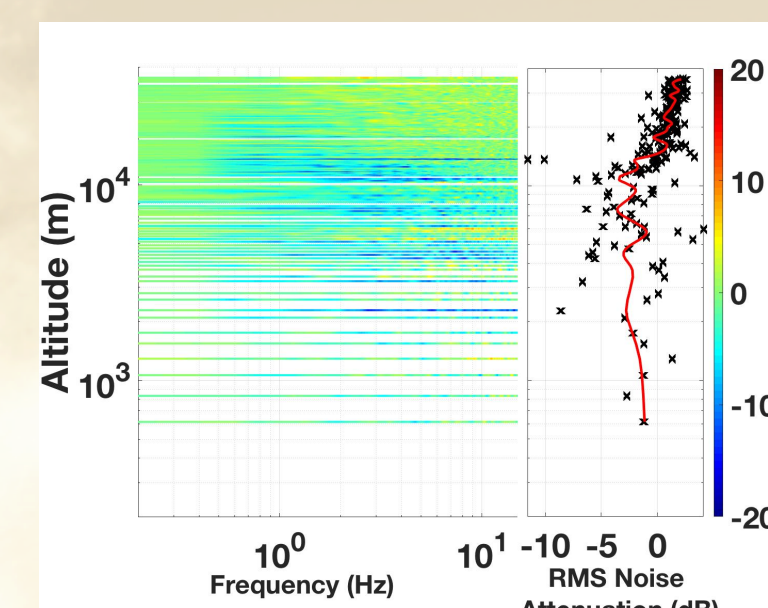
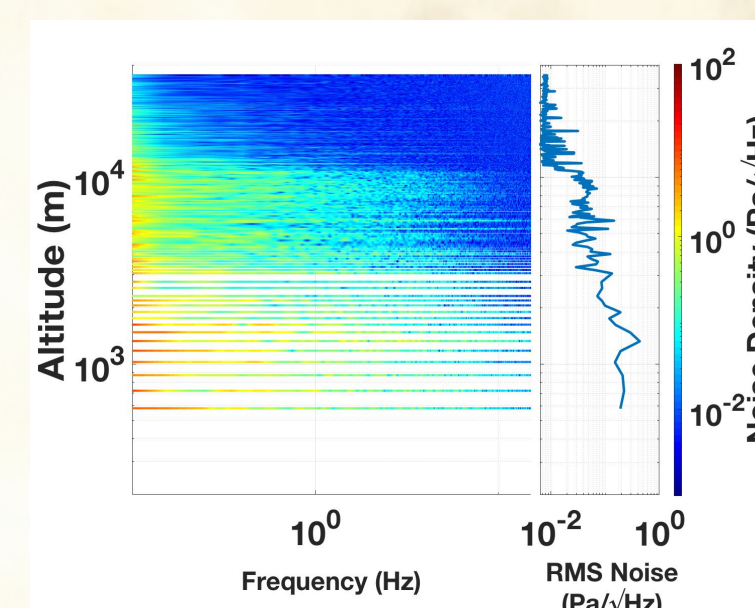
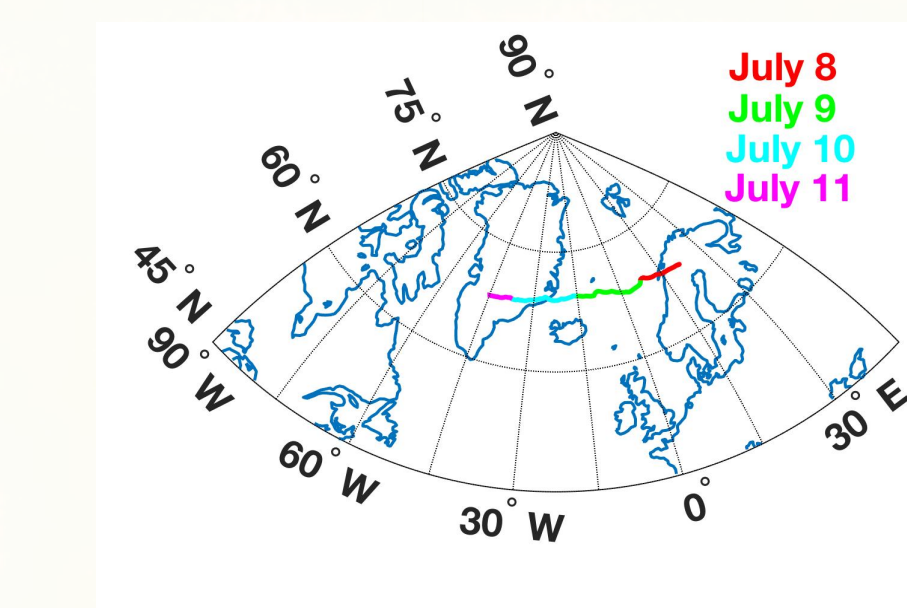
Higher barometer-seismometer wavelet coherence is seen with seismometers in the direction of the balloon than those facing away showing that the acoustic signature also replicates the non-isotropic nature of ground motion near the hammer.



Using multiple shots and time of flight measurements between the two barometers, the seismic hammer (shown by the yellow star) was geolocated. The dotted yellow line in the plot above shows the contour with 90% probability of containing the hammer.

Determination of Infrasound Noise Background

Our Payload for Infrasound Measurement in the Arctic (PIMA) flew on a NASA Long-Duration Balloon from Sweden to Canada in July 2018 and made infrasound background measurements from the lower troposphere to the stratosphere. One of the two infrasound packages in the payload was equipped with a wind noise mitigation system to test its efficacy in the low-density stratospheric environment. Data collection stopped over Greenland on July 11, as shown below.



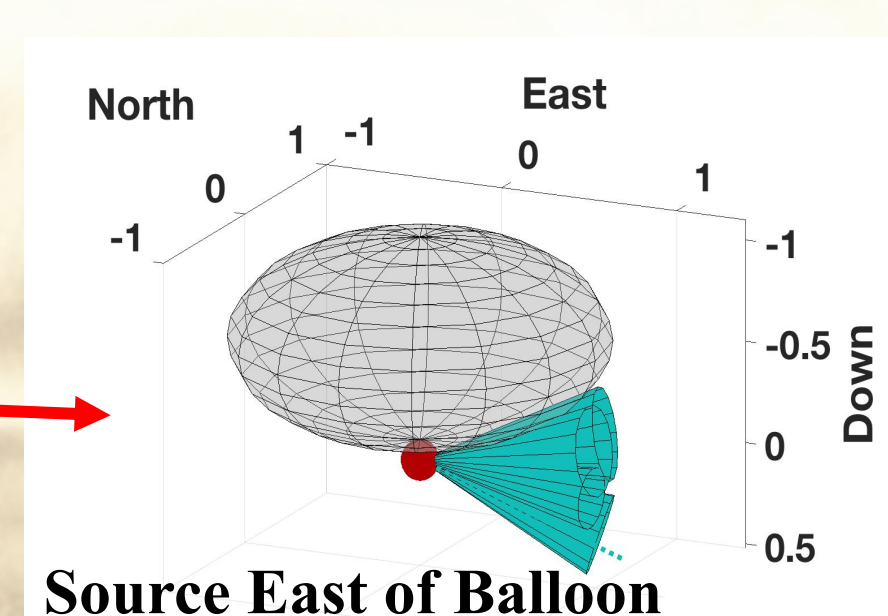
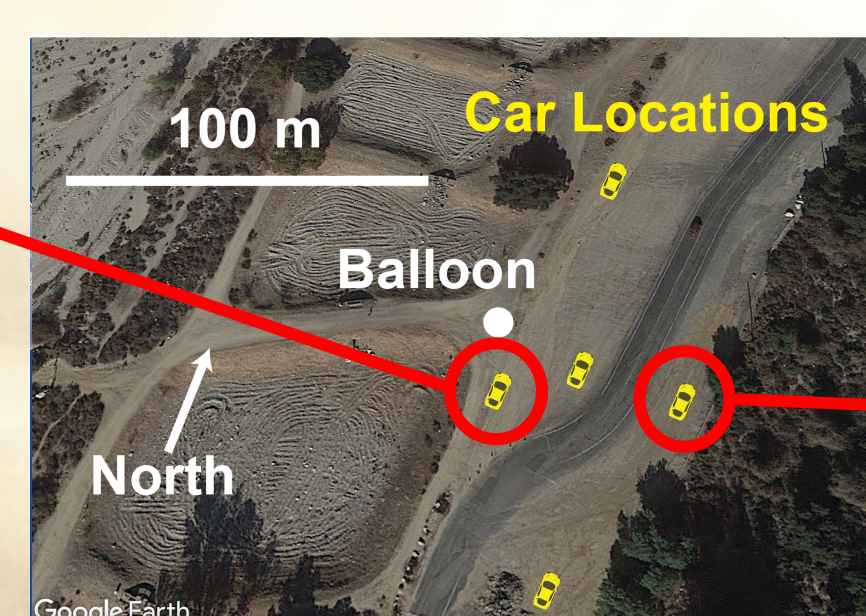
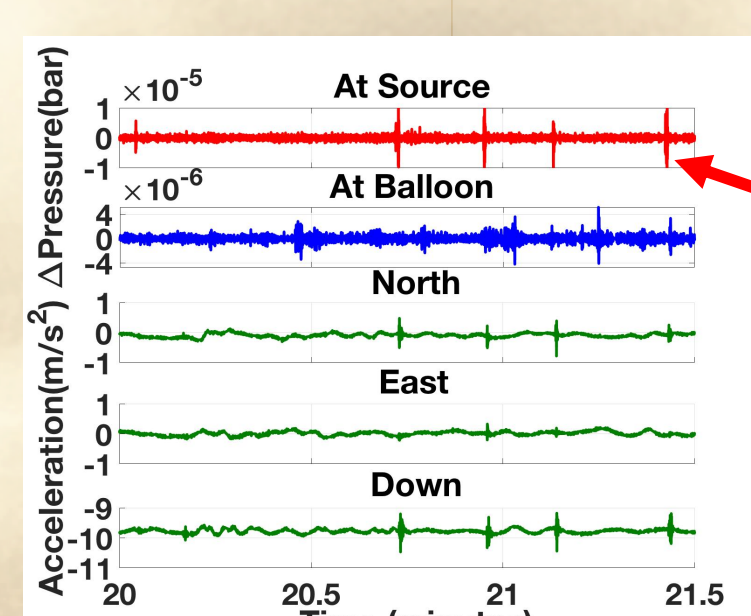
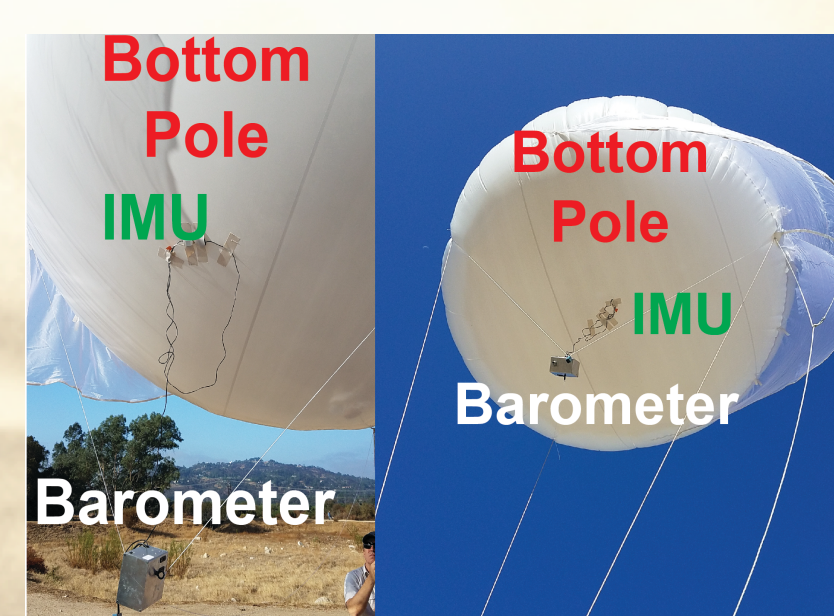
Data taken during the ascent show a **marked drop in background noise at the tropopause at ~10 km**. Venus at 55 km is similar to Earth at 5 km, yielding an RMS atmospheric noise floor of 0.03 Pa/√Hz.

The rightmost plot shows noise attenuation due to the wind noise mitigation system. Bulky hardware **noise mitigation techniques** are effective in the troposphere, but **have no effect in the stratosphere**.

Data are being searched for infrasound signals of opportunity from earthquakes, glacier calving, ocean microbarom, bolides, and auroral activity.

Sensor Miniaturization

Pressure is a scalar and large arrays are needed to perform source geolocation using time of flight. We completed the first demonstration of the **“vector infrasound” instrument concept** in the Arroyo Seco – by measuring a neutrally buoyant balloon's acceleration (a vector) in response to an infrasound pressure wave using a high-precision Inertial Measurement Unit (IMU) along with the pressure, a single station can determine the direction and magnitude of an incoming infrasound wave, circumventing the need for large balloon-borne arrays., greatly miniaturizing the infrastructure needed for balloon-based infrasound seismology.



The balloon was made neutrally buoyant by hanging ballast to cancel the free lift. Infrasound was generated by slamming a car door, seen as spikes in the “at source” pressure signal. The pressure signal from the barometer and the local North, East, and Down components of balloon acceleration from the IMU was combined using a singular value decomposition (SVD) based method to generate a direction estimate for the source. Green cones in the rightmost figure indicate the source direction inverted from data. **The correct octant of the source as seen from the balloon was recovered 75% of the time.** We plan to further develop this instrument by flying neutrally buoyant balloons at 5 km altitude on Earth (equivalent of 55 km on Venus) and generating infrasound from surface chemical explosions.

Key Takeaways

- Venus' surface is too hot for electronics to last long enough to study its seismicity. However, seismic events create pressure disturbances that can be measured from balloons floating in a cooler environment in Venus' upper atmosphere.
- We can begin to unlock the secrets of Venus' interior by producing seismic activity maps without needing to land on it.
- Balloon-based infrasound seismology has unique challenges, such as a moving measurement platform, difficulties in discriminating different geophysical signals, and limitations on sensor infrastructure.
- We are addressing these challenges by combining long-duration flight experiments to measure Earth's infrasound background from a balloon and innovative Earth-based infrasound experiments with theoretical and numerical studies of infrasound propagation.

National Aeronautics and Space Administration

Jet Propulsion Laboratory
California Institute of Technology
Pasadena, California

www.nasa.gov

Copyright 2019. All rights reserved.

The authors would like to acknowledge the Strategic R&TD Program at JPL for funding this research.

Background Image Credit: Tibor Balint (NASA JPL/CalTech)

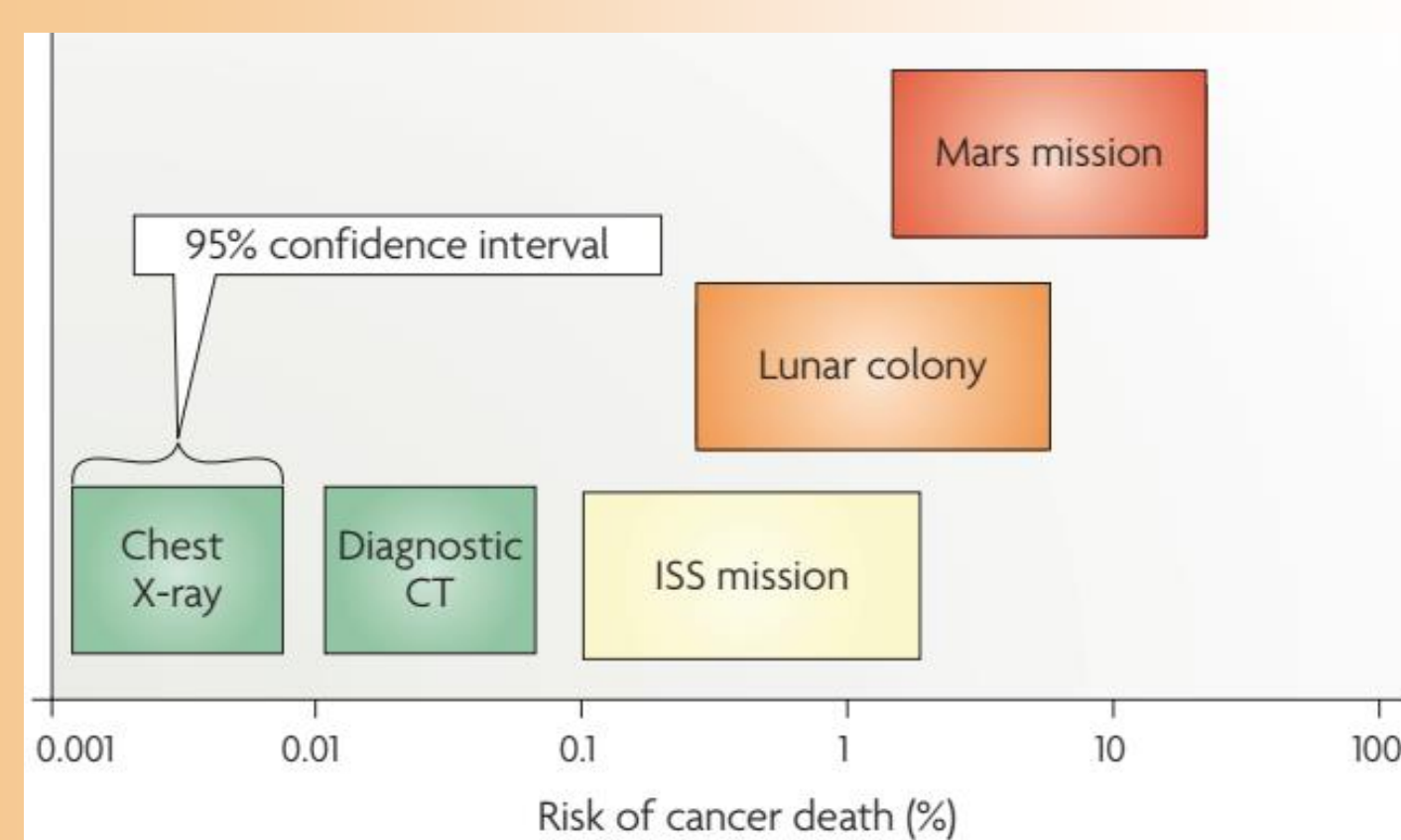
Poster No. T-07

Simulations of Electrostatic Radiation Shielding Configurations

Author: Ashish Goel (389T/347F)

Dragan Nikolic (389T), Stojan Madzunkov (389T), Nikzad Toomarian (3890)

What problem are we trying to solve and why is it important?

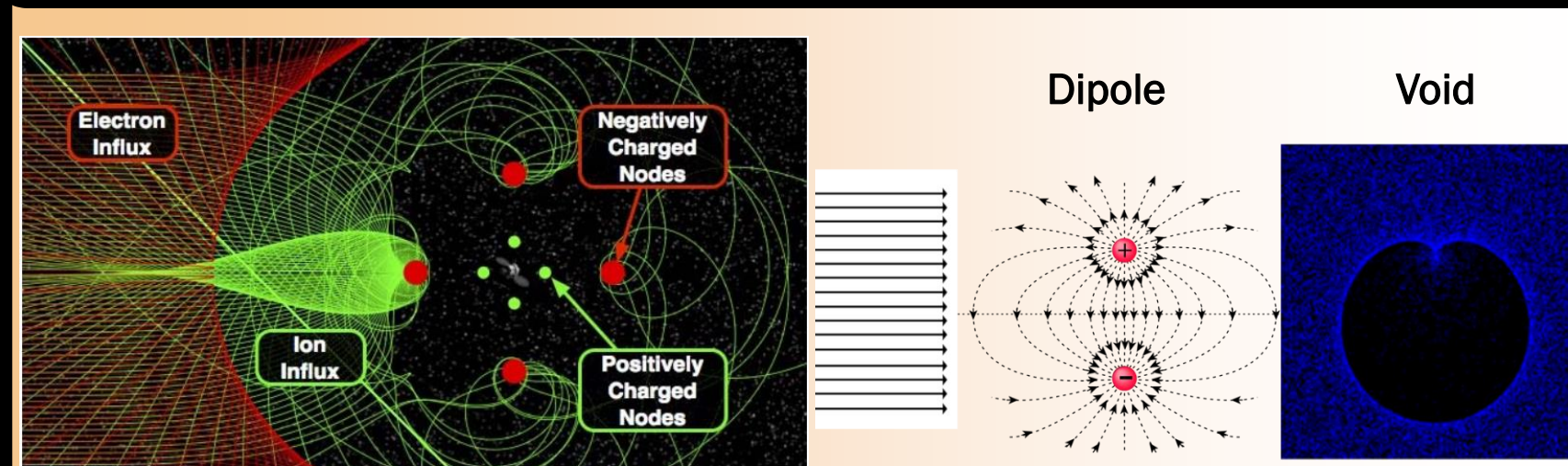


Durante and Cucinotta, Nature Reviews, 2008

- The risk of radiation-induced damage to the health of astronauts and spacecraft electronics is a major challenge to NASA's ambitions for space exploration
- Passive shielding solutions are heavy ✗
- Magnetic shielding solutions require large, cryogenically-cooled superconductors ✗

TL; DR: We need novel solutions for shielding astronauts and electronics from space radiation.

What is the fundamental idea behind using electrostatic fields for radiation shielding?



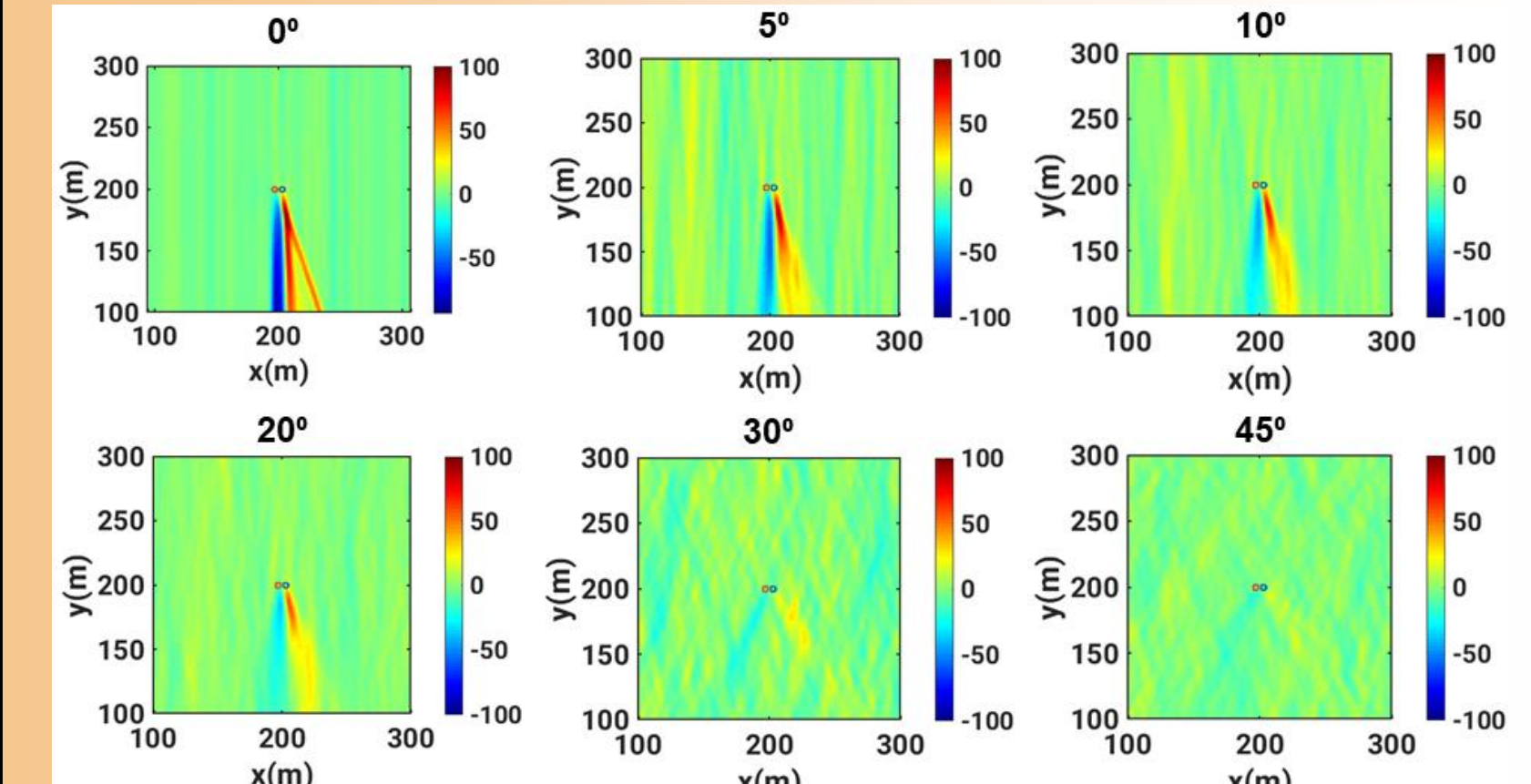
Artistic concept, Tripathi et al., NIAC 2011

- If we place an electric dipole in the path of incoming particles, the electric field deflects particles away from the crew volume, creating a void in its wake
- As the energy of the particles increases, we can produce a void of the same size by moving the dipole farther from the crew volume

TL; DR: The lever-arm effect allows us to use electric fields to shield particles with energies several orders of magnitude higher than the applied voltage

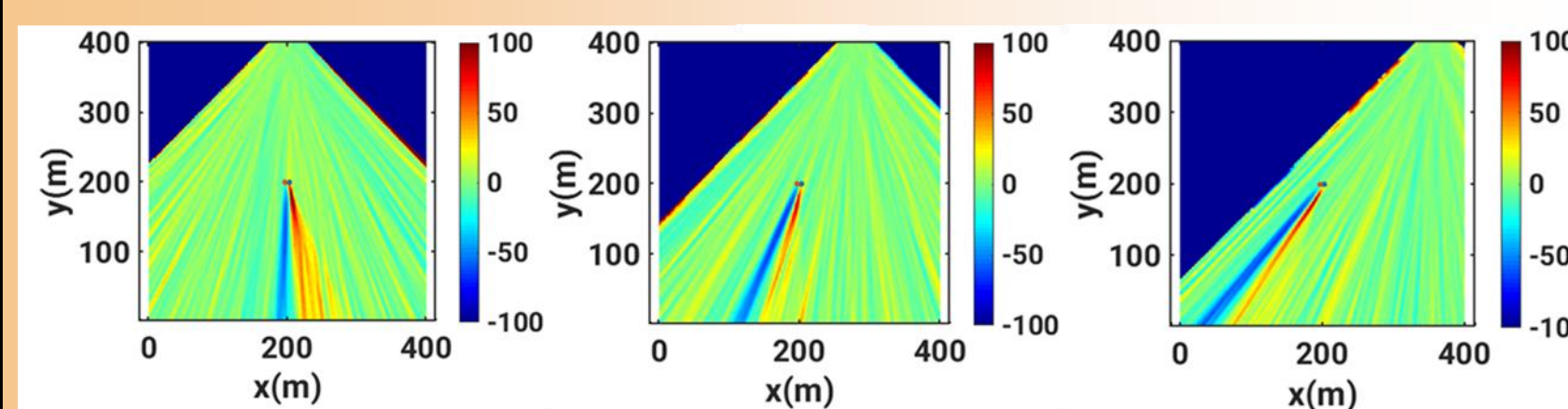
Why is it difficult to extend the fundamental idea into realistic 2D and 3D scenarios?

10 MeV protons, 1 MV potential, Sphere radius = 5 m, results are scale invariant



With one dipole, void fades away when transitioning from 1D to 2D

If we increase the range of angles over which the particles are incident, we see that the void (blue region) becomes weaker, eventually fading away.



Void moves as source moves

- To understand this better, we restrict the section of the top wall from which the particles originate
- A void is created in each of these cases but as the source region shifts, the void shifts too.
- When the particles are incident from all regions simultaneously, the enhancement region (red) from one zone cancels out the void from the neighboring region, with no net flux reduction

- For every particle deflected away from the crew volume, a particle that was going to miss the crew volume gets sucked in
- Need to look at multiple dipole configurations

How do we look for electrode configurations that reduce the radiation flux?

- SIMION simulation approach

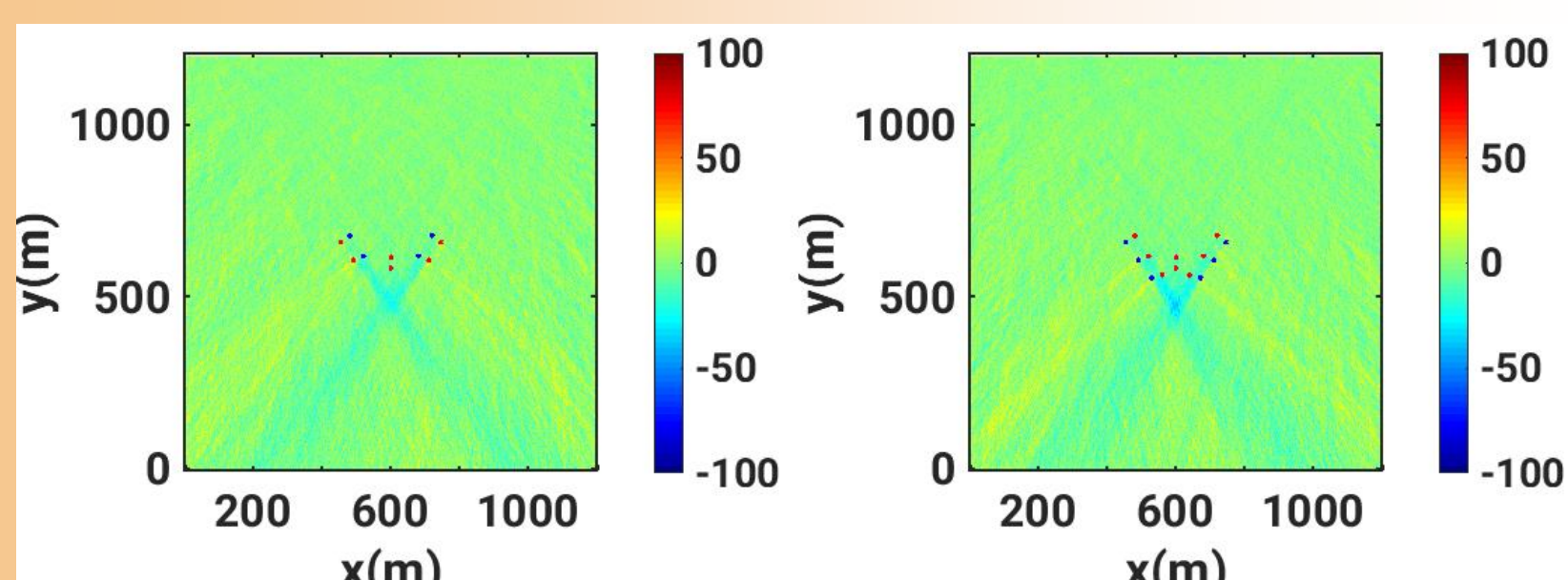
Create the electrode geometry

Solve the Laplace equation to obtain potential and electric field distribution

Define properties of source particles (mass, charge, energy) and their starting locations

Simulate their trajectories and calculate flux distribution

- We first study the sensitivity of shielding efficacy to the size of the spheres and separation between the spheres
- We then fix the position of the central dipole and vary the location of the second dipole until the voids of the two dipoles coincide
- Specifically, we choose configurations where the voids coincide along the y-axis so that the common void remains when the geometry is eventually replicated in 3D

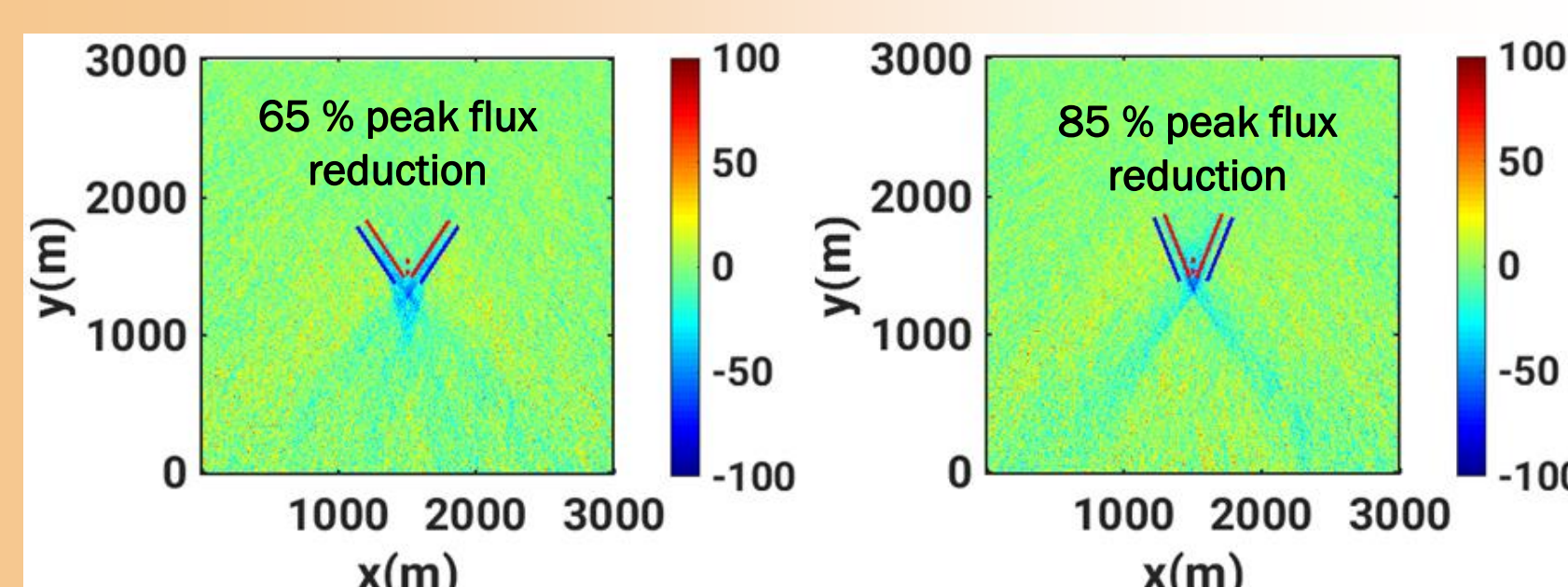


Multiple dipole configurations showing flux reduction in 2D

TL; DR: We optimize the parameters of the dipole and vary their locations until we get the voids from multiple dipoles to overlap

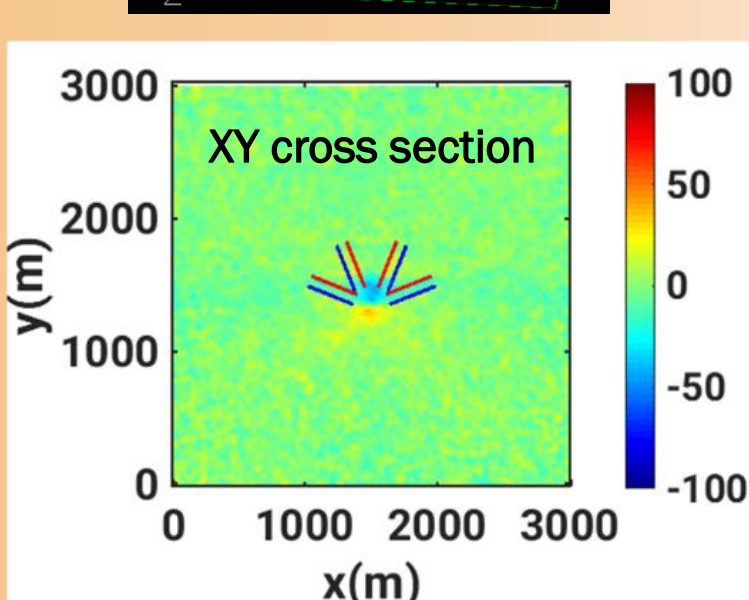
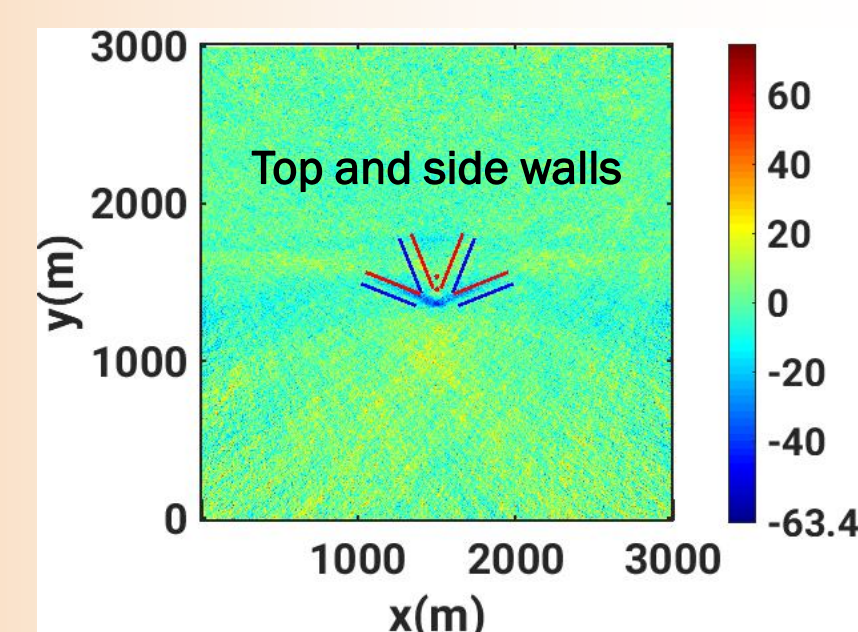
What results do we obtain from the optimized, multi-electrode configurations?

- Replace the string of electrodes with electrostatic rods
- By changing the angle, we can get
 - lower flux reduction (65%) over larger volume
 - higher flux reduction (85%) over smaller volume



Changing angle changes size and intensity of void region

We then shoot particles from the side walls in addition to the top wall, to replicate the scenario on a planetary surface. We add more electrostatic rods to get a peak flux reduction of 63.5%



Extension to 3D

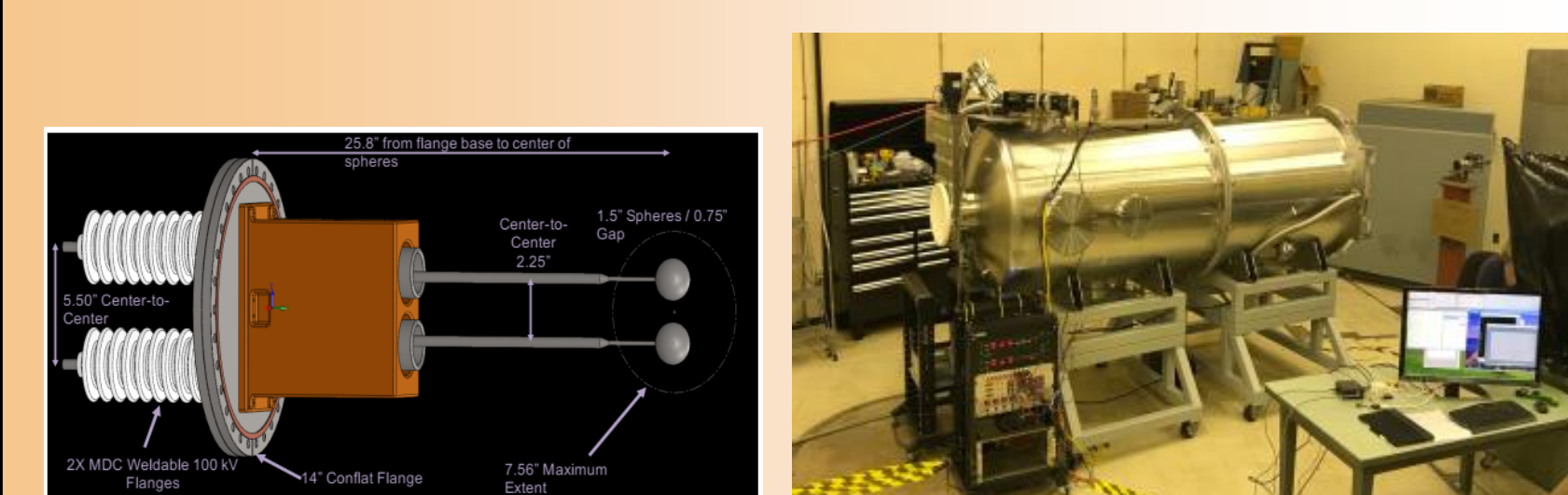
Two ways of extending these geometries to 3D

- Replicate 2D geometry in multiple planes
 - Generate a surface of revolution (cones) from the 2D geometry
- Preliminary results show significant but weaker flux reduction in 3D

TL; DR: We get a peak flux reduction of 63.5 % in 2D

What is the significance of these results and what are the next steps?

- We have shown through numerical simulations that electrostatic shielding can significantly reduce the radiation flux
- These results guide the design of electrode configurations for beam-line experiments scheduled to be carried out at the Brookhaven National Laboratory



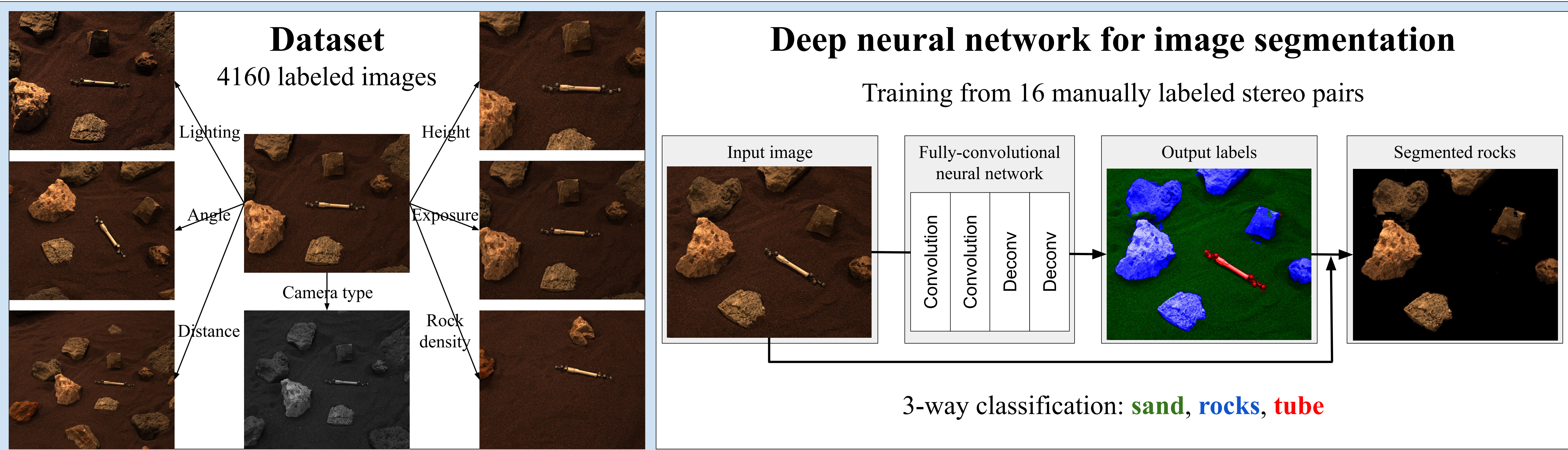
- They also highlight key areas for future research
 - Mathematical optimization of electrode configurations using faster numerical solvers
 - Power supplies capable of producing voltages an order of magnitude greater than current state of the art
 - Novel solutions for avoiding large currents due to the background solar wind plasma

Rover Localization for Mars Sample Return Tube Pickup

Tu-Hoa Pham (347J), Will Seto (347N), Shreyansh Daftry (347J), Alex Brinkman (347G), John Mayo (347M), Yang Cheng (347P), Eric Kulczycki (347C), Renaud Detry (347J)

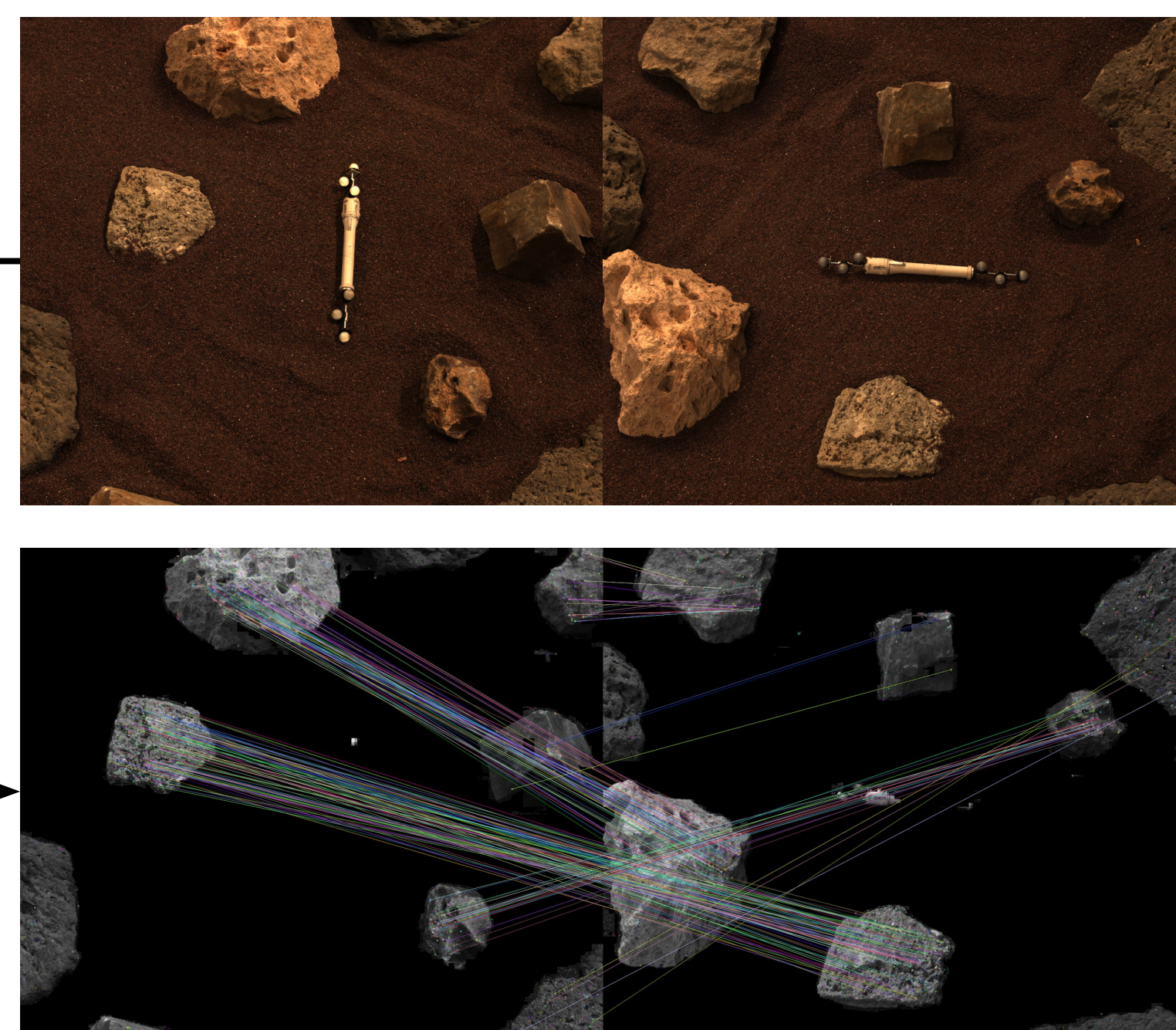
Context: Mars 2020 will collect samples to be stored and left in metal tubes for possible retrieval and return to Earth by a future mission. We study the problem of tube localization and tube pickup.

Challenge: Over years, the sample tubes may get covered in dust and sand, making direct tube observation difficult. Instead, we propose to localize the robot with respect to its surrounding rocks and a cm-scale Mars 2020 map of the depot including tube locations.

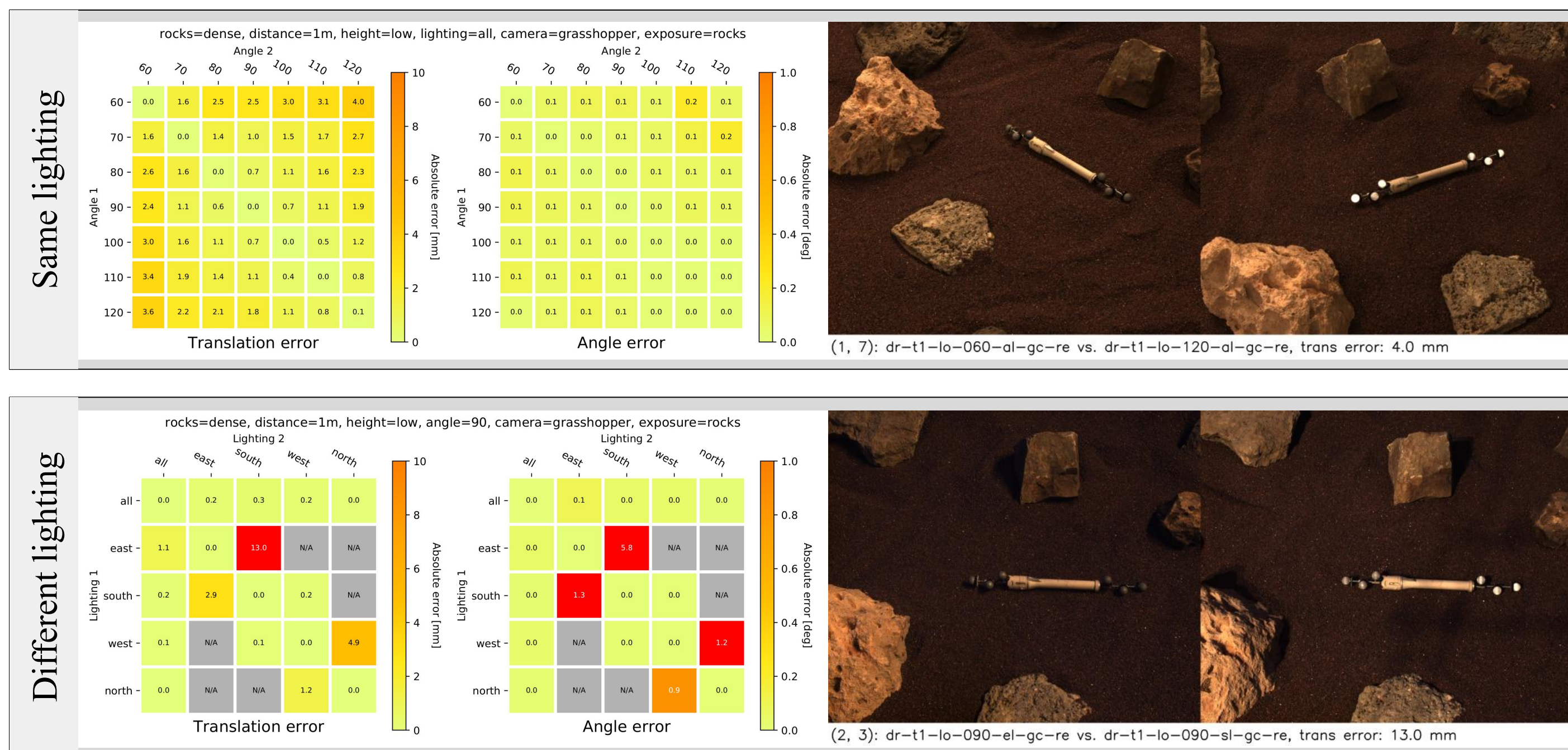


Visual odometry by sparse feature matching

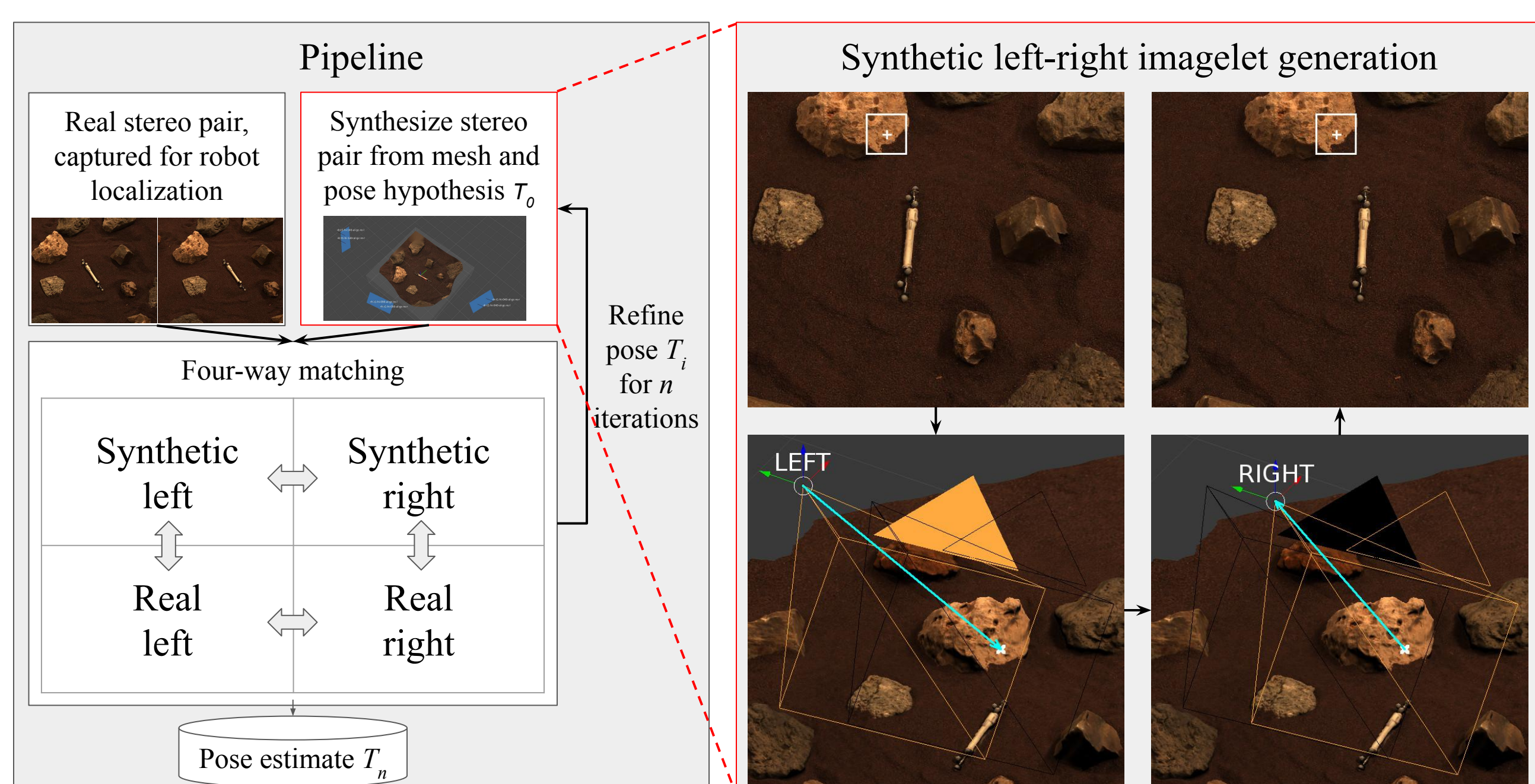
1. Input: two stereo pairs taken from under different conditions
2. Segment out tube and sand: only rely on rocks for localization
3. Compute and match image features (SIFT)
4. Estimate camera motion from matches and project to tube



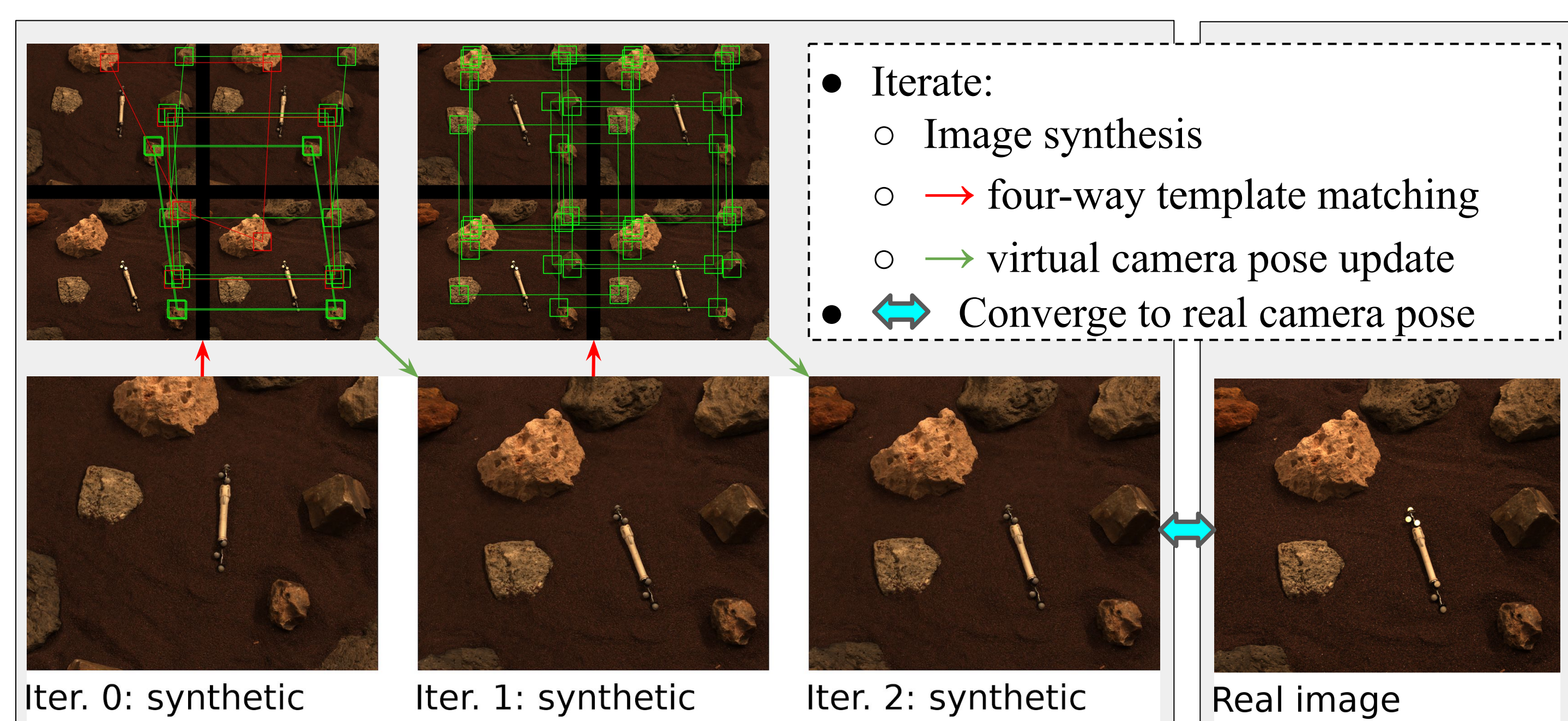
Performance with and without lighting changes



Synthetic imagelet-based pose estimation



Pose estimation by iterative synthesis and matching



Ice screw end effectors for ice climbing and sample collection

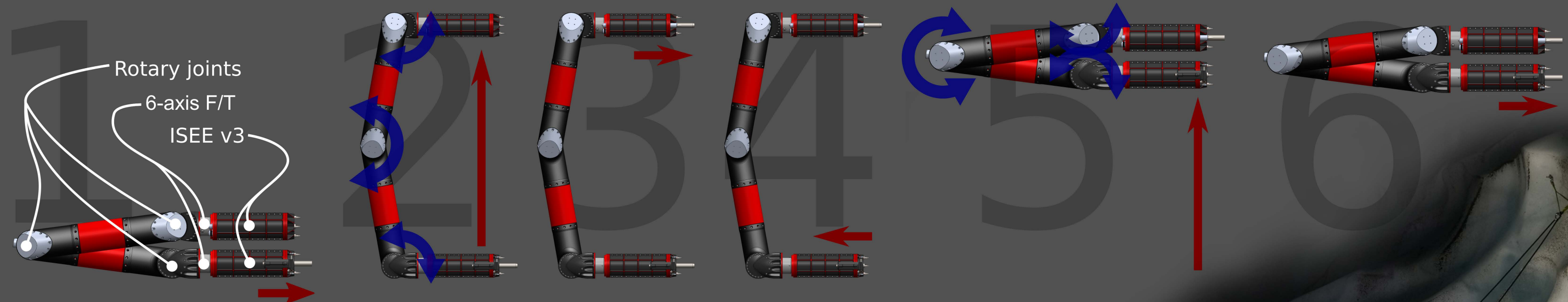
Aaron Curtis and Aaron Parness (347M)

icy terrain mobility

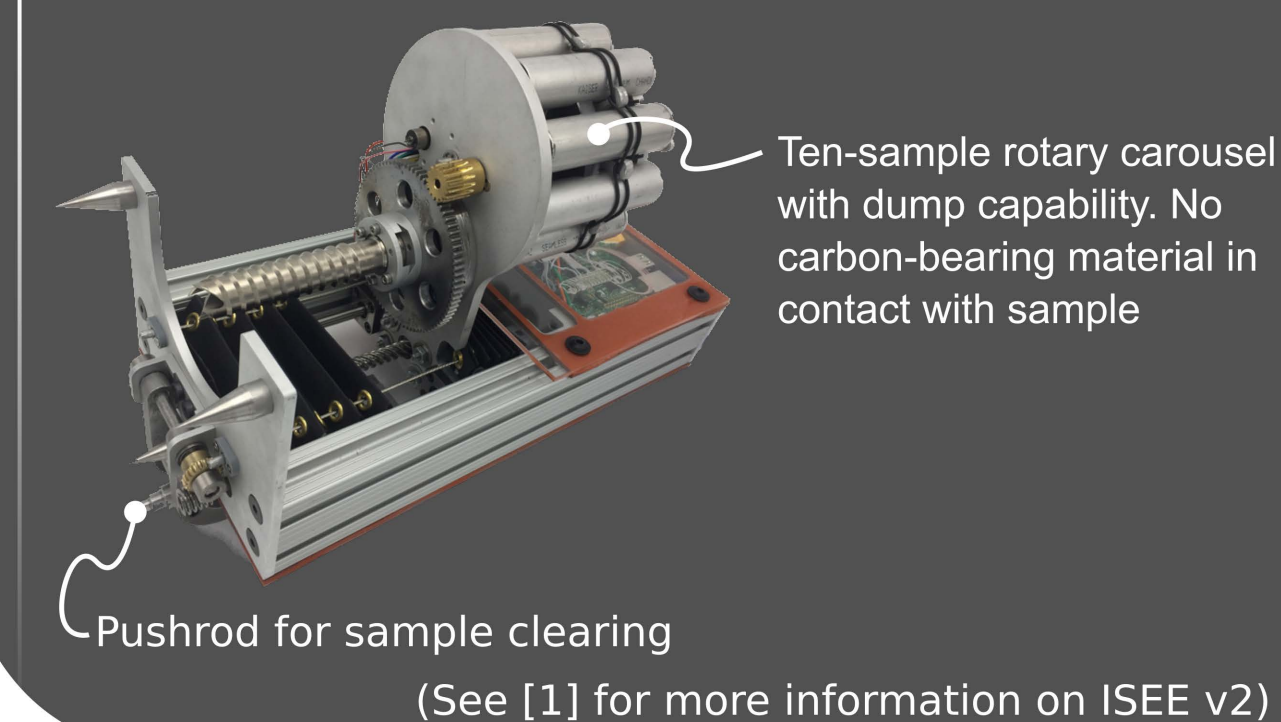
IceWorm allows gravity-agnostic ice mobility. At each step, grippers create a rigid connection to the ice.

This enables movement in low gravity, on slippery ice, or even against fluid flow. Our first prototype, IceWorm Simple, uses hollow ice screws to create that rigid connection.

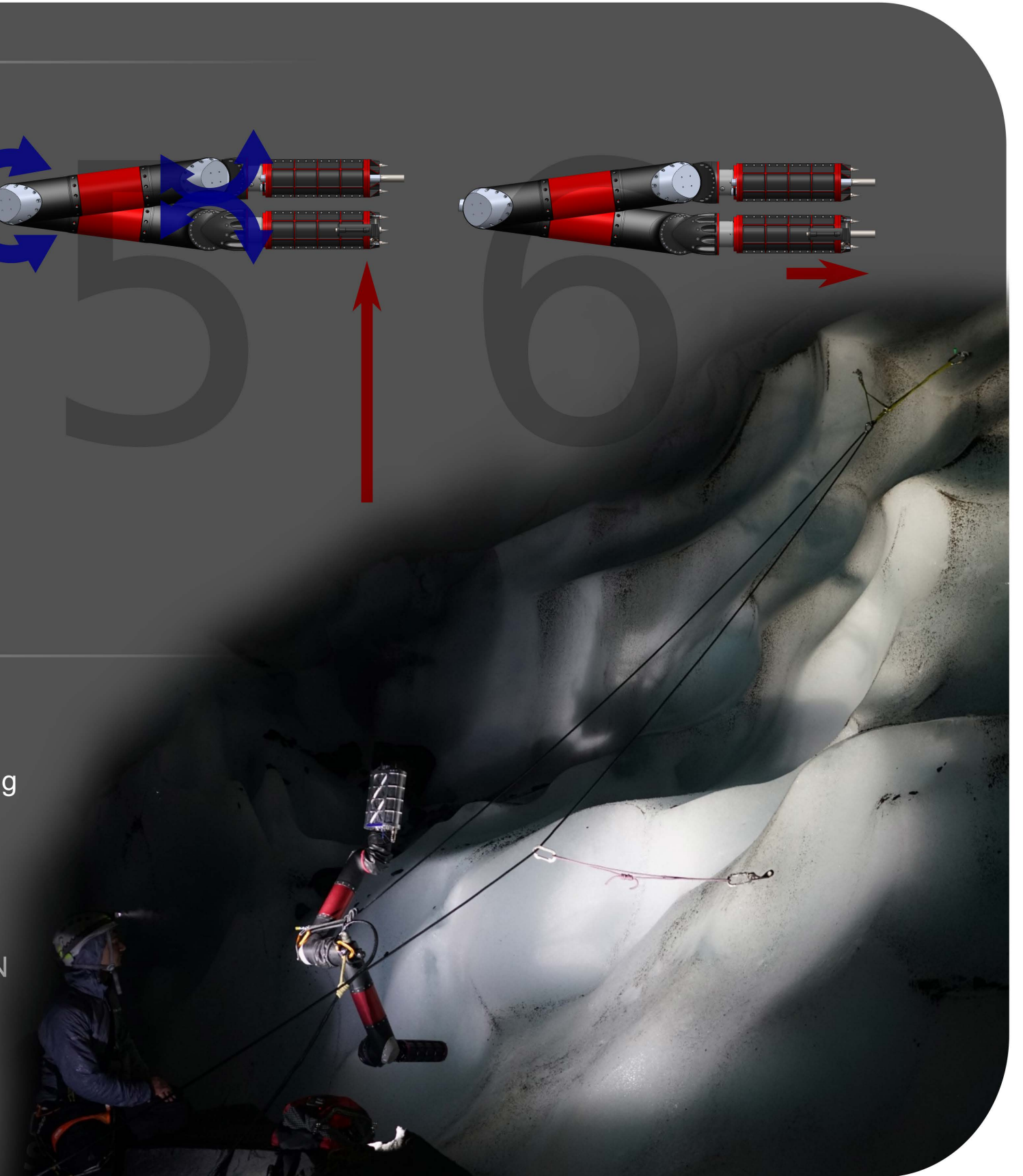
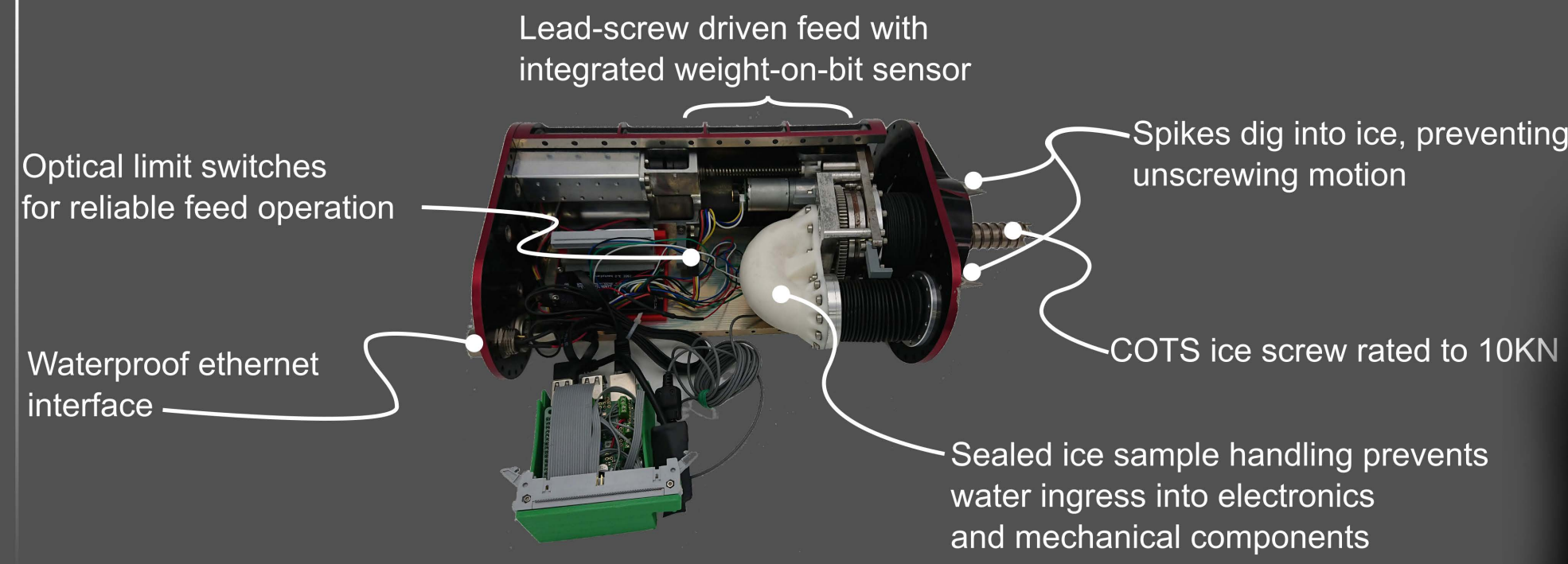
"Inchworm" gait of IceWorm Simple



ISEE v2: Multi-sample caching ice gripper



ISEE v3: Rugged ice gripper



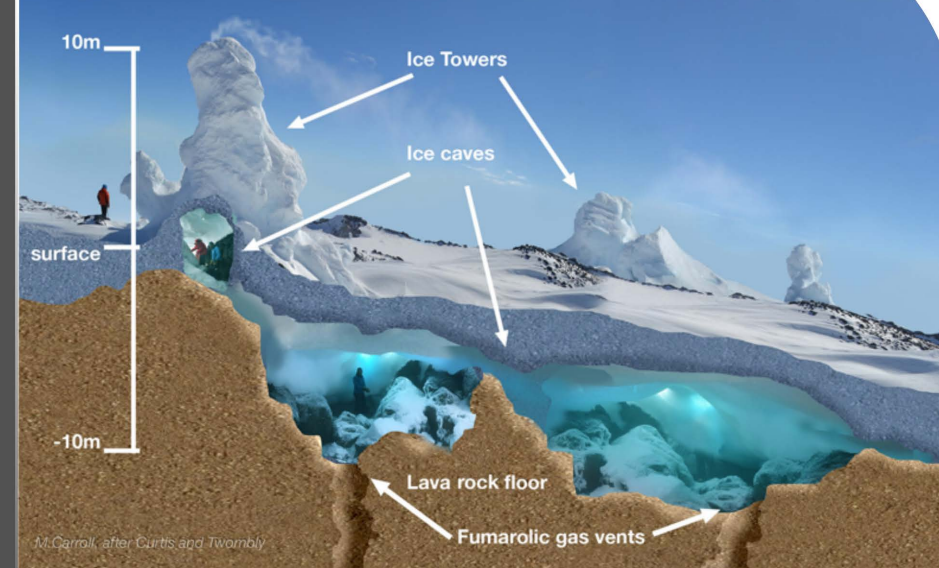
for earth

Fumarolic ice caves (FIC) are the initial science target for IceWorm. Scientific studies require access to FIC to learn crucial information about the state of volcanoes [3] and the origins of life [4]. Human entry into FIC is dangerous due to toxic volcanic gases. Sample collection by ice climbing robot is safer for humans, and also less likely to cause microbiological contamination.

IceWorm in Igloo Cave, Mt. St. Helens



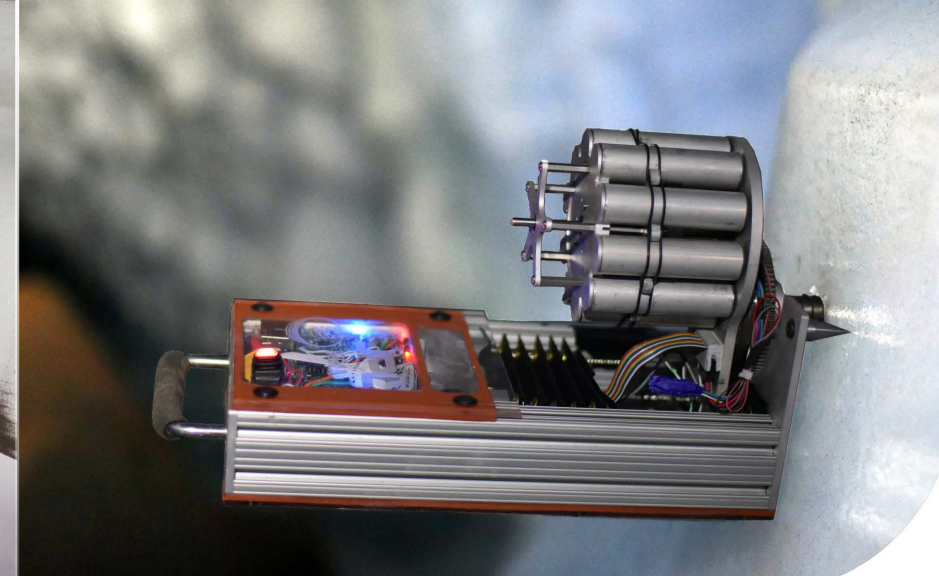
Mt. Erebus FIC (typical)



East Crater Cave, Mt. Rainier



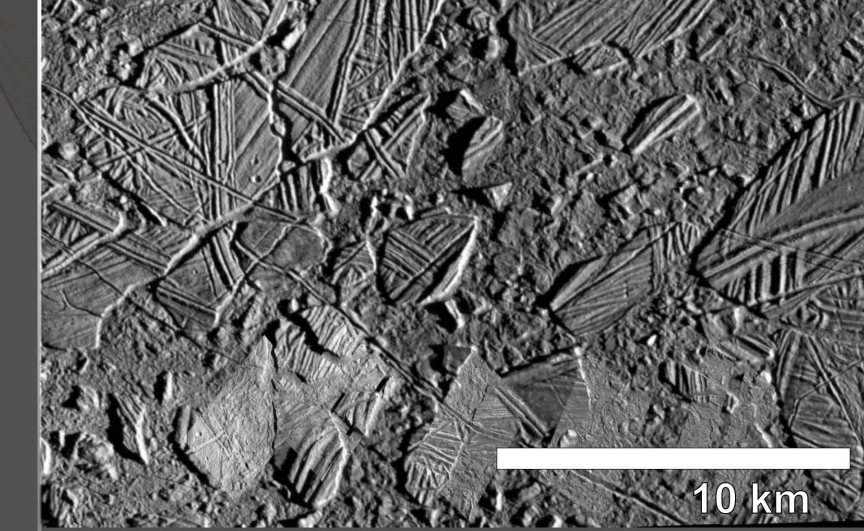
ISEE v2 in East Crater Cave



& planetary science

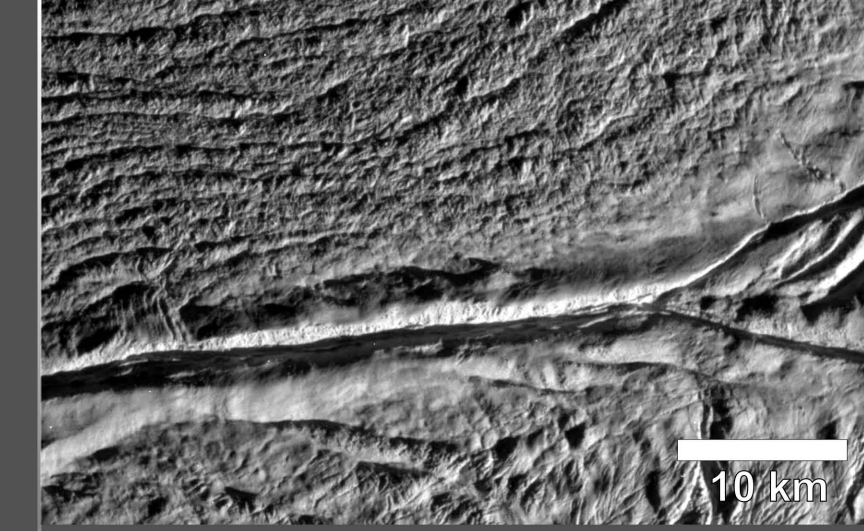
IceWorm technology is intended to be infused into future missions, enabling robotic mobility at places such as:

Europa chaos terrain



Jupiter's moon Europa is the top priority target in NASA's search for life in the solar system. European terrain is universally rugged, and exploring the surface requires a gravity-agnostic robot.

Enceladus tiger stripe vents



Like Europa, Saturn's moon Enceladus is thought to harbor a global ocean, which feeds geysers erupting from its fissured "Tiger Stripe" region. A recent NASA Innovative Advanced Concepts study explored potential methods for accessing the ocean and concluded that sending an ice-screw welding climbing robot down into the fissures would be the best option [4].

Mars North polar cliffs



Spiral cliffs up to ~2km deep cut into Mars' North Polar Layered Deposits reveal stratigraphy thought to date back millions of years [5]. An ice climbing robot could access these layers and investigate Martian climate dynamics.

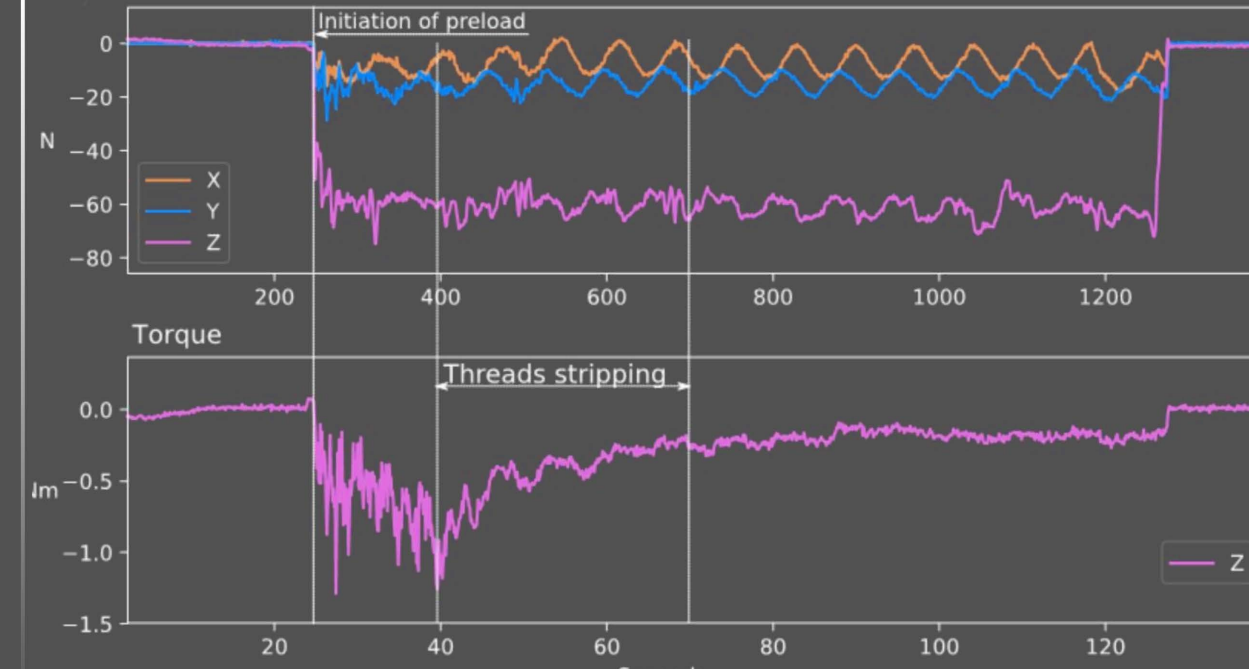
ongoing development

IceWorm Simple is just the first step in the road towards highly capable autonomous ice rovers. We are actively researching and developing:

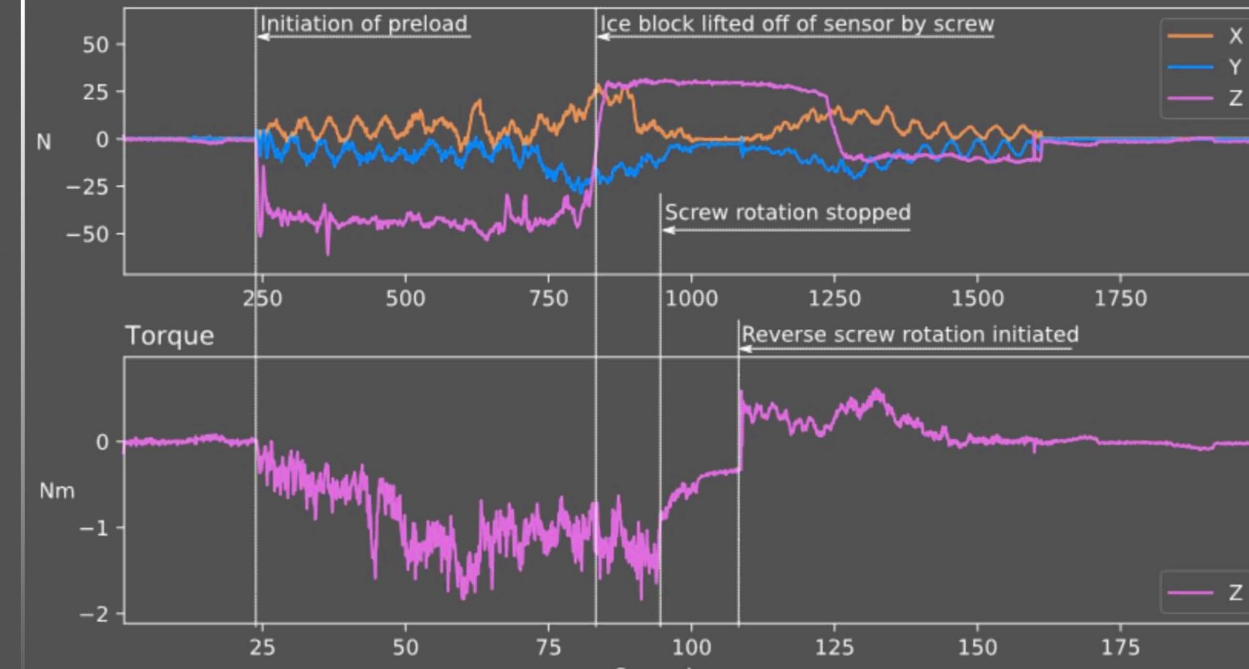
- Systems for ultra cold, high-vacuum conditions
- Autonomy
- Vision / perception systems
- Higher-DOF IceWorm platform kinematics
- Other gripper types, including sublimation-based



Screw insertion failure F/T record



Screw insertion success F/T record



Potential 5-DOF iceWorm gait



Path planning on FIC LiDAR



Work by Ian Rankin

[1] Curtis, A., Martone, M. & Parness, A. Roving on ice: Field testing an Ice Screw End Effector and sample collection tool. in 2018 IEEE Aerospace Conference 1–17 (2018). doi:10.1109/AERO.2018.8396715

[2] Curtis, A. & Kyle, P. Geothermal point sources identified in a fumarolic ice cave on Erebus volcano, Antarctica using fiber optic distributed temperature sensing. Geophys. Res. Lett. 38, L16802 (2011). doi:10.1029/2011GL048272

[3] Tebo, B. M. et al. Microbial communities in dark oligotrophic volcanic ice cave ecosystems of Mt. Erebus, Antarctica. Front. Microbiol. 6, (2015). doi:10.3389/fmicb.2015.00179

[4] Ono, M. et al. Enceladus Vent Explorer Concept in Outer Solar System: Prospective Energy and Material Resources (eds. Badescu, V. & Zacny, K.) 665–717 (Springer International Publishing, 2018). doi:10.1007/978-3-319-73845-1_13

[5] Landis, M. E., Byrne, S., Daubar, I. J., Herkenhoff, K. E. & Dundas, C. M. A revised surface age for the North Polar Layered Deposits of Mars. Geophys. Res. Lett. 43, 3060–3068 (2016). doi:10.1002/2016GL068434

Airships in the Night: Localizing Lighter-Than-Air Vehicles in GPS Denied and Completely Dark Environments

Authors: Robert Hewitt (347T), Matthew Gildner (347C), Jacob Izraelevitz (347C), Donald Ruffatto (347M)

Introduction

Offshore oil tanks are inspected annually for defects to ensure they remain safe to use over their lifetime. They're taken offline for cleaning then ~12 human inspectors inspect the tank over two weeks. Automating this process will reduce cost and improve inspection quality and safety and has been the main objective of the RIOT (Robotic Inspection of Oil Tanks) task at JPL.

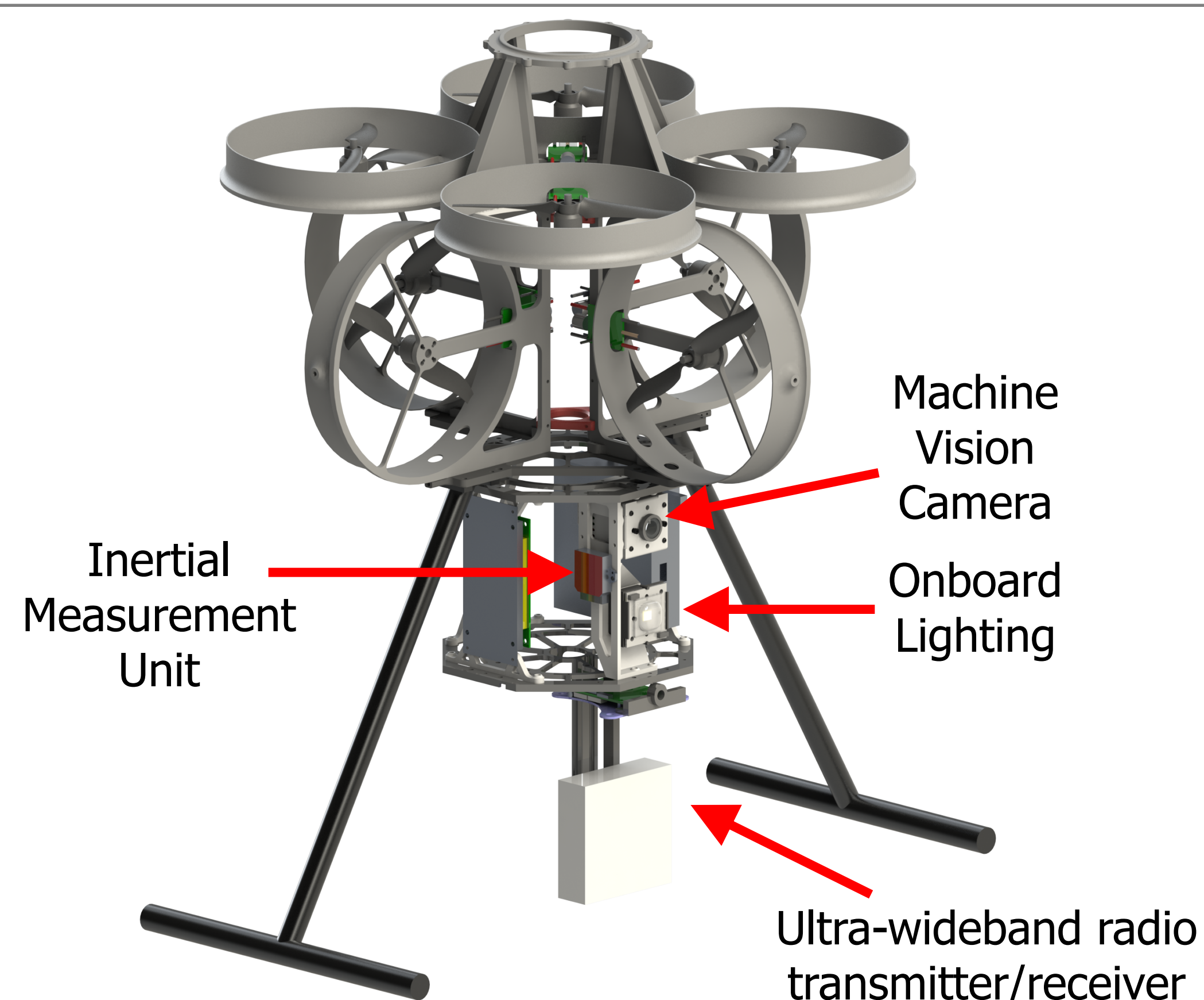


Vehicle and Sensor Description

The tank walls block GPS signals and are completely dark, making localization a key challenge for autonomous flight. We overcome these challenges using a complementary set of sensors that are fused using state of the art visual-inertial odometry (Bloesch, M et al. (2017). *Int. J. Robotics Research*, **36**: 1053-1072). The prototype vehicle is a helium balloon attached to a gondola (pictured below) which contains 8 thrusters for controlled flight and holds the perception sensors payload. The sensor payload includes:

- VectorNav VN-100 Inertial Measurement Unit
- MatrixVision Machine Vision Camera with LED Light
- Pozyx Ultra-wideband radio

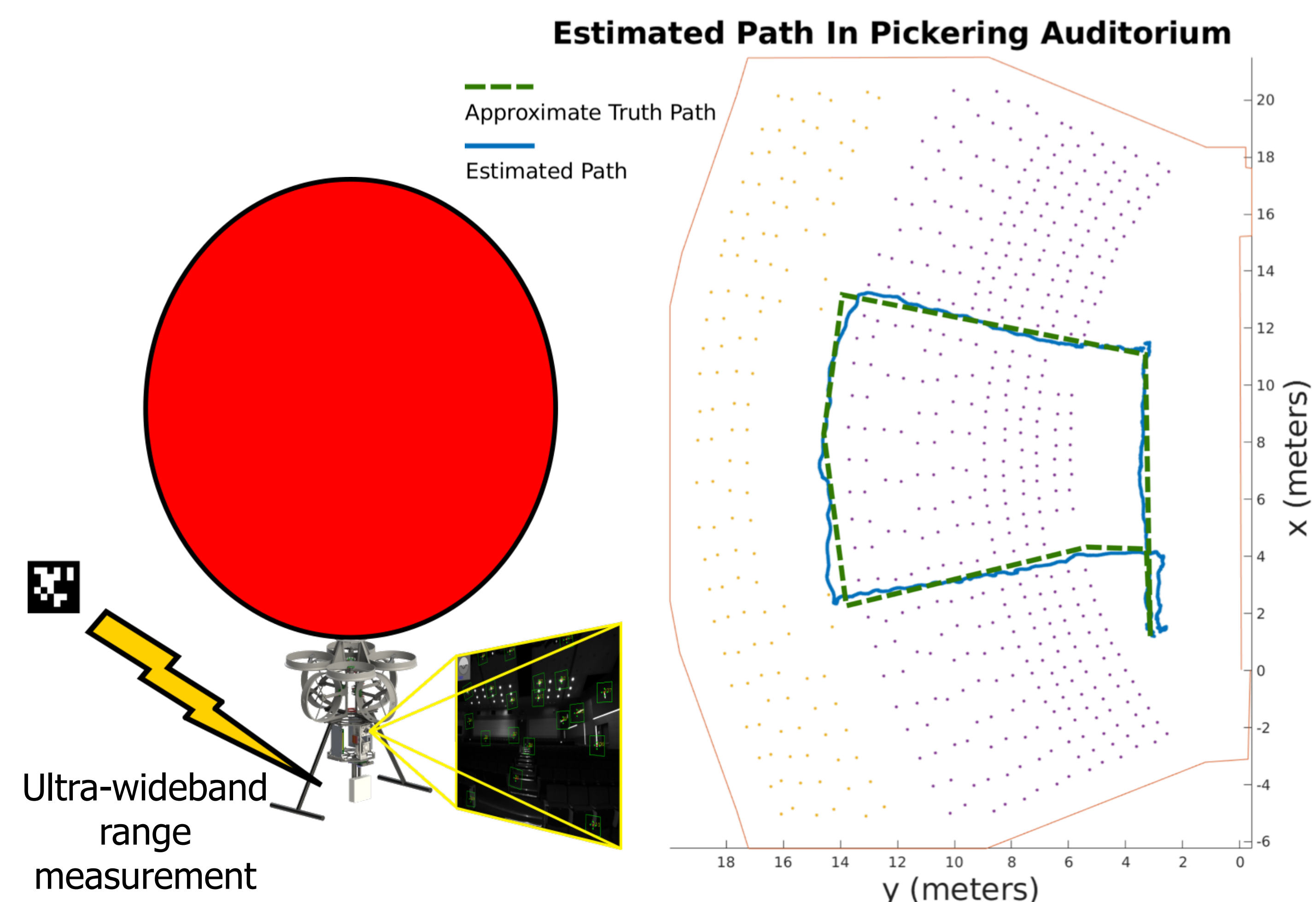
An LED lights the scene, enabling visual-inertial odometry using the camera and IMU sensors. However, feature tracking is less accurate than with normal lighting and results in a larger positional drift error. Additional constraints on the position are provided by fusing range measurements from a Ultra-wideband radio at the starting location (determined with a fiducial) into our estimate. By including range measurements we are able to mitigate positional drift caused by less accurate feature tracking.



National Aeronautics and Space Administration
Jet Propulsion Laboratory
California Institute of Technology
Pasadena, California

www.nasa.gov

Copyright 2019. All rights reserved.



Experiment Description and Results

Experiments were conducted with the balloon in complete darkness in Pickering Hall at JPL. The experimental setup included a Ultra-wideband radio with a fiducial tag attached near the starting location (depicted above). The vehicle then images the tag and initializes its localization reference frame with respect to the transmitter. Once initialized, the fiducial is not in view for the majority of the traverse and is not used for localization.

The resulting trajectory (pictured above) is overlaid onto a floorplan of Pickering Hall to serve as an approximate ground truth. The start and end location are the same, providing a measure of the overall positional error drift over an approximately 80 meter path. We were able to demonstrate our localization system working in complete darkness operating with approximately 1% error in position, matching current state of the art methods in fully lit conditions.

Conclusion

Our system performs localization in the dark with an approximate error of 1% in translation. Going forward, we seek to incorporate our visual-inertial odometry solution as a prior to a Pose-graph Simultaneous Localization and Mapping solution that will reduce error in the traverse estimate after the traverse is completed.



Designing and Fabricating a Three-Dimensional Silicon Stack for a 2.06 THz Receiver Front End

Christine P. Chen (386H)

Darren Hayton (386H), Robert Lin (386H), Cecile Jung-Kubiak (389W), Joseph Lee (386H), Jose Siles (386H), Maria Alonso (386H), Alex Peralta (386H), Imran Mehdi (386H)

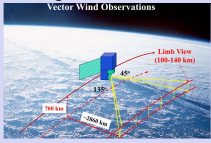
Abstract

NASA's earth science directorate emphasizes understanding complex atmospheric dynamics in Earth's upper atmosphere. A heterodyne receiver front end is being developed to perform measurements in the lower earth atmosphere at 2.06 THz, where a neutral oxygen line exists. The silicon (Si) platform presented in this abstract is created to support a low-parasitic 2.06 THz Schottky diode mixer. The Si stack design is designed with considerations of having system uniformity, accuracy, and repeatability. By using Si micromachining, desired tolerances can be met with faster turnaround time, and losses at 2 THz operation can potentially be minimized relative to existing metal interfaces, thereby improving mixer performance. The capability to leverage Si fabrication and integrate the local oscillator (LO) and intermediate frequency (IF) signal onto a compact Si micro-machined package has the potential to introduce new features and design paradigms. Furthermore, a key challenge for this type of integrated architecture is to perform reliable testing given sub-millimeter constraints. With the features being etched onto two pieces of 350- μm Si wafer, the Si block is designed to be assembled with fine tolerance by incorporating both prior metal block assembly strategies and a novel optical alignment scheme.

Introduction

Terahertz Limb Sounder Enabled by 2 THz Mixer

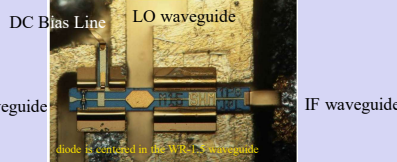
NASA's earth science directorate includes as a focus understanding the atmospheric dynamics in Earth's upper atmosphere. It is scientifically important to measure the lower thermosphere for understanding the transition region between a well-mixed lower atmosphere to a diffusive separated thermosphere.



In order to complete thermospheric measurements, THz receivers with the following specifications is desired:

- Room temperature operation
- Development of local oscillator devices and circuits for THz regime
- Schottky-diode technology for mixers in the one to five THz range

Ref 1: Siles, et al. A New Generation of Room-Temperature Frequency-Multiplied Sources With Up to 10x Higher Output Power in the 160-GHz-1.6-THz Range, 2018.



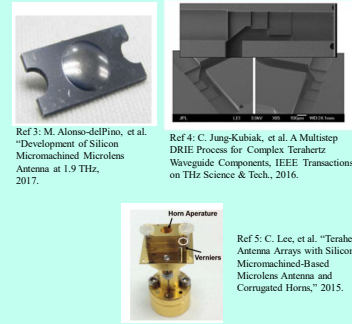
Ref 2: Thomas, et al. 560 GHz, 664 GHz and 1.2 THz Schottky based MMIC sub-harmonic mixers for planetary atmospheric remote sensing and FMCW radar, 2015.

Background

Silicon Micromachining

- Accuracy: can achieve tighter tolerance of μm -level precision
- Repeatability: batch-level process
- Uniformity: circuit-to-circuit variation is reduced at fabrication
- Faster design cycle
- Possibility of 3-d integration
- Reduces mass and volume
- Possibility of reducing losses due to compact designs

Recent Examples of THz Micromachining at JPL



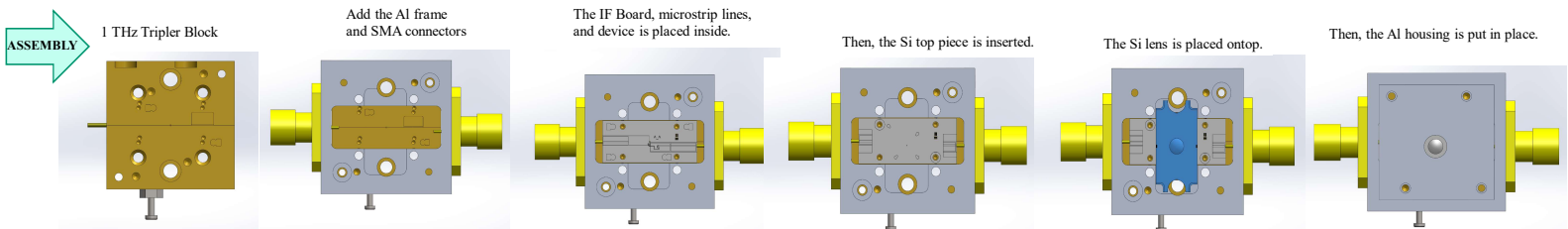
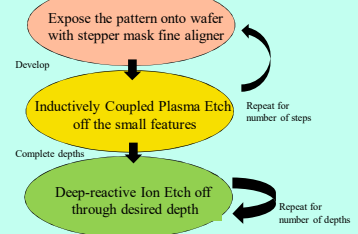
Ref 3: M. Alonso-del-Pino, et al. "Development of Silicon Micromachined Microcavities Antenna at 1.9 THz, 2017.

Ref 4: C. Jung-Kubiak, et al. A Multistep DRIE Process for Complex Terahertz Waveguide Components, IEEE Transactions on THz Science & Tech, 2016.



Ref 5: C. Lee, et al. "Terahertz Antenna Arrays with Silicon Micromachined-Based Microlens Antenna and Corrugated Horns," 2015.

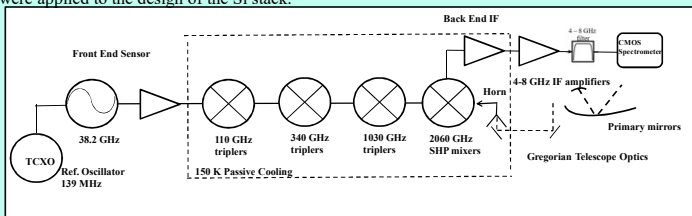
In order to have high-aspect ratio feature size in silicon, deep-reactive ion etching is used: Consists of three-step cycle of etching (SF_6) and passivation (C_2F_8)



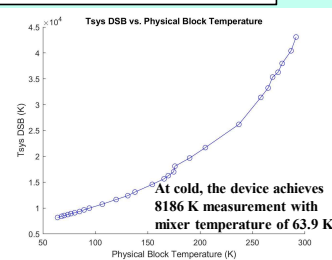
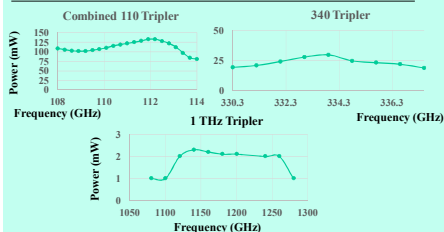
Methodology & Measurement Results

Experimental Setup of CMOS Multiplier Chain

- The local oscillator chain was set up and characterized to perform noise temperature measurements.
- This work was first performed using a metal block for comparison with the Si block. Assembly learnings were applied to the design of the Si stack.



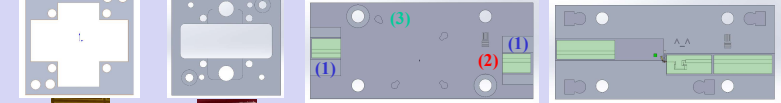
Characterization of Local Oscillator Chain



Integration Results & Discussion

Key Designed Components

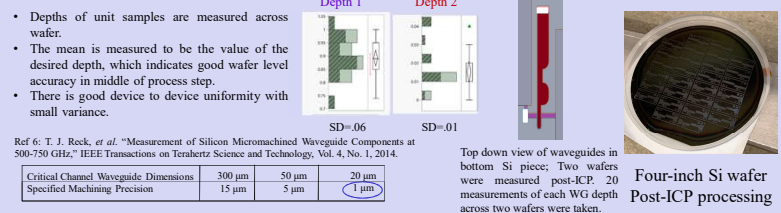
- Backbone: Two possible ways to interface the Si pieces to the metal interface
 - Top and bottom Si pieces: 17.5 mm x 7.5 mm dimensions
 - In order to have miniature dimensions, quartz-based IF boards (1) were designed, maintaining the low crosstalk levels with low-to-high impedance matching within architecture dimensions.



- Indirect monitor (2) of coupling through relative power shuts Significant to design for testing verification
- Interfaces to block via pins (3)
- Two options for coupling out signal via either horn antenna or microlens

Verification of Fabrication Tolerances

In-process waveguide feature depths are measured to verify accuracy and uniformity, key to repeatability.



Conclusion

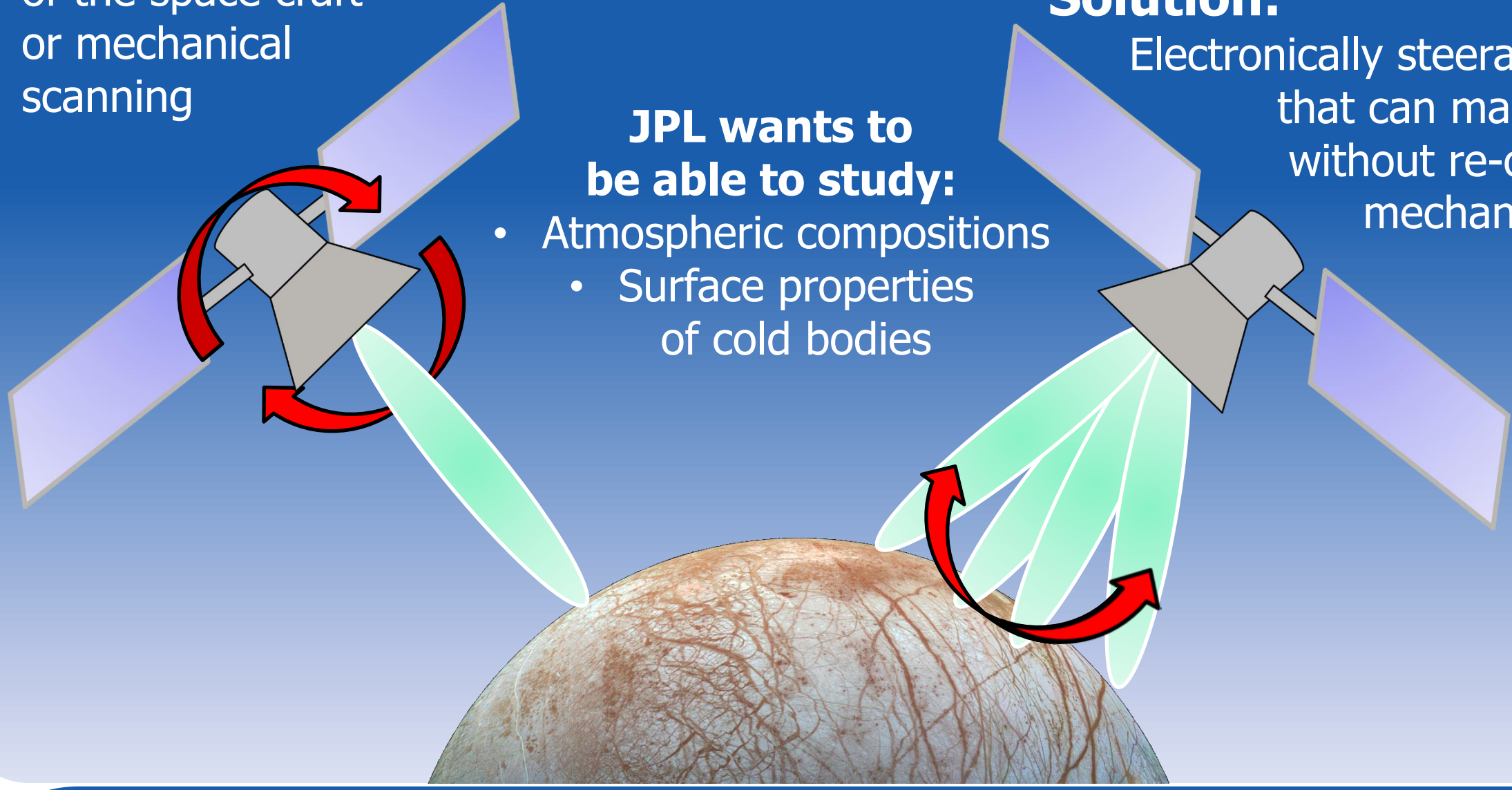
- A fully solid-state receiver has been demonstrated at 2 THz with metal blocks. The Si micro-machined 2 THz mixer block has been designed and is currently being fabricated.
- Si micromachining will allow us to achieve accuracy, repeatability, and uniformity for THz frequencies, enabling components in the 1 to 5 THz range.
- This technology will impact future flight missions by helping to enable larger scale array architecture with reliability at a much smaller area of around 400 mm^2 area than previously demonstrated.

Si RF-MEMS for mapping of planetary surfaces

Author: Sofia Rahiminejad (386)

Maria Alonso del Pino(386), Cecile Jung-Kubiak(389), Mina Rais-Zadeh(389), Goutam Chattopadhyay(386)
Jet Propulsion Laboratory, California Institute of Technology

Today mapping is done by re-orientation of the space craft or mechanical scanning



JPL wants to be able to study:

- Atmospheric compositions
- Surface properties of cold bodies

Background

Solution:

Electronically steerable antennas that can map the surface without re-orientation or mechanical scanning

To do this:

We need an antenna array with phase shifters to electronically steer the beam and switches to continuously calibrate the antenna operating at 550 GHz.

Unfortunately:

- Today's phase shifters cannot operate above 200 GHz.
- There are no commercial switches that are available at these frequencies and have a broad band (500-750GHz)

Objective

Design and fabricate RF-MEMS phase shifters and switches

The phase shifter

- Operating between 500-600 GHz.
- Achieve phase shifts between 0°-180°.
- Low loss i.e. $S_{11} < -20$ dB.

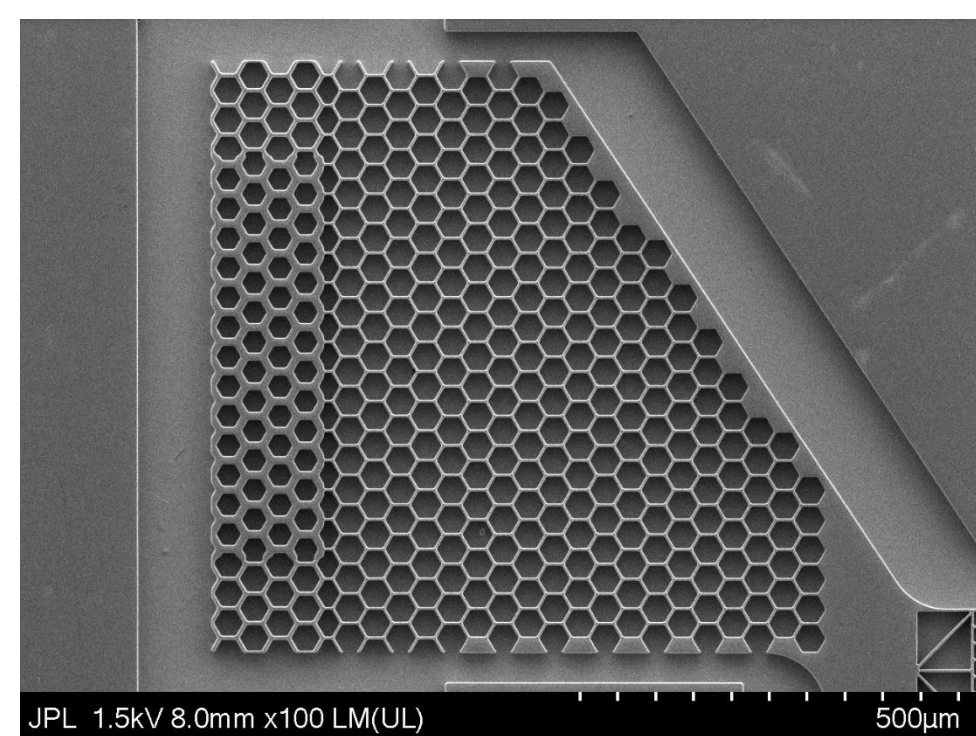
The Switch

- Operating between 500-750 GHz.
- **No contact** when switching.
- Low loss i.e. $S_{11} < -20$ dB.

Both devices need to be fabricated with silicon micromachining.

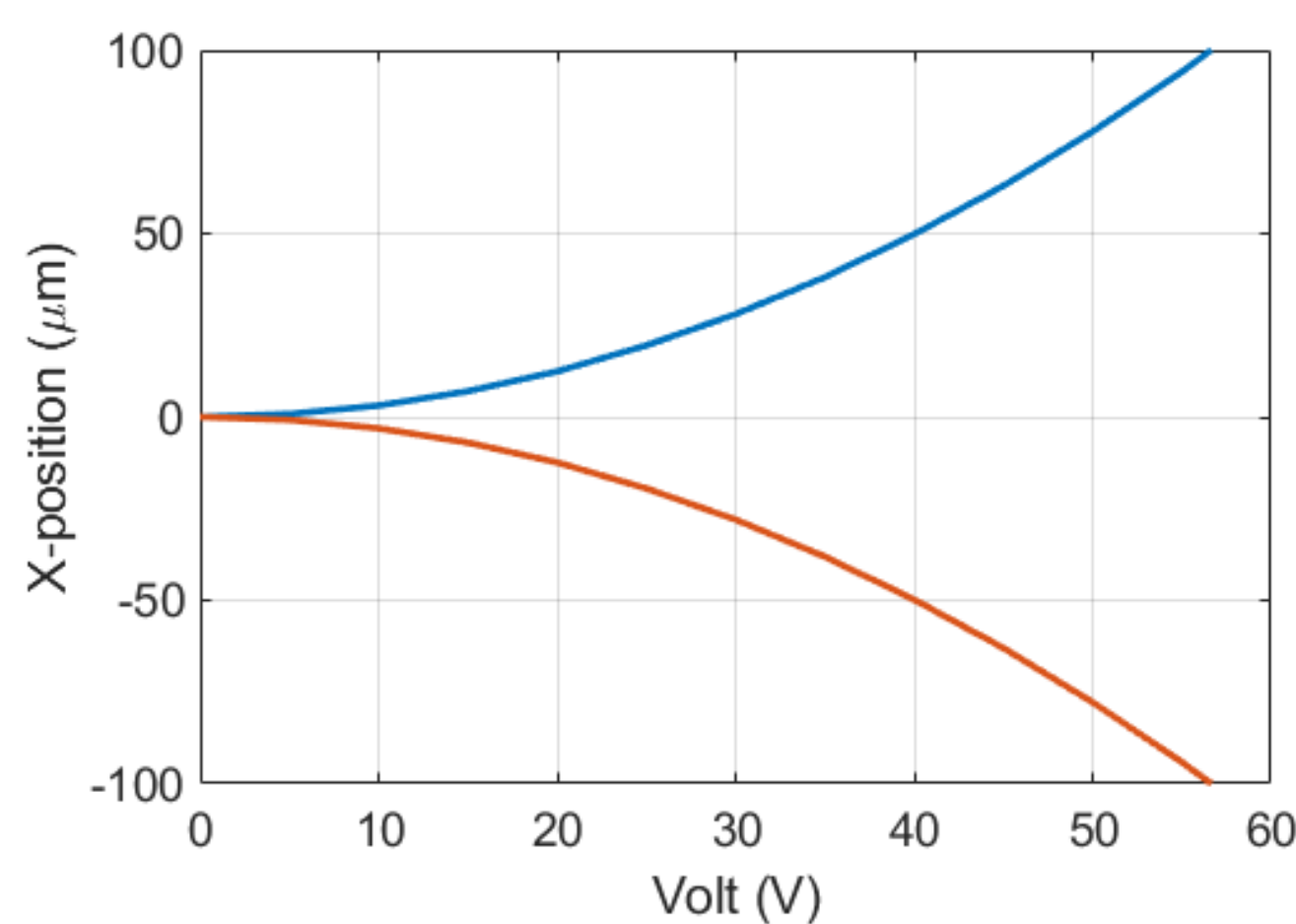
Design and concept of the 180° phase shifter

The insertion of a thin dielectric slab into a waveguide produces a phase shift on the incoming wave. The phase shift depends on the permittivity and thickness of the slab and how much it is inserted into the waveguide.

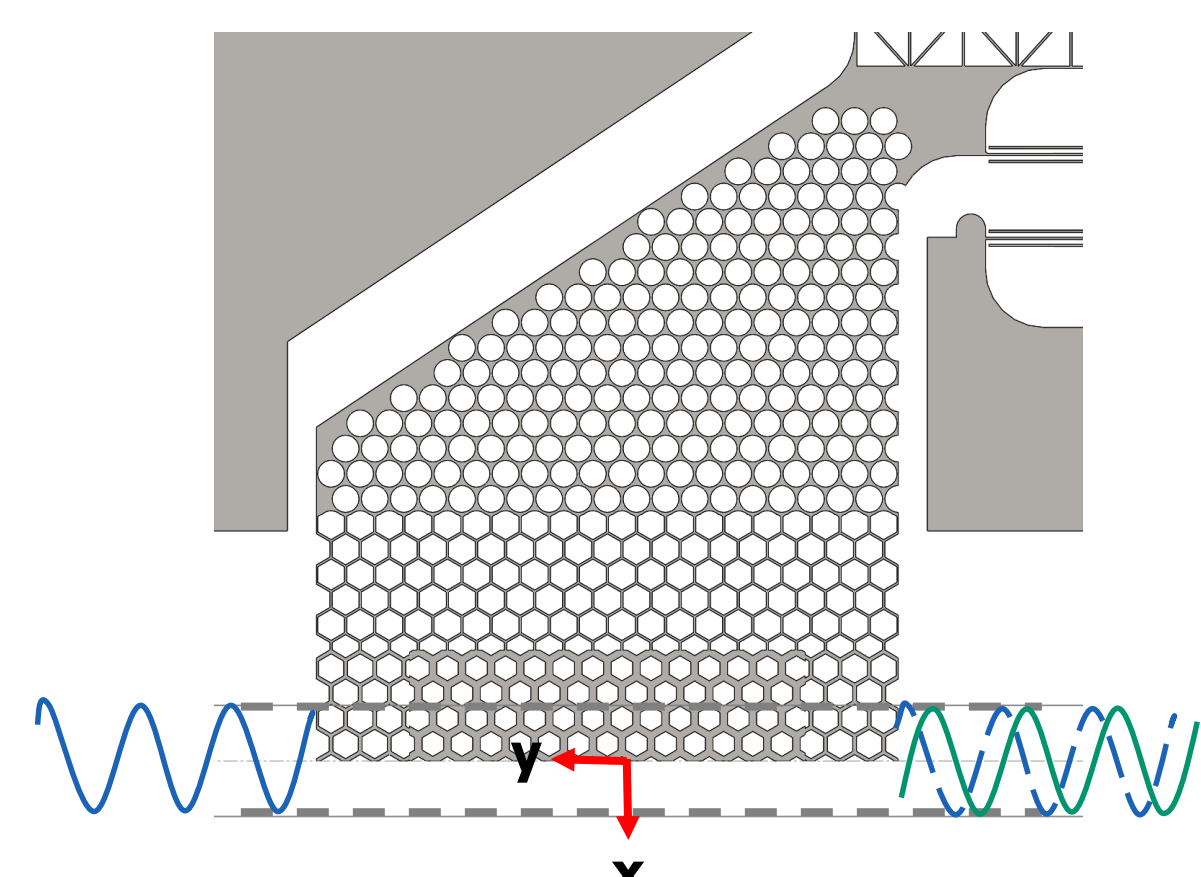
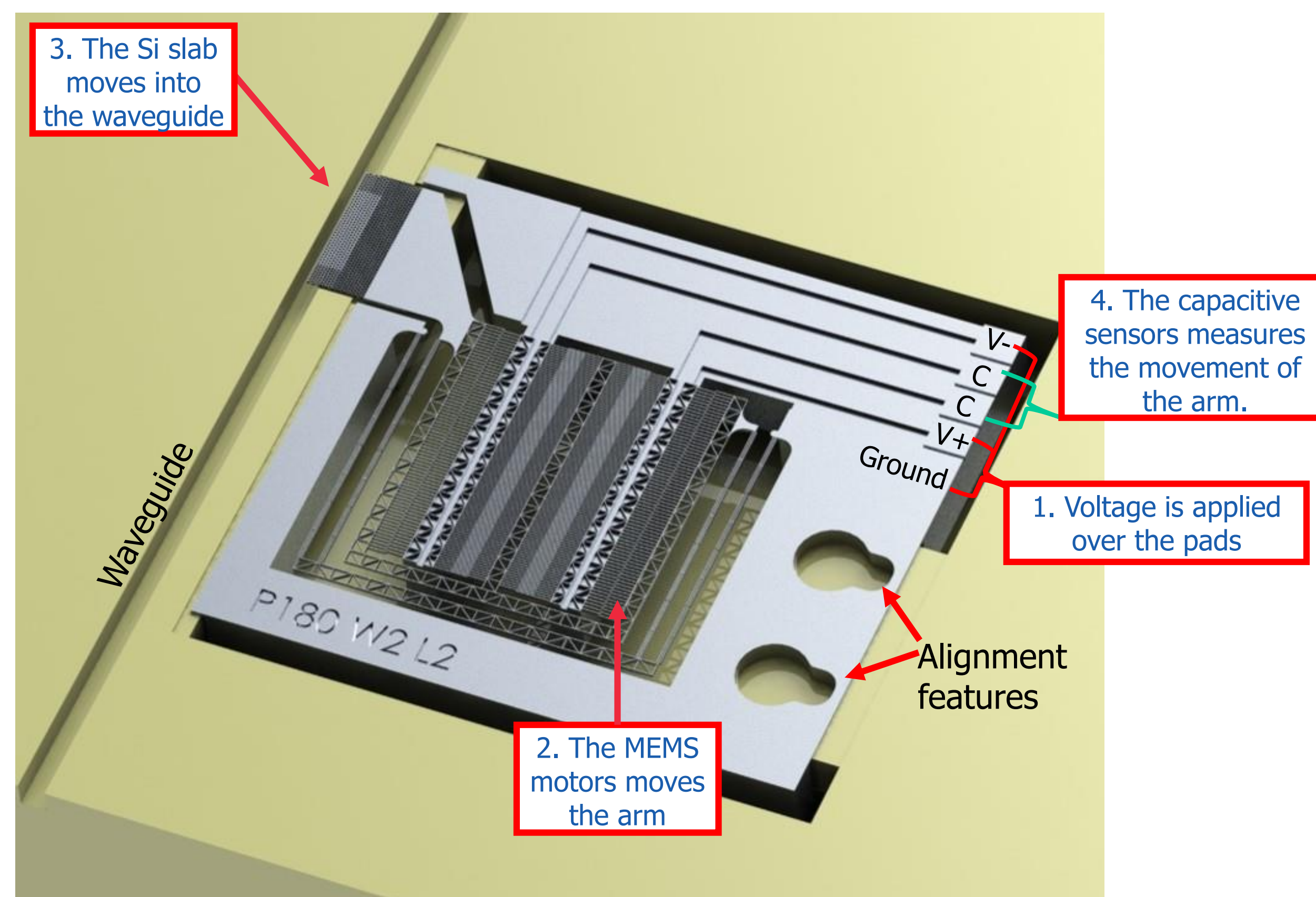


JPL 1.5kV 8.0mm x100 LM(UL) 500µm
SEM close up of the fabricated phase shifters slab

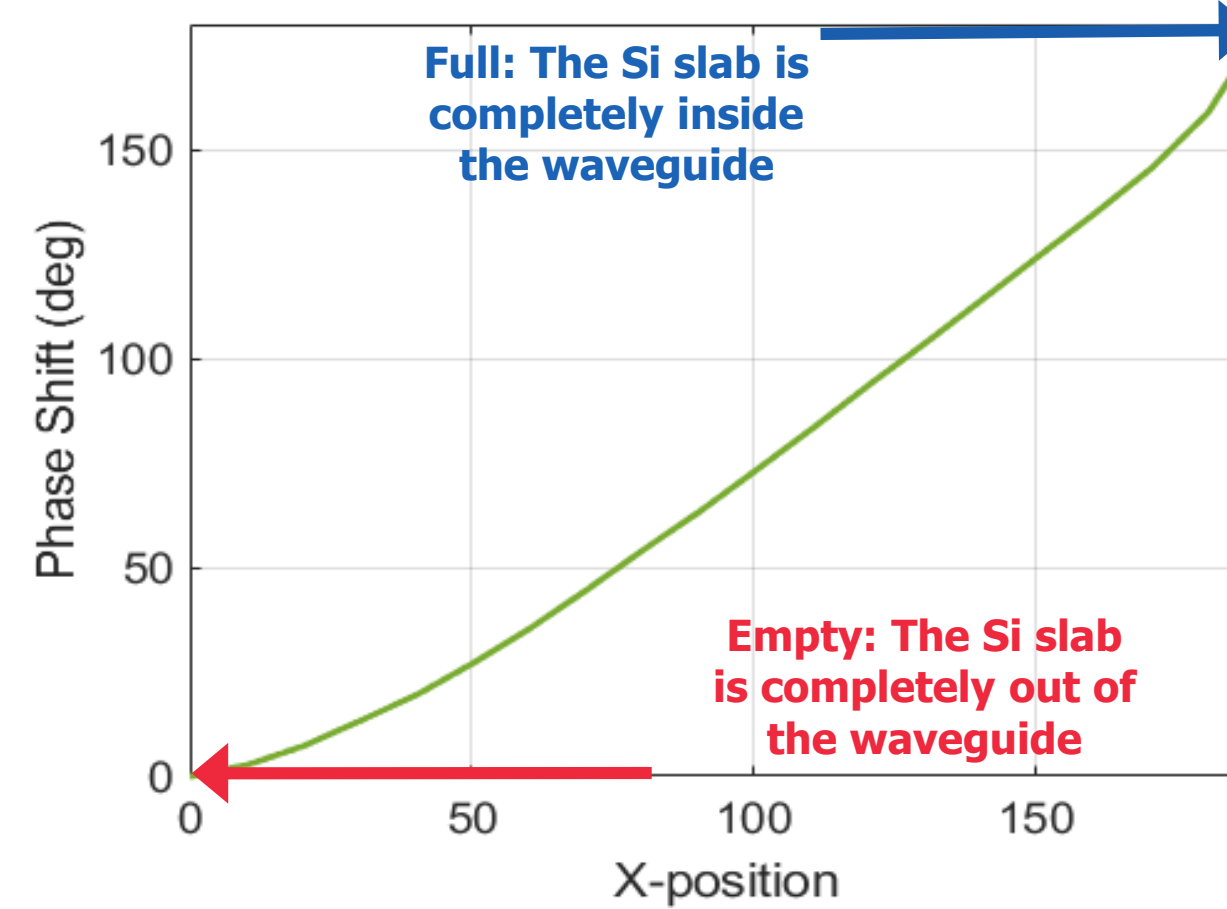
The permittivity of the slab is controlled by etching subwavelength hexagonal holes of a certain aspect ratio (hole diameter/lattice). In this case, permittivities in the range of 1.65-11.9 can be achieved.



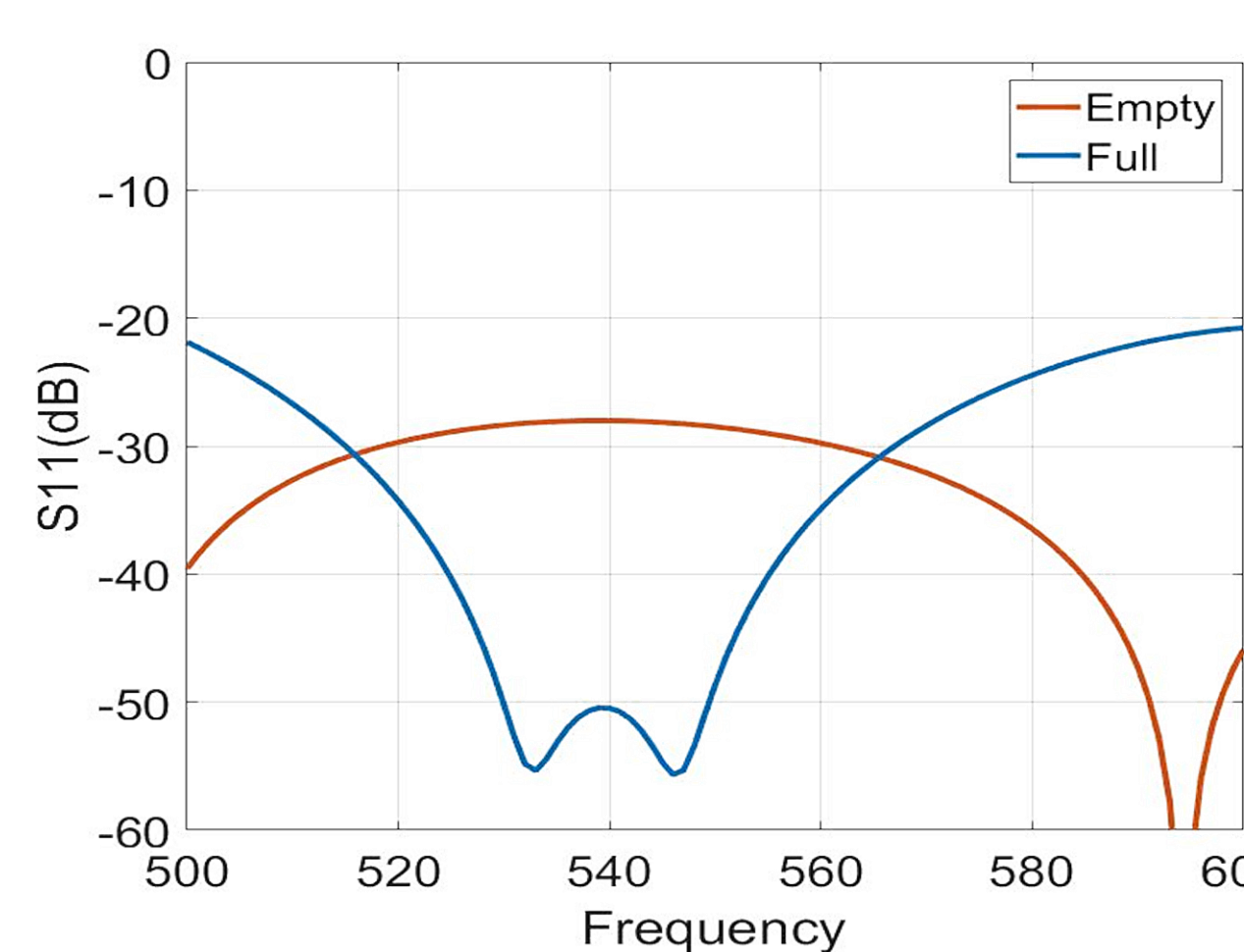
The slab position inside the waveguide depends on the applied voltage. Blue line is when the voltage is applied over pad V+ and Ground. Red line is when the voltage is applied over pad V- and Ground.



The slabs position inside the waveguide defines the phase shift of the incoming electromagnetic wave.



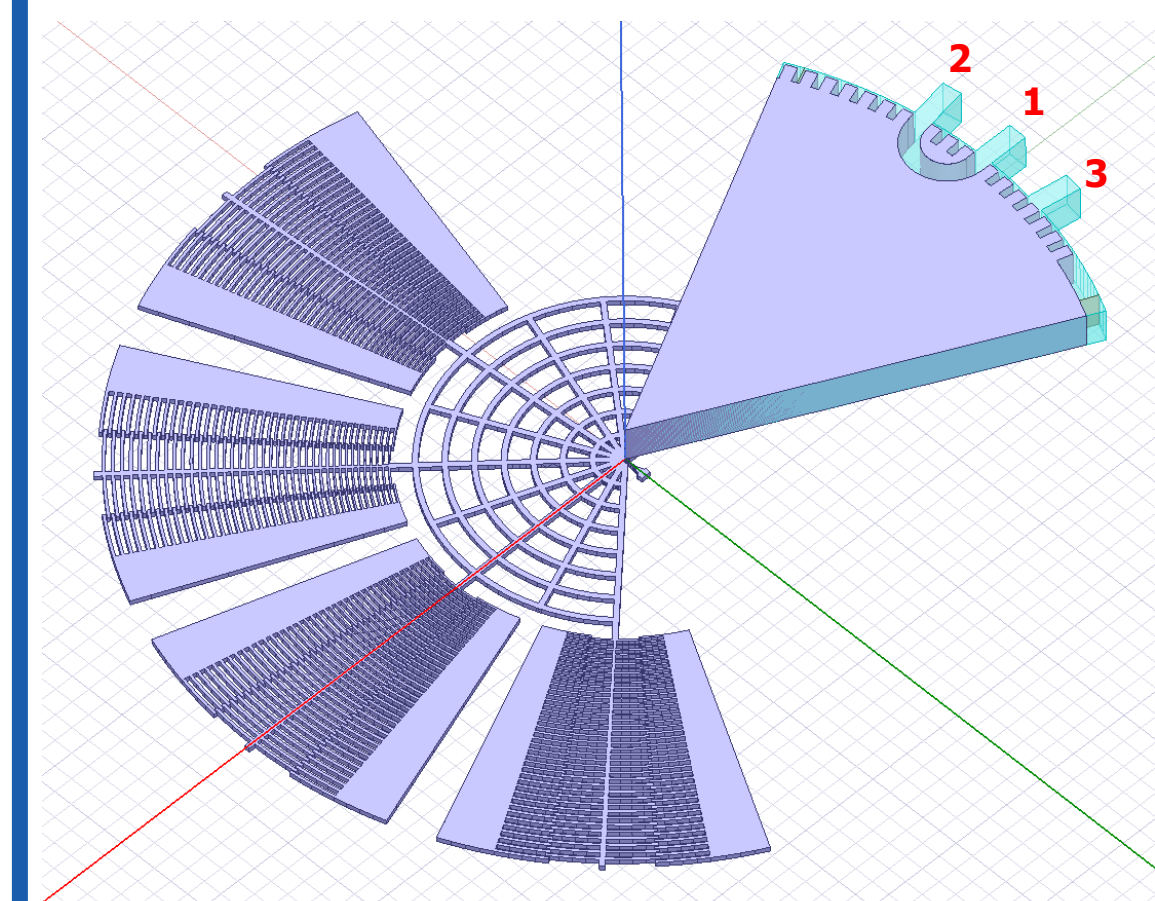
The phase shift depends on how much the slab is inserted into the waveguide.



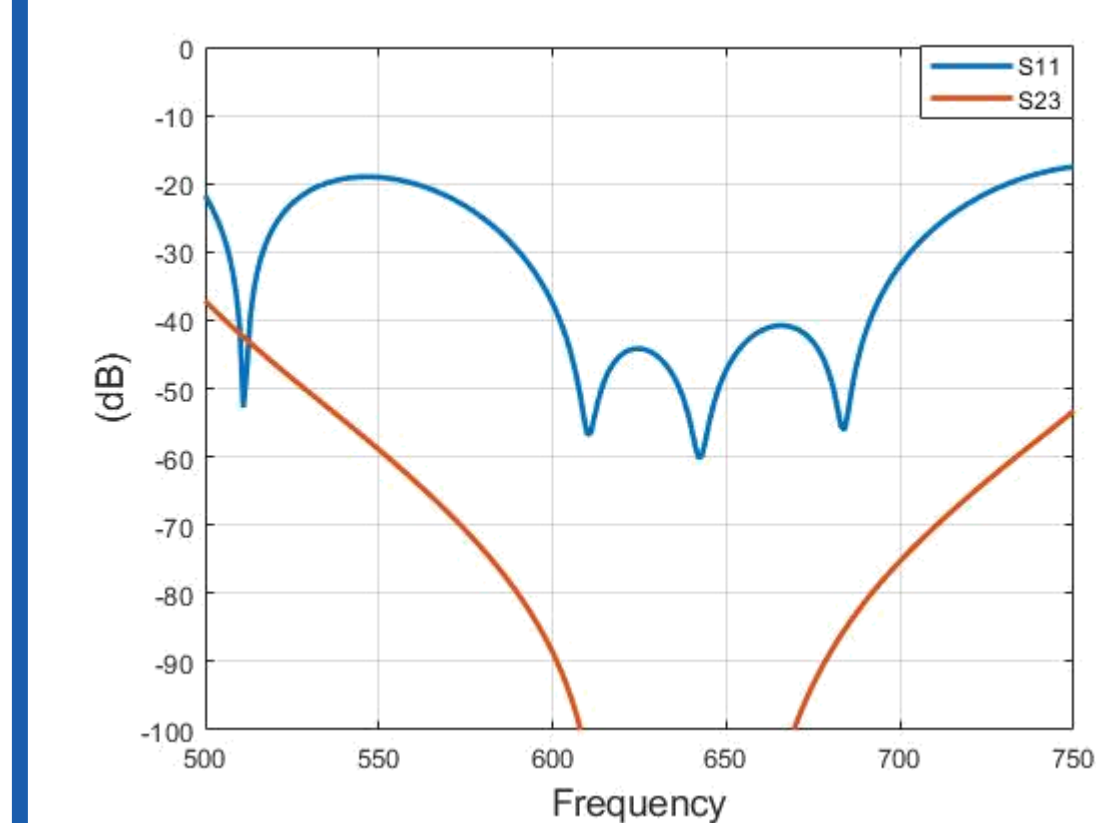
The reflection coefficient S11 for when:

- the slab is completely out of the waveguide (red)
- the slab is completely inside the waveguide (blue)

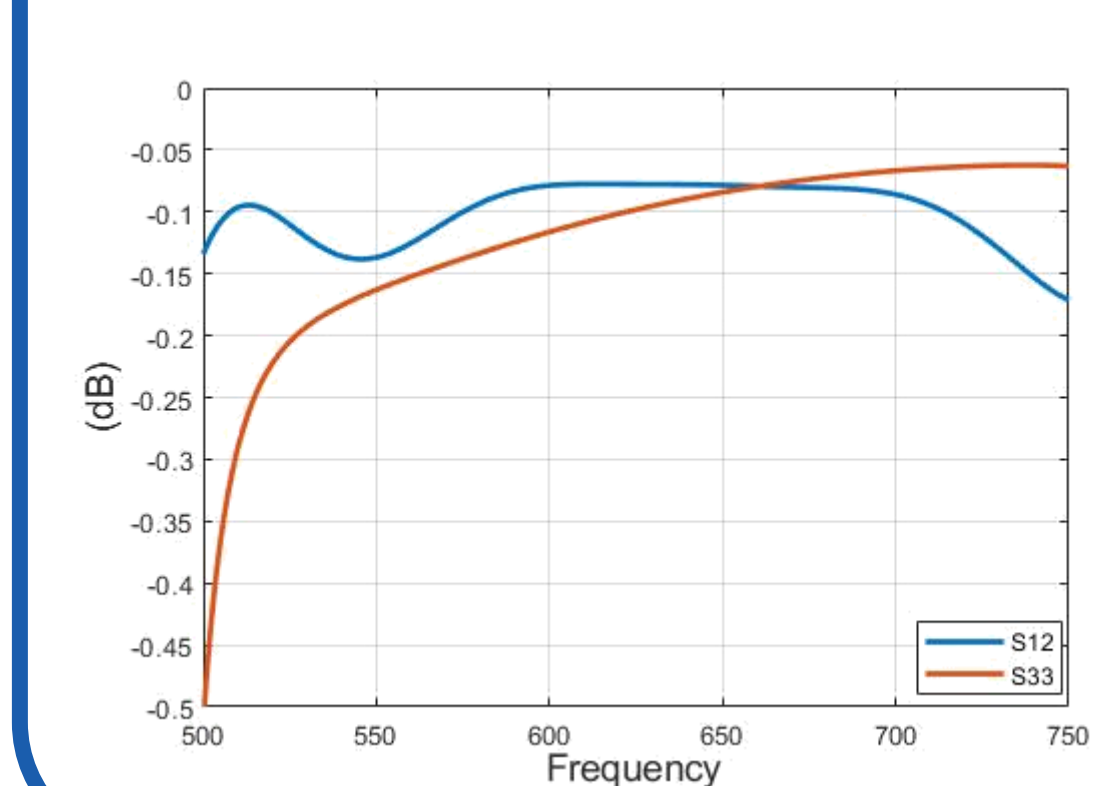
Design and concept of the rotating switch



The motor rotates $\pm 4.5^\circ = 9\text{deg}$, between coupling port 1 and 2, to coupling port 1 and 3. The voltage needed to rotate between positions is 60 V.



The reflection (S11) between the two open ports are below -19 dB, the transmission (S23) between the open port and the closed port are below -35 dB



The transmission (S21) between the two open ports are above -0.2 dB, the reflection (S33) at the closed ports is above -0.5 dB

Summary

- The 180° phase shifter was designed and fabricated to:
 - have a phase shift span of 180°
 - have a reflection coefficient (S11) below -20 dB between 500-600 GHz.
 - have full insertion at 55 V
- The Rotating switch was designed to:
 - rotate 9°
 - have a reflection coefficient (S11) below -20 dB between 500-750 GHz.
 - rotates 60 V

RF-MEMS can enable electrical steerable antennas, that can map planetary surfaces without mechanical movements, thus increased mapping speed at less energy cost.

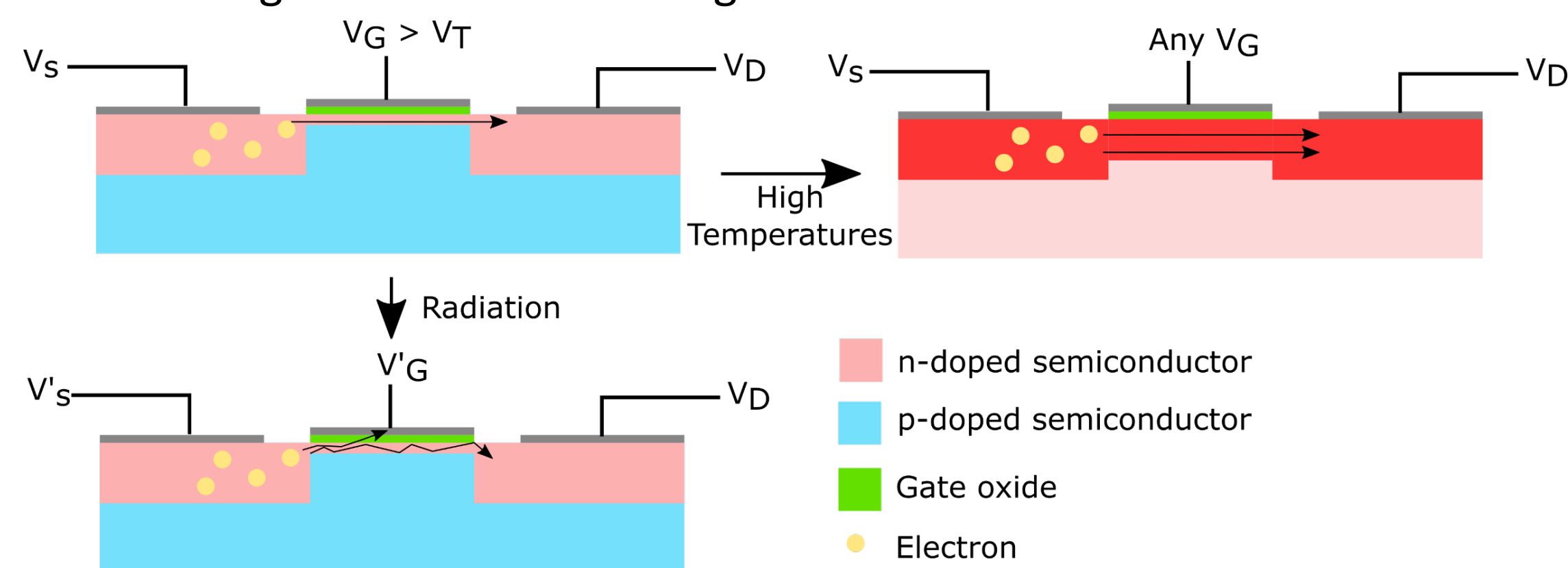
Field Emission Transistors For High Temperature Environments

Author: William Jones (3890)

Siamak Forouhar (3890), Lucia De Rose and Axel Scherer (Caltech)

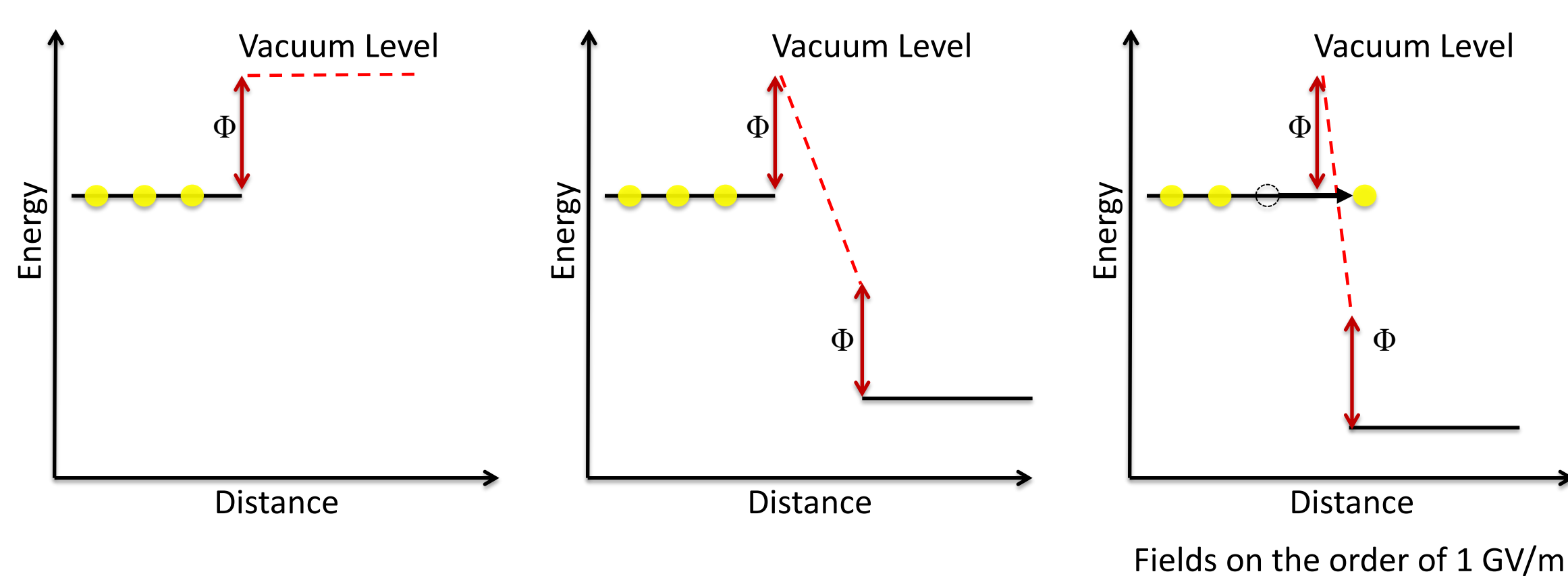
Motivation

- Electronics used in space or extra planetary environments routinely encounter extremes in temperatures and radiation.
 - Wide temperature swings
 - Earth orbit varies from 120 °C to -100 °C
 - Surface of moon varies from 127 °C to -173 °C
 - Surface of Venus is hotter than 480 °C
 - High radiation
 - 20 krad(Si) in low earth orbit
 - >1 Mrad(Si) for Jupiter and Saturn Mission
- Modern semiconductor transistors fail in these environments
 - High temperatures cause transistors to become resistors
 - Radiation creates defects in conduction channels or thin gate oxides, increasing resistance and leakage

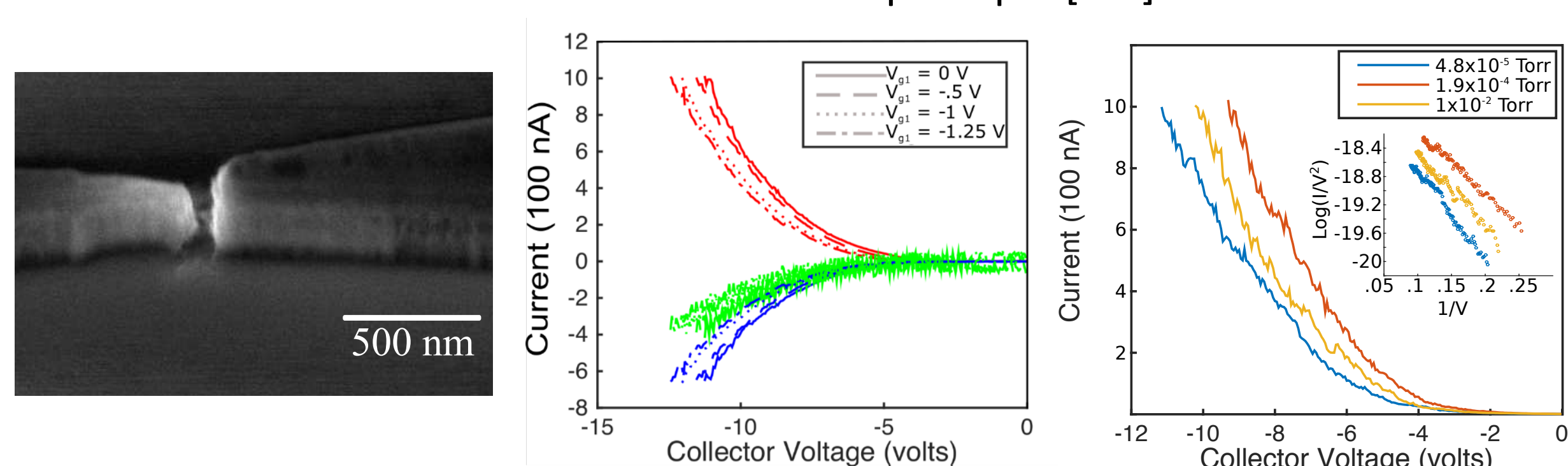


Field Emission Transistors, An Alternate Approach

- Field assisted quantum tunneling of electrons in a conductor to the vacuum
 - Ballistic transport of electrons through vacuum
 - Current depends primarily on the electric field at the emitter surface
 - Modulation done by changing surface electric field
 - Very large electric fields, ~ 1 GV/m
 - Very large voltages, or nanoscale dimensions



- Nanoscale dimensions give you added benefits
 - Extremely short electron conduction times
 - Operation at atmospheric pressures
 - Mean free path of electrons at 1 atm is < 200 nm
- Diodes and transistors can work on this principle [1-2]:

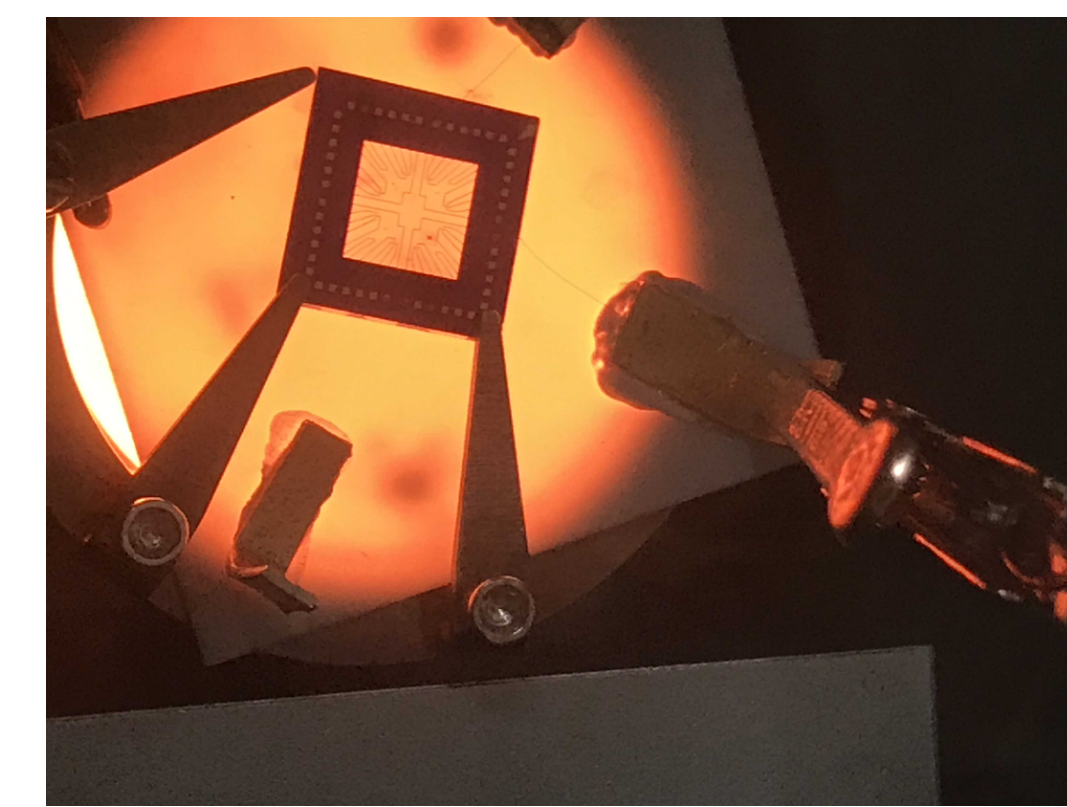
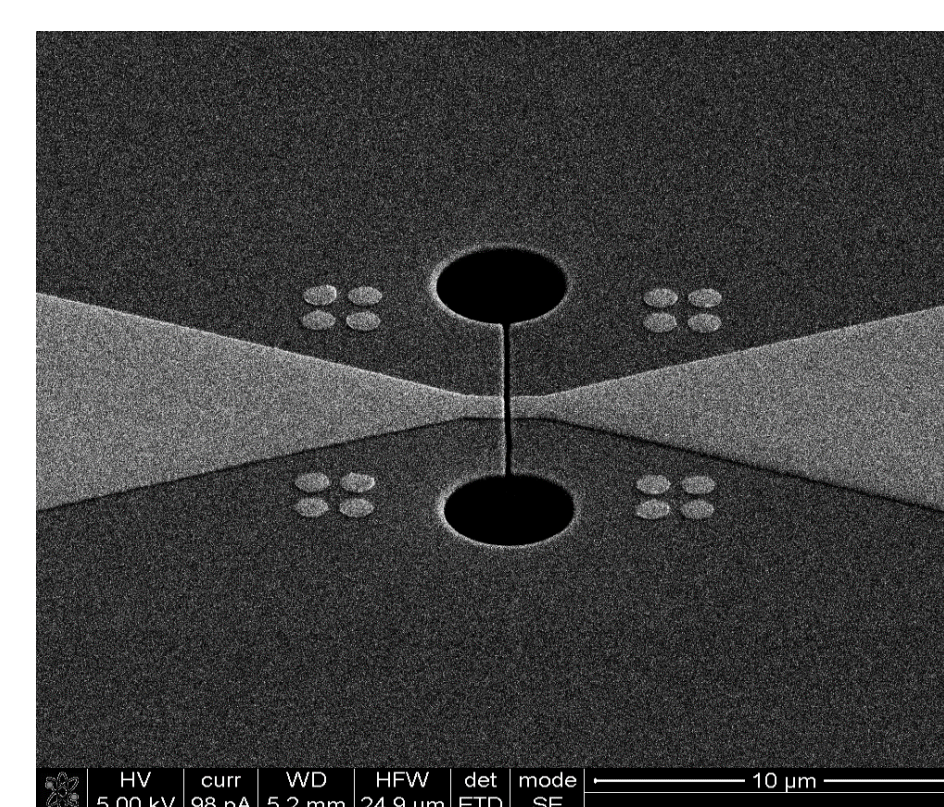
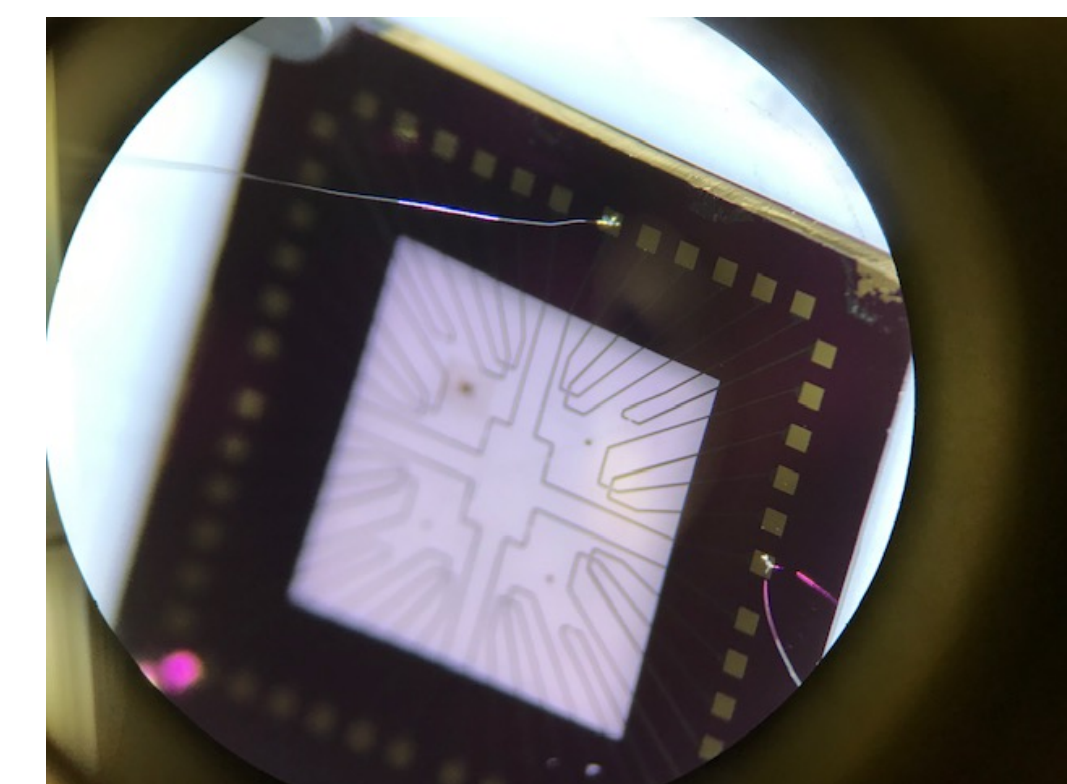
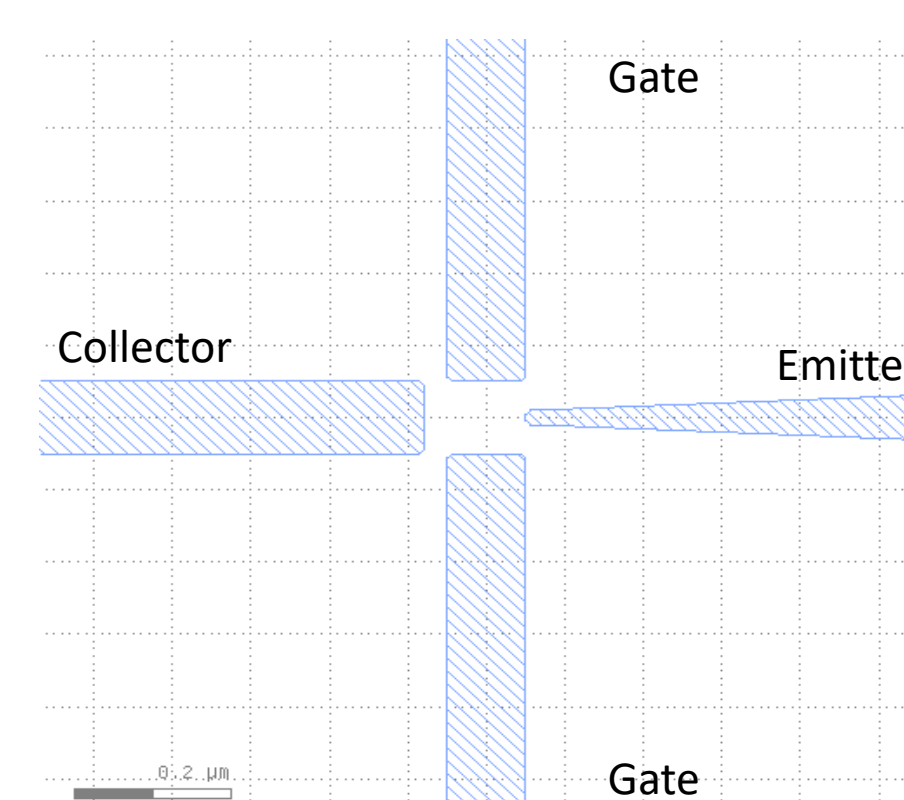


- Nanoscale field emission transistors are robust in extreme environments
 - Non-linear IV curve at high temperatures (< 900 °C)
 - Vacuum channel and amorphous metals are resistant to radiation damage

Design of High Temperature Field Emission Transistors

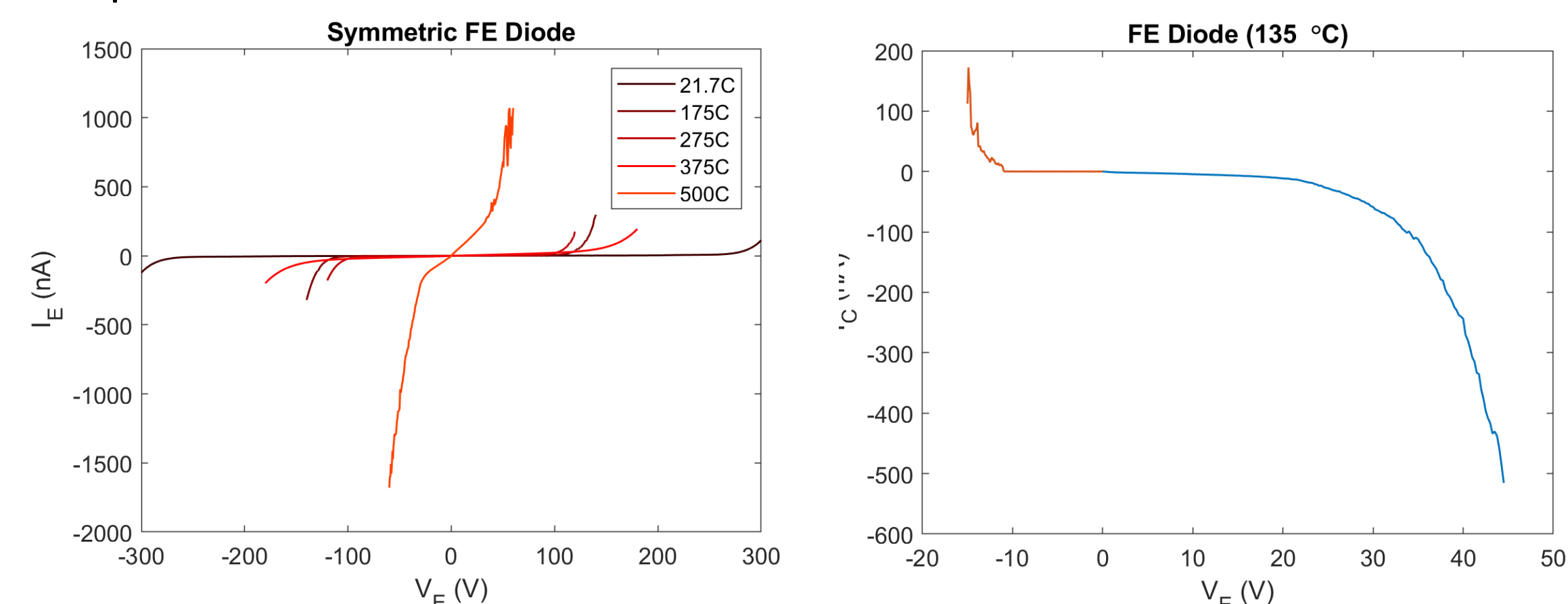
- Leakage current across the surface of the substrate scales with temperature
 - Frenkel-Poole governing equation:

$$J \propto E * \exp\left(\frac{-q(\phi_B - \sqrt{qE/(\pi e)})}{k_B T}\right)$$
- Strategies to overcome leakage current
 - Abandon multilayer structure for four separated terminals
 - Materials choice
 - Stoichiometric Si₃N₄ is a very good electrical insulator at high temperatures
 - Air gapped terminals made by completely removing the substrate near the terminals
- Fabricate air gapped transistors on 200 nm thick Si₃N₄ membrane
 - Use focused ion beam to remove substrate near terminals



Testing and Early Results

- Diodes built by separating two terminals show low turn-on and stability at high temperatures



- Transistors are being built and tested

Future Directions and Impact

- Low temperature testing to demonstrate electronics that operates from -196 °C to 400 °C
- Simple amplifier circuits
 - Incorporate lithographically defined capacitors and resistors
- Provide robust electronics to enable future missions to extreme (and interesting) environments

References

- Jones, W. M., Lukin, D. & Scherer, A. Practical nanoscale field emission devices for integrated circuits. *Appl. Phys. Lett.* **110**, 263101 (2017).
- Han, J. W., Sub Oh, J. & Meyyappan, M. Vacuum nanoelectronics: Back to the future? -Gate insulated nanoscale vacuum channel transistor. *Appl. Phys. Lett.* **100**, 213505 (2012).

Hydration detection and identification with a low resolution mini Raman Spectrometer

Author: Peter H Edwards (389R)

James Lambert (389R), Nicholas Tallarida (389R)

Introduction

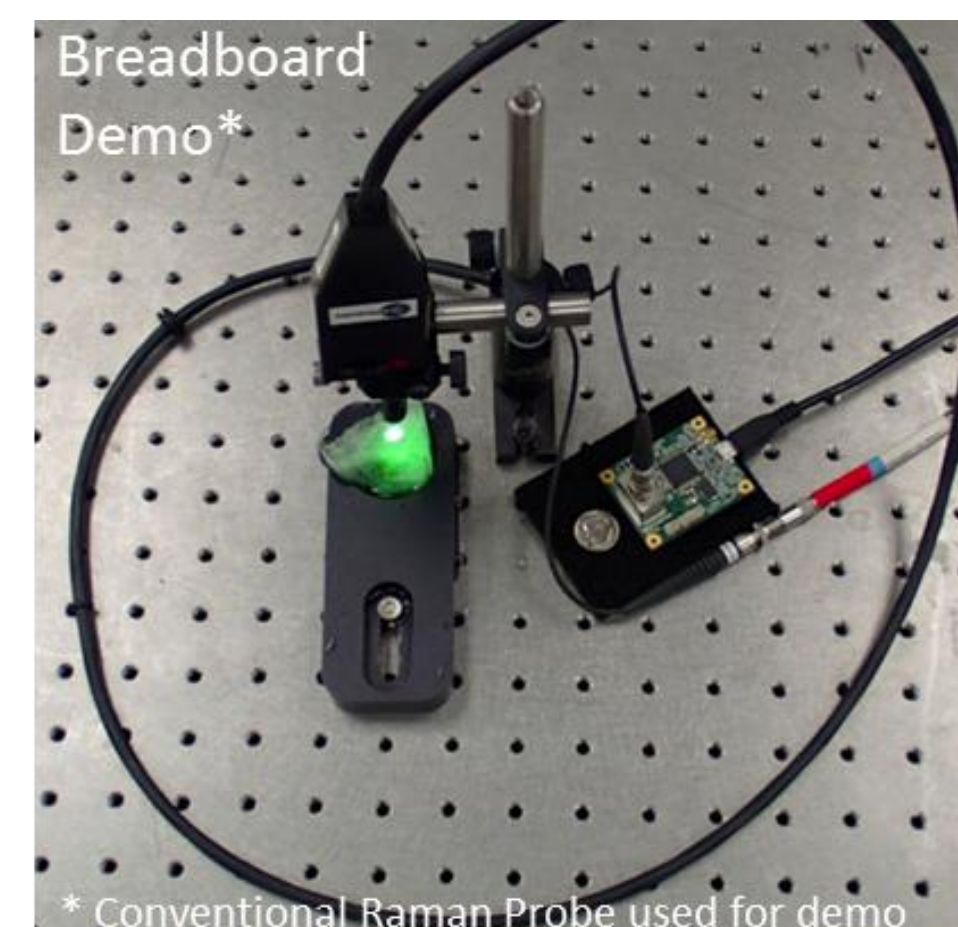
The use of numerous small micro rovers has been proposed as a method of rapidly characterizing a landing site, this will require miniaturized instrumentation.

Raman Spectroscopy has been selected for multiple planetary missions and is a useful tool for examining the molecular structure of a sample. Certain bands within a Raman spectrum (in the 2800-4000 cm^{-1} region) are associated with the molecular bonds found in hydrous material.

This work focuses on the use of a small compact low resolution spectrometer for identifying hydrous material and distinguishing between water, ice and hydrated minerals with these limitations.

Compact low resolution Raman instruments can still provide useful geological hydration data.

Breadboard Setup



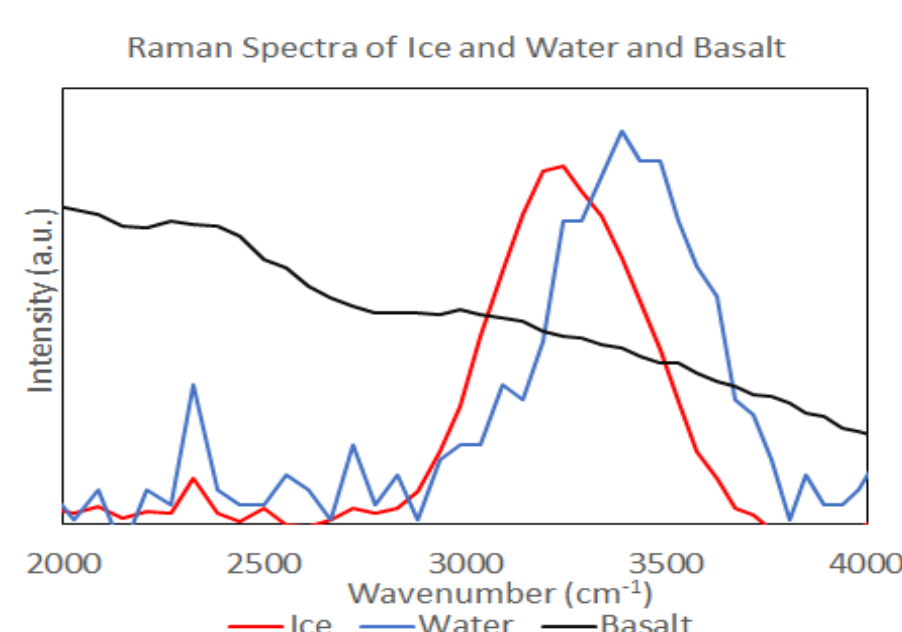
Two lasers were used, a JDSU and a smaller 1.4g OSRAM PL530.

For initial testing a conventional Raman probe head was coupled to a micro spectrometer from Hamamatsu. It is a very compact package at 20.1x12.5x10.1mm and hermetically sealed, with a resolution equivalent to 52 cm^{-1} per pixel in the 2800-4000 cm^{-1} range) and a mass of 5g.

Future tests will use a smaller probe head and compact instrument packaging

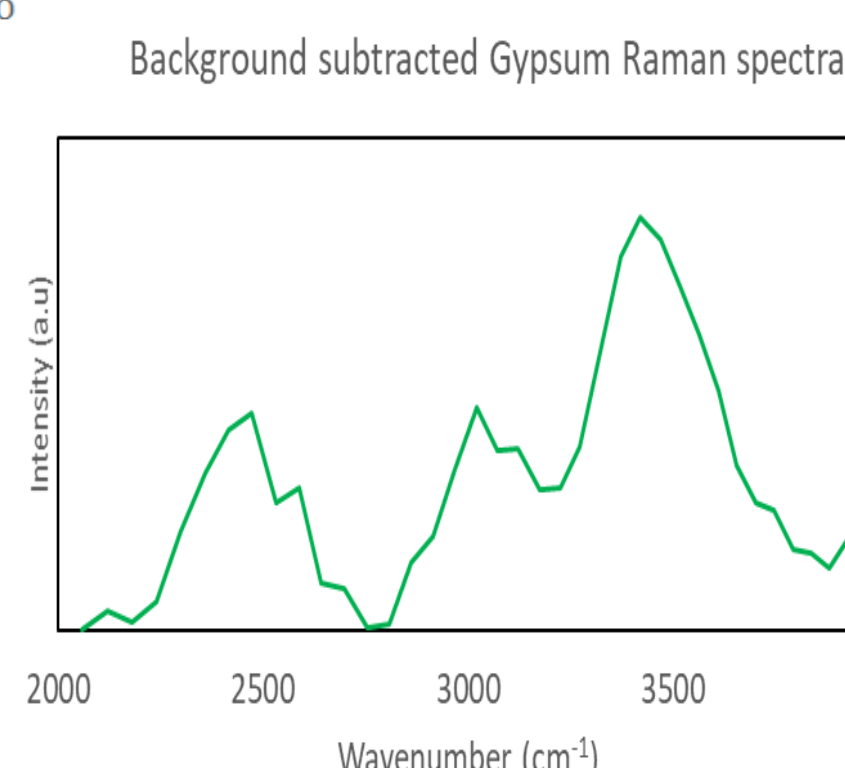
Laser and spectrometer combined total mass of 6.4g.

Data



Spectra of water, ice, and basalt were acquired. The basaltic material showed background fluorescence whilst the water and ice samples showed clear separate Raman bands.

The water peak is 3370 cm^{-1} with ice 3242 cm^{-1} . Literature values are 3270 cm^{-1} and 3140 cm^{-1} respectively, with higher resolution instruments.



Spectra of gypsum, (literature peak maxima at 3400 cm^{-1}), showed a location of 3419 cm^{-1} .

The low resolution spectrometer was capable of clear separation of water and ice samples from basalt. Hydrated minerals had much lower intensity Raman bands.

Classification

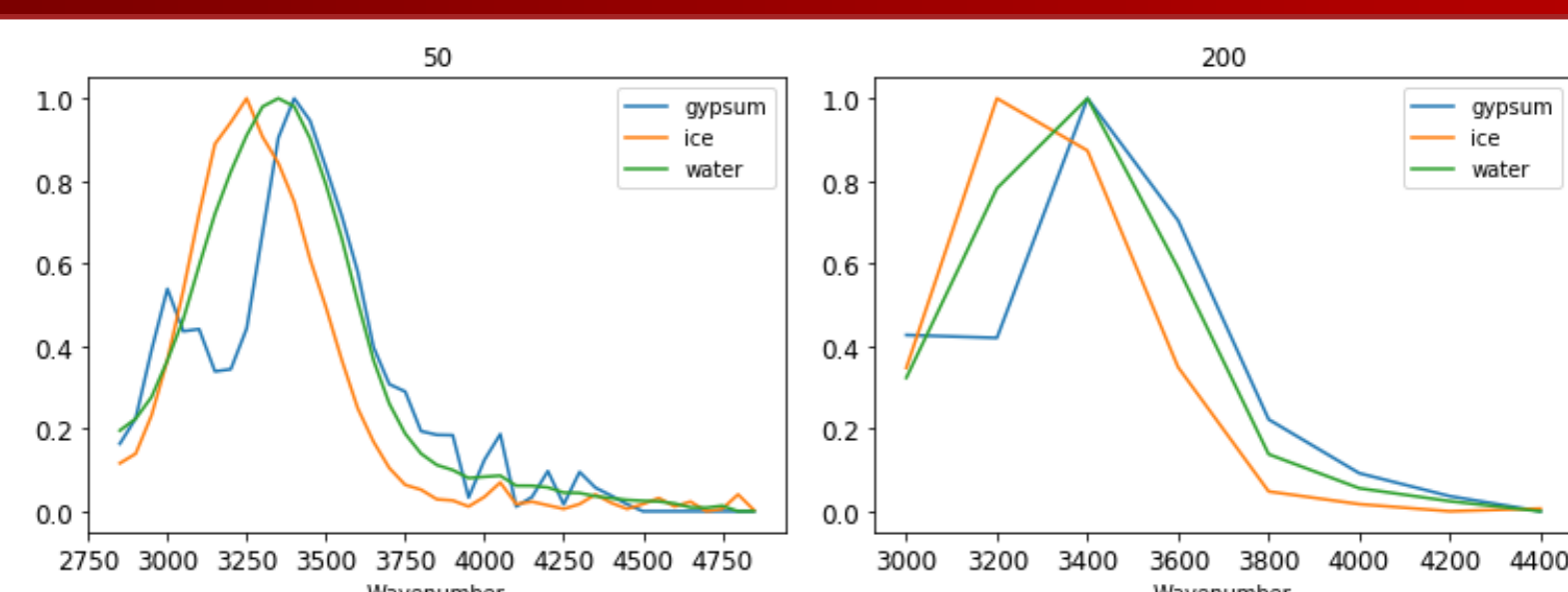
A algorithm was used to classify known spectra, with a focus on avoiding misidentifying any anhydrous material as hydrous. Once hydration has been determined, the algorithm calculates which of liquid water, ice or other hydrated material the sample is most likely composed from.

Further work will examine more mixtures of hydrous and anhydrous material to determine detection limits.

	Precision	Recall	f1-score	Count
Anhydrous Material	0.77	1.00	0.87	10
Hydrated Minerals	1.00	0.95	0.98	22
Ice	0.91	0.91	0.91	32
Water	0.87	0.76	0.81	17

No anhydrous material is a false positive identification. 91% of ice identifications were correct and 87% of liquid water.

Simulations



Simulations modeled from 50 cm^{-1} per pixel to 200, of water, ice and gypsum spectra.

62 cm^{-1} per pixel was the lowest resolution water and gypsum could be consistently distinguished whereas water and ice were more distinct.

At low resolutions (~60 cm^{-1} per pixel in the hydration region) it is still possible to distinguish between liquid water, ice and hydrated minerals.

Conclusions

- Small scale Raman spectrometers can be used to distinguish hydrates at low resolutions
- Anhydrous material is not mistaken for hydrated
- Typically anything lower than 62 wavenumbers per pixel in the hydrations region (2800 – 4000 cm^{-1}) is necessary for separating the water and gypsum Raman bands
- Ice and liquid water can be consistently distinguished as low as 120 wavenumbers per pixel

SiCMAG – the Silicon Carbide Solid State Quantum Magnetometer

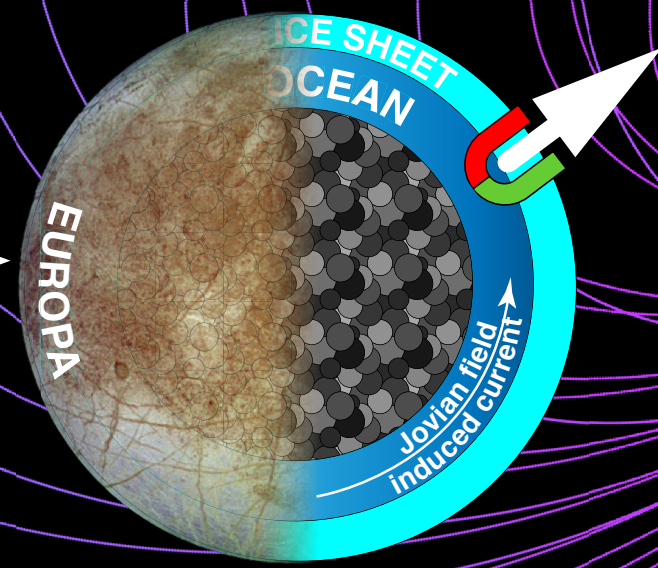
Hannes Kraus^{389R}, James P. Ashton^{389R}, Corey J. Cochrane^{389R}, Kelly Y. Wang^{355L}, Ivan Cisneros^{389T}
 NASA Jet Propulsion Laboratory, California Institute of Technology, Pasadena, CA, USA

Philip G. Neudeck, David J. Spry
 NASA John H. Glenn Research Center, Cleveland, OH, USA

Shin-Ichiro Sato, Yuichi Yamazaki, Takeshi Ohshima
 National Institutes for Quantum and Radiological Science and Technology (QST), Takasaki, Japan

Magnetometry

- high-powered, ultra precise (and expensive) compass
- detects planetary or local, crustal magnetic fields
- gives information about existing, active or erstwhile geodynamos
- can tell what lies beyond, on different scales, e.g.
 - unexploded ordnance
 - submarines
 - mining survey (ores)
 - subsurface oceans
- vector mag: tells direction of field
- scalar mag: tells strength of field



SiCMAG – NASA rationale

leveraging spin-carrying and thus magnetically sensitive atomic-scale quantum centers („defects) in Silicon Carbide (SiC) electronic devices to build a small, light-weight magnetometer

- ✓ **Tiny**
Sensor ~1in², PCB ~ credit card
- ✓ **Simple**
3x DAC, 1x ADC
- ✓ **Lightweight**
m_{sensor} < 0.1 kg, m_{total} < 0.4kg
- ✓ **Low power**
P < 1 W (anticipated)
- ✓ **Sensitivity**
~100 nT
- ✓ **Multiple sensors per spacecraft**
Boom smaller/unnecessary
- ✓ **Self-calibration**
by interleaved vector and scalar mode
- ✓ **No dead zones**
in vector (magnetoresistance) mode
- ✓ **Extreme environments**
SiC is temp- and rad-hard

EPR/EDMR

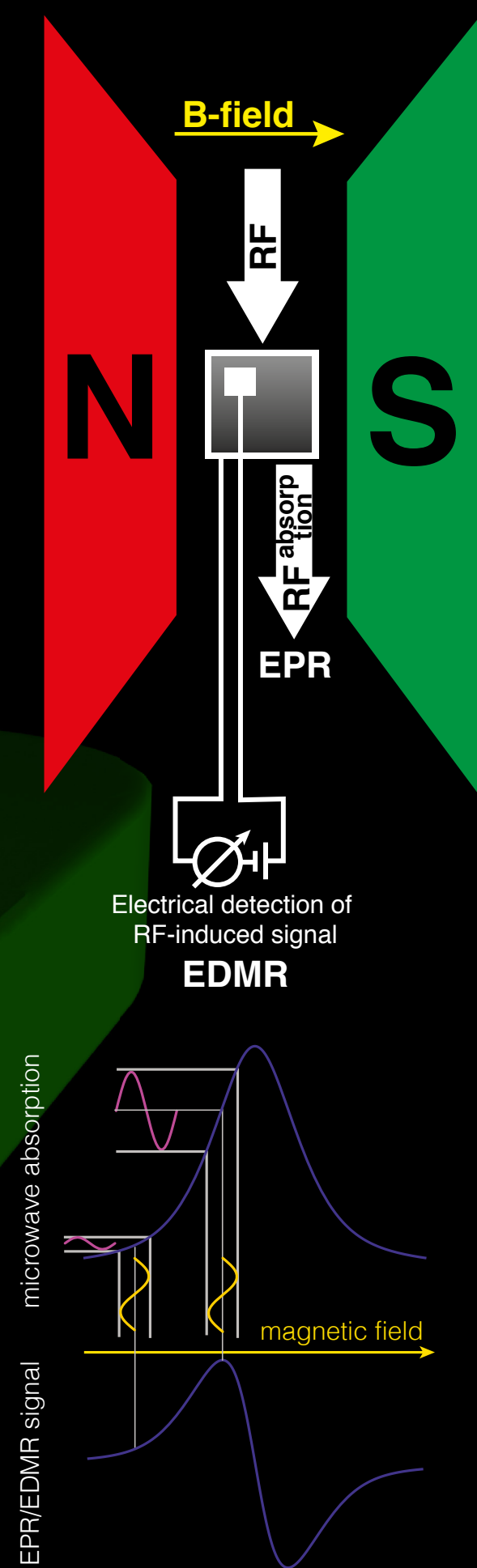
4H Silicon Carbide (SiC) carries optically, electrically and spin-active quantum centers, e.g. **silicon vacancies V_{Si}**

V_{Si} carry a high spin, whose spin states undergo a **Zeeman splitting** under an external magnetic field.

Spin **transitions** can be induced under resonance conditions $E_{Zeeman} = hv = g\mu_{Bohr} B$.

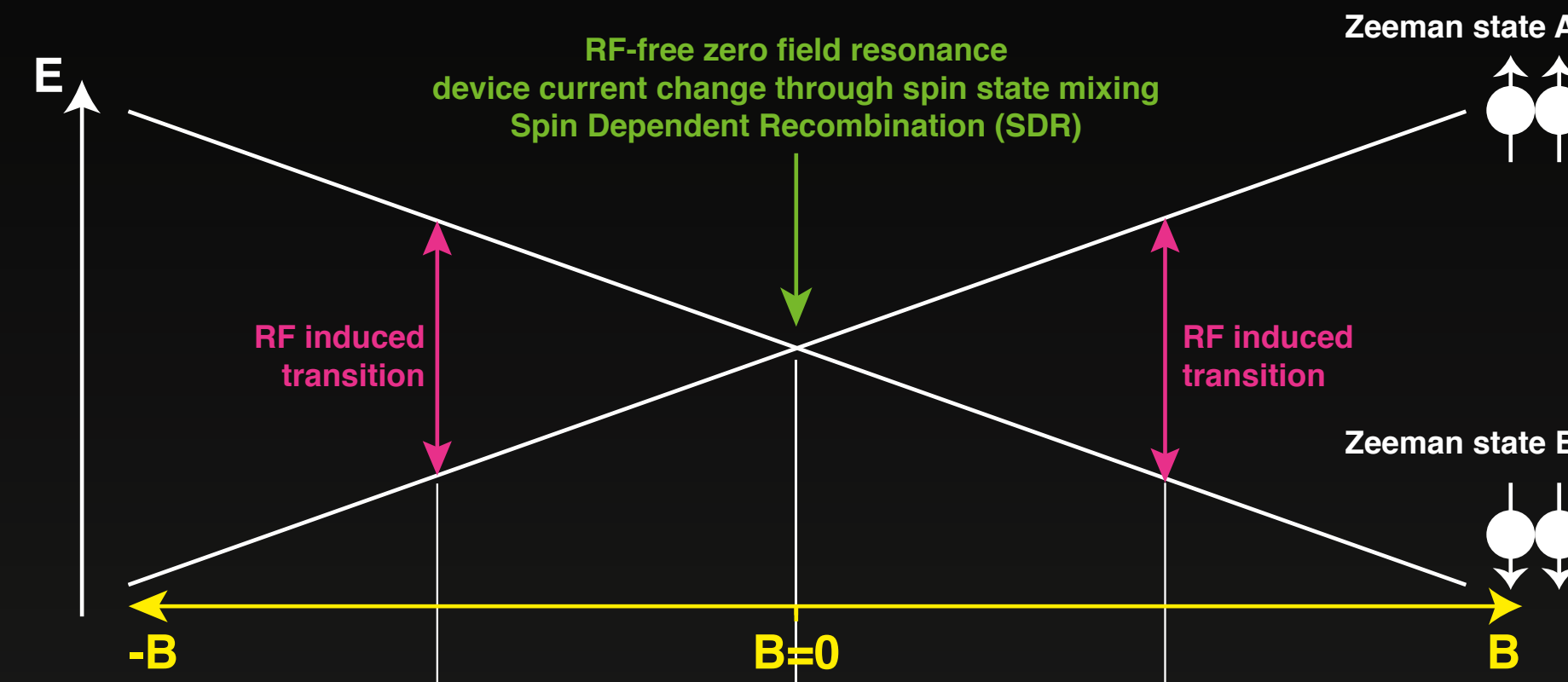
These spin transitions show up as changes in rf absorption (this is called electron paramagnetic resonance – EPR), or as changes in **device current** (electrically detected magnetic resonance – EDMR)

The device current also changes close to **zero field**, even without RF excitation, when the involved spin states become **degenerate** (spin dependent recombination – SDR).

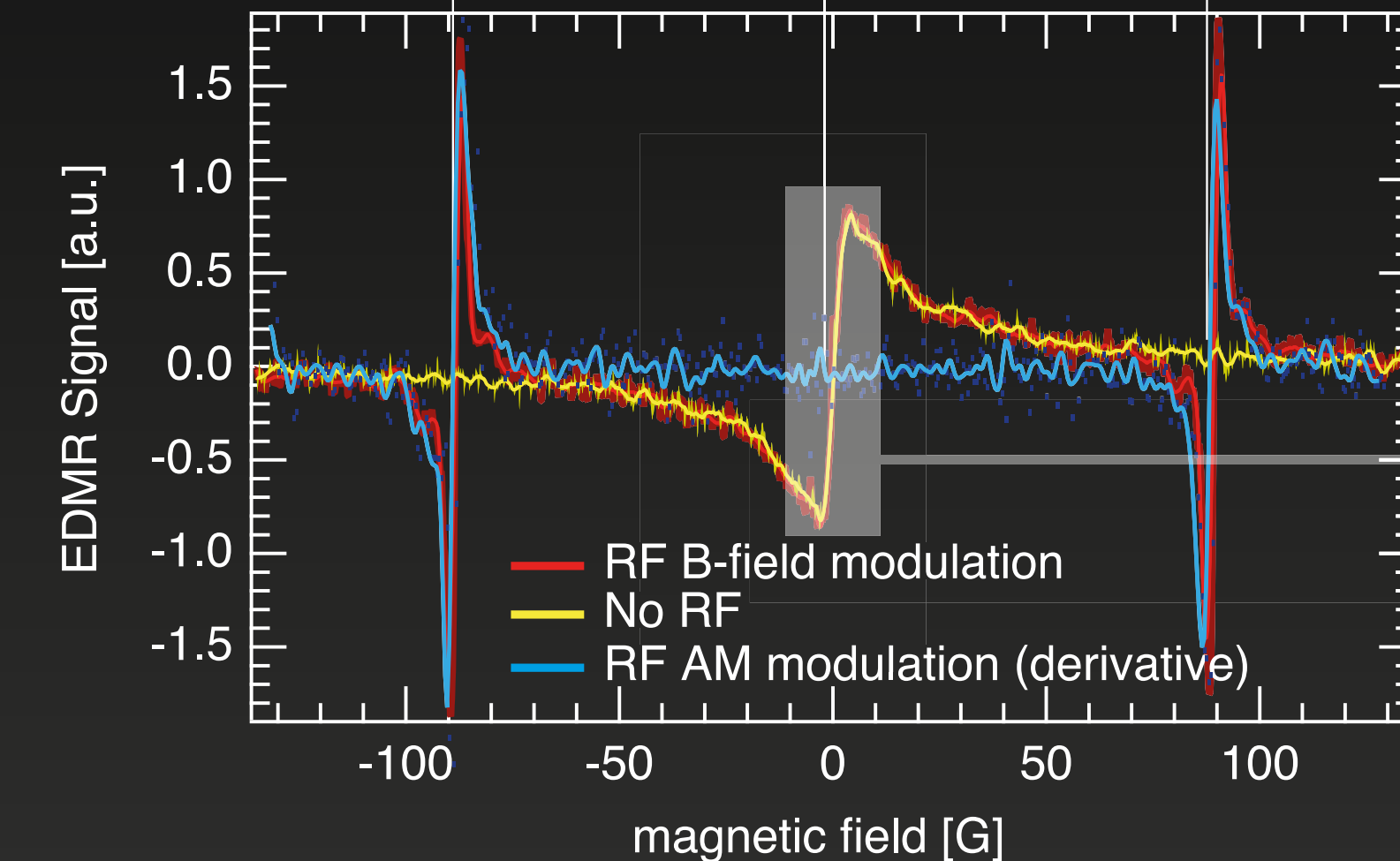


EPR/B-EDMR signal is reconstructed through locking on a kHz modulation of the B-field x-axis, thus the signal response is in **first derivative**.

Strongly simplified Zeeman splitting

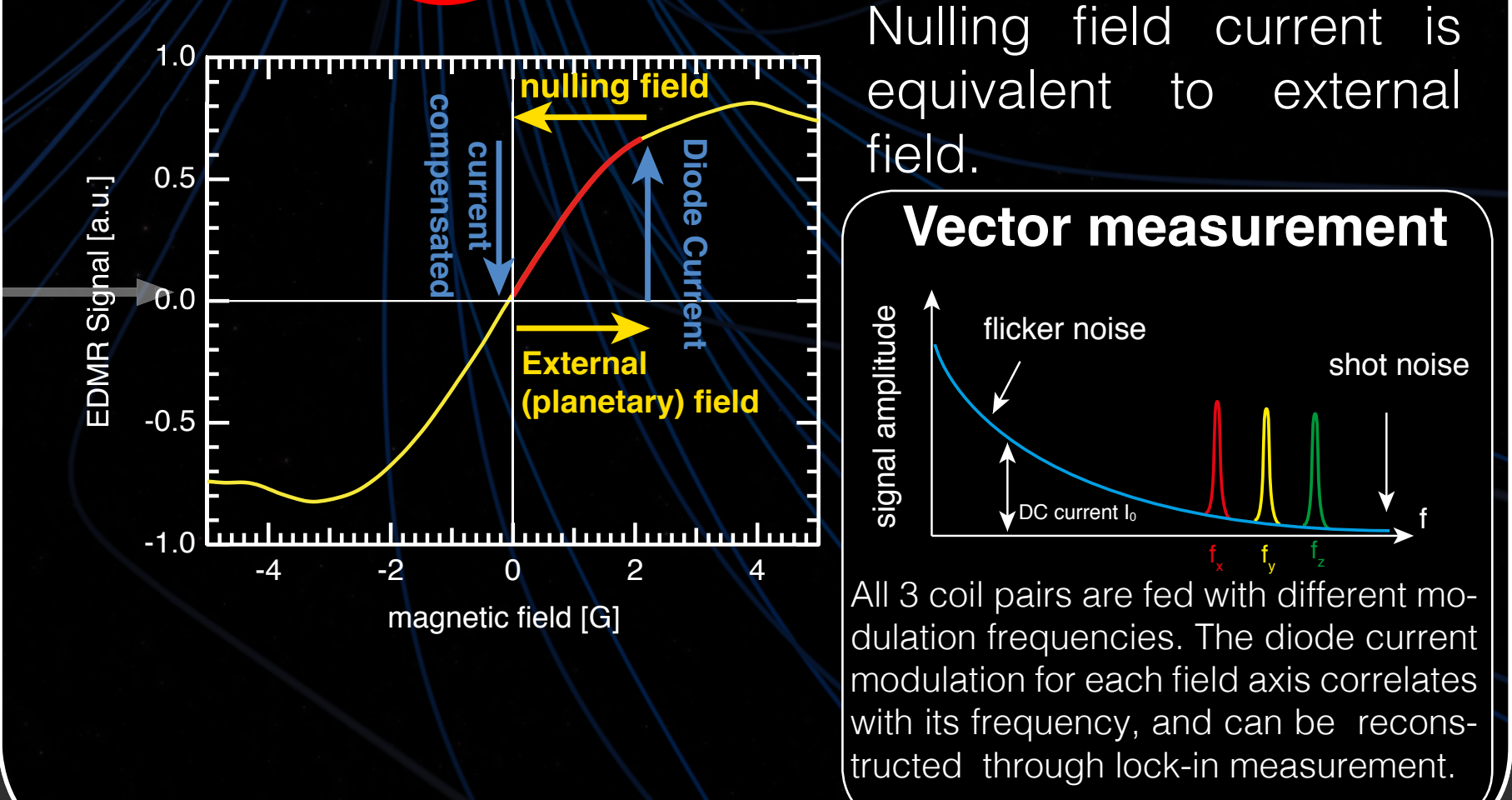
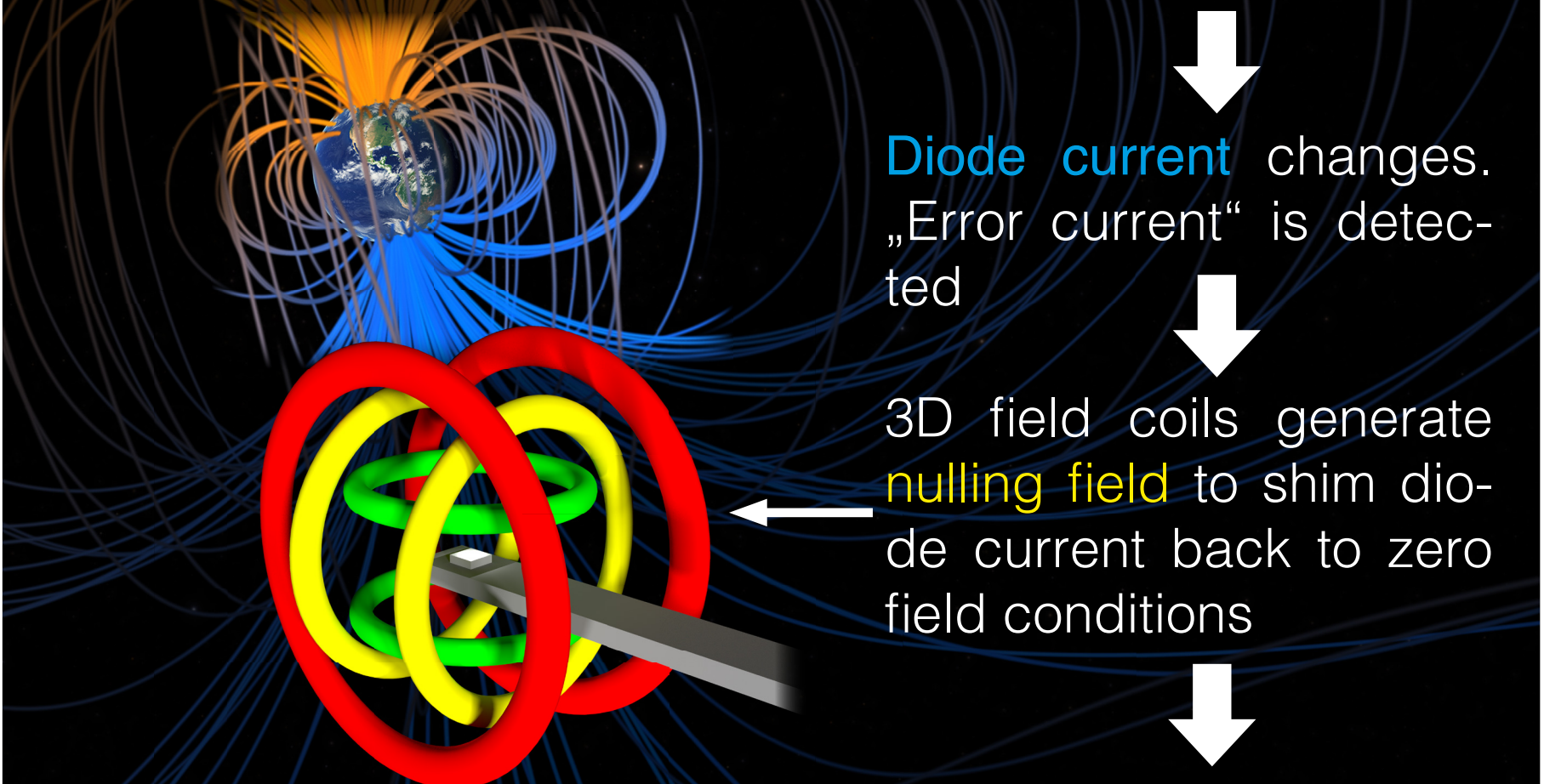


4H SiC EDMR response



SDR Magnetometry

external magnetic field on sensor. External (planetary) magnetic field lifts spin state degeneracy

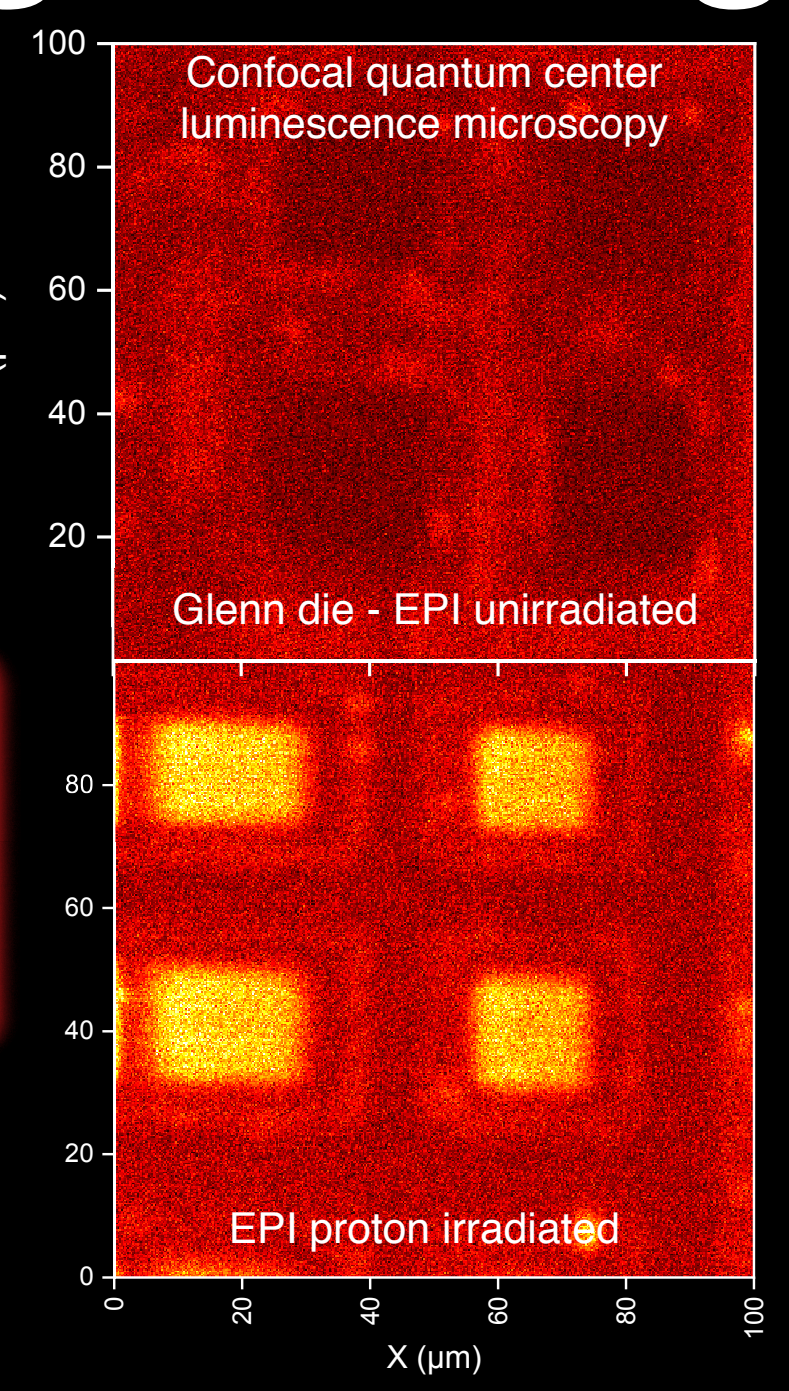
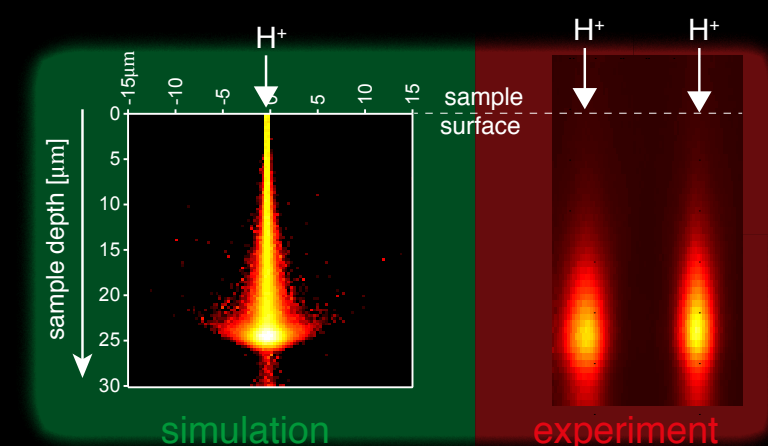
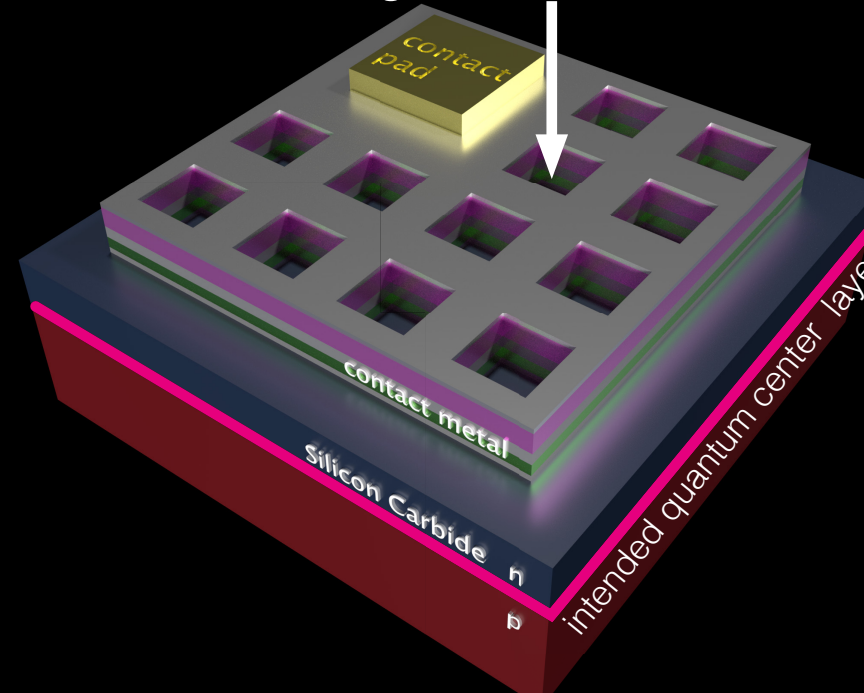


$$\frac{\delta B}{\sqrt{\Delta f}} = 2\sigma\sqrt{\pi e} \frac{\sqrt{I_0}}{\Delta I} \left(\frac{T}{\sqrt{Hz}} \right)$$

Defect engineering

Magnetometer sensitivity is governed by SDR signal strength ΔI – recent sensitivities are in the 100nT/ \sqrt{Hz} range. NASA Glenn provides tailor-made diode devices, which are screened for sensitivity performance and stability. Additionally, device quantum center density is increased through irradiation. Another avenue (going for linewidth σ) are isotopically purified SiC epilayers.

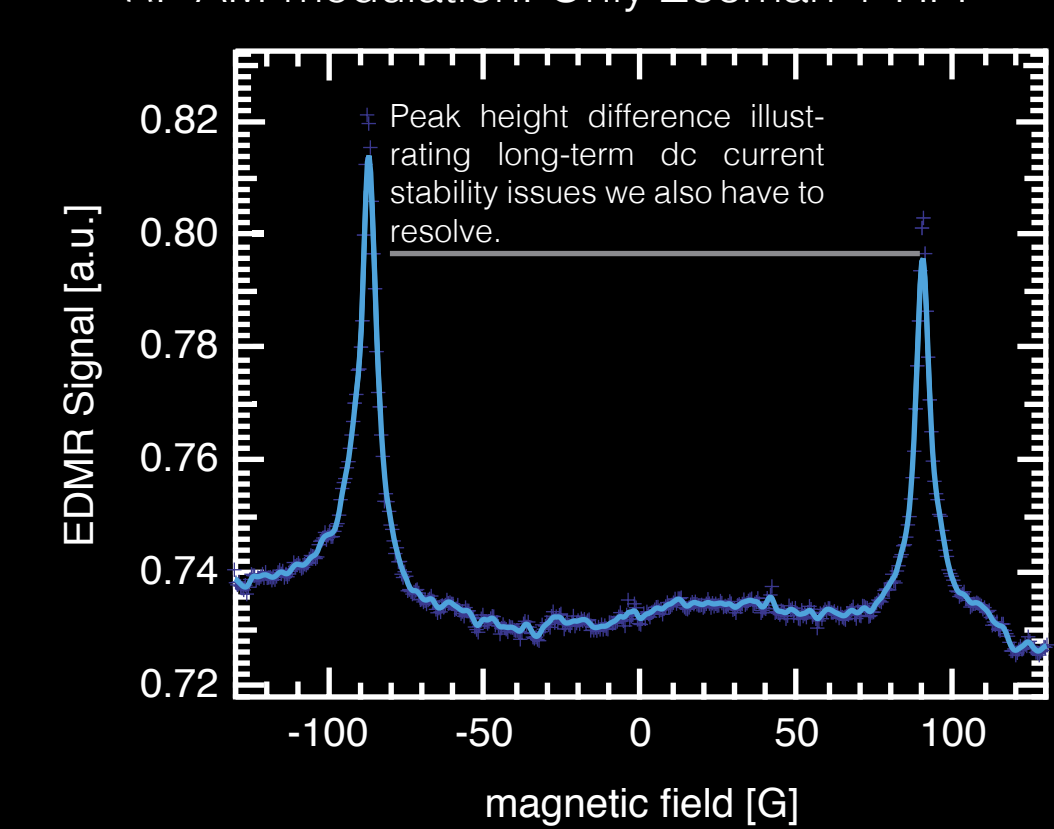
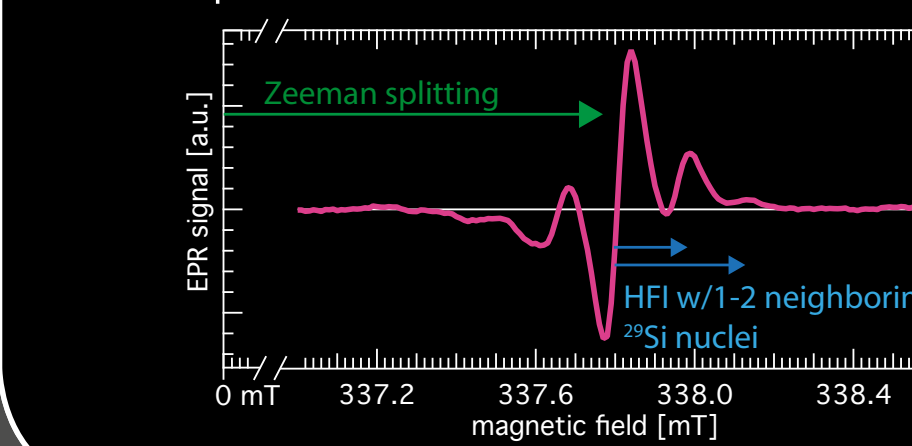
Irradiation through contact windows



Self-calibration

$$\mathcal{H} = g\mu_B S\vec{B} + S^T D S + S^T A I - S_a^T J S_b - g_N \mu_N \vec{B}^T I_Z + I^T Q I$$

Quantum centers in SiC offer potential for self-calibration, as some of the features in the signal are deriving from sections of the spin hamiltonian that are partly or completely relying on natural atomic constants. E.g. the **zeeman splitting** can calibrate the magnetic field against rf frequency, while the **hyperfine interaction (HFI)** returns a completely independent spectral standard.



C. Cochrane et al.
 Vectorized Magnetometer for Space Applications
 Sci. Rep. 6, 37077 (2016)



T. Ohshima, T. Sato, H. Kraus et al.
 Silicon Vacancy [...] towards quantum sensing
 J. Ph. D.: Appl Phys 51, 33 (2018)



H. Kraus et al.
 3D Proton Beam Writing of Vacancy Spins in SiC
 Nano Lett. 17, 2865 (2017)



C. Cochrane, H. Kraus, P. Neudeck, D. Spry, J. Ashton et al.
 Magnetic Field Sensing with 4H SiC diodes: N vs. P implantation
 Mat. Sci. For. 294, 988 (2019)



Electronics

First step of electronics design completed: Two-board approach, with one power- and one measurement/processing board. Next steps: Firmware programming, and ASIC integration.

Injection locking of chip-scale mid-infrared frequency combs based on interband cascade lasers

Author: **Lukasz A. Sterczewski¹ (389R)**

Co-authors: **M. Bagheri¹ (389), C. Frez¹ (389), C. L. Canedy², I. Vurgaftman², M. Kim³, C. S. Kim², C. D. Meritt², W. W. Bewley², and J. R. Meyer²**

¹NASA Jet Propulsion Laboratory, Pasadena, CA

²Naval Research Laboratory, Washington, DC

³Key W Corporation, Hanover, MD

INTRODUCTION

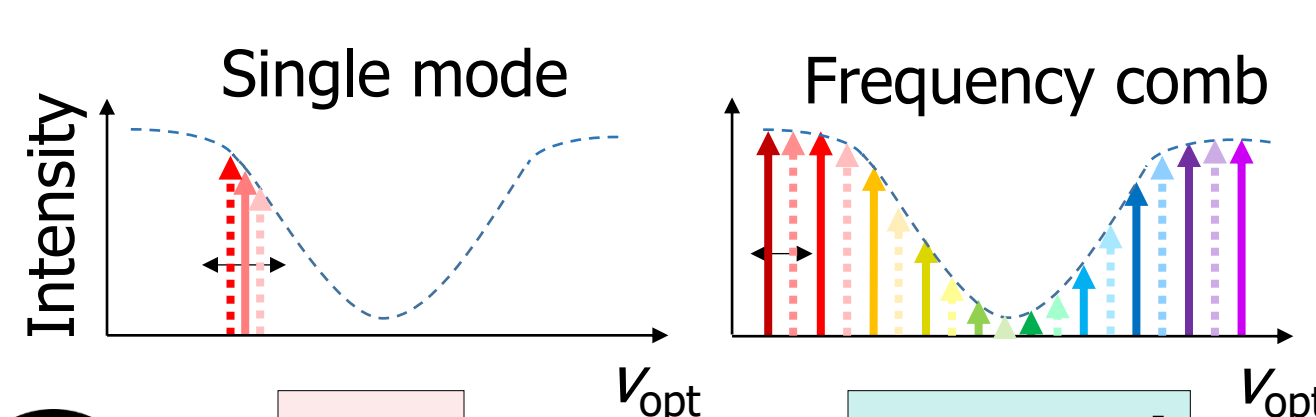
The interband cascade laser (ICL) frequency comb developed in the Microdevices Laboratory is a unique electrically-pumped source of coherent mid-infrared laser radiation for dual-comb spectroscopy, with excellent suitability for scarce power availability conditions. The ICL comb can extend the functionality of tunable laser spectrometers (TLS) by enabling simultaneously broadband and high resolution measurements without any moving parts with <1 W of power consumption.

PROBLEM STATEMENT

The long-term stability of the ICL comb is insufficient. The laser is sensitive to optical feedback and rapidly changes its mode structure. **Here we experimentally verify, if the repetition rate of ICL combs can be controlled and stabilized via external microwave signal injection.**

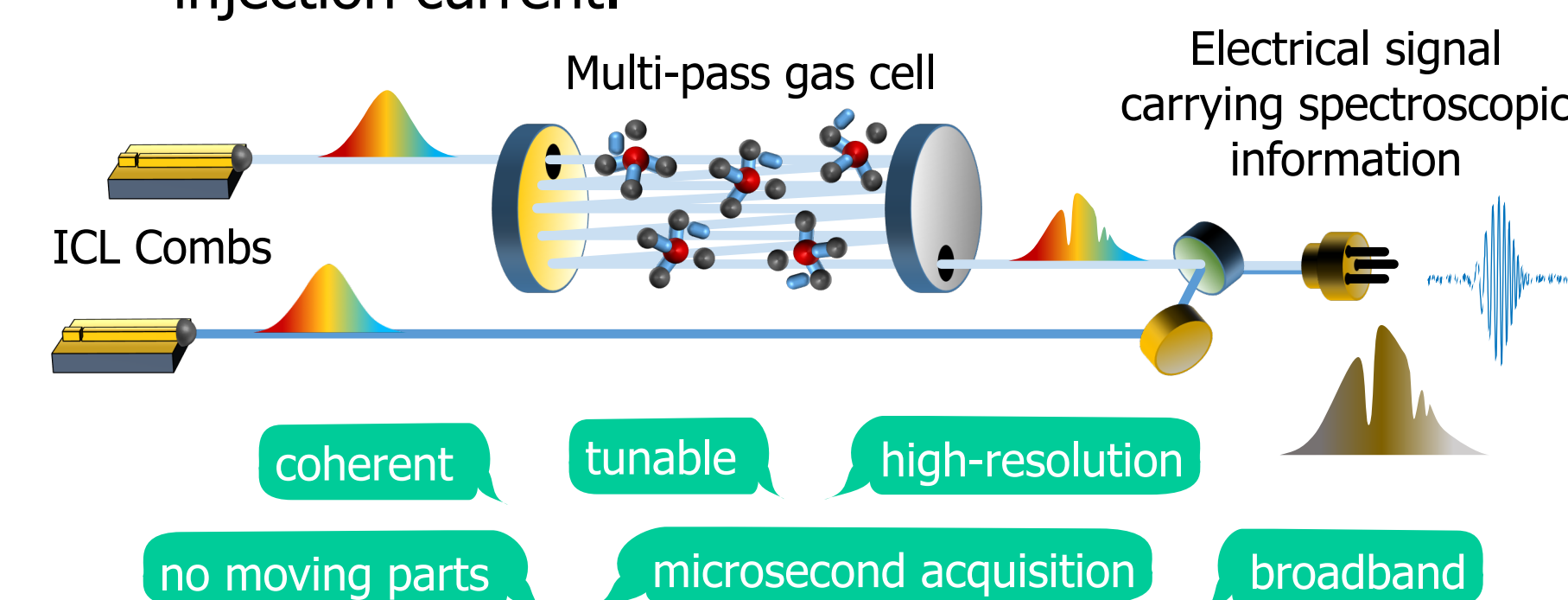


KEY IDEAS FOR THE FUTURE SPECTROSCOPIC INSTRUMENT



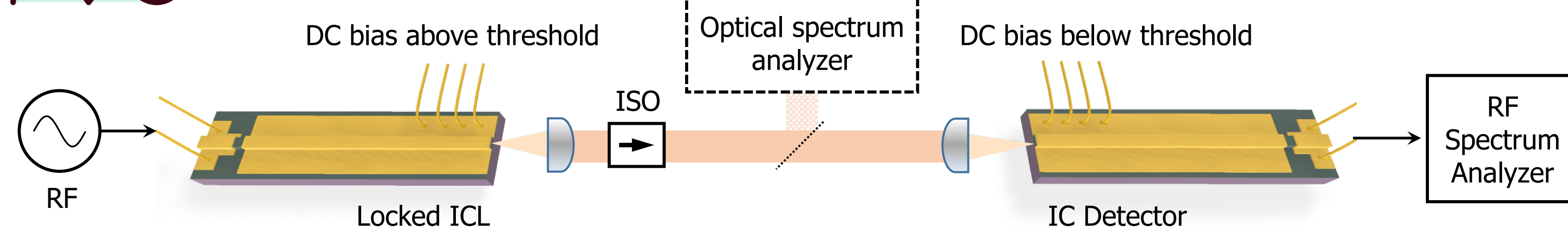
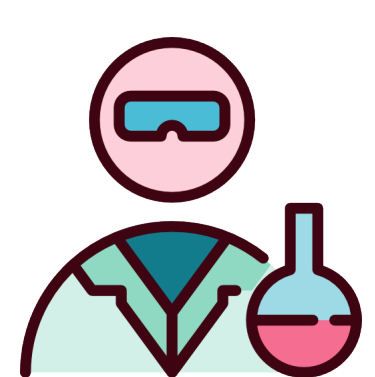
Now A pair of ICL combs is optically beaten on a fast infrared photodetector. This yields an **electrical signal carrying spectroscopic information known as the interferogram**, analogous to that recorded in Fourier Transform Spectroscopy (FTS).

The mid-infrared laser used in the Curiosity mission is a single mode (frequency) source. We propose to use an ICL device emitting more than a **hundred phase-locked lines generated within a mm-size cavity with ~10 μW per line**. All the lines remain locked when their frequency is swept via injection current.

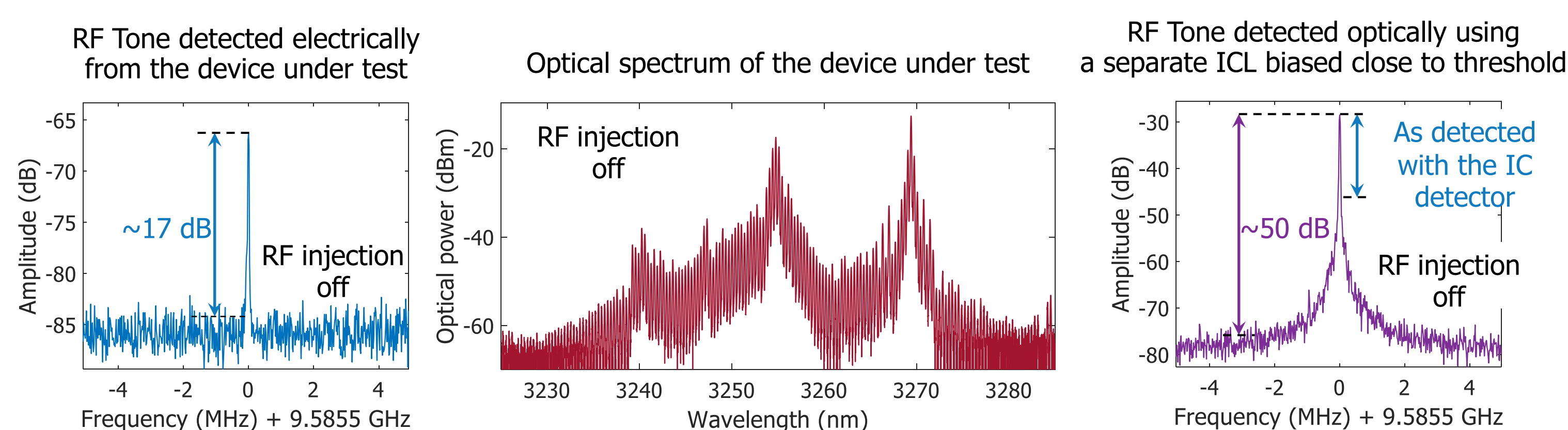


EXPERIMENT

1. We bias an ICL above threshold in a frequency comb regime, while a second device processed from the same wafer operates close to threshold as a fast room-temperature IC photodetector. The isolator (ISO) minimizes optical feedback that would corrupt the comb generation.



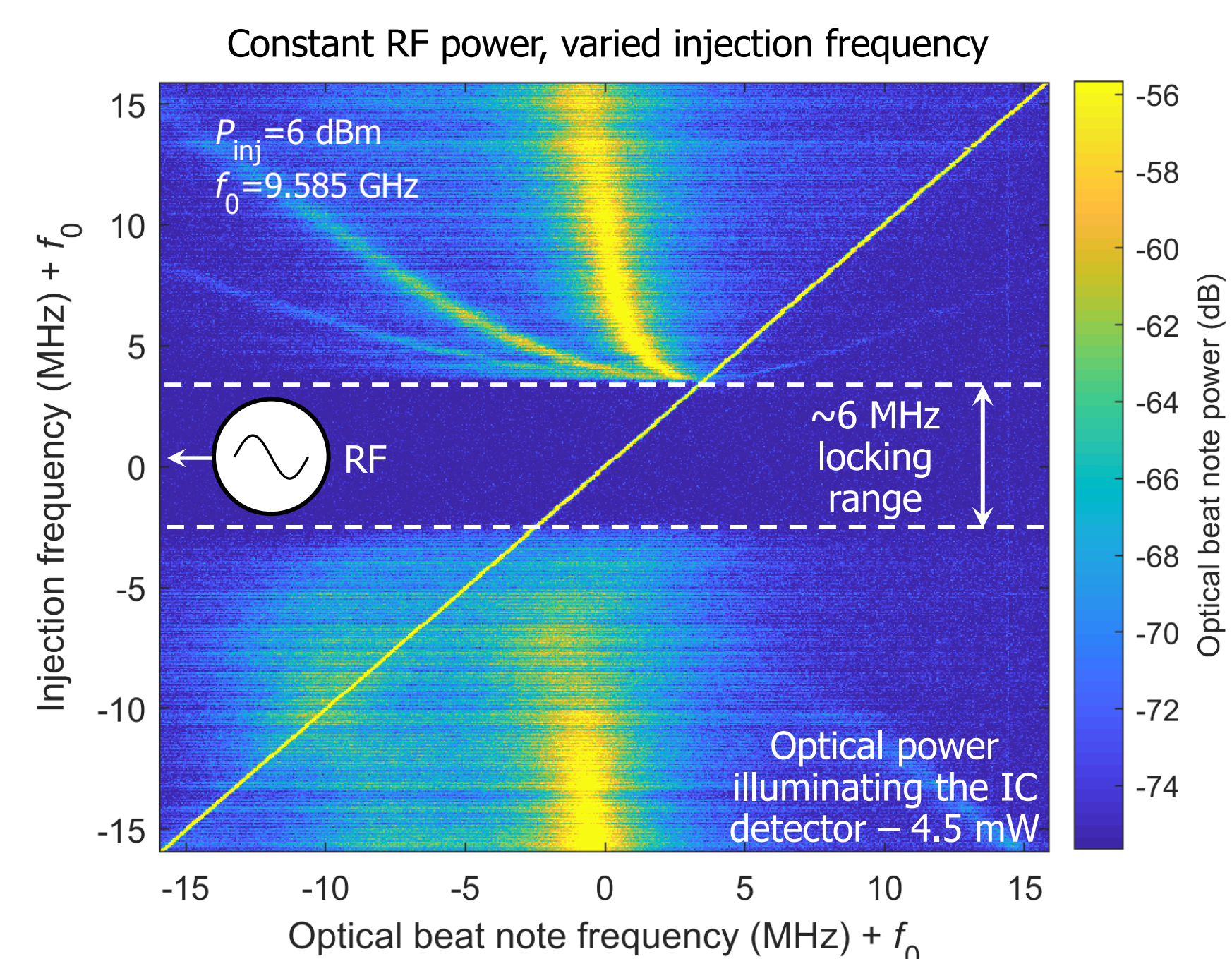
2. We record the characteristics of a free-running device at $I=214$ mA, $U=4.3$ V, $T=12^\circ\text{C}$.



3. We inject an external microwave signal (RF) and repeat the above measurements.

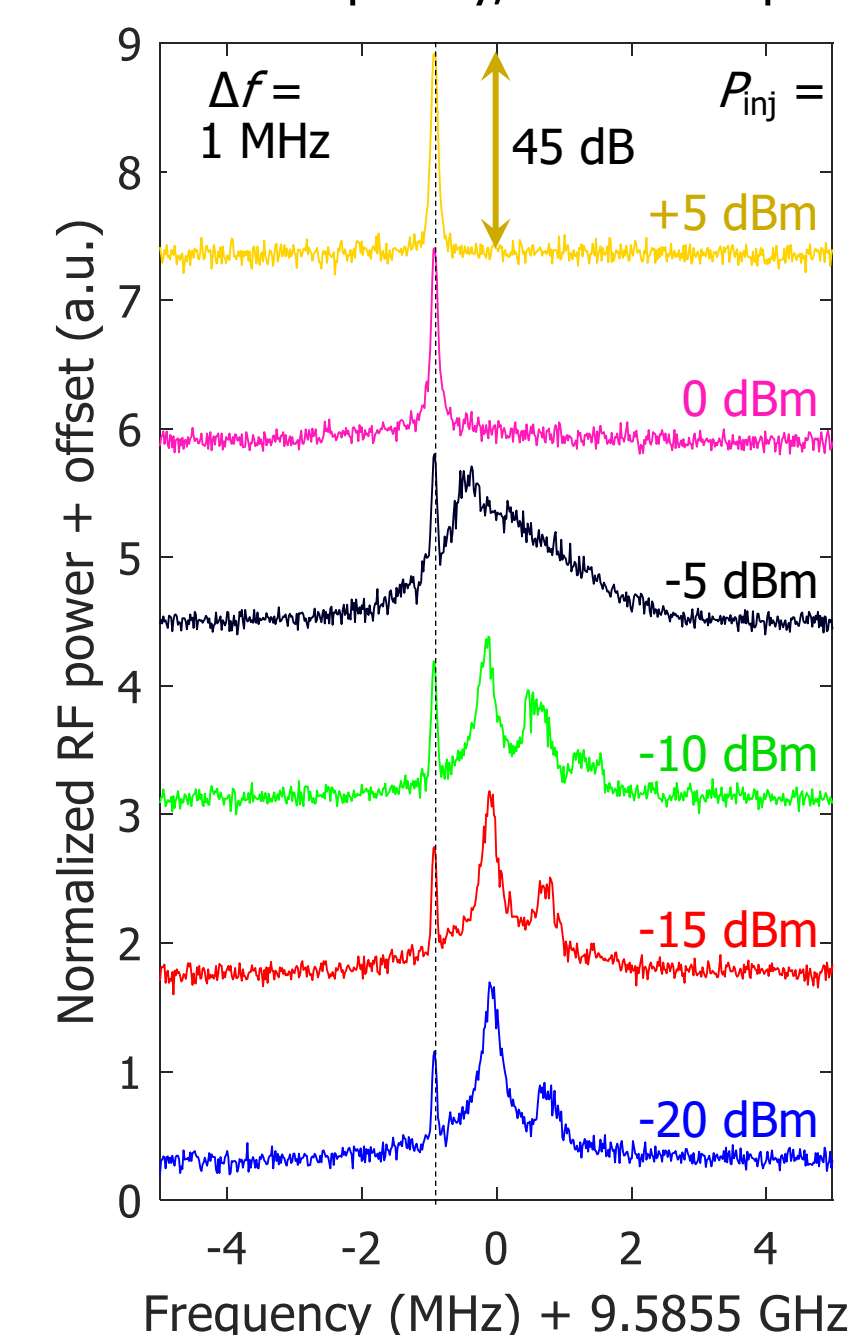
RESULTS

With +6 dBm of injected RF power modulating the absorber section, the locking range reaches 6 MHz.

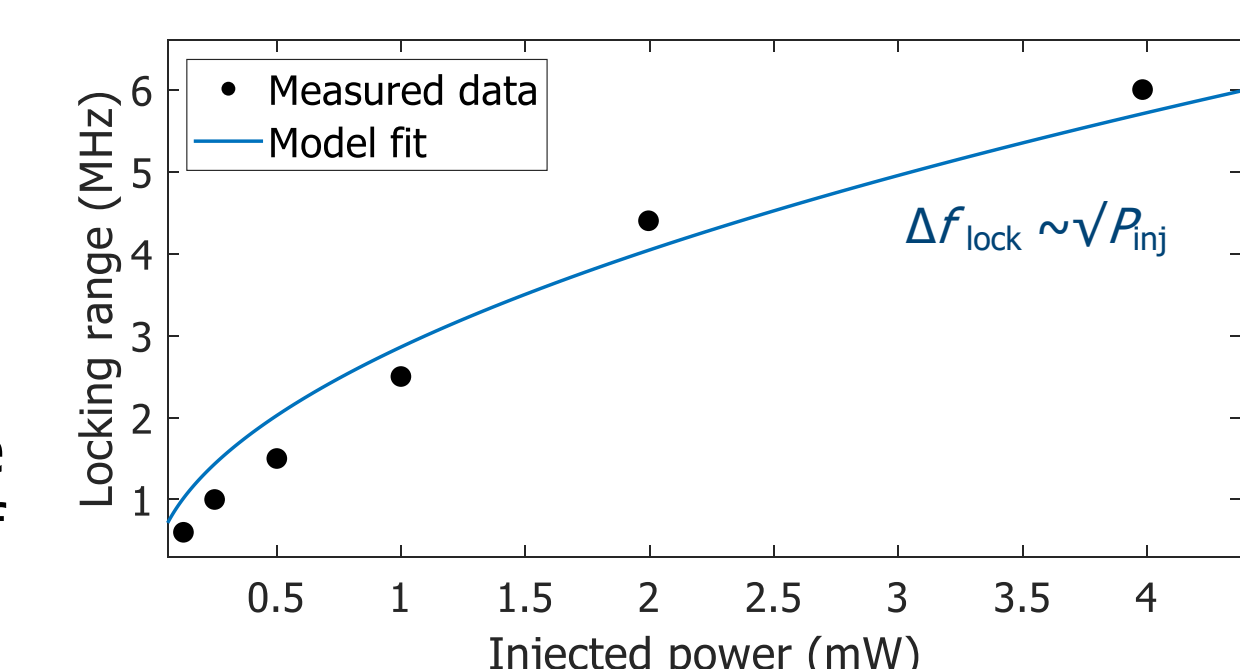
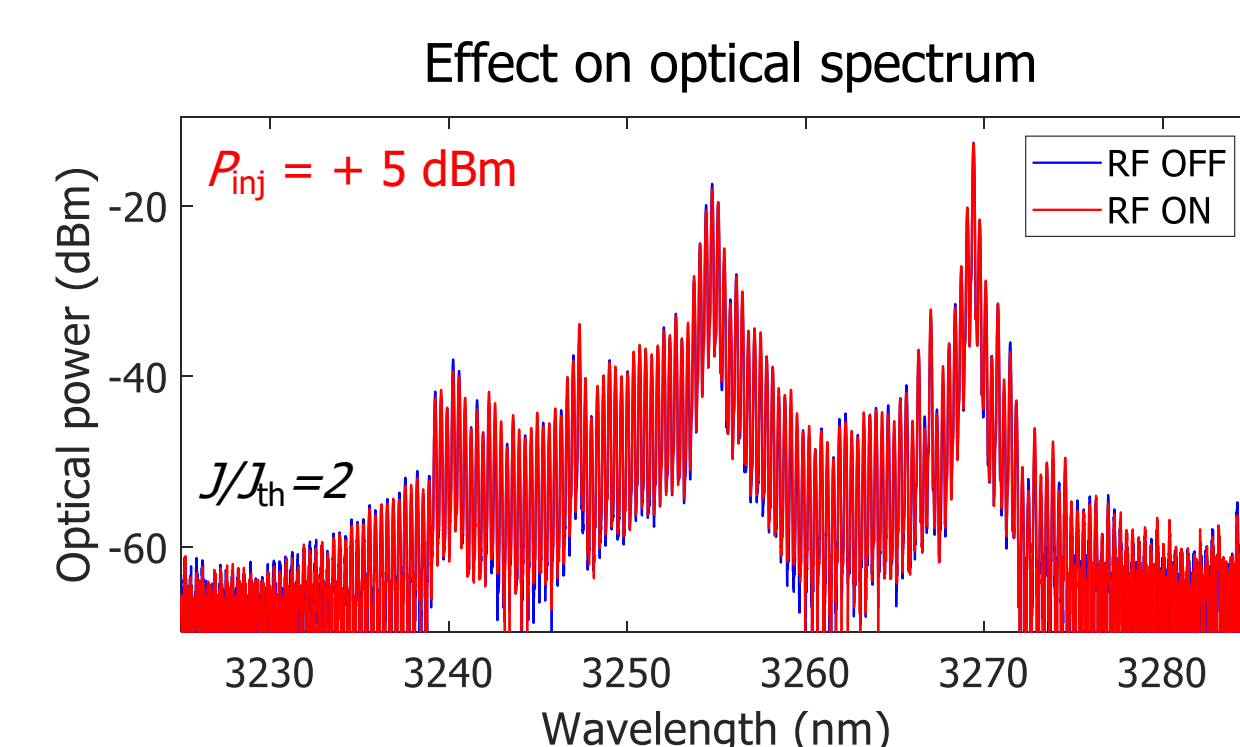


When the injected frequency is 1 MHz away from the natural f_{rep} at power levels above 0 dBm, **the device faithfully follows the injected signal** with more than 45 dB of carrier-to-noise ratio.

Constant frequency, varied RF power



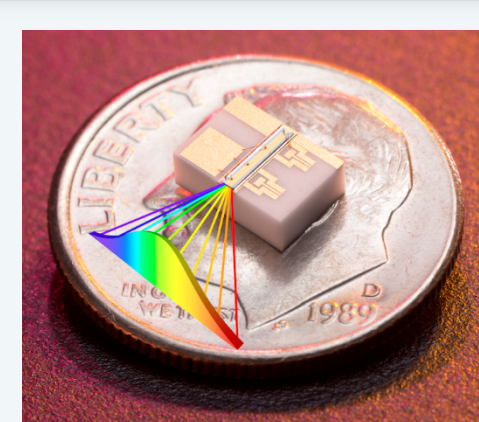
Moderate injected power levels have almost no effect on the shape of the optical spectrum.



The measured locking range follows the square root of injected RF power model with good agreement.

CONCLUSIONS AND OUTLOOK

Interband cascade laser frequency combs can be stabilized using external microwave injection. Milliwatt levels of microwave signal are sufficient to suppress the noise pedestal of the optically detected RF tone, which is a signature of improved comb stability. This will translate into prolonged averaging capabilities.



Microwave injection enables locking of the comb's repetition rate to a frequency standard such as an atomic clock. This feature will facilitate optical frequency axis calibration in the instrument.

To evaluate the gain of the locking technique in spectroscopic terms, we are setting up a dual-comb experiment wherein we will optically multi-heterodyne two injection-locked ICL combs. We are also testing the feasibility of performing **gapless frequency comb spectroscopy** by exploiting the increased current and temperature ranges where a frequency comb is formed thanks to external microwave modulation. Finally, we are trying to flatten the optical spectrum via gain engineering.

Acknowledgements

This work was supported under National Aeronautics and Space Agency's (NASA) PICASSO program and was in part performed at the Jet Propulsion Laboratory (JPL), California Institute of Technology, under contract with the NASA. L. A. Sterczewski's research was supported by an appointment to the NASA Postdoctoral Program at JPL, administered by Universities Space Research Association under contract with NASA.

Isolation, Concentration, and Characterization of Icy Worlds Samples via Flow Cytometry

Author: Nicholas Tallarida (389)

Wayne Schubert (352) and James Lambert (389)

Life on Icy Worlds, if it exists,
is anticipated to be:

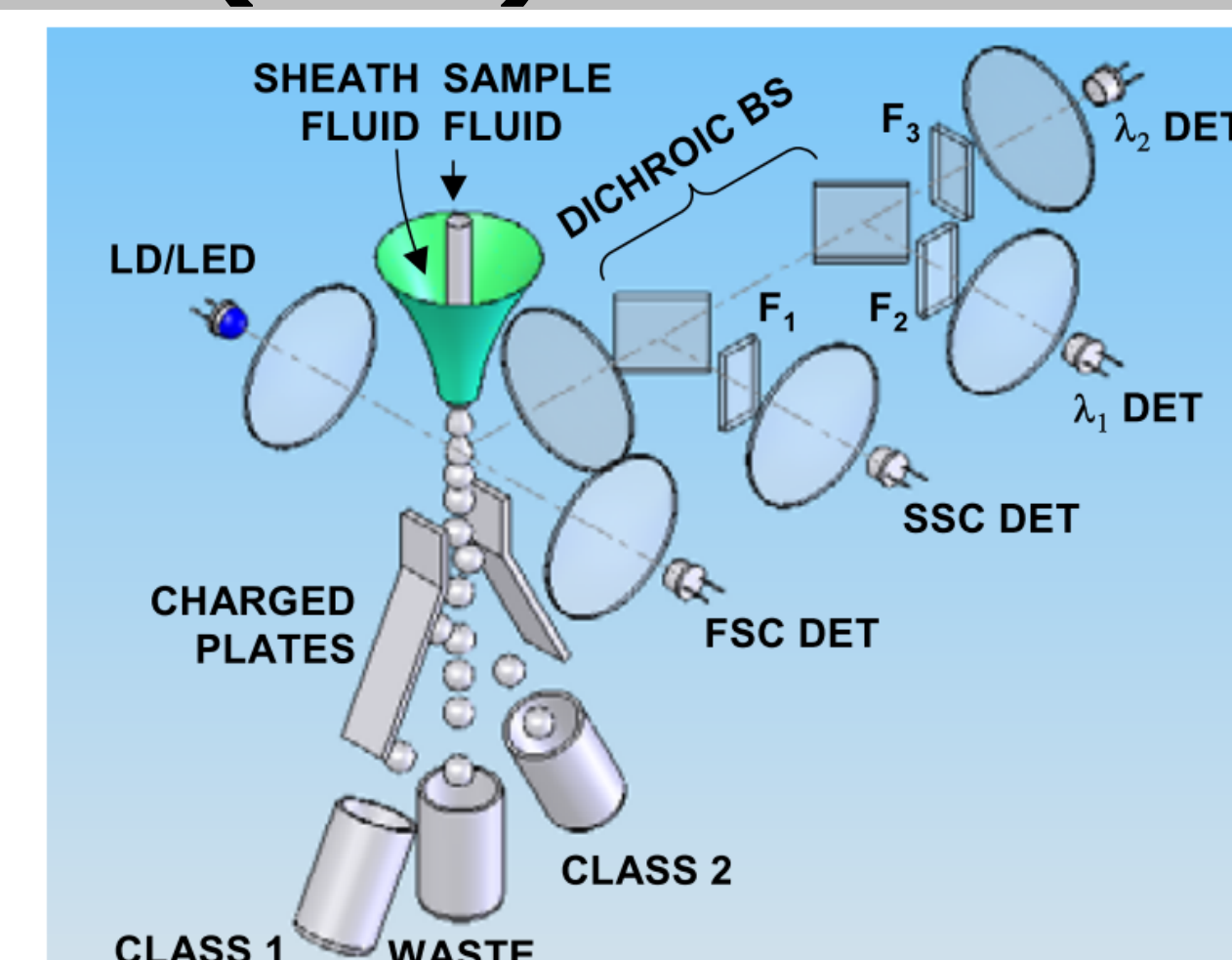
rare, < 300 cells/mL,

microscopic, 0.7 - 3.0 μm , and

hidden under a 80-98% abiotic particle
background.

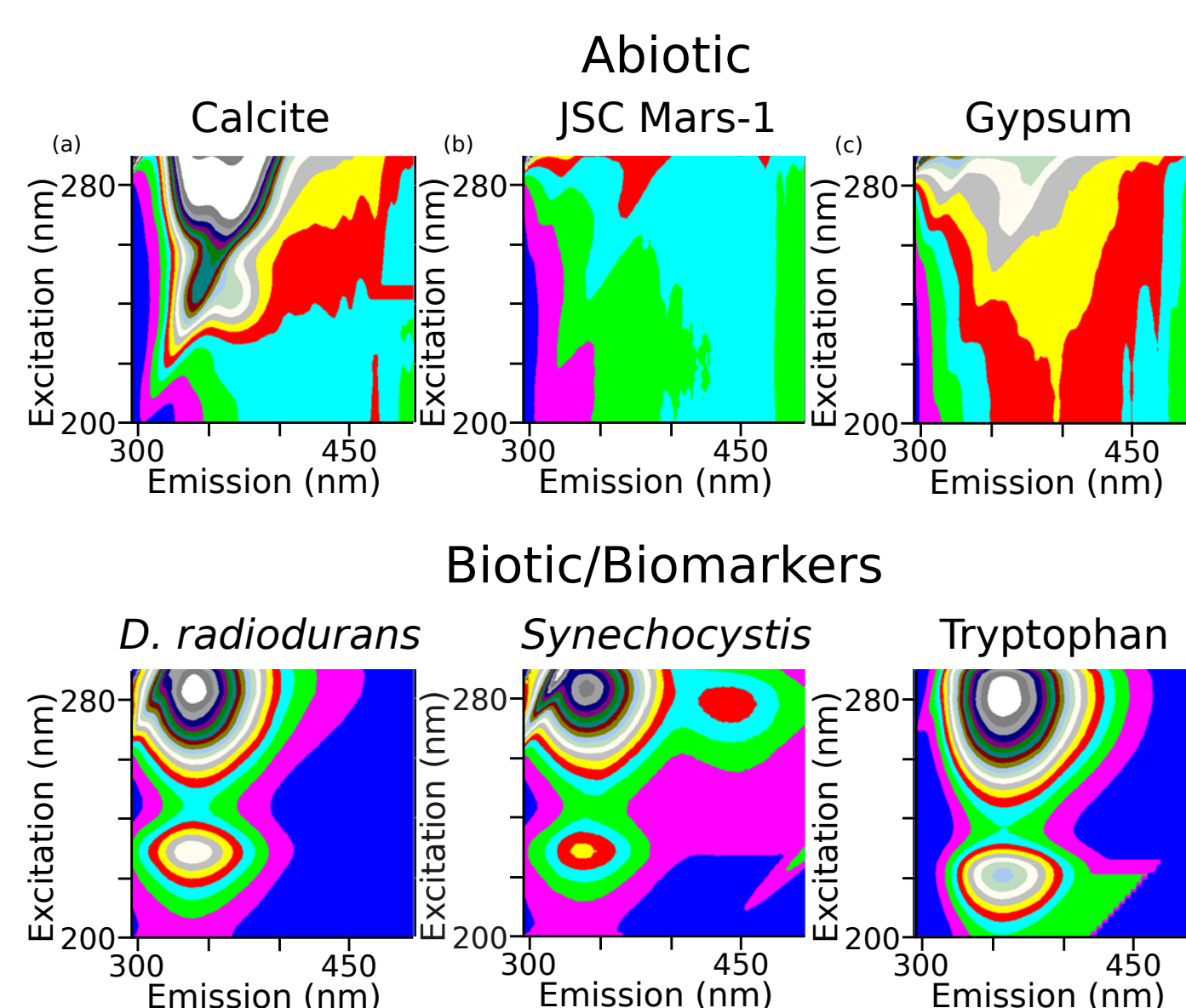
To determine whether life had or does exist in the inhabitable environments of icy worlds like Europa and Enceladus, NASA will have to use techniques capable of measuring microscopic bacterial life at extremely low concentrations (< 300 cells/mL) and in the presence of a large abiotic background. This could require the processing of large volumes of surface water-ice.

While many instruments are great at finding and characterizing bacteria, the flow cytometer is the medical and research industry standard for detecting, isolating, characterizing, and concentrating cells and bacteria. A purpose-built sorting flow cytometer could boost cell concentrations up to 10^6 cells/mL while separating out inorganic contaminants.



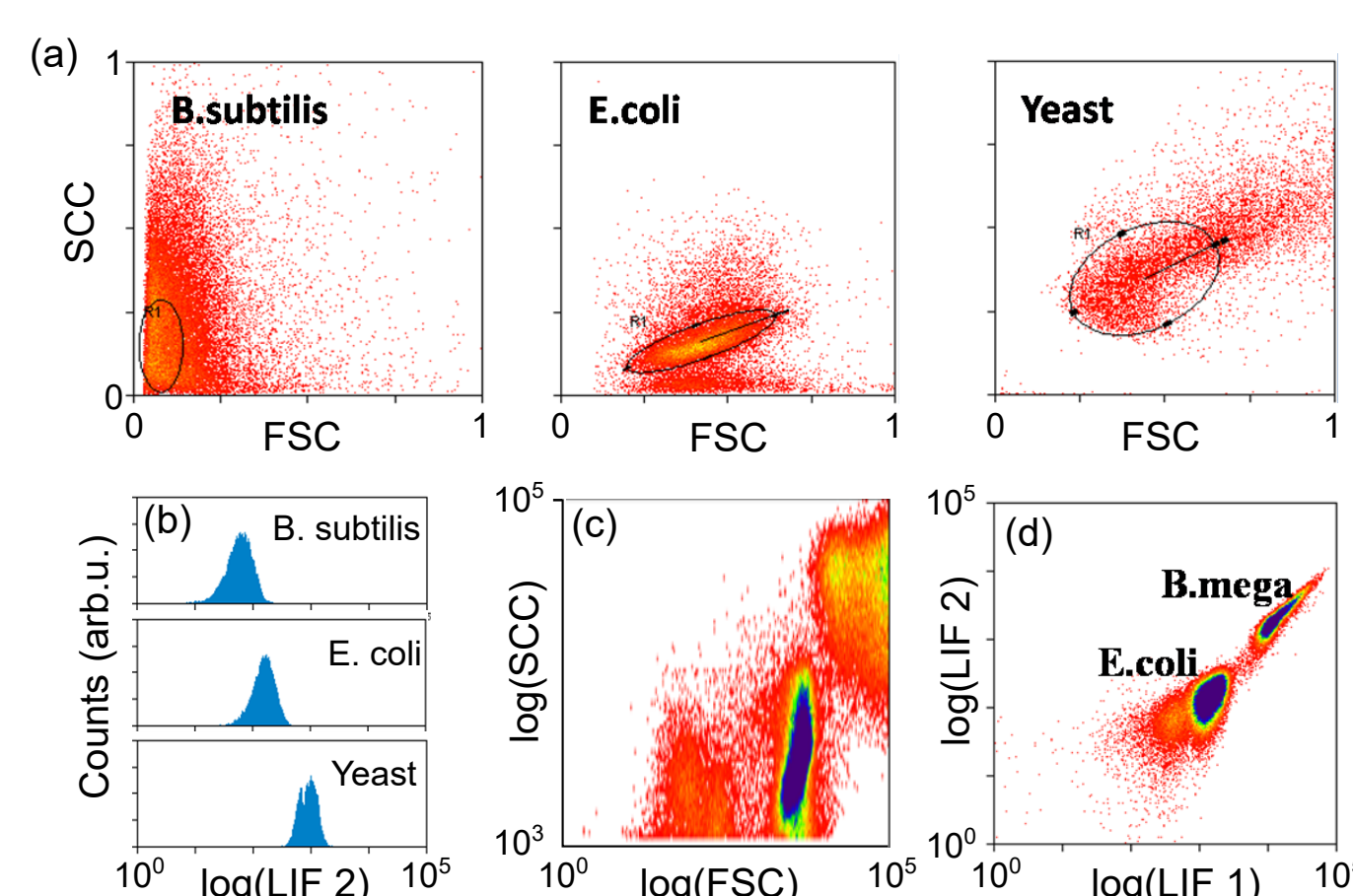
Flow Cytometry irradiates a narrow jet of liquid sample, contain particles, with laser light. Fluorescence and scattered light is collected, sorted by color, and measured on a bank of detectors. The signal intensity as a function of color and scattering angle can be used to classify and sort (via charged plates) particles in real time.

UV-induced fluorescence of
abiotic and biotic samples
differ substantially.



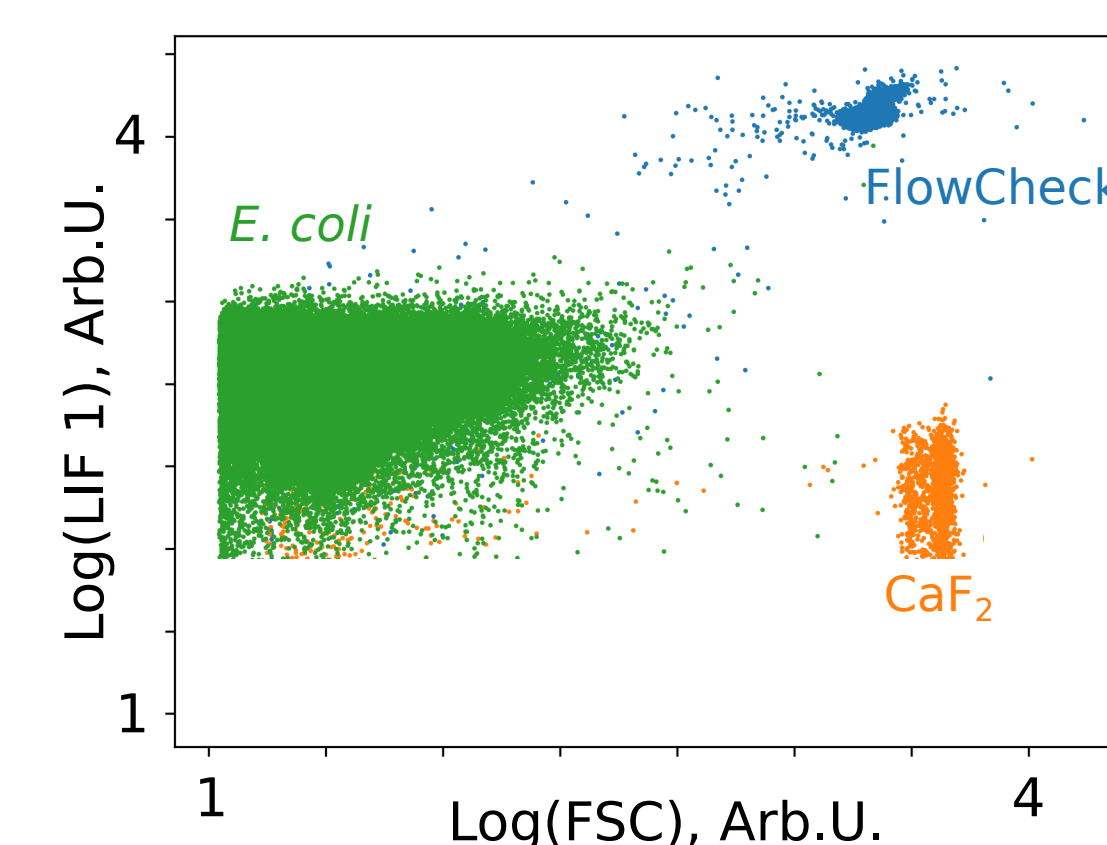
Excitation-Emission Matrices reveal the stark differences between common biotic and abiotic samples. Exciting samples at 275 nm directly excites biotic samples, hitting the large absorption band at ~ 280 nm.

Bacteria can be
detected and isolated
using intrinsic fluorescence,
without reagents.



(a) The forward (FSC) vs side scatter (SSC) plots of the three unstained cell populations captures differences between cell types as larger FSC relates to large cell size. (b) The LIF intensity changes with cell size and composition. (c) While the SSC vs FSC plot for a mixture of *E. coli* and *B. megaterium* shows distinct clustering, the plot of the UV-induced fluorescence (d) shows much better separation of the two cell populations. FSC/SSC - 488 nm excitation, LIF 1/LIF 2 - 275 nm excitation.

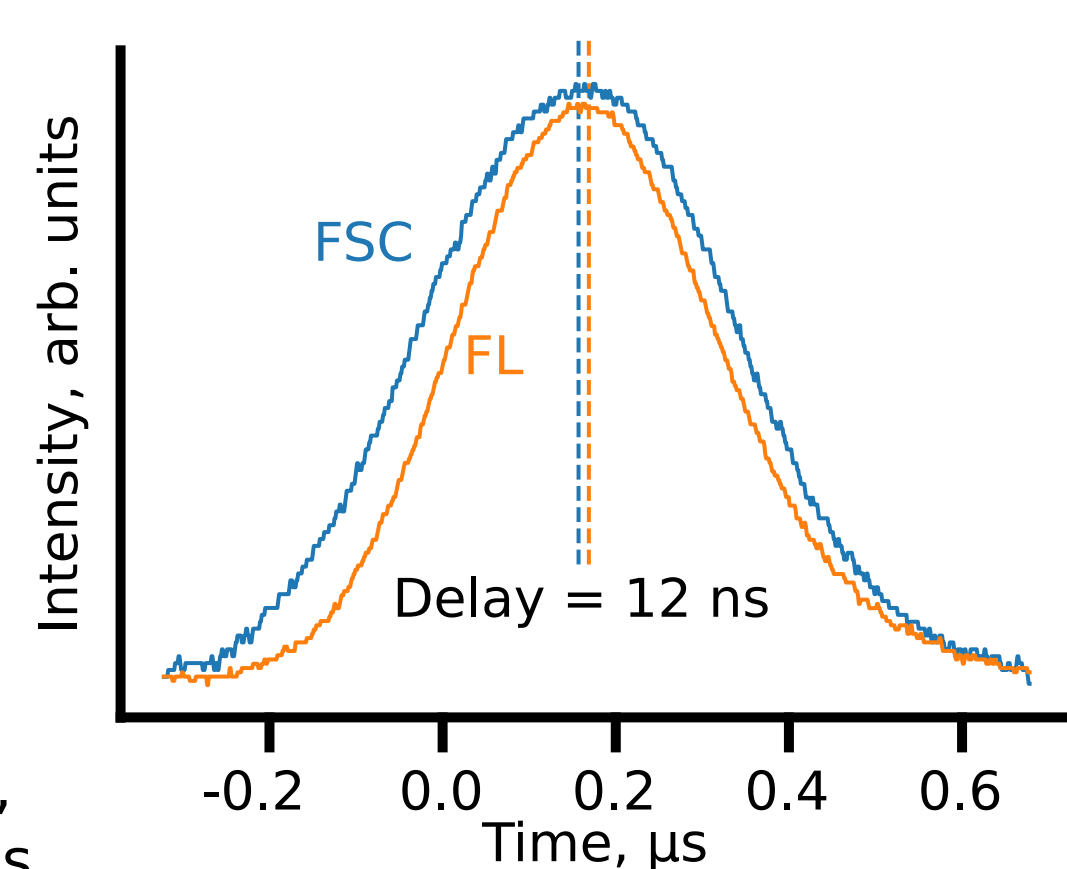
Bacteria can be distinguished from
raw minerals with flow Cytometry



As a step towards the processing of realistic icy worlds simulants, a mixture of *E. coli*, calibration beads (FlowCheck), and raw powdered fluorite (CaF_2) were processed sequentially. Distinct populations are observed with both the scattered light (488 nm excitation) and the fluorescence channel (275 nm excitation, 340 ± 5 nm emission).

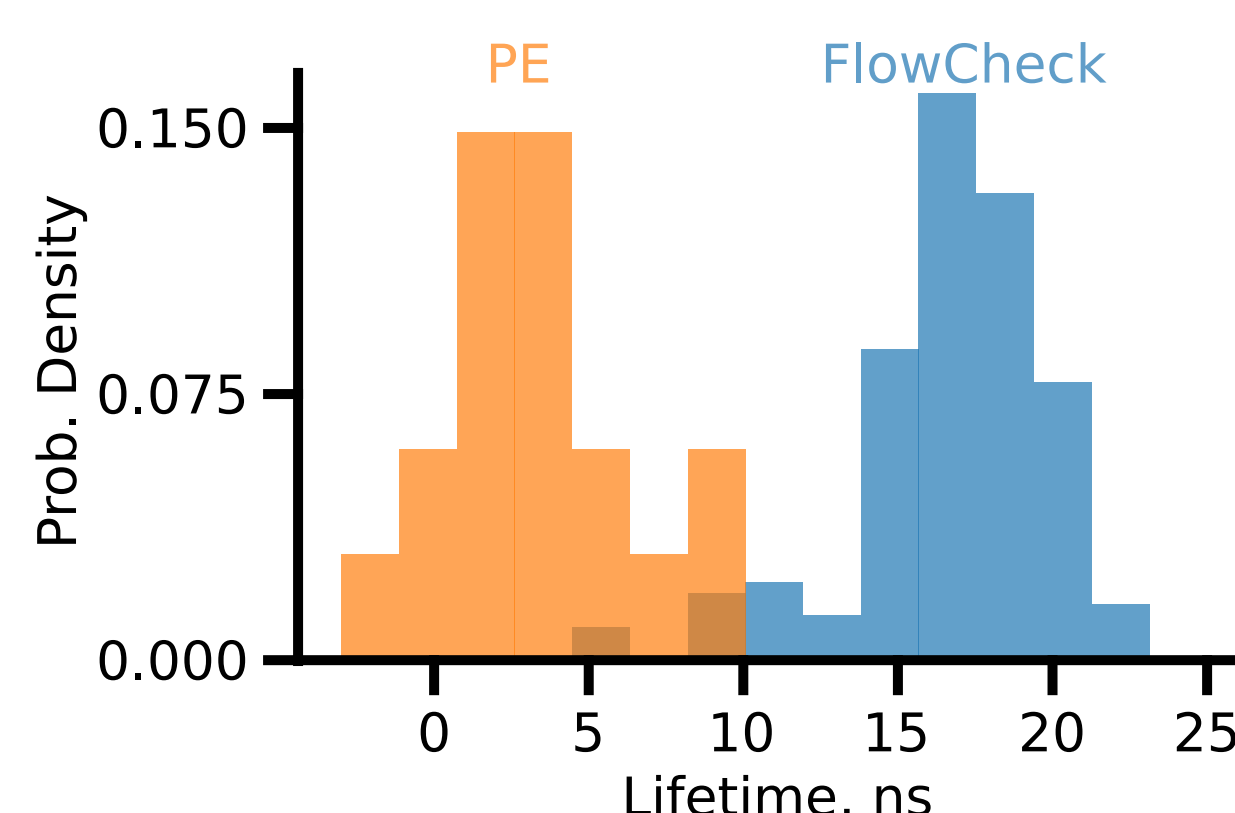
Fluorescence lifetime (FLT)
can be measured without
additional equipment

Inorganic particles have longer lifetimes ($>10^{-6}$ s) than organics ($<10^{-8}$ s). This difference can be used to identify and isolate organics from inorganics, eliminating potentially large abiotic background from the sample. Furthermore, fluorescence lifetime adds an additional sorting parameter, helping to distinguish various organics.



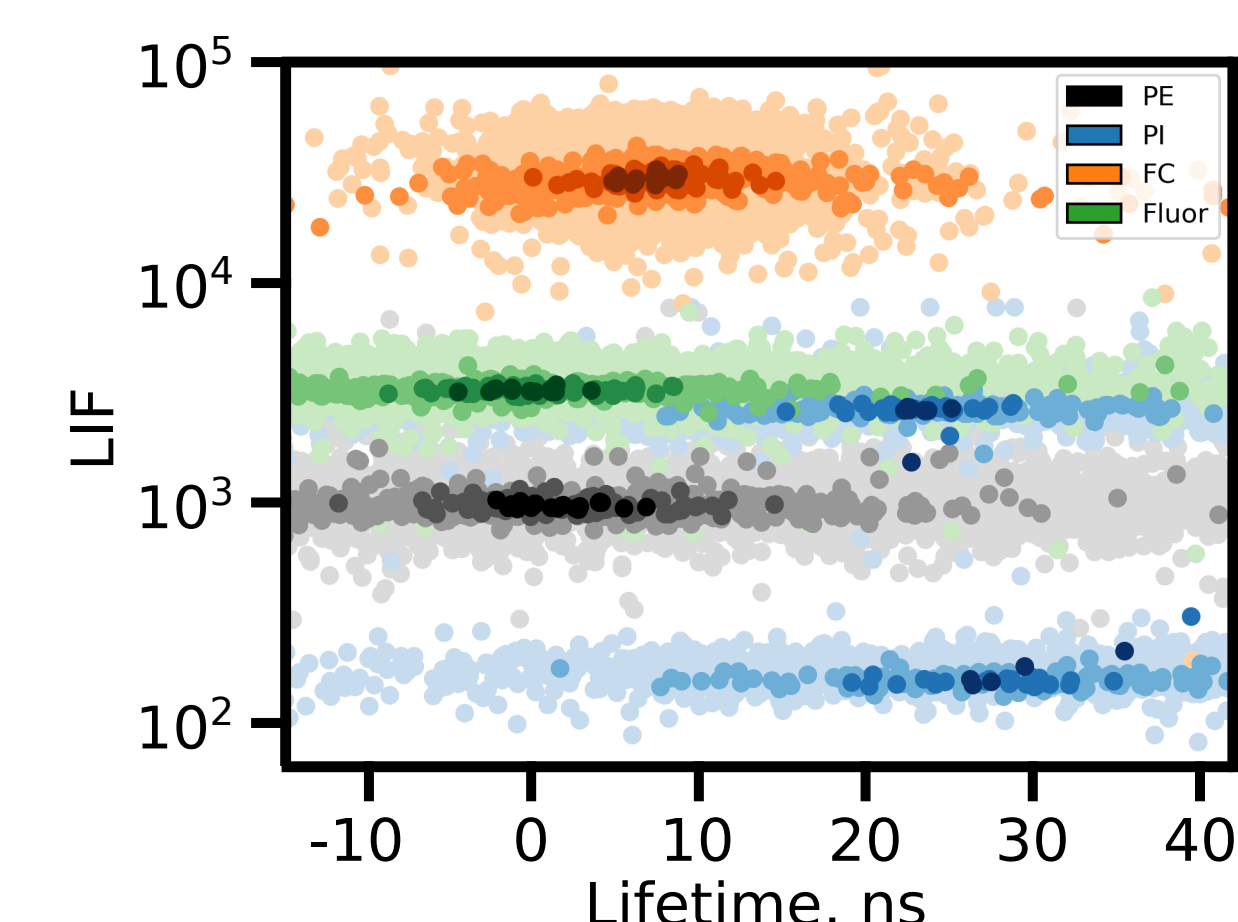
While scattered light, e.g., FSC, is produced instantaneously, fluorescence is a chemical process taking a finite amount of time, defined as its lifetime. Measuring the delay in the arrival times of the two signals at the PMTs gives an estimate of this lifetime.

Cytometry-based FLT has
enough resolution to
distinguish different populations
of organic particles.



Microspheres dyed with fluorescence standards can be distinguished solely based off of this lifetime measurement. Due to alignment errors, flow instabilities, and sometimes low-signal levels, our Beckman Coulter MoFlo XDP has a FLT resolution of roughly 5-10 ns.

Can be used along with
standard fluorescence
intensity to find populations.



The FLT parameter for each particle can then be used along side the standard fluorescence and scattered light parameters to better isolate cell and particle populations. Excitation = 488 nm. LIF = laser induced fluorescence at 580 ± 15 nm. Reference 7.5 μm beads used: PE = R-Phycoerythrin, PI = Propidium Iodide, FC = FlowCheck, Fluor = Fluorescein (FITC)

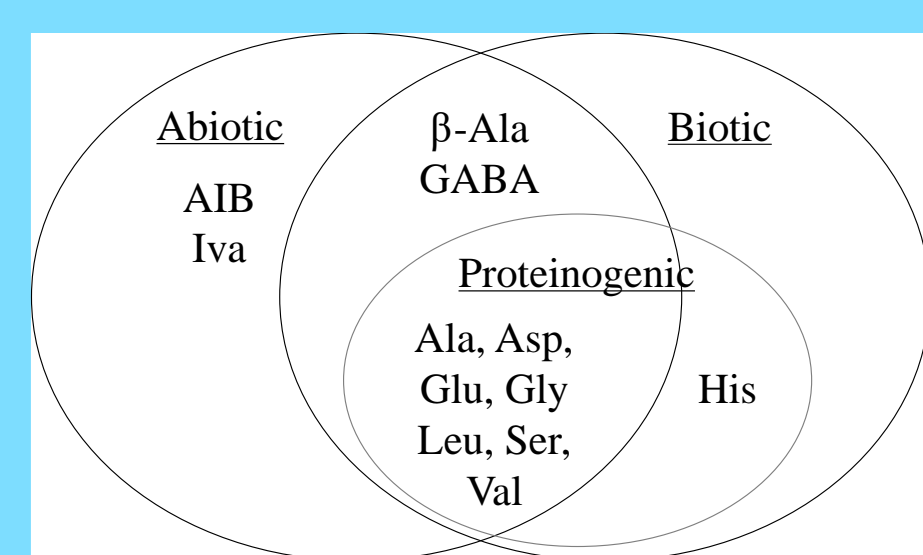
Capillary Electrophoresis and Contactless Conductivity Detection for In Situ Analysis of Samples from Ocean Worlds

Author: Mauro Sergio Ferreira Santos (389U)
Aaron Noell (389U), Maria Fernanda Mora (389U)

Introduction

With growing interest in exploring ocean worlds such as Europa and Enceladus, there is a fundamental need to develop liquid-based analytical techniques capable of handling high salinity samples while performing both bulk and trace species measurements. In this context, capillary electrophoresis coupled to contactless conductivity detection (CE-C⁴D) has tremendous potential. This technique allows the detection of a wide number of charged species (both organic and inorganic) without the need of derivatization.

why amino acids and which ones?



which cations?	Relevance to Planetary Studies
Mg ²⁺	Mars Phoenix Lander; likely Europa relevance
Ca ²⁺	Mars Phoenix Lander
Na ⁺	Mars Phoenix Lander; likely Europa relevance
K ⁺	Mars Phoenix Lander
Li ⁺	Hydrothermal vents, Europa, Enceladus relevance
NH ₄ ⁺	Possible Titan relevance

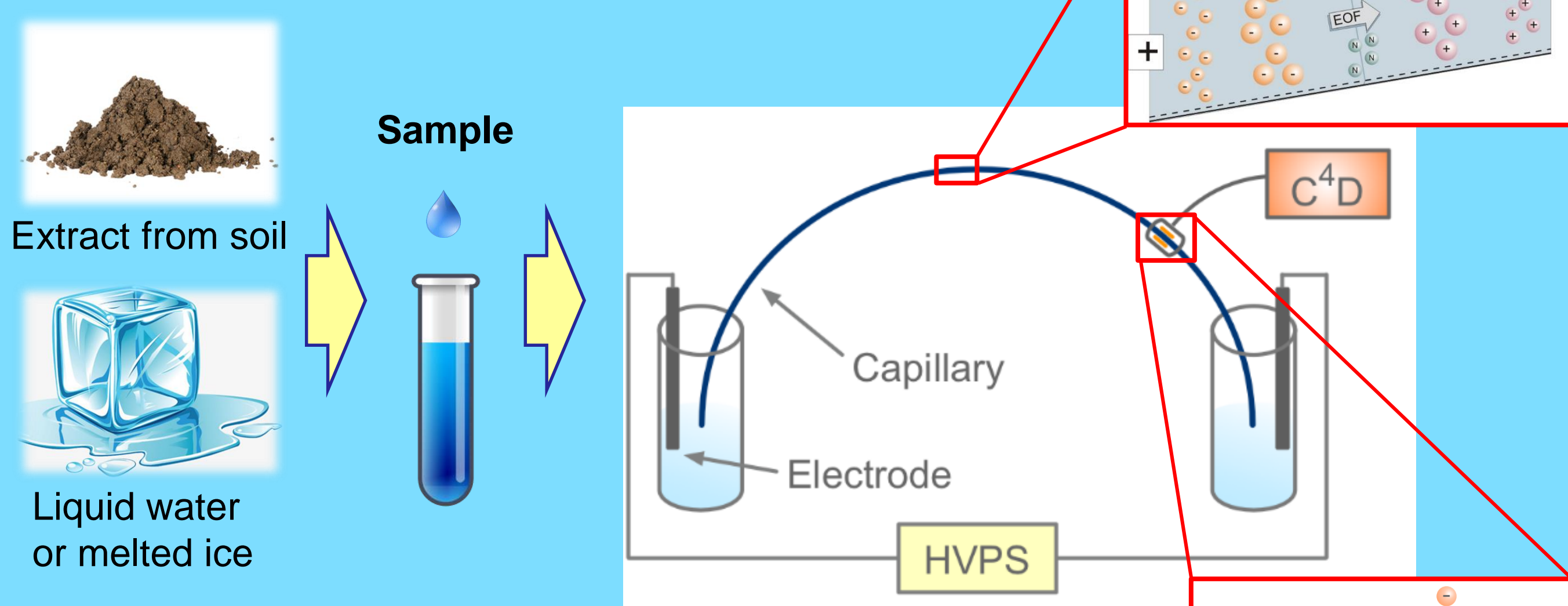
- The distribution of amino acids is a powerful biosignature in the search for life. The distribution of inorganic salts is important to biological activity and its characterization is essential to assess the habitability of an extraterrestrial environment.

Objective and Challenge

To develop a CE-C⁴D method that allows the simultaneous detection of amino acids and inorganic salts regardless the sample salinity, and is also simple and compatible with flight systems (e.g., long term stability, resistant to radiation).

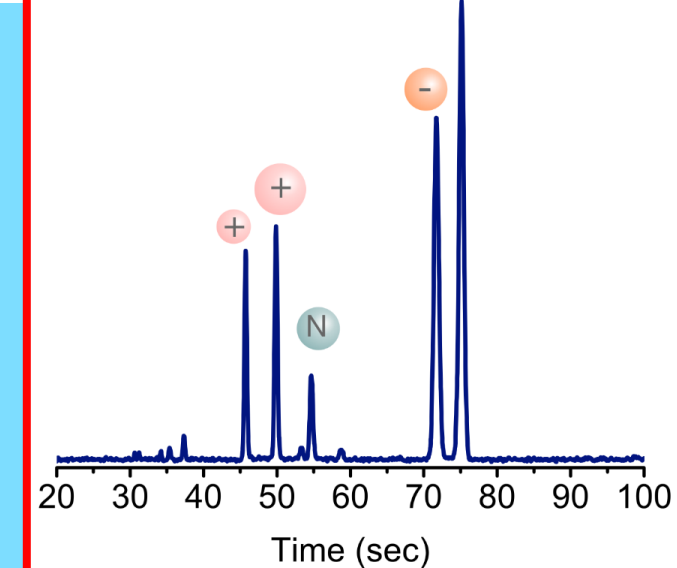
Materials and Methods

- The separation and detection was performed by CE-C⁴D;
- 6 inorganic ions (250 μM) and 12 amino acids (50 μM) were selected as our standard mixture
- Different background electrolytes (BGE) were evaluated;
- Separations were performed under 400V/cm.



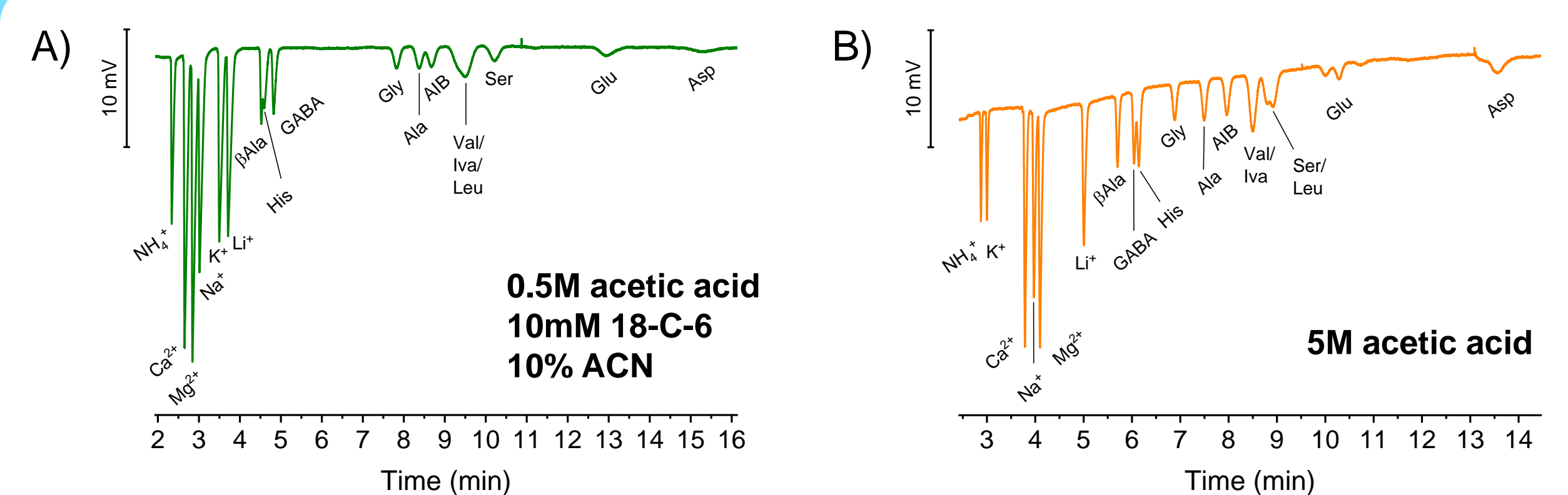
CE-C⁴D:

- It is fast;
- Requires no sample preparation (liquid sample);
- Uses a small sample volume (microliters);
- Can be fully automated (end-to-end analysis);



Results

Two BGEs allowed baseline separation of the inorganic cations and the simultaneous detection of the selected amino acids.



Separation of inorganic cations (250 μM) and amino acids (50 μM) in (A) 0.5 M acetic acid + additives and (B) 5 M acetic acid.

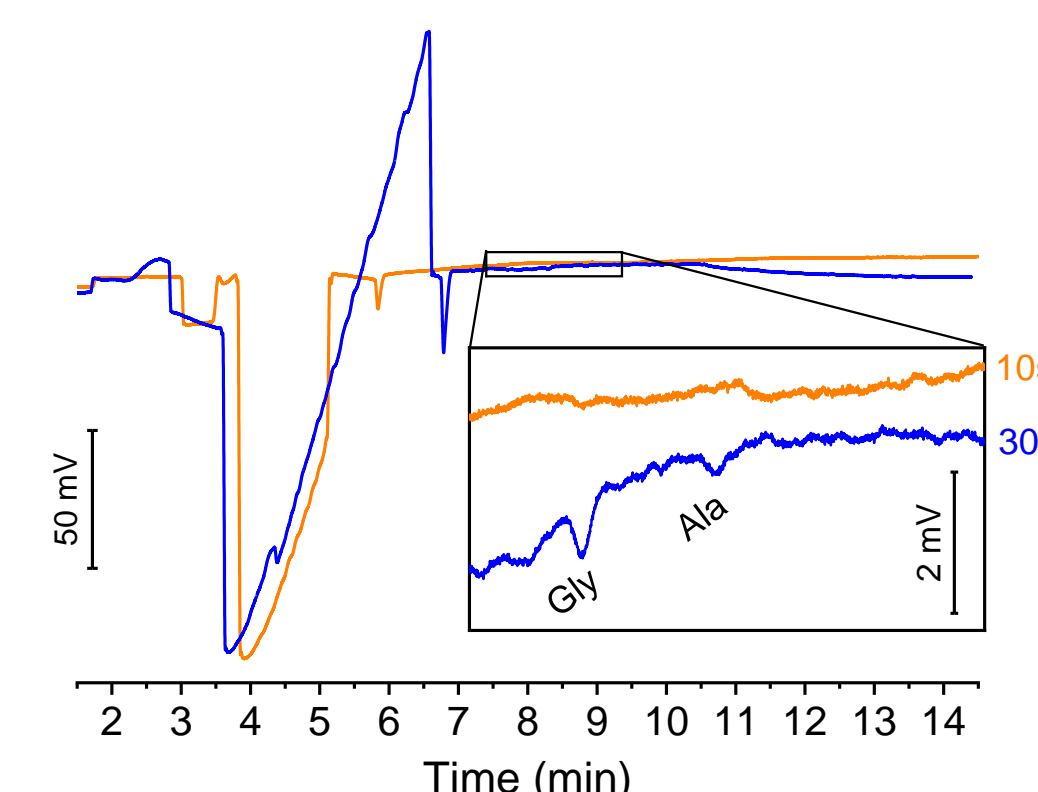
Both methods were validated by analyzing samples of varying salinity from relevant environments (creek, ocean, and salt lake water).



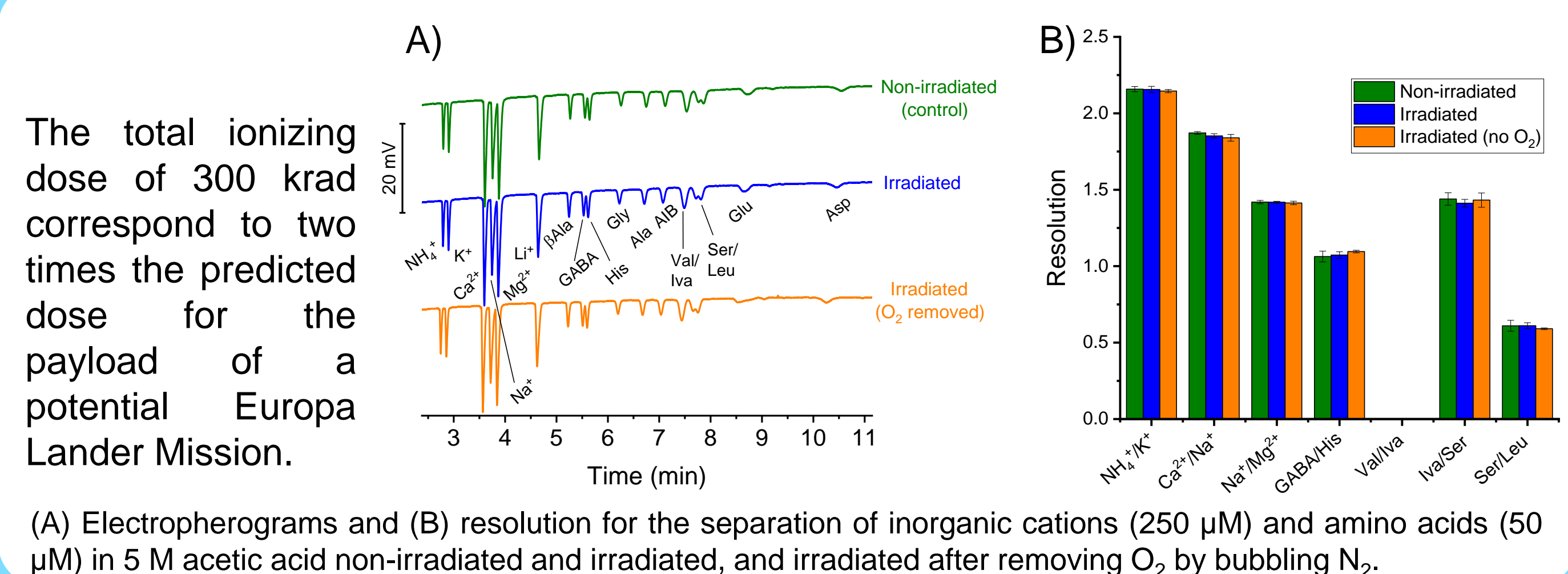
Cation	Hot Creek	Santa Monica	Mono Lake
Ca ²⁺	0.061 ± 0.002	4.0 ± 0.2	ND
Mg ²⁺	ND	30.4 ± 0.7	ND
Na ⁺	4.91 ± 0.07	460 ± 20	245 ± 6
K ⁺	0.210 ± 0.007	5.81 ± 0.01	5.10 ± 0.08
Li ⁺	NQ	ND	NQ

Concentration of inorganic ions (mM) detected on natural samples. ND, not detected, NQ, detected but not quantified.

- Although both methods could be used for quantification of the inorganic cations (after sample dilution), only the BGE composed of 5 M acetic acid could handle high salinity samples, like Pacific Ocean and Mono Lake water;
- Increasing the volume of sample injected allowed the detection of amino acids in the Mono Lake sample.



The stability and performance of the optimized BGE under high levels of radiation (total ionizing dose of 300 krad) was evaluated in order to demonstrate its potential to be used during a future mission to Europa.



The total ionizing dose of 300 krad correspond to two times the predicted dose for the payload of a potential Europa Lander Mission.

(A) Electropherograms and (B) resolution for the separation of inorganic cations (250 μM) and amino acids (50 μM) in 5 M acetic acid non-irradiated and irradiated, and irradiated after removing O₂ by bubbling N₂.

Concluding Remarks

- The method developed allows simultaneous analysis of inorganic cations and amino acids regardless of the sample salinity;
- The method was validated by analyzing natural relevant samples;
- 5 M acetic acid showed no loss in performance after exposure to a total ionizing dose of 300 krad;
- This method could be used in future missions to Ocean Worlds to identify samples with potential biomarkers for further analysis by CE-LIF;
- The optimized BGE is also compatible with CE-ESI-MS.

Inorganic Ion Measurements for *in situ* Habitability Assessment

Author: Elizabeth A Jaramillo 389U

Aaron Noell 389U

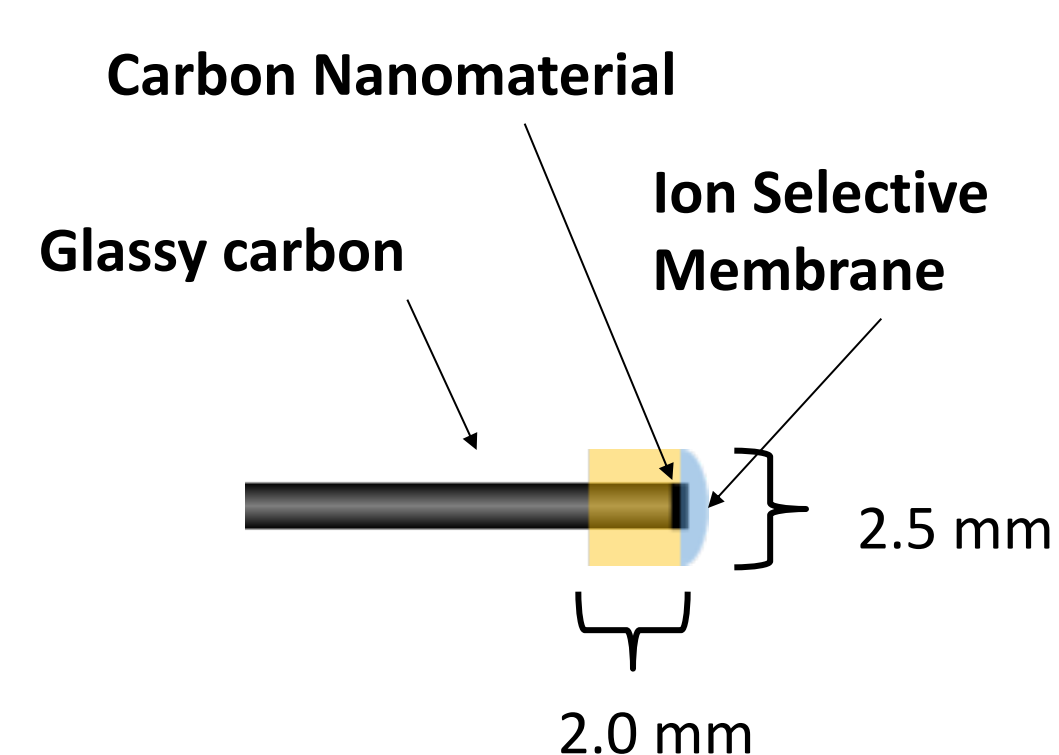
Motivation

The ability to measure inorganic ions in unknown samples is an important contribution to analyses in planetary science. Inorganic ions contribute to our understanding of the broader chemical environment, can potentially interfere with downstream measurements, and affect important indicators of habitability such as **water activity, oxidation reduction potential, and pH**. Ion selective electrodes (ISEs) are simple, low-cost sensors with a large dynamic range, minimal power requirements, and few interferences. We have developed a 3D printed microfluidic ISE array capable of characterizing the inorganic chemistry of an environment as a first step toward habitability assessment.

Instrument design

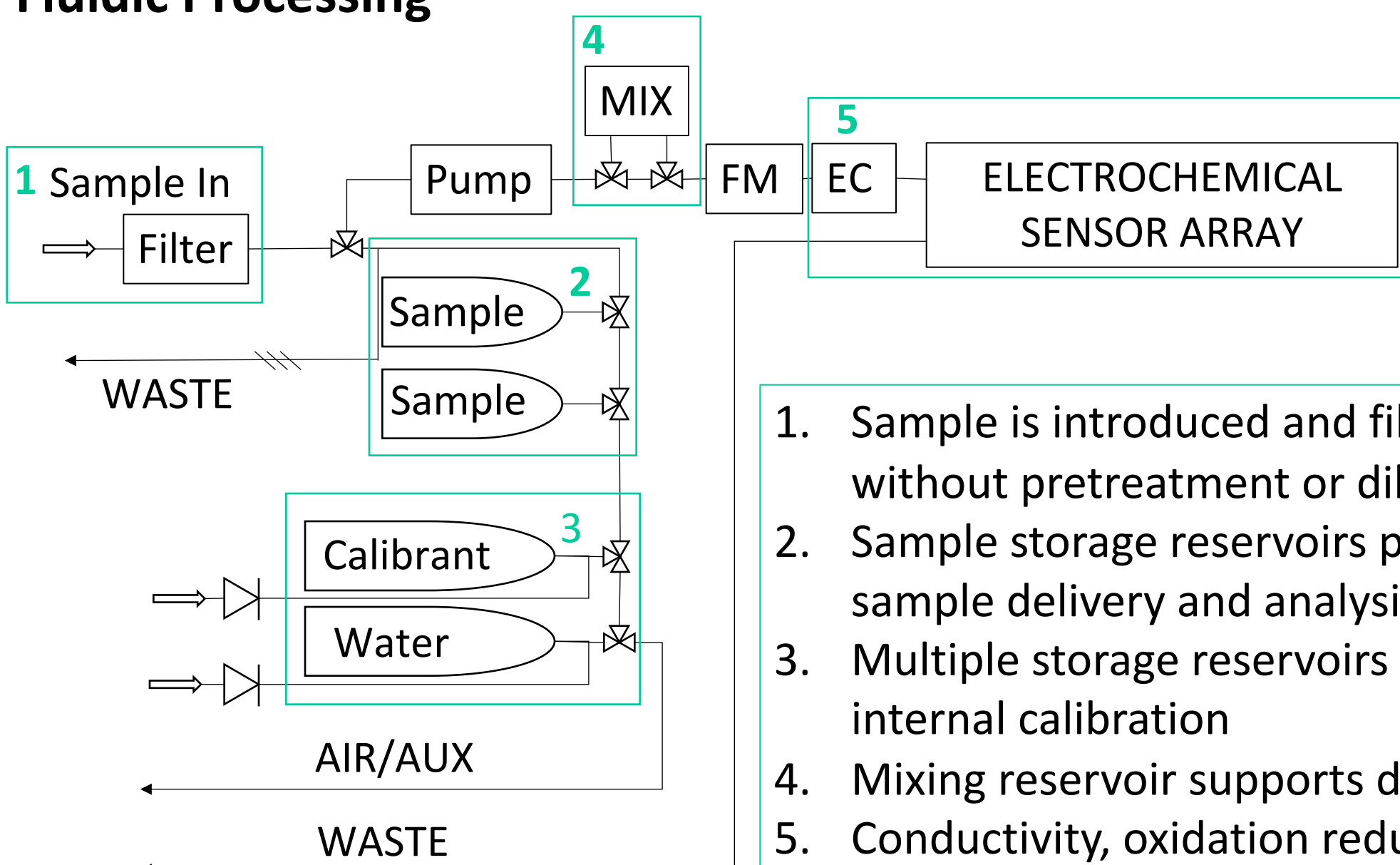
Miniaturization of ion selective electrodes (ISEs):

ISEs use an ion selective membrane in contact with an ion to electron transducer to convert the concentration of ions in solution to an electrical potential.



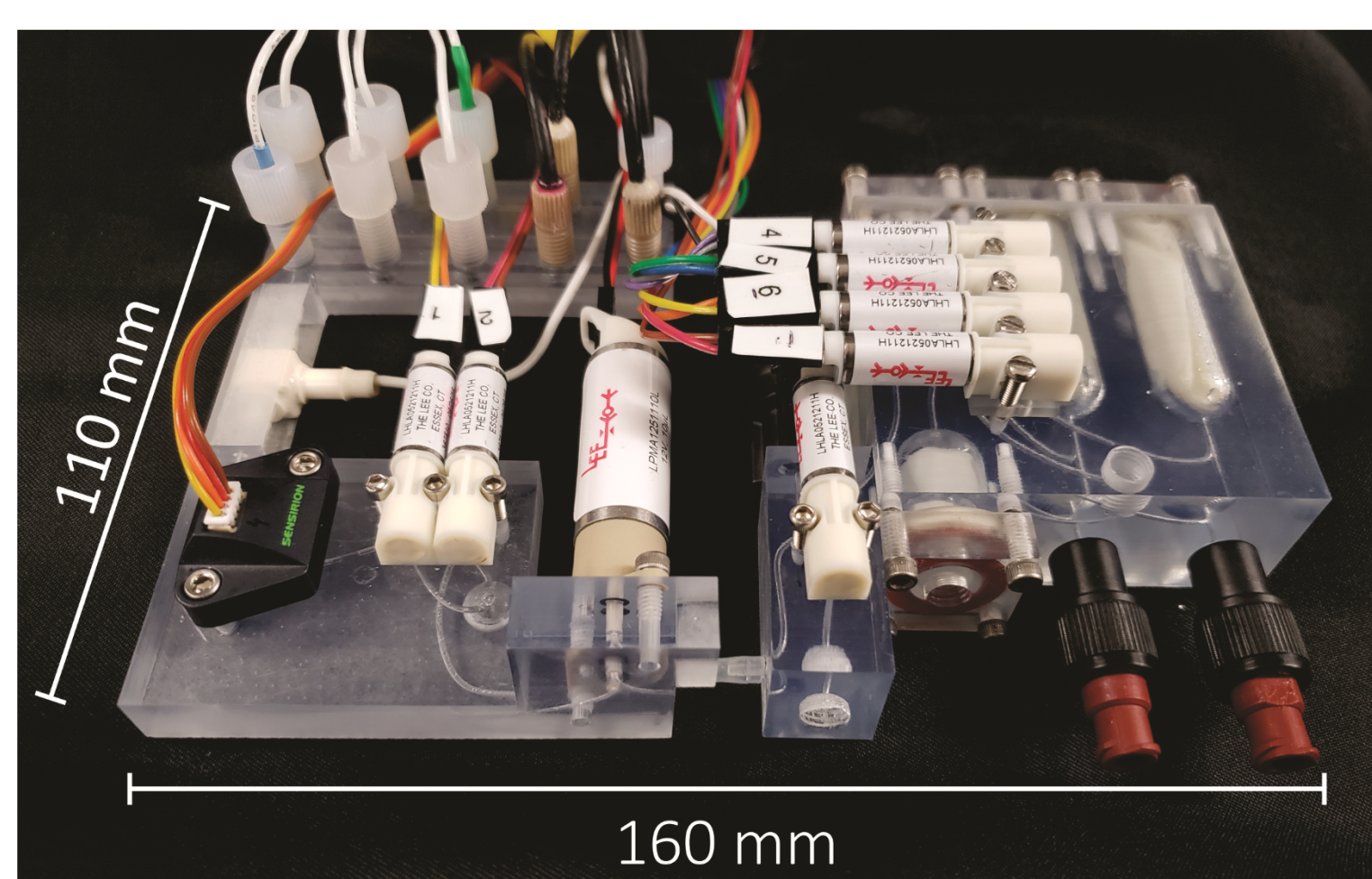
Traditional ISEs use a Ag/AgCl redox mediated transduction mechanism, requiring an electrolyte inner filling solution. We replaced this redox mediated transduction mechanism with carbon nanomaterials, reducing the size of the sensing portion of the ISE by two thirds.

Fluidic Processing



1. Sample is introduced and filtered for direct analysis without pretreatment or dilution
2. Sample storage reservoirs provide flexibility between sample delivery and analysis
3. Multiple storage reservoirs allow for autonomous internal calibration
4. Mixing reservoir supports dilutions up to a 1:25 ratio
5. Conductivity, oxidation reduction potential, pH, and ion concentrations are analyzed with the electrochemical sensor array

= 3-way latching valve
 FM = flow-meter
 EC = conductivity
 = loading port
 = check valve
 = relief valve



Instrument dimensions

- Manifold foot print: 160 mm x 110 mm x 30 mm
- Manifold internal volume: ~330 μ L
- Sample reservoir volume: 2 mL
- Calibrant reservoir volume: 5 mL

Results

Performance Stability

Table 1: calibration slope and correlation coefficient comparison before incorporation into the manifold (beaker), during stabilization period (Feb 25, Feb 26, Mar 5) and after 3 months (Jun 4)

	Feb 22 (Beaker)	Feb 25 (Manifold)	Feb 26 (Manifold)	Mar 5 (Manifold)	Jun 4 (Manifold)
Slope (mV/dec)	49.0	34.0	42.2	46.1	45.5
RSQ	0.9980	0.9906	0.9986	0.9985	0.9872

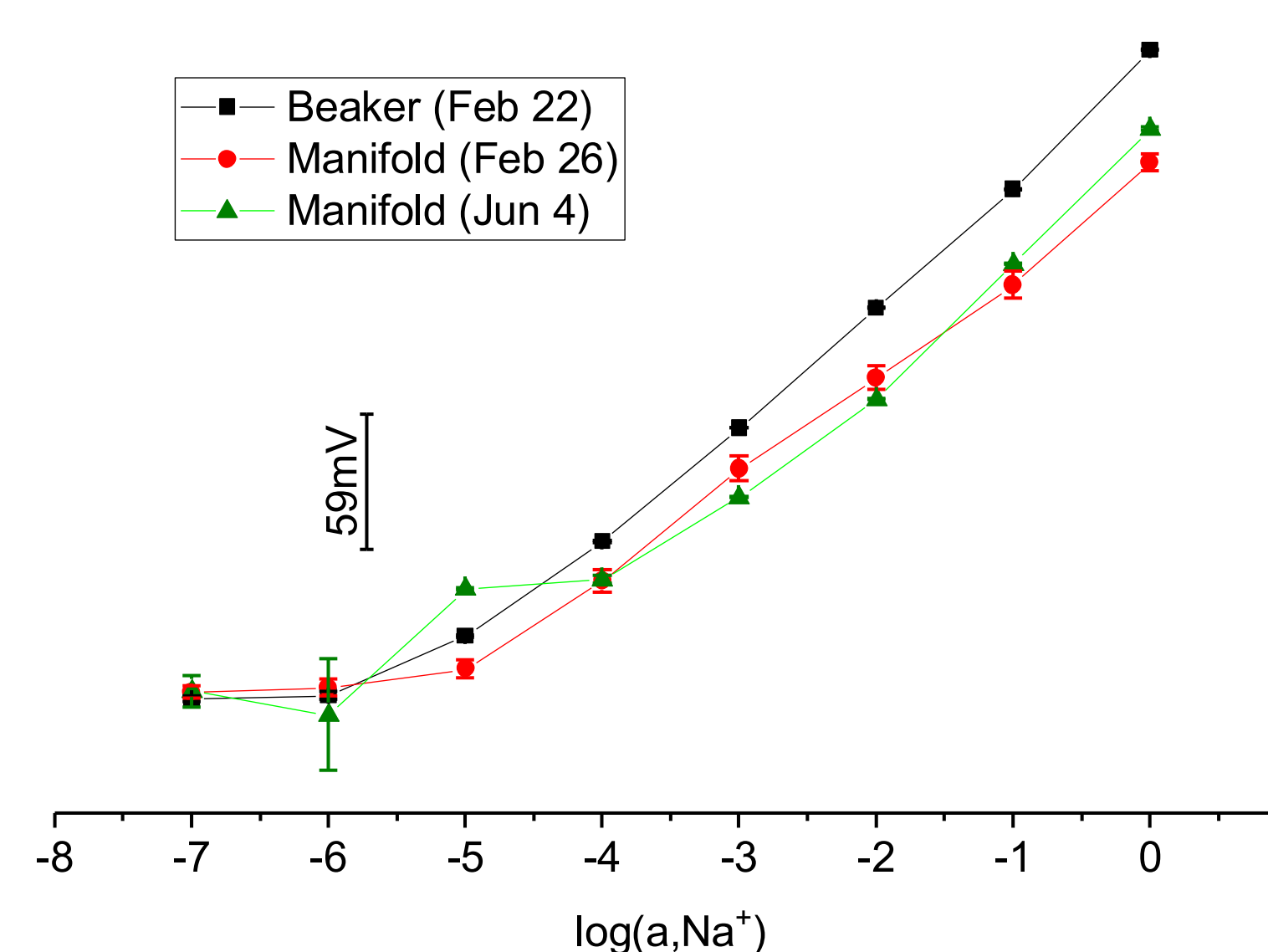


Figure 1: calibration response before incorporation into manifold (beaker), during stabilization period (Feb 26) and after 3 months (Jun 4)

- ISE sensitivity is reduced for the first week when compared to calibrations prior to incorporation in the manifold
- After ISE response stabilizes good performance is maintained after repeated use

ISE performance is stable and reproducible for long-term use after incorporation into the microfluidic manifold

Analysis of Mixed solutions

Table 2: calibration slope and correlation coefficients for ISEs in a multi-ion array

	Ca	Mg	Na	Cl
Slope (mV/dec)	36.5	41.2	50.9	-40.0
RSQ	0.9364	0.9455	0.9909	0.9020

Table 3: comparison of measured response of the multi-ion array to a known solution of artificial seawater

Ion	log(activity) in Mock solution (M)	Measured log(activity) (M)	% error
Ca	-2.61 \pm 0.01	-2.45 \pm 0.01	6%
Mg	-2.11 \pm 0.01	-1.92 \pm 0.01	9%
Na	-0.50 \pm 0.01	-0.6 \pm 0.2	23%
Cl	-0.53 \pm 0.01	-0.7 \pm 0.2	33%

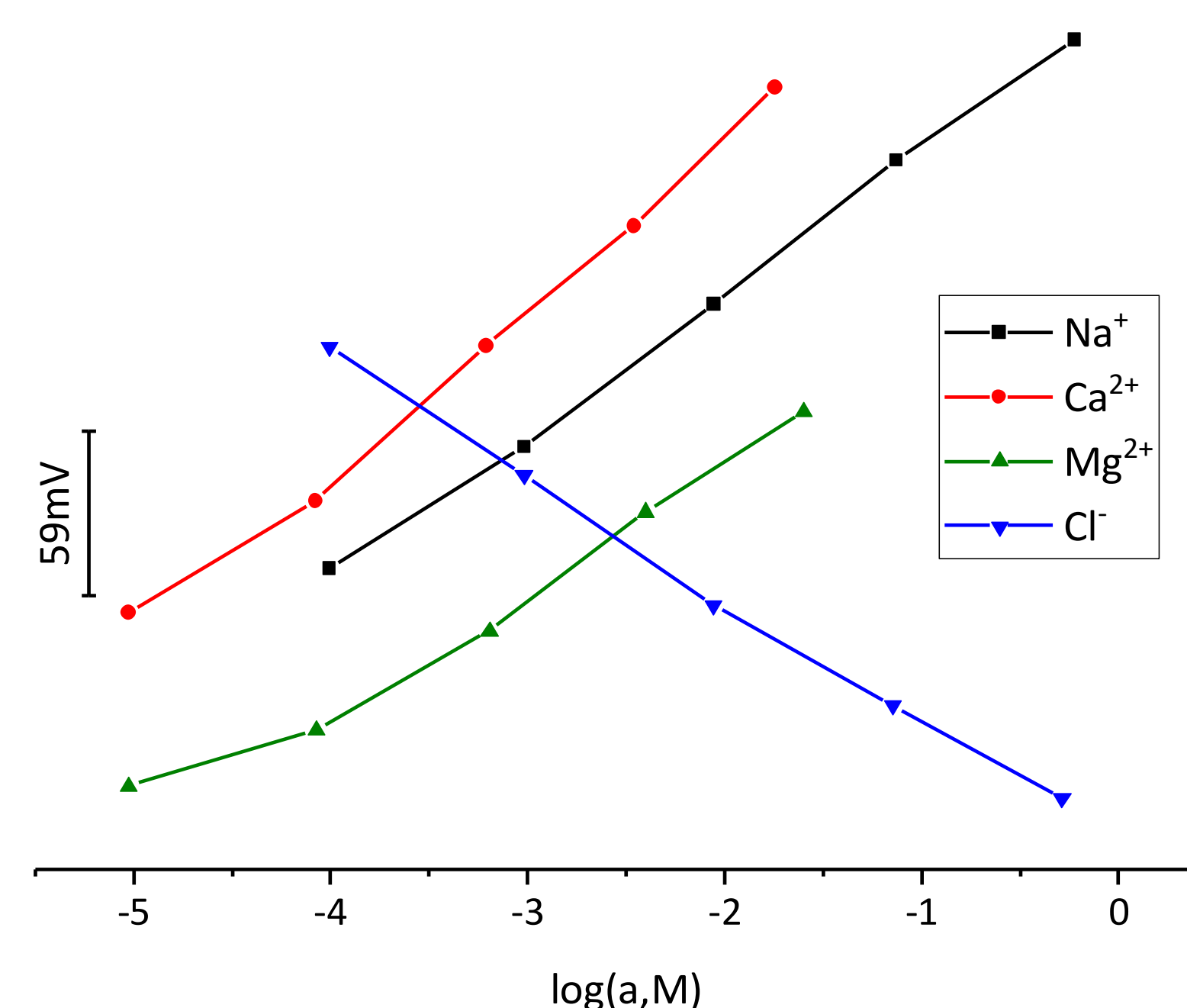


Figure 2: calibration response of multi-ion array

- Calibration of the primary components of seawater in the multi-ion array show a near Nernstian response for all ions
- Error is low for the simultaneous measurement of the primary components of a mock seawater solution without pretreatment or dilution

Multi-ion array is capable of simultaneous quantification of the primary components of seawater without the need for sample pretreatment

Future Enhancements and Testing

- Automation of data analysis
- Field testing in high and low salinity environments
- Channel interface redesign to reduce initial stabilization period

Development of an Automated Microfluidic Sample Processing Unit for Identification of Extant Microorganisms

Author: Dr. Nathan Oborny, 389U

Dr. Scott Perl, Dr. Aaron Noell, Dr. Chris Lindensmith, Dr. Peter Willis

PROJECT OBJECTIVE:

The objective of this effort is to automate the analysis of extant bacteria in liquid water samples by the development of an autonomous microfluidic sample processing unit (SPU). This is performed via a process of identifying presumptive bacterial motion using a digital holographic microscope within microliters of fluid. Following this, bacteria within that volume of fluid are sequentially dyed using fluorescent stains specific for characteristics likely to be common for bacterial life. This system functions as part of a collection of life detection instruments which comprise the Ocean Worlds Life Surveyor (OWLS) instrument suite.

THE ELVIS SAMPLE PROCESSING UNIT

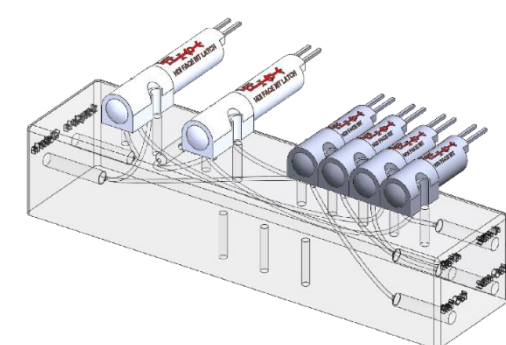
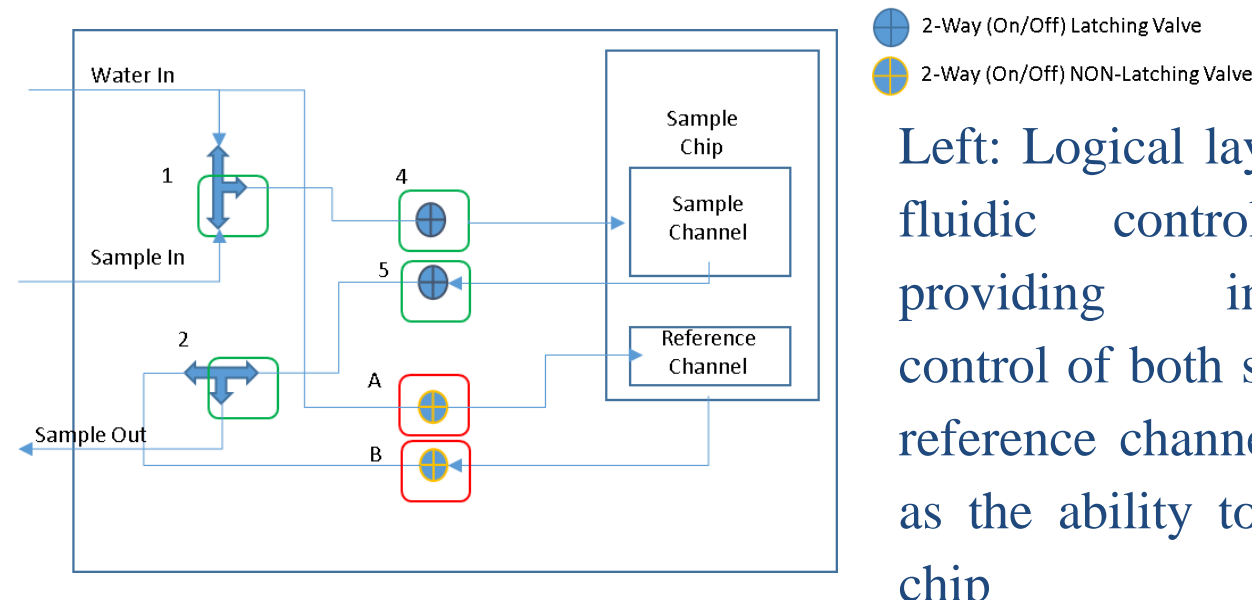
- ELVIS, The Extant Life Volumetric Imaging System, can identify signs of bacterial motion within a $\sim 1\text{mm}^3$ volume of liquid.
- By staining cellular structures via the **sample processing unit (SPU)**, the resulting fluorescence signal can be spatially and temporally correlated to the detected motion^{2,3}.
- Three dyes with different fluorescence emission profiles are used sequentially to stain structures such as cellular membranes, nucleotide sequences, and glycoproteins, increasing detection confidence of non-motile cells^{2,3}.
- The sample fluid handling and staining are performed by the system in an automated fashion.

FLUIDIC CONTROL SYSTEM

The 'control system' is meant to function as a stand-alone module allowing large quantities of motion data to be captured over time. This data can then be used to train the machine learning algorithm. The system can also be used in conjunction with the staining system below.

Right: Fluidic control system.

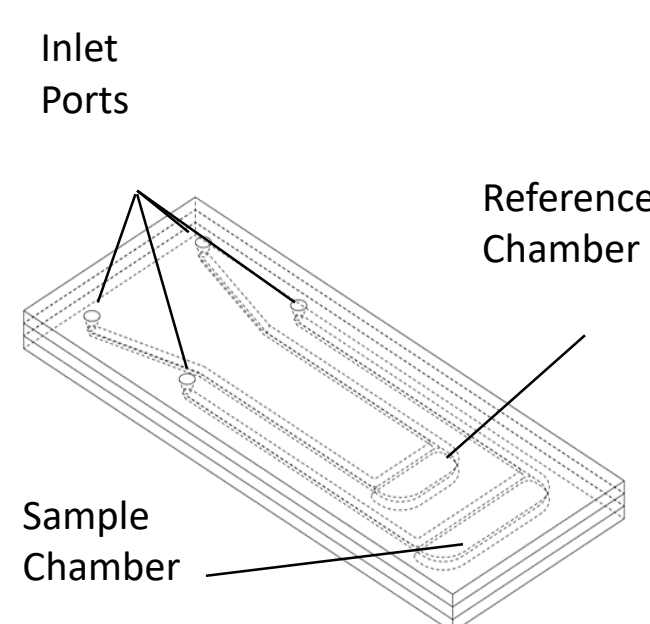
- Three-way valves control sample inlet, dilution and washing.
- Two way valves clamp fluid flow in and out of chip to decrease fluid motion



3-Way Latching Valve
2-Way (On/Off) Latching Valve
2-Way (On/Off) NON-Latching Valve

MICROFLUIDIC SAMPLE CHAMBER

The microfluidic sample chamber was designed to provide both a chamber for individual aliquots of a sample to be analyzed but also for a reference/calibration channel. Images of bacterial motion are analyzed via machine learning to identify motion.



- Microfluidic chip measures $\sim 45\text{mm}$ long x 18mm wide and 3mm tall
- Thermally bonded borosilicate glass
- Channels etched in middle layer $\sim 300\ \mu\text{m}$ square
- Sample and reference chambers 1mm wide

DYE SELECTION AND USE

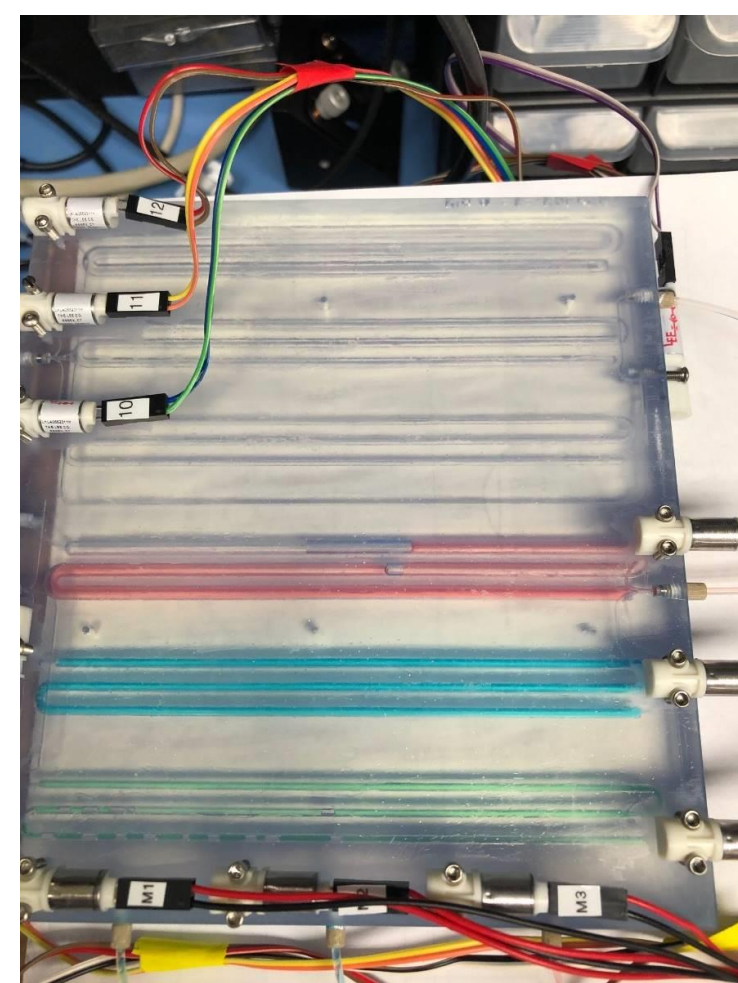
- Dyes were selected to cover a range of cellular characteristics¹.
 - Specifically targeted are cellular membranes, glycoprotein structures, and nucleic acids.
- Water solubility – material compatibility with polymer structures and valves
- Excitation/Emission via a single laser and optical filters

Dye	Characteristics	Excitation/Emission
Acridine Orange ⁴	<ul style="list-style-type: none"> • Binds nucleic acids, Both DNA and RNA • Indicator of low pH cellular structures such as lysosomes 	
FMI-43 ⁴	<ul style="list-style-type: none"> • Structure results in transmembrane insertion • Water soluble but intensely fluorescent when membrane bound • Can be used to monitor changes in cellular membranes and vesicle release 	
Fluorescein-Wheat Agglutinin Conjugate (WGA) ⁴	<ul style="list-style-type: none"> • WGA coupled dyes bind glycoproteins such as sialic acid and N-acetylglucosamine residues • Typically used to stain bacterial cell walls 	

AUTOMATED BACTERIAL STAINING

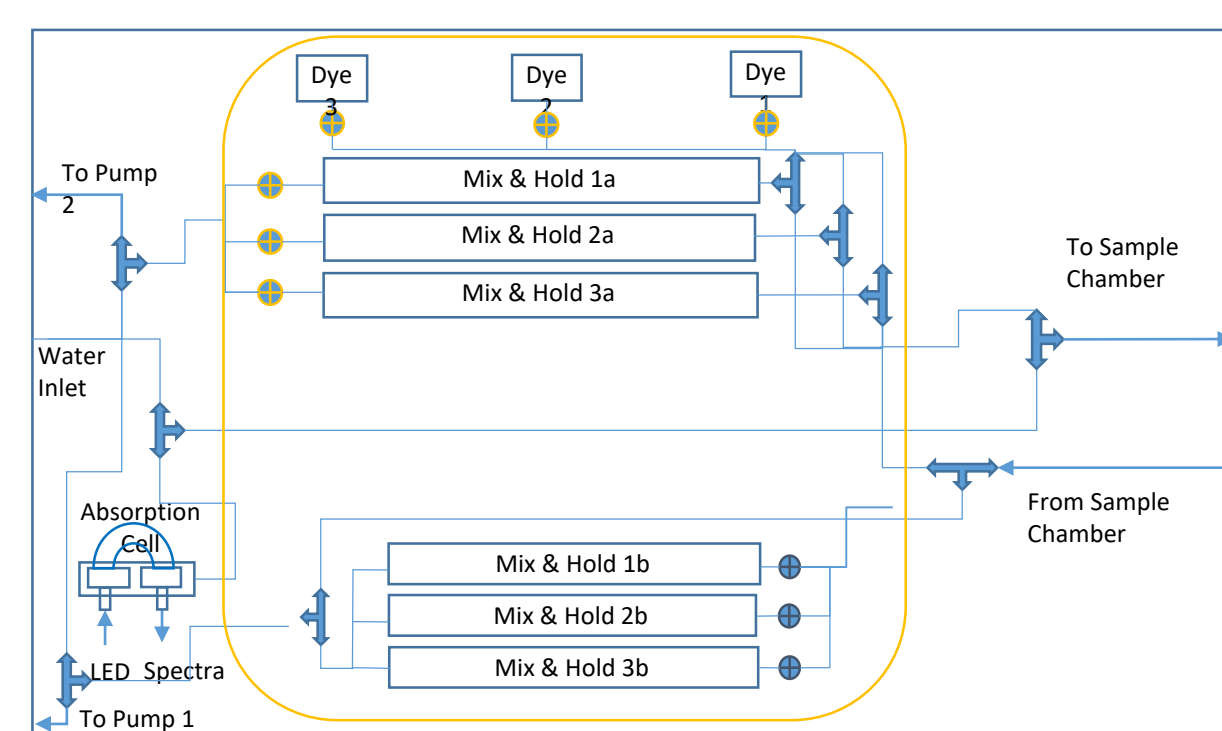
Once bacterial motion has been identified in a sample, it is routed to the mixer chamber using one of two piezo electric pumps. The sample is subsequently stained using one of the three dyes. Once this is complete, that volume is transferred to the sample chamber for analysis. This process proceeds an additional two times, after which the sample can be repeatedly processed to generate a large dataset of images.

Shown on the right are samples stained with different colors. Three way valves in each channel provide both mixing and the ability for variable dilution of both dye and sample allowing us to tune concentrations and conserve dye.



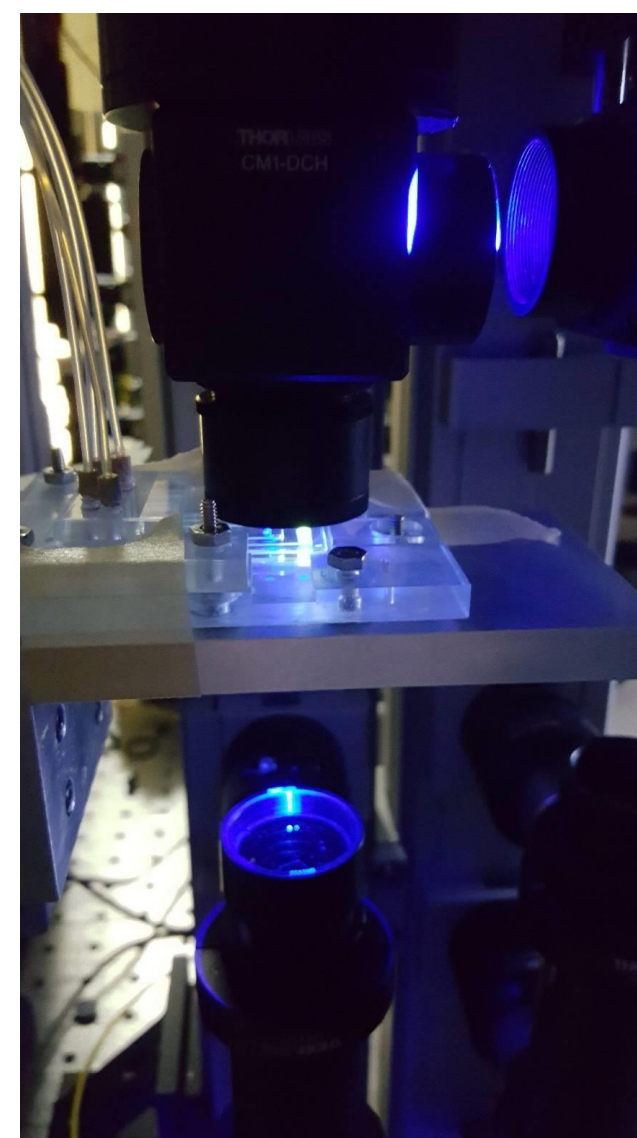
Left: The logical block diagram of the automated staining system.

- Sample enters the system through an absorption cell allowing a quick measurement an estimation of sample density.
- Based on this the sample can be diluted with water if necessary
- Sample then passes to the control system and chip until motion is detected.
- Following this, sample is routed to a mix & hold chamber for staining.
- This volume of fluid is then passed back and forth through the chip initially from 1a to 1b, then as the volume increases as dye is added from 1b to 2b until all dyes have been added.

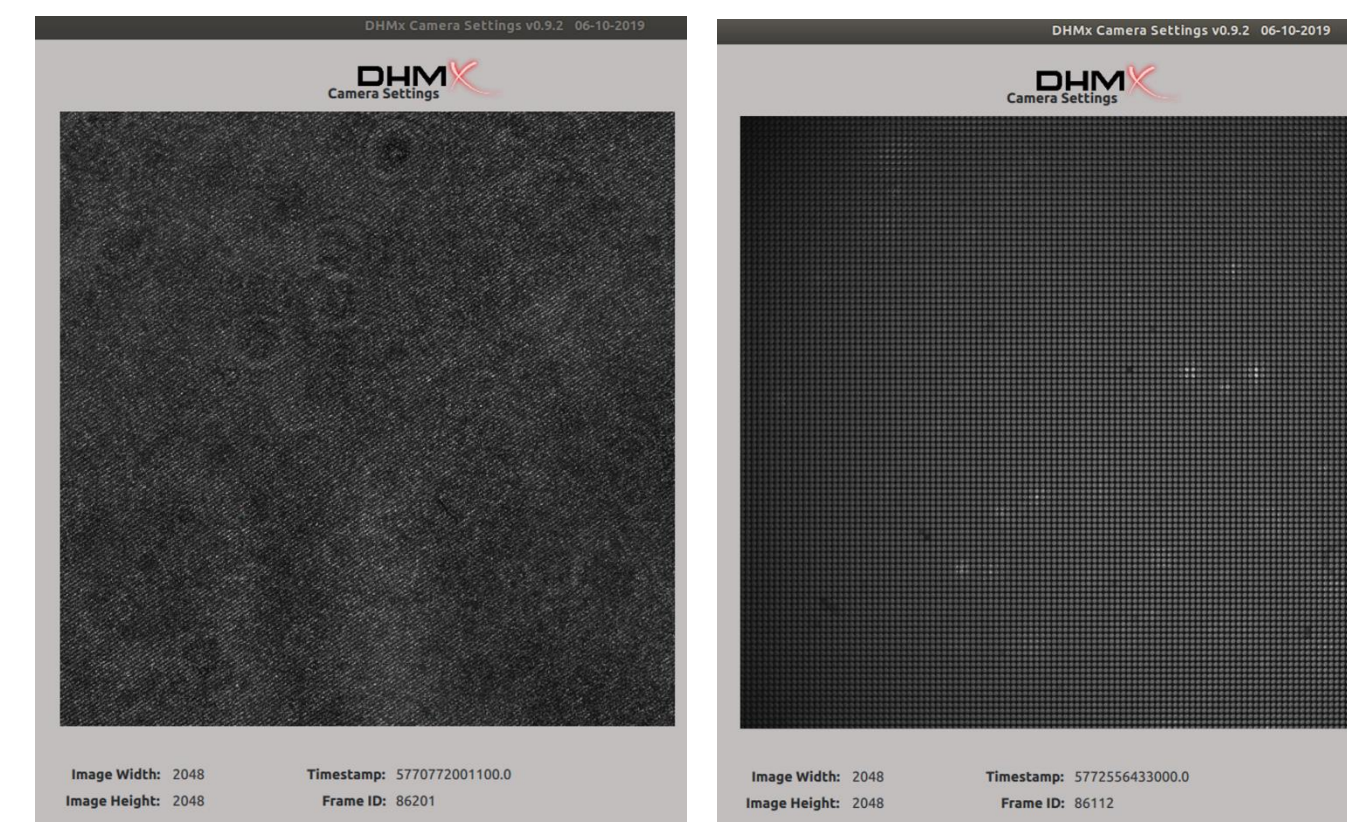


BACTERIAL DETECTION VIA DHM/VFI

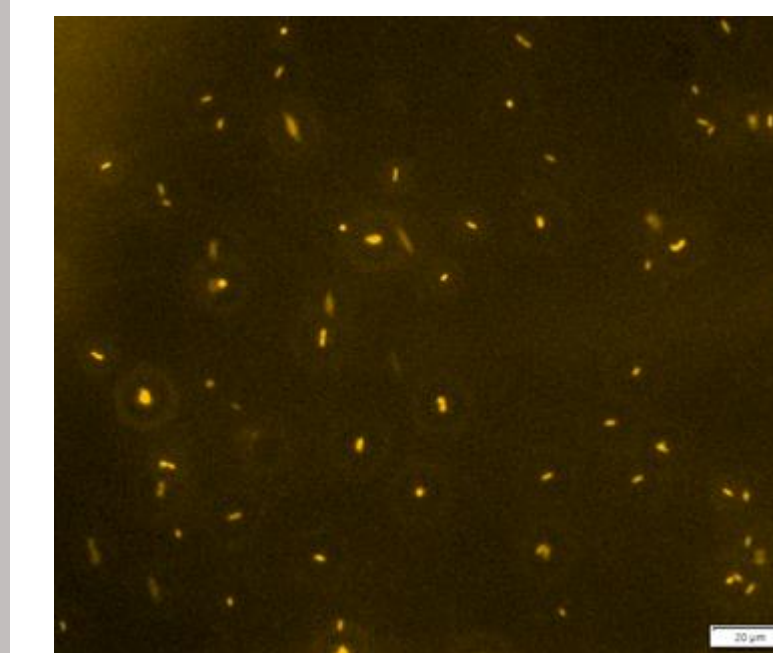
The sample chamber mounted (Left) in a combined digital holographic microscope / volumetric fluorescence imager (DHM/VFI) developed at JPL. Using a 405nm laser as an excitation/illumination light source, the DHM can detect cell-like objects and bacterial motion. Following fluorescent staining, the VFI system can be used to correlate the location of that motion to fluorescence emission. These combined signals increase the probability of detected life².



A sample chamber mounted in the DHM/VFI



DHM (left) /VFI (right) images of Acridine Orange stained *B. Subtilis* in motion.



Acridine Orange stained *B. Subtilis*, $\sim 10^4$ cells/mL for comparison – Image taken via traditional microscopy

REFERENCES

1. Nadeau, Jay L., et al. "Fluorescence microscopy as a tool for in situ life detection." *Astrobiology* 8.4 (2008): 859-874
2. Nadeau, Jay L., et al. "Improved tracking and resolution of bacteria in holographic microscopy using dye and fluorescent protein labeling." *Frontiers in chemistry* 4 (2016): 17
3. Bedrossian, Manuel, Chris Lindensmith, and Jay L. Nadeau. "Digital holographic microscopy, a method for detection of microorganisms in plume samples from Enceladus and other icy worlds." *Astrobiology* 17.9 (2017): 913-925.
4. <http://www.thermofisher.com>

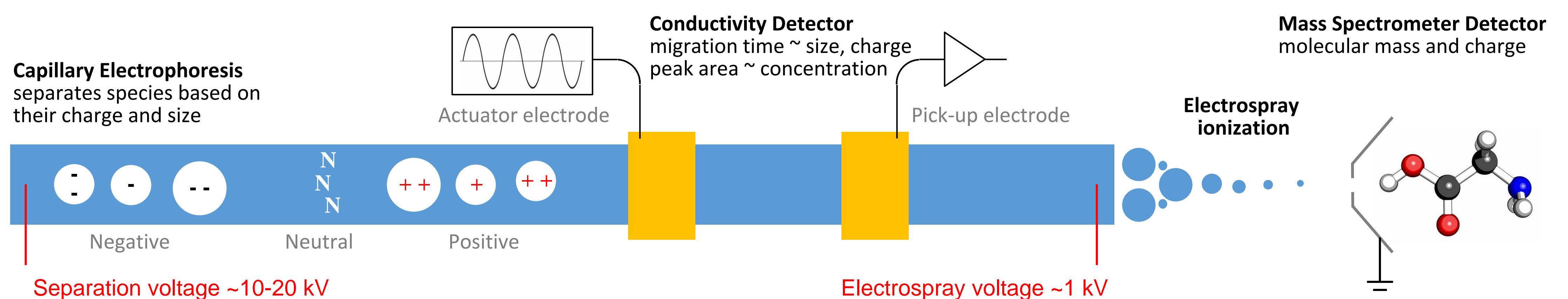
A Portable, Automated Capillary Electrophoresis System for Multiple Mode Detection of Organic and Inorganic Species

K. Zamuruyev (389U)
M.S. Ferreira Santos, E. Kurfman, A. Noell, P. Willis

Problem:
 Life detection, method and instrument

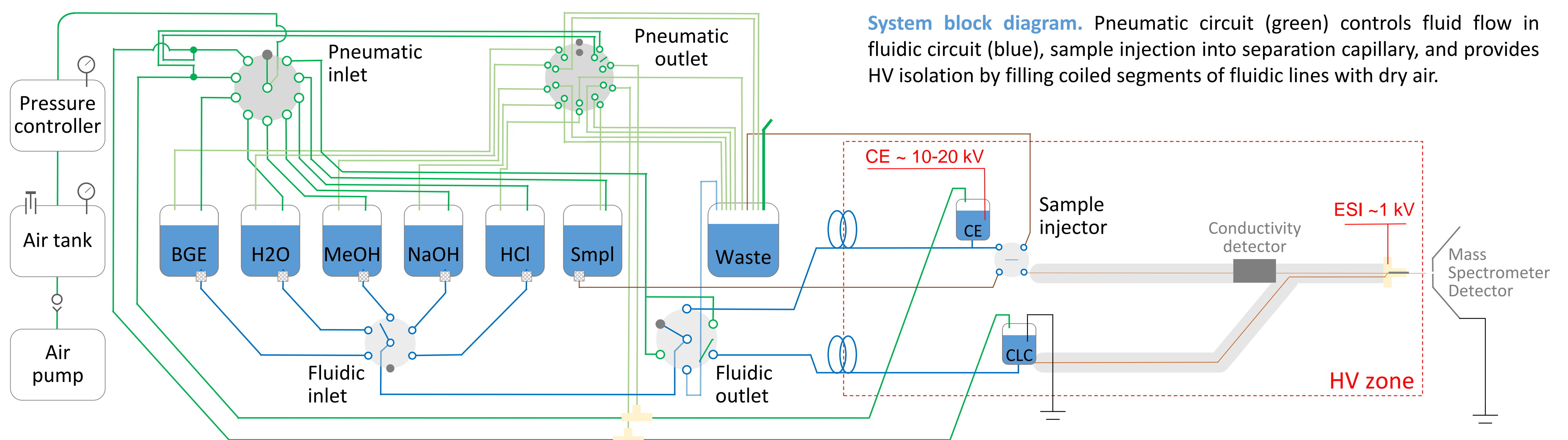
Method:
 Separate + detect amino acids

The search for past or present life elsewhere in the Solar System is one of NASA's science goals. Detection of carbon-based molecules and analysis of their molecular properties could provide the very best evidence for possible past or present life. The use of liquid-based extraction, chemical separation, and detection enables analysis of a wide range of polar organic compounds potentially indicative of life, as well as inorganic compounds that can serve as indicators of habitability. To detect this broad range of compounds in a single instrument, it is essential to incorporate mass spectrometric (MS) detection as one of the detection modes. Two other extremely powerful complementary detection modes include laser-induced fluorescence (LIF) and contactless conductivity detection (C4D) for analysis of amino acids and carboxylic acids. Here we report the first proof-of-principle demonstration of a fully automated, portable capillary electrophoresis (CE) analyzer that can be interfaced with MS, LIF and C4D detectors.



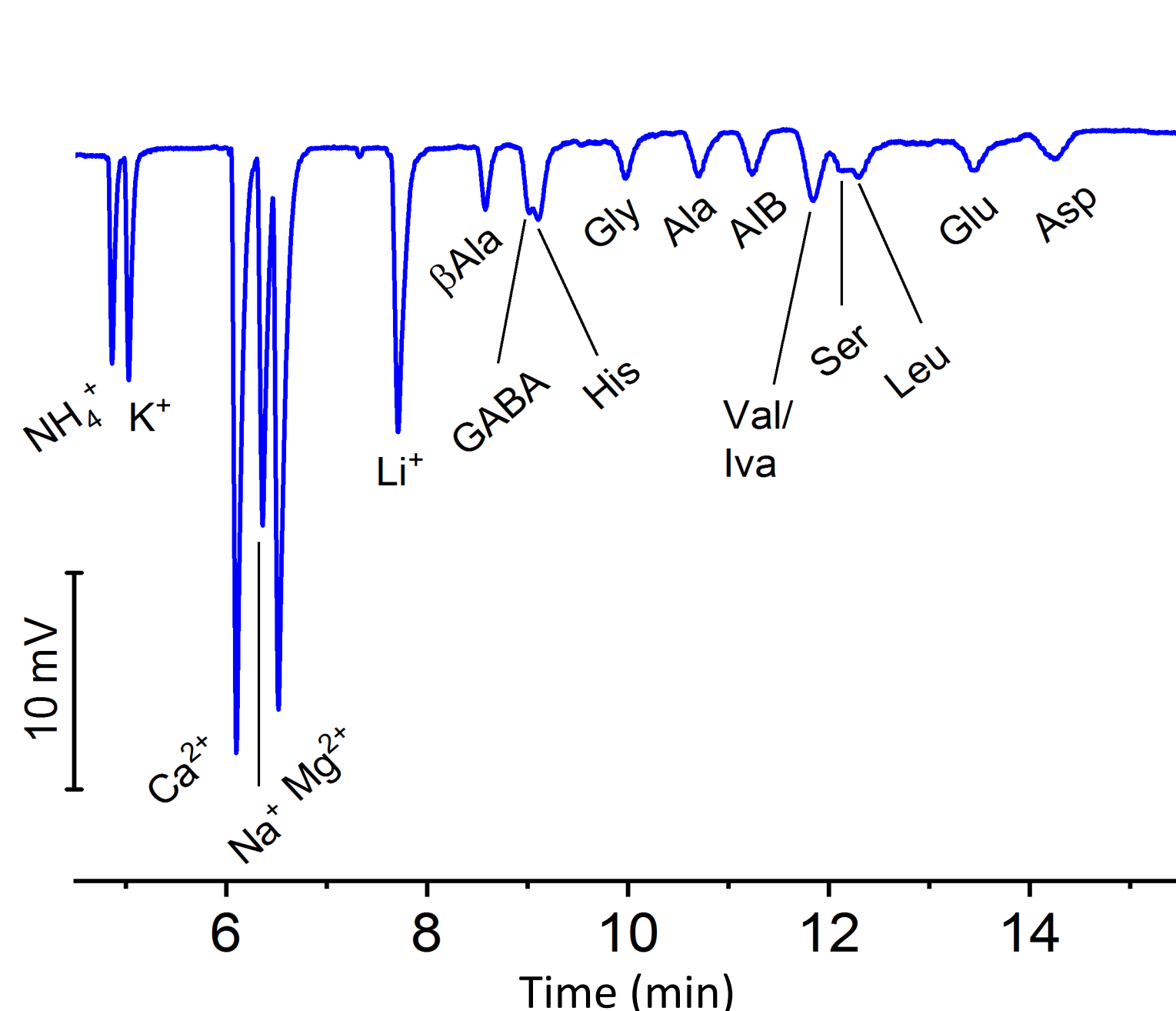
CE-ESI-MS system

- Fully automated
- HV isolation
- Precise sampling

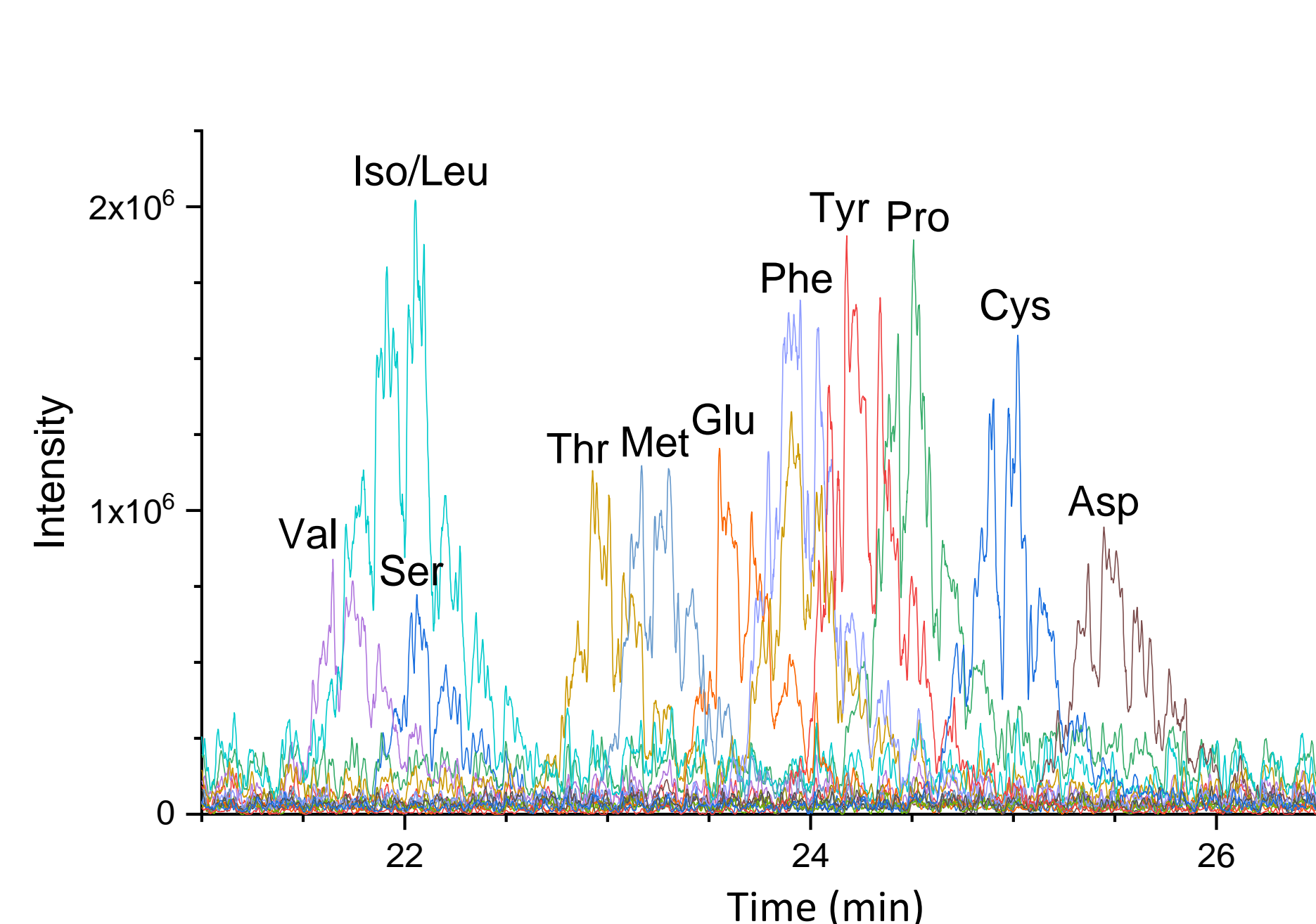


Results:
 Detection of building blocks of life

Accurate and repeatable measurement of multiple amino acids has been demonstrated with our system, using two different detectors.



Conductivity detection:
 Conditions: 250 μ M inorganics, 50 μ M amino acids; BGE: 5 M acetic acid; injection volume: 8 nL; separation voltage: 20 kV; capillary length: 67 cm (effective: 47 cm); 50 μ M i.d. capillary.



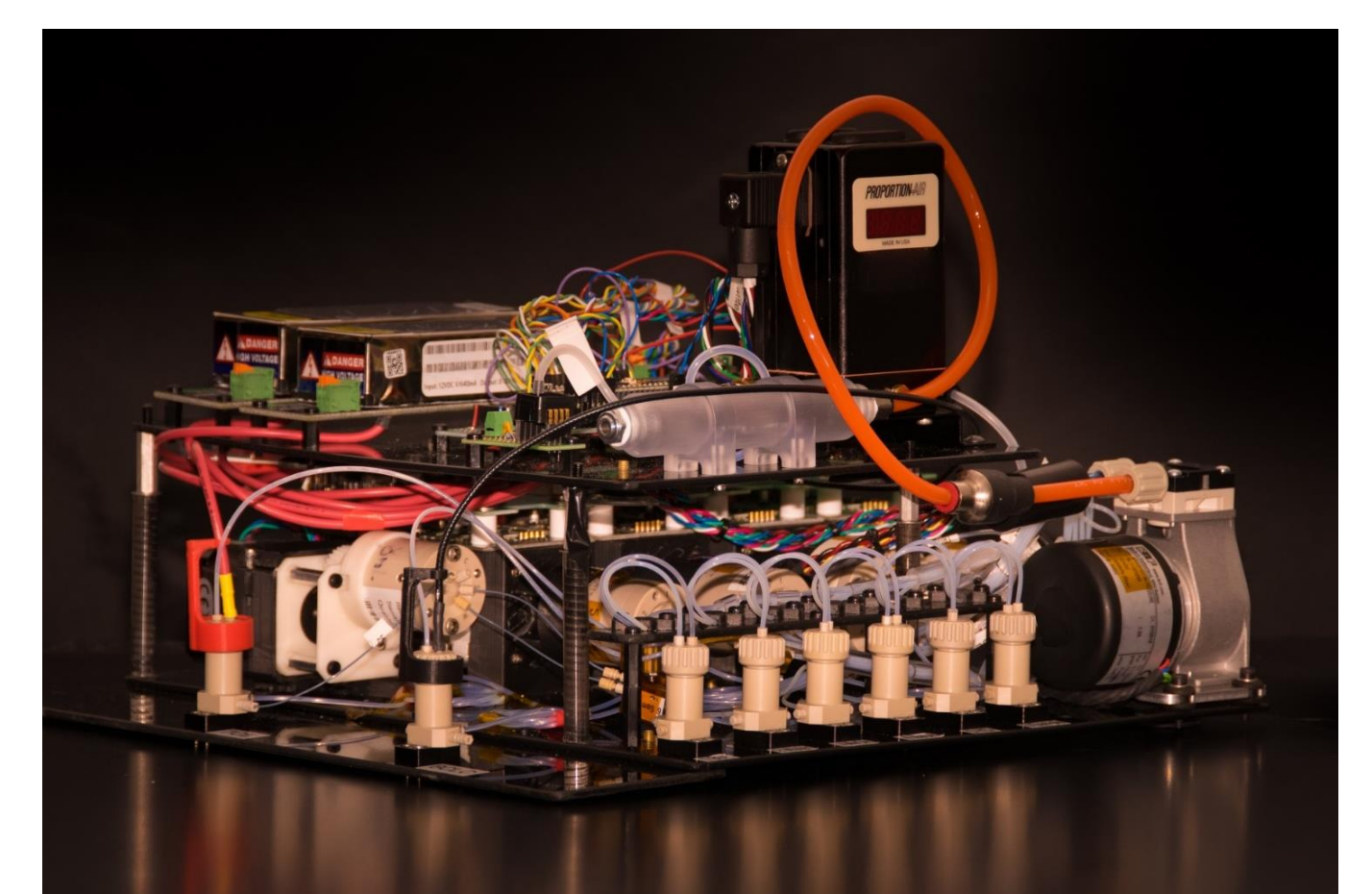
Mass spectrometry:
 Overlay of extracted ion chromatograms. Conditions: 50 μ M amino acids; BGE: 10% acetic acid; injection volume: 4 nL; separation voltage: 20 kV; separation pressure: 5 psi; capillary length: 90 cm; 50 μ M i.d. capillary; spray voltage: 1.5 kV.

Conclusions:
 Simple and robust analysis

Future steps: Field tests, integration into autonomous instrumental suite, multiplex separation capillaries and electro spray sources, brass board design.

Conclusions: An original design combining microfluidic and pneumatic circuits with custom rotary valves solved the most challenging problems of microfluidic instruments: automation, HV isolation, and sample injection.

We demonstrated the first fully automated CE-C4D-ESI-MS system with similar detection limits to commercial benchtop equipment. The instrument can detect a broad range of soluble species that can be ionized, polar organic and inorganic. We demonstrated, as a first step, the detection of ions relevant to ocean world environments and amino acids.



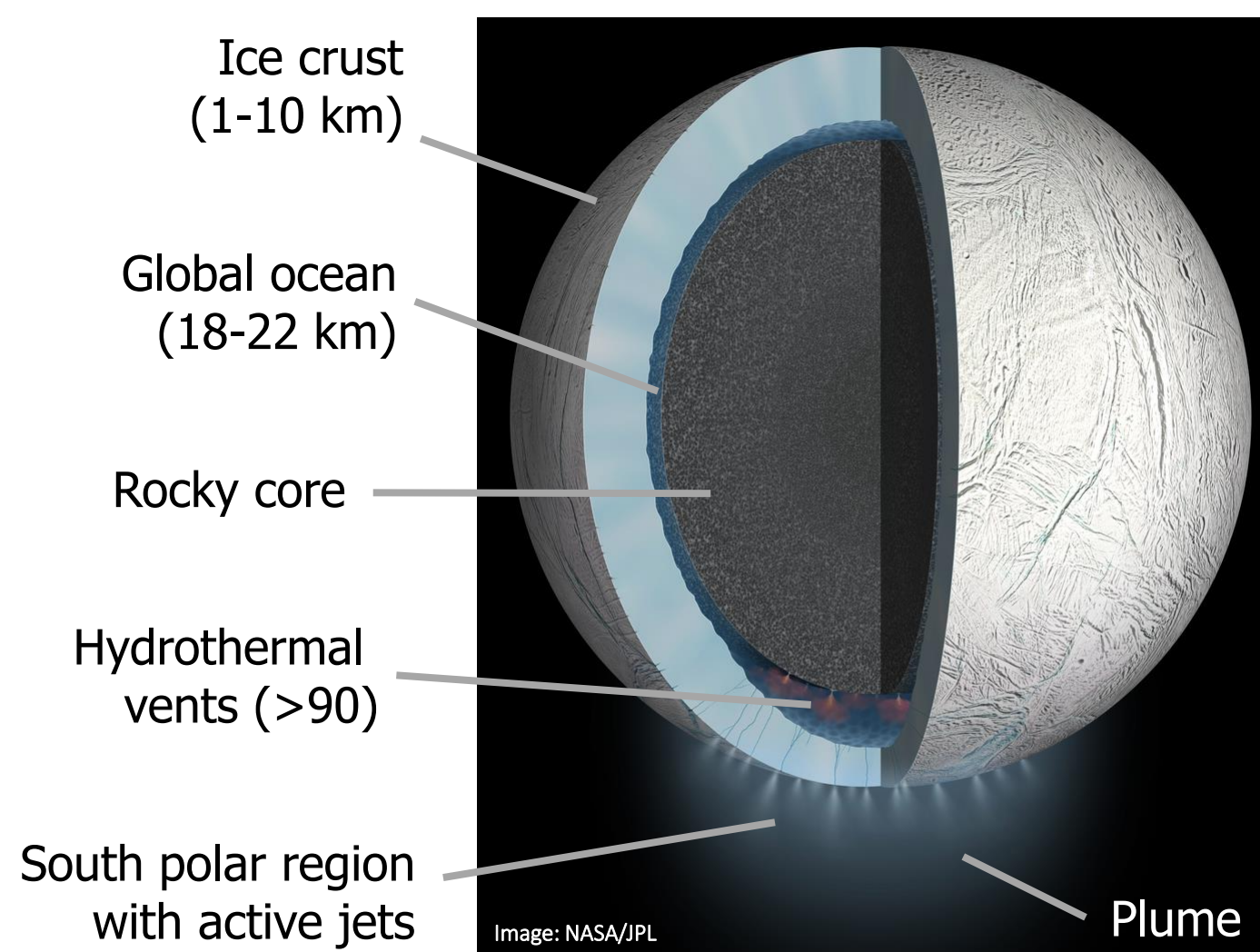
Prototype of Automated Capillary Electrophoresis System for Multiple Mode Detection. NTR-51143.

First Steps to Measuring Enceladus' Plume Constituents at Hypervelocity

Author: Sarah E. Waller (389T)

Anton Belousov (389T), Nicholas R. Tallarida (389R), Stojan M. Madzunkov (389T), Murray R. Darrach (3890), Robert P. Hodyss (3227), and Morgan L. Cable (3225)

Background and Motivation



On the shoulders of giants: The Cassini mission revealed Enceladus to be an active, dynamic world with a global, subsurface, liquid-water ocean with a plume at its South pole.

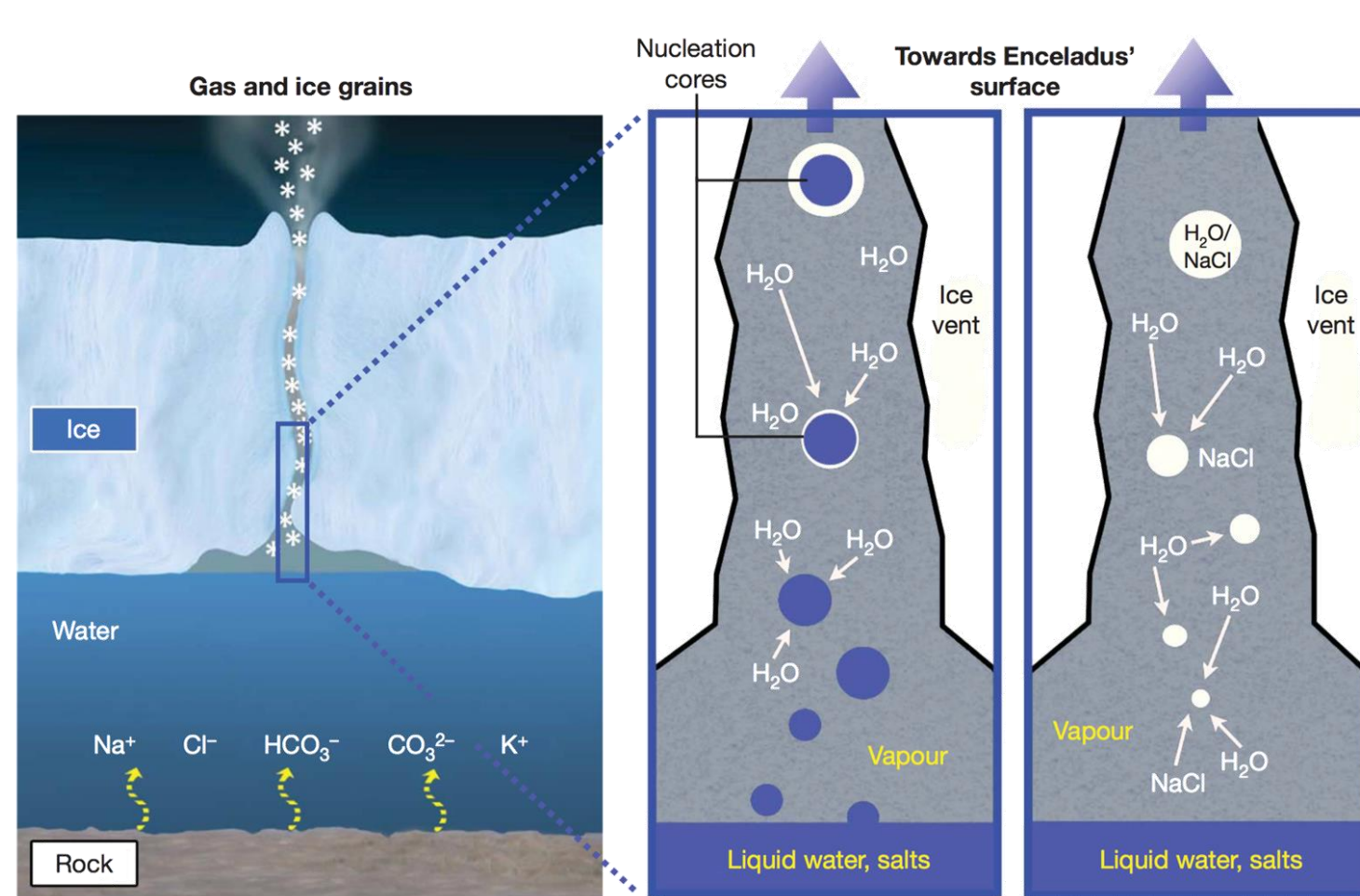
Is it hot in here or is it just Enceladus? The presence of methane, molecular hydrogen, and silicon nanograins in the plume is strong evidence for hydrothermal vents on the sea floor.

- Silica nanograins can only form >90 °C.
- Methane and molecular hydrogen production indicate chemistry is taking place in the ocean.

These make Enceladus a key target for astrobiological missions.

Enceladus is one prime target to search for aqueous-based life.

- Energy, chemistry, liquid water



A look at the plume through Cassini's eyes:

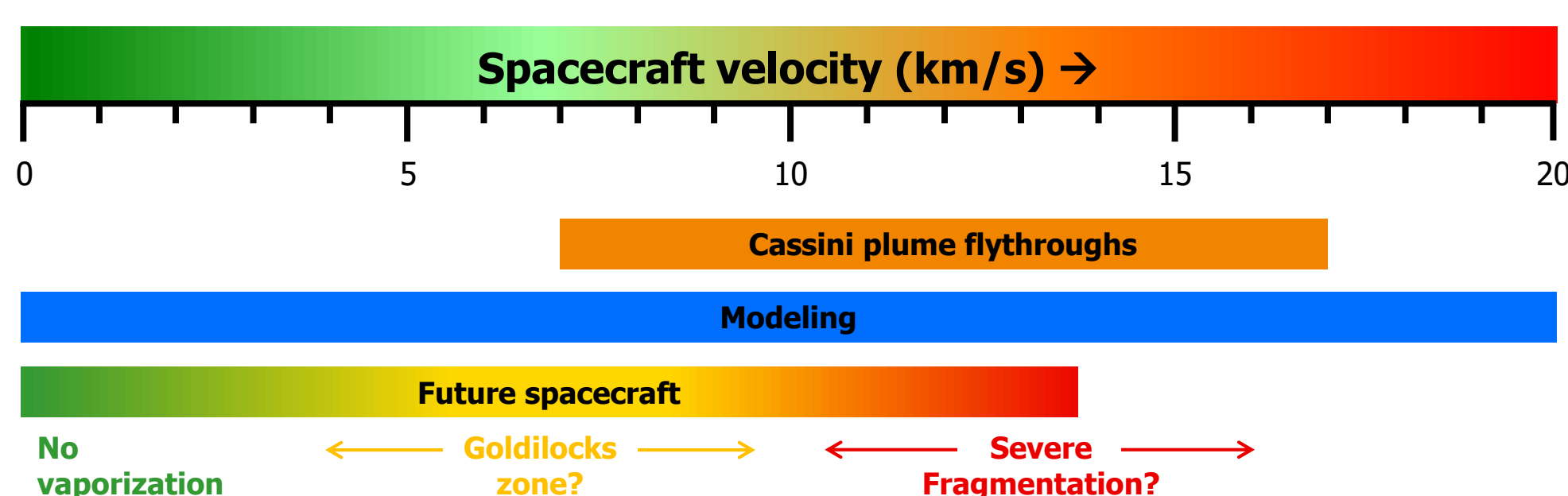
Gas component

- Ion and Neutral Mass Spectrometer (INMS)
 - H_2O , CO_2 , CH_4 , NH_3 , and H_2
 - Simple and complex organics

Solid component

- Cosmic Dust Analyzer (CDA)
 - Water-ice
 - Salts (mostly NaCl)
 - High Mass Organic Cations

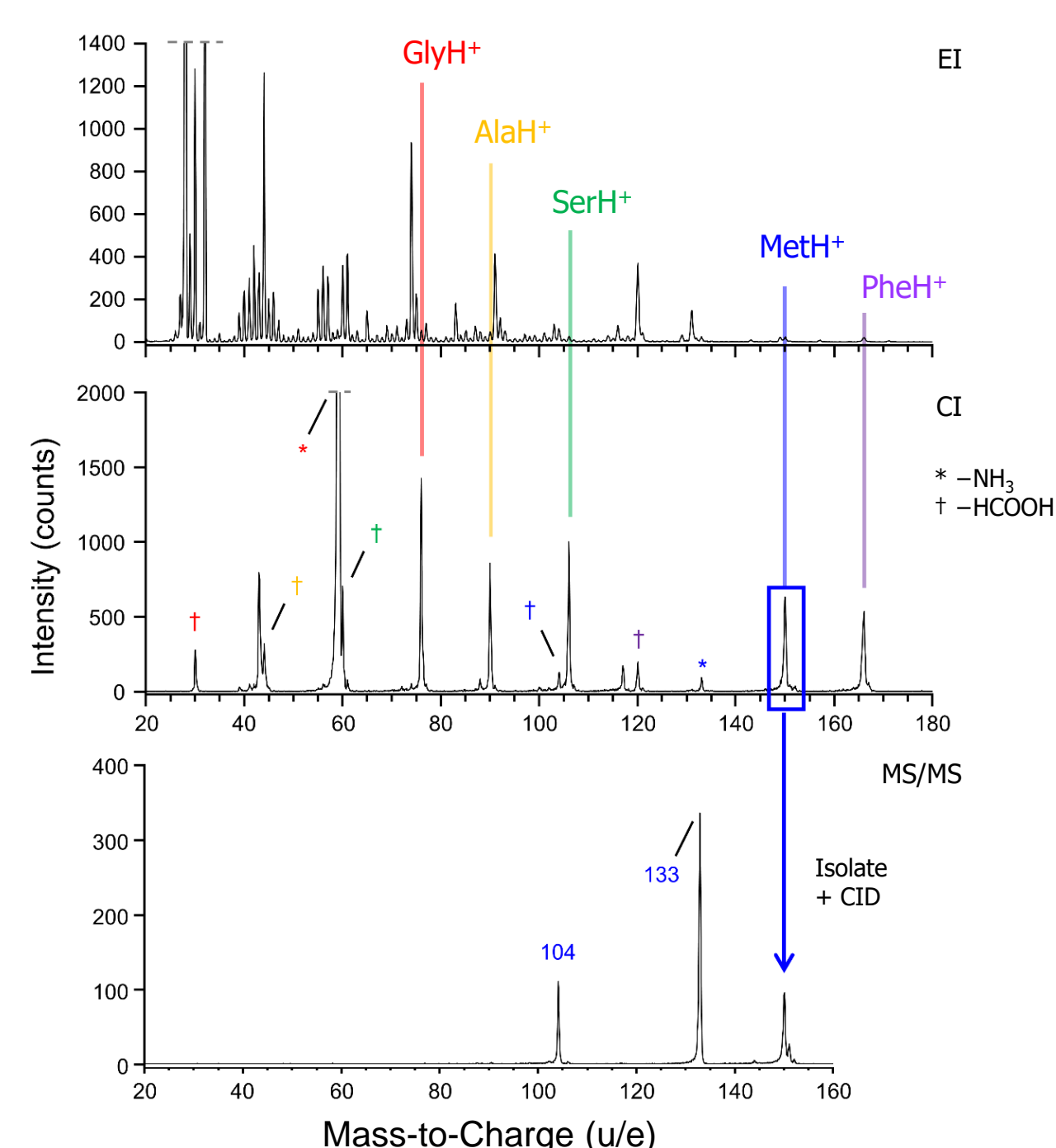
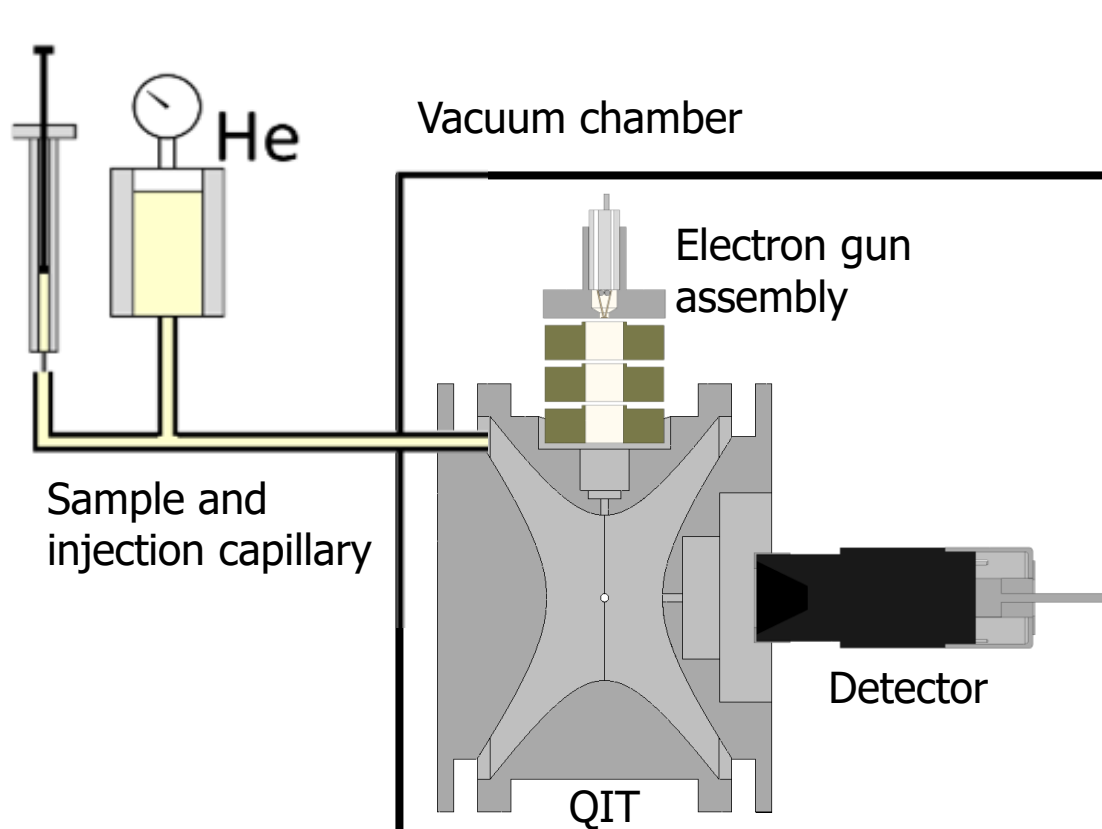
- The plume expresses the subsurface ocean into space
- Enables sampling with a flyby spacecraft –easier than an orbiter or lander
- **Challenge:** hypervelocity (>1 km/s) sampling can induce fragmentation, but where do the thresholds lie?



I aim to determine Goldilocks zone and severe fragmentation thresholds with lab-based instrumentation

There is a need to validate instrumentation and methodologies for future missions utilizing hypervelocity sampling.

Quadrupole Ion Trap Mass Spectrometer (QITMS)

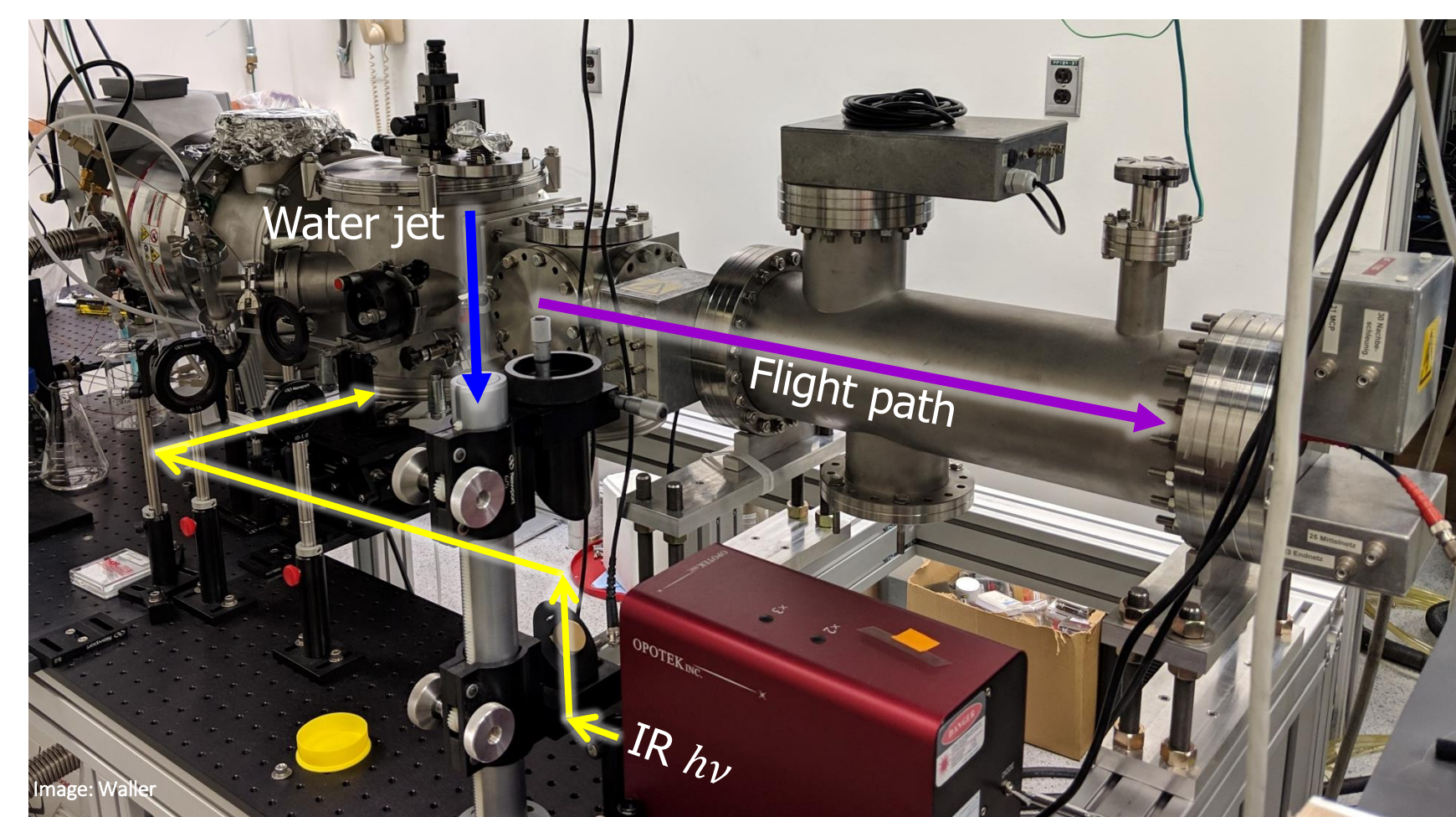


- Chemical ionization (CI):
 - Reduces fragmentation
 - Enables tandem MS (MS/MS)
 - Increases sensitivity
- MS/MS produces a chemical fingerprint
- Chemical fingerprints ease MS analysis

A lab-based instrument that generates hypervelocity ice and molecule analogs is currently being build and characterized to validate flight instrumentation.

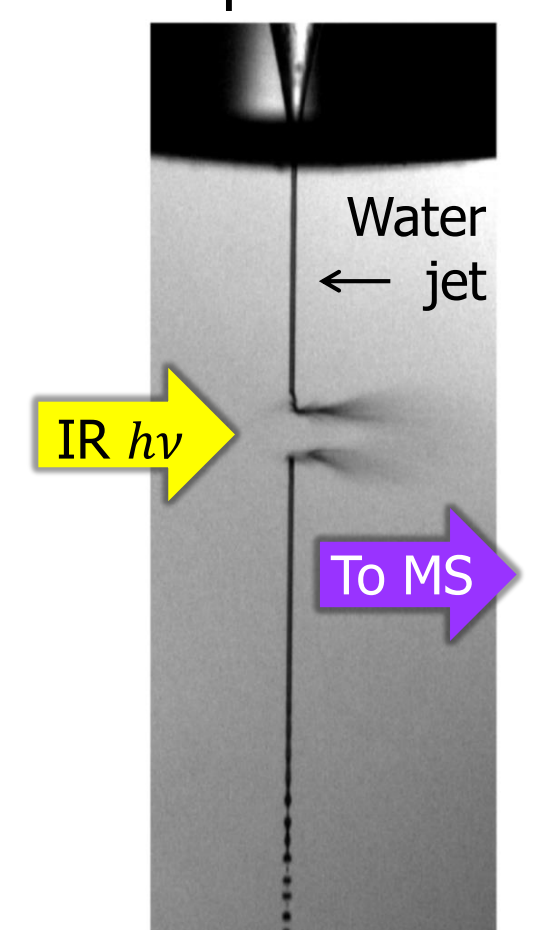
This will be the ONLY instrument on the planet with such capabilities.

Meet HIGS (Hypervelocity Ice Grain System)

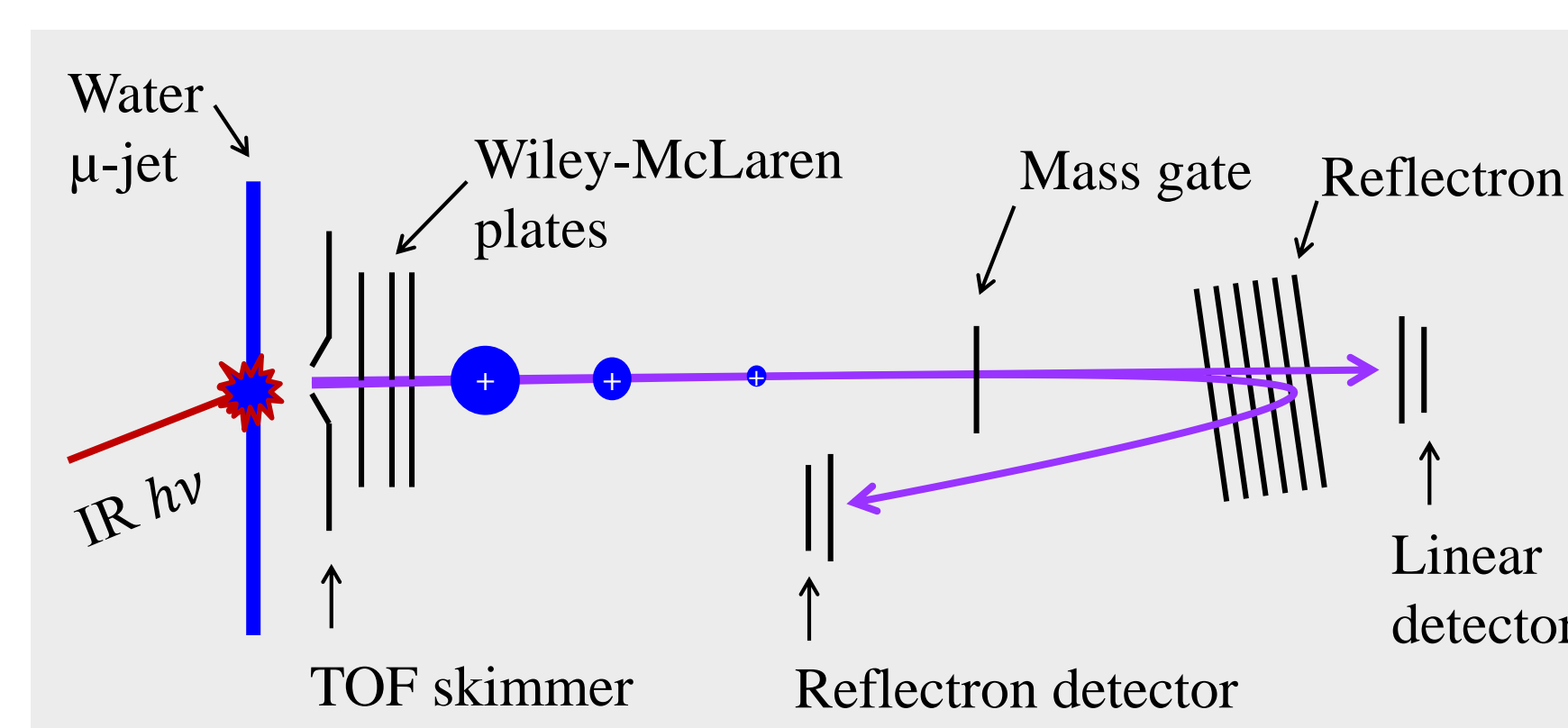


- Laser induced desorption (LID)
- Time-of-flight (TOF) mass spectrometry
- Generates charged and neutral species
- Used to reproduce CDA data

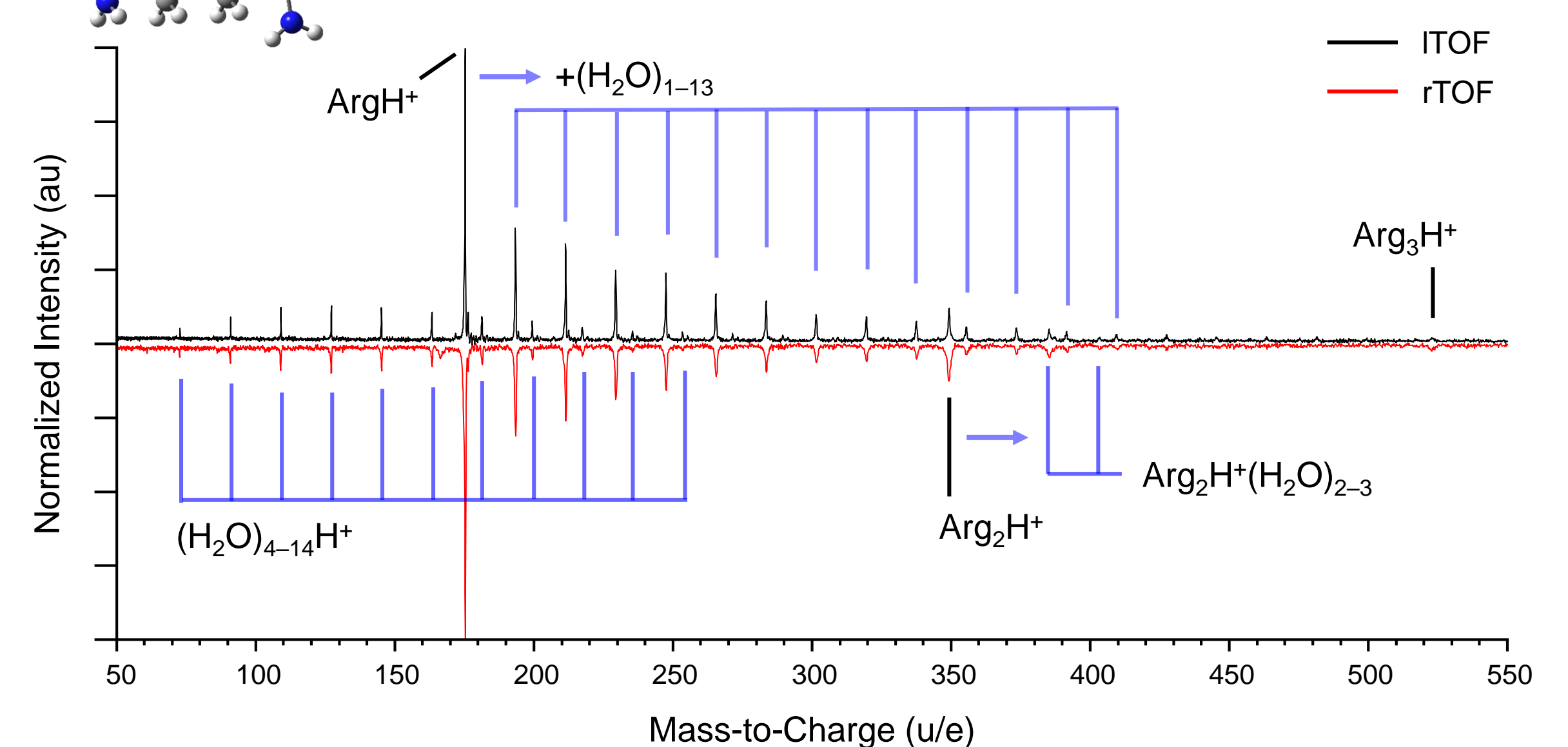
LID: Explosive action!



Wiedersheim et al. (2015) PCP, 17, 6858-6864.



10 mM Arginine (Amino Acid): ITOF vs rTOF



- Water clusters
- Monomers and *n*-mers of amino acids
- Amino acid-water clusters
- ITOF and rTOF distributions are identical
- Velocity of ArgH+ 8×10^4 m/s

The work detailed here represents a strong start to developing instrumentation and methodologies that can analyze species upon hypervelocity impact.

Can't Stop, Won't Stop

Methodologies:

- Chemical fingerprint library
- Structural isomer identification
- Quantitation investigation

Experimental:

- Enceladus brines (NaCl, KCl)
- Enceladus pH's (8.5-9)
- Amino acid mixtures, polypeptides, fatty acids
- Anion distributions

Instrumentation:

- Adaptive interface –to couple instruments for validation
- Phosphor screen – to characterize ion & neutral beam

Acknowledgements

I gratefully acknowledge the JPL Strategic Research and Technology Development Program for funding this work. I am also thankful to the Planetary Mass Spectrometry group (389T) for allowing me to use their MS.

Special thanks to Morgan L. Cable for her wonderful mentorship and insights into Enceladus and other astrobiological targets. Additional thanks to the amazing Hypervelocity Sampling Team.